Stimuli-Triggered Ionic and Molecular Transport through Track-Etched Nanopores

Vom Fachbereich Material- und Geowissenschaften
der Technischen Universität Darmstadt

zur Erlangung des akademischen Grades eines
Doktor rerum naturalium (Dr. rer. nat.)

genehmigte

Dissertation

von

M.Phil. Saima Nasir
aus Sahiwal (Pakistan)

Darmstadt 2014
D17

Stimuli-Triggered Ionic and Molecular Transport through Track-Etched Nanopores
Stimuli-getriggerter ionischer und molekularer Transport durch spurgeätzte Nanoporen

genehmigte Dissertation von Saima Nasir aus Sahiwal (Pakistan)

1. Gutachten: Prof. Dr. rer. nat. Wolfgang Ensinger
2. Gutachten: Prof. Dr. rer. nat. Jörg J. Schneider

Tag der Einreichung: 25.06.2014
Tag der Prüfung: 03.11.2014

Erklärung zur Dissertation

Hiermit versichere ich, die vorliegende Dissertation ohne Hilfe Dritter nur mit den angegebenen Quellen und Hilfsmitteln angefertigt zu haben. Alle Stellen, die aus Quellen entnommen wurden, sind als solche kenntlich gemacht. Ein Teil der Dissertation wurde bereits in wissenschaftlichen Journalen veröffentlicht, siehe *List of Publications*, und ist in der Dissertation mit Erlaubnis der Herausgeber der Journale reproduziert. Diese Arbeit hat in gleicher oder ähnlicher Form noch keiner Prüfungsbehörde vorgelegen.

Darmstadt, den 07.11.2014

_____

(Saima Nasir)

Diese Arbeit wurde unter der Leitung von Prof. Dr. rer. nat. Wolfgang Ensinger im Fachgebiet Materialanalytik des Fachbereichs Materialwissenschaft der Technischen Universität Darmstadt in der Zeit von April 2011 bis Mai 2014 durchgeführt.

Acknowledgements

Firstly, all praises to Allah Almighty, the most omnific, omniscient and omnipresent. All respects are for His Holy Prophet Muhammad (Peace be upon him), who enabled us to recognize our creator.

I would like to express my deepest appreciation to my respected and gracious supervisor Prof. Dr. Wolfgang Ensinger for his encouraging attitude, remarkable suggestions and keen interest during my research work. Additionally, providing the opportunity to attend very interesting and informative international conferences where I have presented my research work in the form of oral talks and posters.

I pay my gratitude to Prof. Dr. Christina Trautmann for the opportunity to perform my doctoral work at the Materials Research Department at GSI. Especially for providing me irradiated samples, research facilities and flexible environment to do my research work. I would also appreciate her nice behaviour during my stay at GSI.

I also express my sincere thanks to Prof. Dr. Jörg J. Schneider accepting to be the second referee of this research work.

I am obliged to express my thanks to Dr. Mubarak Ali for being a source of inspiration and enlightment for me. I thank his guidance for the new ideas, discussions and experiments. Especially for the time he spent in reading and correcting to improve my written work.

I am thankful to Dr. Maria Eugenia Toimil Molares for giving basic lab instructions, friendly behaviour and solving problems related with chemistry laboratory.

I pay my thanks to Dr. Quoc Hung Nguyen for introducing me to the field of mass transport experiments and his guidance in calculation work and using FESEM.

I am also thankful to our theoretician collaborators from Spain Prof. Dr. Patricio Ramirez (Universitat Politècnica de València) and Prof. Dr. Salvador Mafe (Universitat de València) for the theoretical modelling of the experimental results.

Dr. Muhammad Nawaz Tahir (Johannes Gutenberg-Universität, Mainz) is highly acknowledged for making possible access to instrument for UV light irradiation experimnets and the synthesis of chemical compounds.

Dr. Ishtiaq Ahmad (Karlsruhe Institute of Technology, Karlsruhe) is highly acknowledged for the synthesis of photolabile molecules.

I am thankful to all the members of Material Research Group (Dr. Marilena Tomut, Dr. Kay-Obbe Voss, Loic Burr, Marco Cassinelli, Christian Hubert, Janina Krieg, Katharina Kupka, Liana Movsesyan, Anton Romanenko, Anne Spende, Michael Wagner, Umme Habiba Hossain) for a very pleasant and friendly working atmosphere. Especially, Dr. Ina Schubert who always gave positive response.

I also would like to thank Dr. Markus Bender and Dr. Daniel Severin for their support with computer related programming issues, and Elko Schubert for his help in the designing of apparatus used in diffusion experiments.

I also express my sincere gratitude to Mr. & Mrs. Nayyar Iqbal for their moral support.

I thank from the bottom of my heart to my loving and gracious parents Mr. & Mrs. Muhammad Abdullah Nasir for their endless affection, patience, support and encouragement throughout my academic career and life. I will comit a moral laps if I do not mention my sweet, caring and friendly brothers Muhammad Khurram Abdullah, Muhammad Farrukh Abdullah and Muhammad Qasir Abdullah. I am also thankful to my uncle Muhammad Tahir for everything which he did for me.

My very special love and thanks to my parents-in-law Mr. & Mrs. Muhammad Rafique, and brothers-in-law Mr. & Mrs. Rafaqat Ali, Tariq Ali and Tahir Ali for their love affection and support.

The acknowledgement may remain incomplete if I do not mention the love and support from my husband, and especially the great sacrifice of my son Zeeshan Ali to spend whole day without Mama.

I also gratefully acknowledge financial support (partial) by the Beilstein-Institut, Frankfurt/Main, within the research collaboration NanoBic.

Abstract

In nature, ion channels facilitate the selective transport of ions, water and small organic molecules across the cell membrane. Under the influence of external stimuli, biological ion channels change their conformation states in order to enhance/inhibit the ionic transport across the membrane, allowing functions such as communication between cells, nerve conduction and signal transmission. Inspired from the functionality and responsiveness of natural ion channels, an attempt to design artificial nanopore-based stimuli-responsive membranes is demonstrated in this thesis. To achieve this goal, the swift heavy ion irradiation of polymer membranes is performed at the UNILAC linear accelerator (GSI, Darmstadt). The damaged zones (latent ion tracks) in the polymer membrane are selectively removed via asymmetric and symmetric track-etching techniques, leading to the fabrication of conical and cylindrical nanopores, respectively. Due to heavy ion irradiation and the concomitant chemical etching process, chemical moieties on the inner pore walls are produced. The native carboxyl (–COOH) groups on the pore walls are further exploited for the chemical attachment of stimuli-responsive molecules having primary amine in their backbone through carbodiimide coupling chemistry. Thermo-responsive membranes are prepared by the immobilisation of amine-terminated polymer (PNIPAAM–NH_2) chains on the inner pore wall via "grafting-to" approach. The effective pore diameter is tuned due to swelling/shrinking of the polymer chains by changing the environmental temperature, leading to decrease/increase in the ionic transport through the modified nanopores. The experimental results exhibit the reversible temperature-dependent variation in the analyte permeation across the multi-pore membranes and ionic conductance of single-pore membrane in response to thermal changes in the electrolyte solution in contact with the nanopores. Light-sensitive nanopores are prepared by decorating the pore walls with monolayers of photolabile molecules. The terminal uncharged photosensitive pyrene moieties are cleaved from the pore surface through UV irradiation, leading to the generation of carboxylate ($–COO^-$) groups. The photo-triggered permselective ionic transport is evaluated experimentally and theoretically by current–voltage (*I–V*) and analyte permeation measurements of single-pore and multi-pore membrane, respectively. Moreover, dual-responsive nanopores, i.e., nanopores that respond to both light and pH, are prepared by functionalizing the nanopore surface with photosensitive "caged" lysine chains. The uncharged and hydrophobic photo-labile 4,5-dimethoxy-2-nitrobenzyl (NVOC) groups, protecting the amine and carboxylic acid groups of lysine, are removed by exposing the modified pores to UV light, resulting in the production of hydrophilic amphoteric groups on the inner pore walls. In this experiment, polymer membranes having single and arrays of asymmetric nanopores are used for the light-triggered pH-tunable transport of ionic and molecular analytes through the nanopores. In addition to above mentioned stimuli-responsive systems, the modulation of ionic transport is also achieved through biomolecular conjugation inside the confined geometries. To this end, nanopore surface is modified with a suitable biorecognition element (ligand). Firstly, iron-terPy complex (ligand) is immobilized on the pore walls. The Fe(II) ions incorporated in the iron-terPy complex recognize and bioconjugate with lactoferrin through specific metal ion–protein interactions. The bioconjugation processes inside the nanopore significantly decrease the effective pore diameter available for the transport of ions, resulting in the reduction of ionic flux across the membrane. Secondly, an attempt is made to fabricate nanopore which exhibits reversible biomolecular recognition and conjugations via lectin–carbohydrate interactions. For this purpose, nanopore surface is decorated with mannopyranoside moieties which have the ability to selectively bioconjugate with lectin (ConA) protein. The biomolecular binding (bioconjugation) and unbinding inside the confined geometries gives measurable changes in the conductance of single-pore membrane and permeation rate for the case of multipore membrane. Moreover, the ConA binding/unbinding events inside the confined environment are reversible, allowing several measuring cycles by simply washing the bioconjugated membrane with a mannose solution. Such stimuli-responsive nanoporous systems, described in this PhD research work, have huge potential for biosensing, drug delivery and the design of controlled release platforms, especially when the modulation of nanopore transport properties under biological conditions is required.

Zusammenfassung

In der Natur dienen Ionenkanäle zum selektiven Transport von Ionen, Wasser und kleinen organischen Molekülen durch Zellmembranen. Durch externe Stimulation verändern biologische Ionenkanäle ihre Konformationszustände um Ionentransport zu verstärken oder zu blockieren und so Funktionen wie Kommunikation zwischen Zellen, Leitung in Nervenbahnen und Signaltransport zu ermöglichen. Inspiriert durch die Funktionalität und Reaktionsfreudigkeit von Ionenkanälen ist in dieser Arbeit ein Weg zur Herstellung von künstlichen, gezielt ansprechbaren, nanoporen-basierten Membranen aufgezeigt. Zu diesem Zweck wurden Schwerionenbestrahlungen von Polymerfolien am UNILAC Linear Beschleuniger (GSI, Darmstadt) durchgeführt. Die geschädigten Zonen (latenten Spuren) im Polymer werden durch asymmetrisches bzw. symmetrisches Spurätzen selektiv herausgelöst, um konische bzw. zylindrische Nanoporen herzustellen. Mittels Schwerionenbestrahlung und anschließendem chemischem Ätzen werden chemische Bausteine an der Poreninnenwand erzeugt. Die ursprünglichen Carboxylgruppen (-COOH) an der Porenwand werden mittels Carbodiimide-Kopplungs-Chemie für die chemische Bindung von gezielt ansprechbaren Molekülen ausgenutzt, die primäre Amin in ihren Hauptsträngen besitzen. Auf Temperatur reagierende Membranen werden durch Immobilisierung von Polymerketten, die auf Amingruppen enden, (PNIPAAM-NH_2) an der Poreninnenwand mittels dem sogenannten “grafting-to” Verfahren hergestellt. Durch Veränderungen der Umgebungstemperatur wird der effektive Porendurchmesser durch Schwellen oder Zusammenziehen der Polymerketten kontrolliert. Dies führt zu Abschwächung bzw. Verstärkung des Ionentransports durch die modifizierten Poren. Die experimentellen Ergebnisse zeigen reversible temperaturabhängige Veränderungen beim Durchfluss des Analyten durch eine Multipormembran sowie der ionischen Leitfähigkeit von Einzelpormembranen als Reaktion auf Temperaturveränderungen im Elektrolyt im Kontakt mit der Nanopore. Lichtsensitive Nanoporen werden durch dekorieren der Porenwand mit Monolagen von photolabilen Molekülen hergestellt. Die ungeladenen photosensitiven Pyren-Bausteine werden von der Porenoberfläche durch UV Bestrahlung abgelöst. Dies führt zu Erzeugung von Carboxylatgruppen (-COO^-). Der durch Licht ausgelöste selektiv-permeable Ionentransport wird experimentell und theoretisch durch Aufnahme von Strom-Spannungs-Kurven und Durchflussmessungen an Einzelporen- und Multiporen-membranen untersucht. Zusätzlich werden doppelt ansprechbare Nanoporen, die sowohl auf Licht als auch auf pH-Wert-Änderungen reagieren, hergestellt. Dies geschieht mittels Funktionalisierung der Nanoporenoberfläche mit photosensitiven “caged” Lysinketten. Die ungeladenen und hydrophoben photo-labilen 4,5-Dimethoxy-2-Nitrobenzyl-Gruppen, die Amin und Carboxylsäuren des Lysin schützen, werden bei Bestrahlung der modifizierten Poren mit UV Licht herausgelöst. Dies führt zur Entstehung von hydrophilen amphoteren Gruppen an der inneren Porenwand. Bei diesem Experiment werden sowohl Einzelkanalmembranen als auch Vielkanalmembranen für den durch Licht und pH-Wert kontrollierbaren Transport von ionischem und molekularem Analyt durch die Poren eingesetzt. Zusätzlich zu den oben erwähnten gezielt ansprechbaren Systemen, wird die Ionentransport-Veränderung durch biomolekulare Konjugation innerhalb der begrenzten Geometrien erzielt. Dazu wird die Nanoporenoberfläche mit geeigneten Elementen (Liganden) modifiziert. Zuerst, wird ein Eisen(III)Py-Komplex (Ligand) an der Porenoberfläche immobilisiert. Die Fe(II)-Ionen inkorporiert in Eisen-terPy Komplex biokonjugieren mit Lactoferrin durch spezifische Metallionen-Protein Wechselwirkungen. Der Biokonjugationsprozess innerhalb der Nanopore verringert signifikant den effektiven Porendurchmesser, der für den Porentransport zur Verfügung steht und resultiert in einer Verringerung des Ionenflusses durch die Membran. Anschließend wird ein Versuch gemacht Nanoporen, die reversible biomolekulare Erkennung und Konjugation haben, mittels Lectin-Carbohydrat- Wechselwirkungen herzustellen. Zu diesem Zweck wird die Nanoporenoberfläche mit Mannopyranosid dekoriert. Dieses besitzt die Eigenschaft zur selektiven Biokonjugation mit Lectin (ConA) Proteinen. Die biomolekularen Bindungs- und Lösungsereignisse innerhalb der begrenzten Geometrien führen zu messbaren Veränderungen der Leitfähigkeit von Einzelkanalmembranen und Durchflussraten im Falle der

Multiporenmembran. Zusätzlich sind die ConA Bindungs/Lösungsereignisse innerhalb der begrenzten Umgebung reversibel d.h. durch einfache Spülung der biokonjugierten Membran mit Mannoselösung werden vielfache Messzyklen ermöglicht. Solche gezielt ansprechbaren nanoporösen Systeme, die in dieser Arbeit untersucht werden, haben großes Potential als Biosensoren, Medikamentenverabreichung und zum Design von kontrollierten Abgabeplattformen, insbesondere wenn die Modulation der Nanoporenparameter bei biologischen Bedingungen notwendig ist.

Table of Contents

Table of Contents ..... **vii**

1. General Introduction **1**

1.1 Nanopore preparation and functionalisation 1

1.1.1 Biological ion channels / nanopores 1

1.1.2 Solid-state nanopores 2

1.2 Stimuli-responsive nanopores 4

1.2.1 Thermo-sensitive nanopores 4

1.2.2 Photo-sensitive nanopores 4

1.2.3 pH-sensitive nanopores 5

1.2.4 Metal ion-sensitive nanopores 5

1.2.5 Biomolecular-sensitive nanopores 5

1.3 Aims and Objectives 6

2. Experimental **9**

2.1 Nanopore fabrication in polymer membranes 9

2.1.1 Heavy ion irradiation 9

2.1.2 Chemical etching of latent ion tracks 13

2.1.2.1 Fabrication of conical nanopores 14

2.1.2.2 Fabrication of cylindrical nanopores 16

2.2 Geometrical characterization of nanopores 17

2.3 Current-voltage (*I*–*V*) measurements 18

2.3.1 Estimation of single pore diameter 20

2.4 Tuning nanopore surface chemistry 21

2.5 Analyte permeation experiments 23

2.6 Fabrication of stimuli-responsive nanopores 25

2.6.1 Materials and chemicals 25

2.6.2 Preparation of thermo-sensitive nanopores 25

2.6.2.1 Functionalisation of PNIPAAM–NH_2 brushes 25

2.6.2.2 Characterization 25

2.6.3 Preparation of photosensitive nanopores 26

2.6.3.1 Synthesis of 4-oxo-4-(pyren-4-ylmethoxy) butanoic acid 26

2.6.3.2 Functionalisation of 4-oxo-4-(pyren-4-ylmethoxy) butanoic acid 27

2.6.3.3 UV light irradiation 27

2.6.3.4 Characterization 28

2.6.4 Preparation of photo-triggered pH-sensitive nanopores 28

2.6.4.1 Synthesis of “caged” lysine amino acid (7) 28
2.6.4.2 Functionalisation of “caged” lysine chains 30
2.6.4.3 UV light irradiation 30
2.6.4.4 Characterization 31
2.6.5 Lactoferrin protein sensitive nanopore 32
2.6.5.1 Synthesis of 1-amino-5-(2,2′:6′,2″-terpyrid-4′-yl-oxy)pentane (terPy–DEG-NH_2) 32
2.6.5.2 Functionalisation of terPy–DEG-NH_2 32
2.6.5.3 Formation of iron–terpyridine complexes 33
2.6.5.4 Characterization 33
2.6.6 Lectin (ConA) protein sensitive nanopores 34
2.6.6.1 Functionalisation of p-aminophenyl α-D-mannopyranoside 34
2.6.6.2 Characterization 34
3. Results and discussion 35
3.1 Thermally Controlled Permeation of Ionic Molecules through Synthetic Nanopores Functionalized with Amine–Terminated Polymer Brushes 35
3.1.1 Introduction 36
3.1.2 Immobilzation of polymer chains 36
3.1.3 Analyte permeation 37
3.1.3.1 Cylindrical nanopore arrays 37
3.1.3.2 Conical nanopore arrays 40
3.1.4 Single conical nanopore 42
3.1.5 Conclusions 43
3.2 Optical Gating of Photosensitive Synthetic Ion Channels 45
3.2.1 Introduction 46
3.2.2 Immobilization of photo-labile PYBA molecules 47
3.2.3 Single conical nanochannels 47
3.2.4 Theoretical Modeling 48
3.2.4 Multichannel membranes 49
3.2.5 Logic functions and controlled release 52
3.2.6 Conclusions 52
3.3 Nernst-Planck Model of Photo-Triggered, *pH*–Tunable Ionic Transport through Nanopores Functionalized with “Caged” Lysine Chains 53
3.3.1 Introduction 54
3.3.2 Synthesis and immobilization of Photosensitive “caged” amino acid lysine 54
3.3.3 Single asymmetric nanopore 55
3.3.4 Multipore membranes 57
3.3.5 Theory 60
3.3.5.1 A single pore with COOH groups 63

3.3.5.2 A single pore with amphoteric groups....63
3.3.5.3 Estimation of the pore parameters....64
3.3.5.4 Permeation of MV^{2+} and NDS^{2-}....67
3.3.6 Conclusions....69
3.4 Metal Ion Affinity-based Biomolecular Recognition and Conjugation inside Polymer Nanopores Modified with Iron–Terpyridine Complexes....71
3.4.1 Introduction....72
3.4.2 Immobilization of amine-terminated terpyridine ligand....73
3.4.3 Single conical nanopore....74
3.4.3.1 Bioconjugation inside a confined environment....75
3.4.3.2 Sensitivity and specificity of the nanopore biosensor....75
3.4.3.3 Control experiment....77
3.4.3 Multipore membranes....78
3.4.4 Conclusions....80
3.5 Carbohydrate-Mediated Biomolecular Recognition and Gating of Synthetic Ion Channels....81
3.5.1 Introduction....82
3.5.2 Ligand immobilization and bioconjugation....83
3.5.2.1 Single-channel membrane....84
3.5.2.2 Modelling....88
3.5.2.3 Multichannel membrane....89
3.5.3 Conclusions....91
4. Summary and outlook....93
5.1 Summary....93
5.2 Outlook....94
5. References....95
Appendix....105
List of Abbreviations....105
List of Chemicals....107
List of Figures....108
List of Tables....112
List of Publications....113
Curriculum Vitae....115

1. General Introduction

Ion channels/ pores are ubiquitous in nature and play a vital role in almost all physiological processes occuring in living organisms. These are the sign of life because physiological functions such as energy storage, signal transduction in nerves and muscles to communicate within the cellular system depend strongly on the regulation and transport of ions across the cell boundaries.[1] In living organisms, ion channels are mainly formed by the self-assembling of proteins that populate the cell membrane. The integration process of membrane proteins into channels/pores is quite reproducible. The biological ion channels/pores serve as "smart" gates which open and close in response to external stimuli to regulate the flow of ions across the cellular system. Moreover, they also exhibit permselective behaviour and very selectively transport ions (e.g., Na^+, K^+, Ca^{2+} or Cl^-) through their selectivity filter.[2-5] They also facilitate the flow of water and other organic molecules such as drugs, nutrients or toxins through the biological membranes.

Inspired from the structure, function, operation and responsiveness of ion channels, an increasing number of scientists are still making attempts to understand the gating mechanism and permselective characteristics of biological membranes. For this purpose, solid-state nanopores are fabricated in a variety of organic/inorganic materials.[6-9] The synthetic nanopores show some advantages over their biological counterparts such as stability, tunable pore dimensions (size and shape), possibility of integration into nanofluidic devices, and tailored surface properties. They also exhibit ionic transport properties such as current rectification, voltage-dependent current gating, and permselectivity similar to those of biological pores. Moreover, phenomena like drug delivery, hemodialysis, diagnostics, incorporation into artificial organs, coatings for medical devices, tissue regeneration and biosensing can be studied using synthetic membranes.[9-13] Industrially, synthetic membranes have found application in ultra-filtration, microfiltration, reverse osmosis, gas separation, pre-evaporation, and electro-dialysis.[12-20] Synthetic nanopores seem to be perfect choice for building devices with controlled mass transport.

1.1 Nanopore preparation and functionalisation

To understand the mechanism of natural ion channels, a variety of techniques have been developed to prepare pores of biological origin in which proteins self-assemble and reproducibly integrate into pores/ionchannels which are supported in a lipid bilayer. Also, different methods were explored to fabricate synthetic nanopores in organic and inorganic materials as described below.

1.1.1 Biological ion channels / nanopores

Initially, the protein pores such as K^+-selective ion channels, particularly α-hemolysin which is a pore-forming toxin secreted by Staphylococcus *aureus* and the pore formed by protective antigen in Bacillus *anthracis* were studied experimentally for sensing purposes.[2,21,22] Amongst the variety of biological ion channels, the α-hemolysin (αHL) pore is most widely and frequently employed in nanopore analytics. It is a bacterial protein pore (heptameric structure) formed by the self-assembly of seven identical polypeptides.[21] The αHL pore has been explored as a highly sensitive sensor for rapid detection and sequencing of single molecule, i.e., DNA.[11] The other biological pores used in sensing purposes are originated from the porins.[23] The first one is the OmpG porin, which is composed of a single polypeptide chain and found in the outer membrane of Gram-negative bacteria. As compared to multimeric α-hemolysin pore, single point mutation is easily carried out in monomeric OmpG pore. The MspA is another porin from Mycobacterium *smegmatis*.[24] The MspA pore is

comprised of a short and narrow channel constriction suitable for the DNA sensing. Another class of protein pore includes peptide antibiotics such as gramicidine and alamethicin.[25] But these pores are not commonly used in nanopore analytics. Similarly, semi-biological ion channels are also available such as de-novo designed protein and peptide[26] pores as well as barrel-like pores formed by the interaction of peptides on rods.[27]

Chemical modification / engineering:

In order to expand the sensing capabilities, artificial binding sites (ligands) that interact with a specific analyte (receptor) were introduced into protein pores through chemical modification (or engineering). The engineering of protein pores is achieved mainly through mutagenesis, targeted chemical modification as well as incorporation of adapters via non-covalent modification techniques.[7,11,28,29] The majority of chemical modification/engineering work is dedicated to αHL pore because of its well studied X-ray structure as well as its ability to withstand harsh purification conditions and mutagenic changes. The interior (lumen) of the pore can be modified with suitable amino acids via mutagenesis. In this way, amino acid side chains differing in polarity, shape, size and reactivity can be introduced. For example, the histidine and arginine have been successfully introduced into the αHL pore for the detection of heavy metal ions and insitol 1,4,5-triphosphate, respectively.[30,31] For the case of target chemical modification, specific reagents (e.g., short oligonucleotides) having different functionalities are incorporated into the lumen of the pore by selective functionalisation of the side chain of amino acid, i.e., cysteine residue.[32] For the case of non-covalent modification, binding sites, i.e., host molecules (adapters, e.g., cyclodextrins) for the detection of small analytes (drugs and organic solvents) are introduced into the transmembrane barrel of αHL pore.[26]

In addition to αHL pore, other protein pores have also been engineered to improve their sensing abilities. For example, a moveable peptide loop in OmpG porin is removed and stabilized by the insersion of disulfide bond in order to avoid current fluctuations.[33] For the case of MspA porin, negativey charged residues are deleted to overcome the electrostatic repulsion forces during DNA analysis.[24] Moreover, current rectification properties of OmpF porin have been achieved by substitution with electrically charged amino acids.[34]

Biological ion channels/pores (αHL) embedded in lipid bilayer are prepared reproducibly with precisely controlled geometry and interfacial chemistry, and have therefore been proved to be very useful for a variety of interesting applications in nano/biotechnology such as sensing and manipulation of single molecules. However, the fragility and sensitivity of the embedding lipid bilayer induced by external parameters such as pH, temperature, salt concentrations, etc. restrain their suitability for more practical purposes. Conversely, synthetic nanopores fabricated in solid-state materials have recently attracted a great deal of interest as their dimensions, geometry and surface properties can be tuned on demand. Moreover, they also exhibit excellent chemical and mechanical robustness.

1.1.2 Solid-state nanopores

To date, various routes based on electron beam technology,[35,36] laser technology,[37] electrochemical etching,[38] anodic oxidation method[39] and ion-track-etching technology[40-42] have been investigated to fabricate synthetic nanopores in a variety of insulating solid-state materials like silicon, glass, alumina and polymer membranes. For the case of silicon materials, a nanosized hole in silicon nitride (Si_3N_4) membrane was drilled through ion beam sculpting technique.[35] In this method, first a wide pore (50-100nm) was drilled via focused ion beam and subsequently, the pore was narrowed due to surface diffusion to desired opening (e.g., ~ 1nm) diameter by using a diffuse beam. A feedback mechanism is employed to monitor the pore shrinking process. In silicon dioxide (SiO_2), an electron-beam is used to fabricate single nanopore with diameter ranges from 20 to 200 nm.[36] Moreover, focused electron beam is also used to fabricate pores in a free standing thin silica layer with a thickness of only 10 nm.[36] The fabrication of nanopores in silicon material can also be achieved via asymmetric

etching in potassium hydroxide (KOH) solution.[43] In addition to single pore, an array of nanopores in silicon membranes was prepared by lithography technology.[44]

The glass nanopipettes were prepared by microprocessor-controlled laser pullers. In this case a glass capillary was heated in the middle with laser and then mechanically pulled to break it at the narrow neck to form conical openings. In this technique, it is possible to obtain pipettes with pore opening diameter down to ~ 20 nm by tuning the heating and mechanical pulling parameters.[45,46] In addition to quartz nanopipettes, fabication of submicrometer pore structures in borosilicate glass coverslides was achieved by employing femtosecond-pulsed laser.[47] Recently, Drndic´ and his team have developed a method to fabricate nanopores in a vey thin graphene membrane in combination with electron-beam sculpted nanopores for the DNA translocation.[48]

Anodic aluminium oxide (AAO) membranes have been increasing interest due to self-organization and unique structure. AAO membranes have been widely studied for filtration and separation of molecules.[49,50] Fabrication process consists of the anodization of aluminium of high purity in an acidic solution applying a constant high voltage. Acidic solution consists of oxalic, sulphuric, chromic or phosphoric acids. Under these conditions, aluminium oxide is generated but it contains many defects due to concentration of electric field. This localized electric field increases acidic dissolution of the oxide at the bottom of the pores while leaving the pore walls intact. This process results in the formation of pore arrays which are self organized on the substrate. Then the remaining Al substrate is etched away by immersion in dilute acid which also affects the pore size. The geometry and morphology of the nanopores can be easily controlled by adjusting the conditions during the anodization processes. The AAO membrane has a packed array of columnar hexagonal pores ranging typically from 4 to 200 nm in diameter.

The fabrication of nanopores in ion tracked polymer membranes such as polyethyleneterephthalate (PET), polycarbonate (PC) and polyimide (PI) was achieved by track-etching technique.[40-42] Track-etching is the oldest fabrication technique for single solid-state nanopores. In this technique, a dielectric film is first irradiated with energetic heavy ions. As a result of this irradiation process, local damaged zones are created. Pores are fabricated from these latent tracks by chemical etching process. Track-etching technique is used to control the pore size by adjusting the conditions of etching process (etching time, temperature, and etchant concentration).

Moreover, Martin and his co-workers have developed a sophisticated approach to produce gold (Au) nanotubes in track-etched porous membrane via electroless plating method. In this way they are able to tune the pore size by controlling the Au-layer thickness as well as obtained reactive surface to functionalize the inner pore walls.[15,17,51]

Chemical functionalization:

In order to miniaturize nanopore based sensing/separation devices, it is highly desirable to have an active control over pore surface chemistry. For this purpose pore surface is chemically modified to match the specific requirements concerning hydrophobicity, selectivity, and interaction with a variety of bio(chemical) analytes. The chemical moieties on the pore walls may serve as binding sites for analytes or may interact with ions/molecules passing through the pore. For the case of solid-state nanopores, chemical modification strategies mainly rely on the inherent functionalities originated during pore formation process. Therefore, modification methodologies vary from one type of pore to another, depending on the material in which they are prepared.

The surface characteristics of Si_3N_4 nanopores were modified by depositing a layer of aluminium oxide through chemical vapour deposition.[52] Wanunu and Meller have reported the functionalization of different organosilanes by using the native oxide layer on the inner walls of Si_3N_4 pore.[53] Nilsson et al. have reported the localized functionalization of Si_3N_4 pore by depositing an oxide layer on the pore entrance.[54] Similarly, silane chemistry was also employed to tune the surface properties of nanoporous alumina membranes.[49,50,55] For the case of glass nanopipettes and glass pores, silanol (Si-OH) groups on the pore surface serve as sites to tether variable functionalities and responsive molecules via silanization[56,57] or electrostatically at neutral pH conditions.[46]

The surface properties of track-etched nanopores can be tuned via covalent modification through carbodiimide coupling chemistry[10,58-67] or electrostatic self-assembly[68,69] of functional molecules by exploiting the native carboxylic acid groups generated during pore fabrication process. The responsive polymer brushes were also tethered on the pore surface via "grafting-from" techniques, such as atom transfer radical polymerization (ATRP)[70-74] and plasma-induced grafting.[75,76] The grafting-to approach was also used to immobilize end-functionalized polymer chains onto the pore surface.[77] Moreover, surface chemistry of track-etched nanopores was changed by first depositing a Au layer on the pore surface through electroless deposition.[15,17,18,51]. Subsequently, the attachment of molecules containing SH or S-S was achieved via the spontaneous formation of S-Au bond on the metal coated pore surface.[15,17,18,51]

1.2 Stimuli-responsive nanopores

In membrane science and technology in particular stimuli-responsive nanoporous membranes have achieved remarkable attention because their physicochemical properties can be modulated in response to changes in their surrounding environment.[14] These membranes have the capability to regulate ionic and molecular permeation upon the application of external stimuli such as pH, temperature, ionic strength, light, electric field and (bio)chemicals.[12] The stimuli-responsive membranes containing either single-pore or an array of nanopores (multipore membrane) were prepared via the immobilization of polymer brushes[78] or self-assembled monolayers[7,10,11,79] of functional molecules on the surface and inner pore walls.

1.2.1 Thermo-sensitive nanopores

In living organisms the thermosensation process occurred via the direct activation of thermally gated ion channels located in the membrane surface of sensory neurons.[80] These thermo-responsive channels belong to the transient receptor potential (TRP) family of ion channels.[81] The protein pore can also respond to temperature [82]changes by the incorporation of an elastin-like polypeptide loop within the lumin of αHL pore.[83] For the case of synthetic nanopores, temperature sensitive pores were prepared by the immobilization of temperature-responsive polymer brushes on the pore walls. These polymer brushes change their conformational state (swell/shrink) by the variation of environmental temperature. The attachment of polymer chains onto the pore surface was achieved via "grafting-from" or "grafting-to" approach. Mainly poly(*N*-isopropylacrylamide) (PNIPAM) polymer was used for the preparation of thermo-sensitive nanopores because of its solubility in water.[10,57,70,73,77,84,85] Below the lower critical solubility temperature (LCST ~32 ˚C) the PNIPAM brushes were in swollen state, leading to reduction of the effective pore diameter which in turn blocked/decreased the ionic flow across the membrane. While above the LCST, PNIPAM polymer brushes are in collapsed state due to sharp conformational changes. This resulted in an increase in the effective pore diamter as indicated from the high ionic flux. Moreover, nanopore responsive to both temperature and pH were also fabricated by the grafting of dual-responsive copolymer brushes on the pore walls.[76,86]

1.2.2 Photo-sensitive nanopores

In addition to temperature as an external stimulus, light has equally attracted attention in the field of stimuli responsive nanopores.[87] In natural ion channels a variety of photochemical tools have been developed to control ionic flux across the biological membranes.[88] In order to create photo-responsive synthetic nanopores, photo-chromic molecules such as azobenzene,[89] spiropyran,[55,56,90] and coumarin[91] were incorporated onto the pore surface. Depending on the chromophore, light responsiveness behaviour of the pore can either be reversible or irreversible. For the case of reversible light-gated nanopores, the photoresponsive molecules undergo a

reversible isomerisation upon irradiation. Reversible photo-isomerization (photo-chromism) switches a chromophoric moiety between two or more states, leading to a change in polarity, charge, and size of the immobilized molecules in response to light irradiation which in turn controls the mass transport through the nanopores. Furthermore, transport properties of nanopores responsive to both light and pH were also investigated.[92]

An irreversible light-responsive behaviour can generally be observed in molecules having photolabile protecting groups (PPGs) instead of isomerizable photochromic units.[61,90,93-97] These photolabile groups act as protecting moeities, which mask the activity of ionizable moeities in the backbone of molecules. When such systems were exposed to UV irradiation, the wavelength of the light to be used was absorbed only by the protecting group, while other parts of the molecule attached onto the pore surface remained unaffected. Upon irradiation, the light photolabile moiety of the corresponding attached molecule would then be cleaved, leading to the generation of polar functional groups. But this transformation is an irreversible process. Nanopores modified with "caged" lysine chains exhibit photo-triggered pH–tunable ionic transport properties.[97]

1.2.3 pH-sensitive nanopores

In biological system, environmental pH condition plays an important role in almost all electrochemical reactions. The ionic/molecular flux across the biological membranes is regulated through ion channels which act as ionic/molecular gates. These gates can be opened / closed in response to pH changes, leading to the passage/hinderence of ions/molecules through the ion channels depending on the ionization state of incorporated chemical groups. The simplest pH-gated ion channel in biological system is a tetrameric M2 protein from influenza in which the protonation state of its histidine residues control the passage of ions. For the case of synthetic nanopores, a variety of ionizable functional groups (polymer brushes and monolayers) have been incorporated which change their conformational state or polarity in response to pH conditions. The most frequently studied pH-sensitive polymer brushes which were grafted inside the synthetic nanopores include polyvinyl pyridine (PVP),[72] zwitterionic poly(methacryoyl-L-lysine),[46,71] poly-2-(methacryloyloxy)ethyl phosphate (PMEP),[74] poly(methacrylic acid) (PMAA)[75,98] and polypeptide brushes.[98] Moreover, self-assembled monolayers of amphoteric chains,[65,99] polyprotic acid chains[62,100], uniprotic chemical moelcules[58,67,101-103] and DNA molecules [63,104,105] were also immobilized onto the inner pore walls to achieve pH-regulated ionic flux across the membranes. Similarly, a self-assembly of organosilane introduced pH-sensitivity in the silicon nitride pore.[53]

1.2.4 Metal ion-sensitive nanopores

Transport properties of synthetic nanopores can also be modulated through the introduction of specific metal ions in the electrolyte solution. For this purpose, metal chelating ligands were immobilized on the inner pore walls. Metal ion-ligand complexes were formed when the modified pore was exposed to solutions with very low concentration of metal ions, leading to a significant change in the ionic flux across the membrane. For example, native carboxylate groups on the surface of track-etched single conical nanopores exhibit calcium-induced gating behaviour by forming a complex with calcium ions dissolved in the electrolyte solution.[106,107] Calcium-induced gating was also observed in the nanopores modified with phosphonic acid chains.[62] Also nanopores modified with oligonucleotides respond to metal ions such as calcium and zinc.[108,109]

1.2.5 Biomolecular-sensitive nanopores

Biomolecules also act as external stimuli and their presence or absence in the solution in contact with the nanopore significantly affects transport properties across the membrane.[7,11,18,63,64,69,110-116] The nanopores

sensitive to specific biomolecule have novel applications in the field of biosensors. The detection and biosensing of specific molecules can be achieved by interaction with recognition sites (ligands) attached on the pore surface and the inner walls. The working principle of nanopore-based biosensing devices mainly depends on the electronic readout originated from the ionic transport across the nanoporous membranes. The ionic current modulation in these biosensing devices is mainly achieved by two methods. In the first strategy, the selected biomolecule is driven through the pore under the influence of an applied voltage, and by measuring the *transient* changes in the ionic current/electrical signal, one is able to detect individual molecules.[117-119] In addition, the degree and duration of ion current reduction provide information about structure and length of translocating biomolecules. The second strategy is known as "*steady-state*" approach, in which the bio-recognizable elements (ligands) are immobilized into these nanoscale architectures. On the addition of analyte molecules (receptors) in the surrounding environment, biorecognition via ligand-receptor interactions confined into a nanopore would lead to volume exclusion and/ or electrostatic-based effects, which govern the ionic transport across the nanopore.[60,63,65,67,69,113,115,120] For the case of volume exclusion principle, the molecular size of analyte is comparable to the tip opening of the nanopore. This leads to the partial or complete occlusion of the pore opening, thus hindering the flow of ions across the membrane.[60,69,113] For the case of electrostatic-based effects, the analyte binding results in a change in the pore surface charge polarity/density which in turn has an impact on ion transport properties, *i.e.*, ion current rectification and permselectivity of the nanopore.[59,63,115]

1.3 Aims and Objectives

The main aim of the present work is to prepare stimuli-responsive membranes and to investigate their ionic transport properties. These membranes can be prepared by incorporating stimuli-responsive molecules on the inner pore surface via chemical modification techniques. The responsive molecules could be light-sensitive molecules in the form of photolabile protecting groups (PPGs), zwitter-ionic groups (e.g., lysine chains), temperature-sensitive polymer chains, or biomolecular sensitive chemical groups (ligands). The immobilized molecules (chemical groups / polymer chains) undergo physicochemical/conformational changes in response to environmental cues. This leads to variation in the degree of swelling/shrinking of polymer chains, with the consequence of changes in the ionic permeation across the membrane. The hydrophilic / hydrophobic behaviour of inner pore surface can also be tuned by the application of external stimuli which inturn affect the permeability and ionic selectivity of membrane.

The following objectives have been kept in mind before starting the experimental work on this research project to pursue my PhD thesis.

The first goal was the selection of suitable material and technique for the preparation of nanopores. Amongst the various materials and methodologies available, polyethylene terephthalate (PET) and polyimide (PI) membranes of 12µm thickness were selected for nanopore fabrication by using heavy ion track technology because of the following reasons. i) Firstly, heavy ion irradiation can be performed on a variety of polymer membranes having thickness ranging from 5 to 100 µm, depending on the requirement. Secondly, ion fluence can be controlled from 1 ion to 10^9 ions cm^{-2}, enabling the production of single/multi-pore membranes. ii) By tuning the chemical track-etching parameters, one is able to exert control over the pore diameter and geometry (*e.g.*, cylindrical, conical and biconical). iii) Most importantly, due to heavy ion irradiation and subsequent track etching process, chemical functionalities originate on the surface and inner pore walls. These inherent chemical groups can be used as a starting point for the introduction of other potential functionalities for the further expansion of application spectrum of these nanoporous membranes.

For the preparation of nanopores, polymer membranes were first irradiated with swift heavy ions having an energy of 11.4 MeV/nucleon at heavy ion accelerator UNILAC (UNIversal Linear Accelerator) at GSI Helmholtzzentrum für Schwerionenforschung. Cylindrical or conical shaped nanopores (single or nanopore

arrays) were fabricated in polymer membranes by selective chemical etching of the damage trails caused by the swift heavy ions along their trajectories via symmetric or asymmetric track-etching techniques, respectively. The internal pore geometry was determined by imaging cross-sections of etched multipore membrane with field emission scanning electron microscopy (FESEM) or by the deposition of metal wires inside the track-etched nanopores and inspecting them under the FESEM after removal from polymer membrane.

After the successful preparation of the nanopores, the next goal was the integration and incorporation of stimuli-responsive molecules on the pore surface via exploiting the inherent chemical groups on the surface and inner pore walls. By keeping in view the advantages and the recent developments in the field of heavy ion track technology, the main objective of this PhD work was to establish a link with nano/biotechnology. This was accomplished by the incorporation of monolayer/polymer assemblies of functional molecules on the inner pore walls that respond to external physical or chemical stimuli, and performing current-voltage measurements for single-pore membranes and mass transport experiments for multipore membranes in a controllable manner, as precisely as nature does in biological membranes, where the amino acid sequence of proteins not only tune the pore diameter but also their selectivity and transport properties.

To investigate the temperature-dependent transport properties of track-etched membranes, I have used "grafting to" technique to introduce thermo-sensitive polymer chains on the surface and inner pore walls. This led to covalent attachment between amine-terminated groups of polymer chains and carboxylic acid groups on the inner pore walls. The effective nanopore diameter was tuned by the environmental temperature due to the swelling/shrinking of polymer brushes attached to the nanopore surface, leading to a decrease/ increase in the ionic transport across the membrane, respectively.

The next objective of this work was to investigate the transport behaviour of light-sensitive nanopores. For this purpose, synthetic nanopores were decorated with photolabile protecting groups (PPGs). Upon UV light irradiation, the hydrophobic and uncharged PPGs were cleaved at the point of weak bonds, leading to the generation of hydrophilic and charged moieties on the pore surface. Therefore, the inner environment of the nanopore was switched from a hydrophobic nonconducting (off) state to a hydrophilic conducting (on) state, allowing for the permselective transport of ionic species. Moreover, transport properties of dual-responsive nanopores, i.e., nanopores that respond to both light and pH were also studied. To achieve this goal, the nanopore surface was functionalized with photosensitive "caged" lysine chains. The uncharged and hydrophobic photo-labile 4,5-dimethoxy-2-nitrobenzyl (NVOC) groups, protecting the amine and carboxylic acid groups of lysine, were removed by exposing the modified pores to UV light, resulting in the production of hydrophilic amphoteric groups on the inner pore walls.

In addition to above mentioned stimuli-responsive systems studied in this PhD work, the modulation of ionic transport was also achieved via biomolecular conjugation inside the confined geometries. To this end, biorecognition elements (ligands) were tethered onto the surface and inner pore walls. Firstly, iron-terPy complex (ligand) is immobilized on the pore walls. The Fe(II) ions incorporated in the iron-terPy complex recognize and bioconjugate with lactoferrin through specific metal ion–protein interactions. The bioconjugation processes inside the nanopore significantly decrease the effective pore diameter available for the transport of ions, resulting in a significant reduction in the ionic flux across the membrane. Secondly, an attempt was also made to fabricate nanopore which exhibits reversible biomolecular recognition and conjugations via lectin–carbohydrate interactions. For this purpose, the nanopore surface was decorated with mannopyranoside moieties which have the ability to selectively bioconjugate with lectin (ConA) protein. The biomolecular binding (bioconjugation) and unbinding inside the confined geometries gives measurable changes in the conductance of single-pore membrane and permeation rate for the case of multipore membrane.

The main requirement for the successful application of stimuli responsive nanopores is a fundamental understanding of their properties and the way through which these properties influence the transport of ions or molecules. Transport through cell membranes is fundamentally important for cell functions. In living organisms, the ion channels facilitate the selective transport of ions and small organic molecules across the cell membrane. Under the influence of external stimuli, these channels change their conformation states in order to enhance or

inhibit the transport across the membrane, allowing functions such as communication between cells, nerve conduction and signal transmission.

Inspired from the functioning and responsiveness of biological ion channels, stimuli controlled permeation of ionic analytes through the track-etched membranes containing single pore or an array of nanopores (cylindrical or conical) modified with responsive molecules was investigated in this PhD work. Typical questions of interest in terms of ion transport can be ion conductance, ion binding, permeation, ion selectivity, and gating properties of these nanopores. Answer of these questions are searched by using these track-etched membranes with fixed surface charges, which act as ionic filter for the separation of ionic analyte molecules. By modifying the pore surface with responsive functional groups, one can play with the polarity of the inner pore walls by the application of external stimuli, which in turn results in the modulation of ionic transport across the membrane. Ionic species having same charge as that of the pore walls are repelled, while oppositely charged ions are attracted and selectively transported through the nanopores of the membrane. In this way, electrostatic interactions between immobilized responsive molecules and ionic analytes control the molecular flux across the modified membrane. These processes should permit thermal, optical and biomolecular gating for the controlled release of ionic drugs through the nanopores.

2. Experimental

2.1 Nanopore fabrication in polymer membranes

Ion track technology involves the creation of damaged zones by irradiating solids with swift heavy ions. These damaged zones can be selectively etched, leading to conical or cylindrical nanopores. The damaged material along the track can be removed quicker than the bulk material by using suitable chemical etchant to create a pore along the trajectory of ion track. Size and shape of these nanopores can be controlled by controlling various parameters.

2.1.1 Heavy ion irradiation

Sample preparation:

The starting polymer membranes were received from the supplier in the form of rolls (Figure 2.1a). In this study, polyethyleneterephthalate (PET, Hostophan RN 12, Hoechst) and polyimide (PI, Kapton 50 HN, DuPont) membranes of 12µm thickness are used as template for heavy ion irradiation. The first step in the sample preparation involves the cutting of about A4 size sheets from the membrane rolls. Then the six polymer sheets are placed on each other (thickness of six membranes is 72 µm) between the two sheets of paper in order to avoid adherence with the sample cutter. Then these sheets are mounted on the top of a 30 mm diameter cutter situated on cutting machine to prepare round shaped membrane samples (Figure 2.1b). Then the stack of polymer samples are filled in the sample holders (Figures 2.1c to 2.1e). The sample holders are packed in magazine which contains 20 slots for heavy ion irradiation (Figure 2.1f).

Irradiation process:

Prior to heavy ion irradiation experiments, taking part in the radiation safety instructions and personal dosimeter are the basic requirements for entering in the radiation chamber (cave X0). The magazine packed with membrane samples was placed in such a way that the incident ion beam should be oriented perpendicular to the surface of the membrane. As a result the irradiated membranes contain ion tracks strictly parallel and perpendicular to the surface. In the irradiation chamber when beam is on, each sample holder with membranes is taken out from the magazine automatically by pulling with a puller. After irradiation, the sample holder then again automatically moves back into the magazine. Similarly, all of the 20 samples packed in the magazine are irradiated. Then the beam is stopped in order to replace irradiated magazine with non irradiated one. The irradiation process is monitored online from the control room.

The irradiation of polymer membranes was performed with swift heavy ions (^{238}U, ^{197}Au or ^{206}Pb) [I] having a kinetic energy of up to 11.4 MeV per nucleon. The irradiation of polymer membranes was performed at heavy ion accelerator UNILAC (Universal Linear Accelerator) at GSI Helmholtzzentrum für Schwerionenforschung

[I] People from the Materials Research Department (GSI) are highly acknowledged for their help and support during the heavy ion irradiation of samples.

GmbH, Darmstadt, Germany. This linear accelerator is 120 m long and has the ability to accelerate the heavy ions up to ~15 % of the speed of light.

During irradiation process, the highly charged ions penetrate into the material (sample) and lose their energy through different routes, such as,

i) Excitation of target electrons and ionization. This process is termed as electronic energy loss.

ii) Elastic collisions with target atoms which is referred to as nuclear energy loss.

iii) Through the capturing of electrons.

iv) Through electromagnetic radiations processes such as Bremsstrahlung and Cherenkov effect. These effects did not play significant role at such kinetic energies.[121]

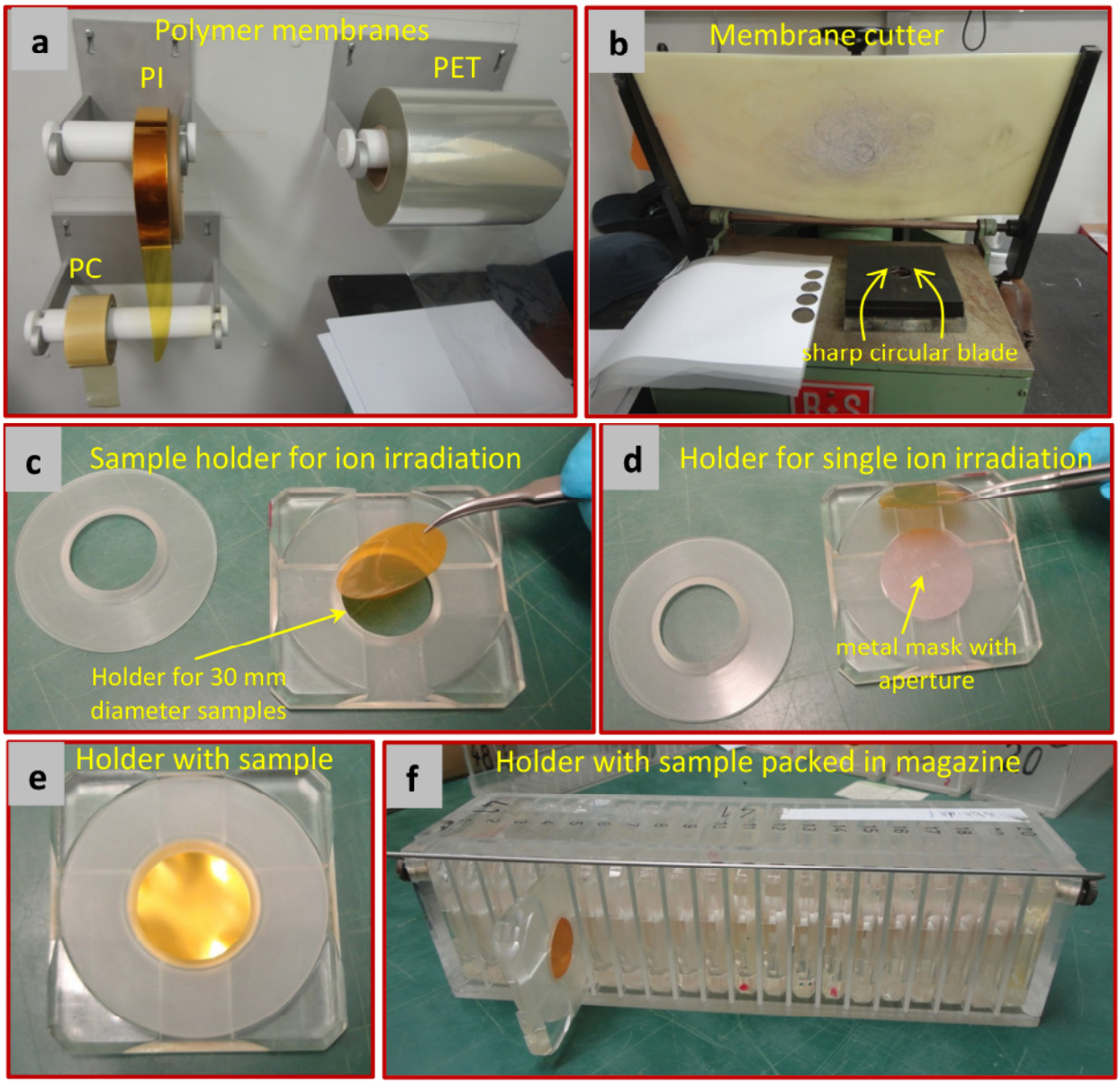

Figure 2.1: a-f) Presentation of steps for the preparation of samples and packing of samples in magazine.

For the case of Pb ion irradiation, the electronic energy loss dominates at energies higher than 2.6 MeV which correspond to ~ 0.01 MeV/nucleon as shown in Figure 2.2a. In this case, the total energy loss achieves a plateau and the nuclear energy loss is dominated at lower energies. The main characteristic of swift heavy ions

is that their maximum electronic energy loss takes place just before they stop. This maximum is reffered as Bragg-peak and is shown in Figure 2.2b. For the case of heavy ions (^{206}Pb or ^{238}U) the Bragg-peak is rather broad, while for light ions (carbon) it becomes very pronounced. When the irradiated sample is very thick, the incoming ion is stopped inside the material by losing its energy completely rather than passing through the sample.

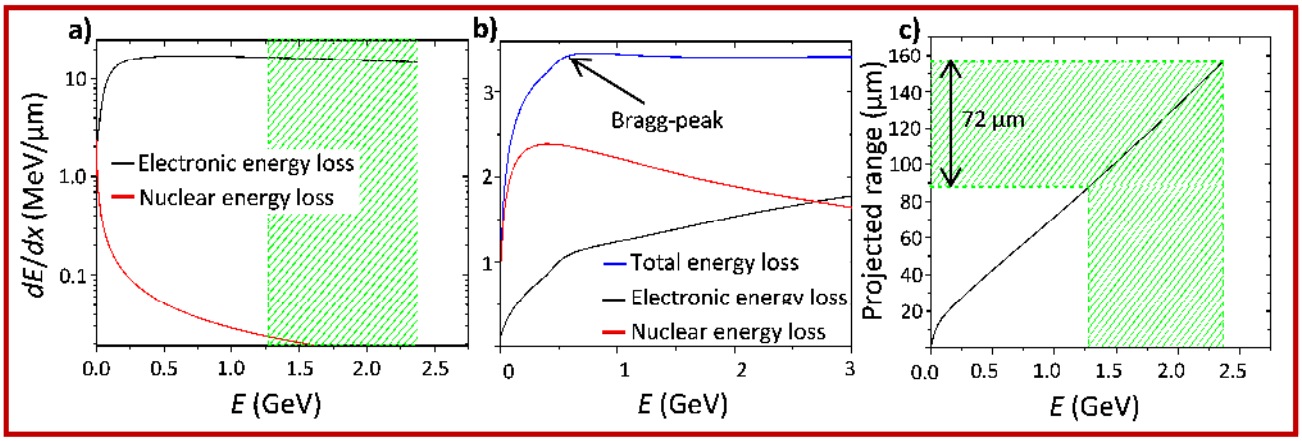

Figure 2.2: a) Electronic and nuclear energy loss of lead (^{206}Pb) ion during the irradiation of a stack of PET membrane samples of 72µm thickness. b) Energy loss versus specific energy E (GeV) at low energies. c) Projectile range of ^{206}Pb ion in PET sample with respect to specific energy. The energy loss and projectile range for ^{206}Pb ion was calculated by using SRIM code.

The projectile range (R) at which a bombarding ion can penetrate into the irradiating sample material shortly before it stops is calculated by the following equation:

$$R = \int_{o}^{Eo} \left(\frac{dE}{dx} \right)^{-1} dE \qquad 2.1$$

The SRIM code is employed to calculate the energy loss dE / dx and projected range R of heavy ions.[122]
The electronic energy loss (dE/dx) can be described by the Bethe-Bloch formula:

$$\frac{dE}{dx} = 4\pi \frac{Z_{eff}^2 n_e e^4}{m_e c^2 \beta^2} \left(\ln \left(\frac{2 m_e c^2 \beta^2}{I\left(1-\beta^2\right)} \right) - \beta^2 \right) \qquad 2.2$$

where

Z_{eff} : effective charge of the projectile ion, see eq. 2.3
n_e : electron density of the target material: $n_e = Z_t n_t$
Z_t and n_t denote atomic number and number density of target atoms, respectively
m_e : free electron mass
e : elementary charge
β : v/c where v denotes the velocity of the projectile
I : ionization energy

The interaction of a projectile ion with a material (target) mainly depends on the effective charge (Z_{eff}). This effective charge in turn depends on the velocity of the incoming ion. When the velocity of the projectile is very high compared to the orbital velocities of its electrons, the slow moving electrons will be stripped off completely. This resulted in an increase in the charge state of the projectile ion. On the contrary, the projectile

ions with low kinetic energy retain some of their electrons. Thereby, Z_{eff} increases with the kinetic energy of the projectile. This relation is described by the following Barkas formula:

$$Z_{eff} = Z_t\left(1-\exp\left(-\frac{130\beta}{Z_t^{2/3}}\right)\right) \qquad 2.3$$

So it is obvious from equations 2.2 and 2.3 that only swift heavy ions bear high effective charge and concomitant high energy. This is indeed required for the production of continuous and etchable ion track target material, especially polymer membranes. The minimum energy loss required to produce etchable ion track in PI membrane is ~2-5 KeV/nm.[123]

In this work polymer foils of 12 μm thickness are used for nanopore fabrication. These folis are first irradiated with swift heavy ions (^{238}U, ^{206}Pb, ^{197}Au) of energy 11.4 MeV/u from the UNILAC in stacks containing six foils (6×12 = 72µm thickness). The energy loss throughout the stack should be in the region of the plateau and almost constant as shown in the Figure 2.2a. The region highlighted with green lines in Figures 2.2a and 2.2c is corresponding to the total thickness of the stack (72 μm) of polymer foils.

All the irradiation experiments at UNILAC are performed at room temperature. The applied ion fluence can be changed in order to vary the density of ion tracks in the material. Usually fluences of maximum 10^7 to $5\cdot10^8$ ions /cm^2 are applied for nanopore fabrication. Higher track densities can cause a great overlap in the etched nanopores. A set of electromagnetic lenses named as Quadrupole magnets widen or focus the incoming ion beam to vary the track density of the membrane. The variation of fluence can also be achieved by the choice of irradiation time during which the target is exposed to an ion beam with a constant flux. The Faraday cup is used to measure the electric current of the ion beam. This signal can be converted into a beam current value for a given area and charge state of the ion beam. The Faraday cup can not be used during irradiation because it is a beam stopping device. A secondary electron transmission monitor (SEETRAM) is used to monitor the accumulated flux on the monitor. The SEETRAM consist of three aluminium foils, each foil is 1µm thick. The middle foil is connected to a current amplifier, while the two outer foils are biased with +100V to sweep out the free electrons. The SEETRAM emission current is calibrated against the Faraday cup and it is left in front of the sample during irradiation, leading to a small reduction in energy from 11.4 to ~11.1 MeV/u.

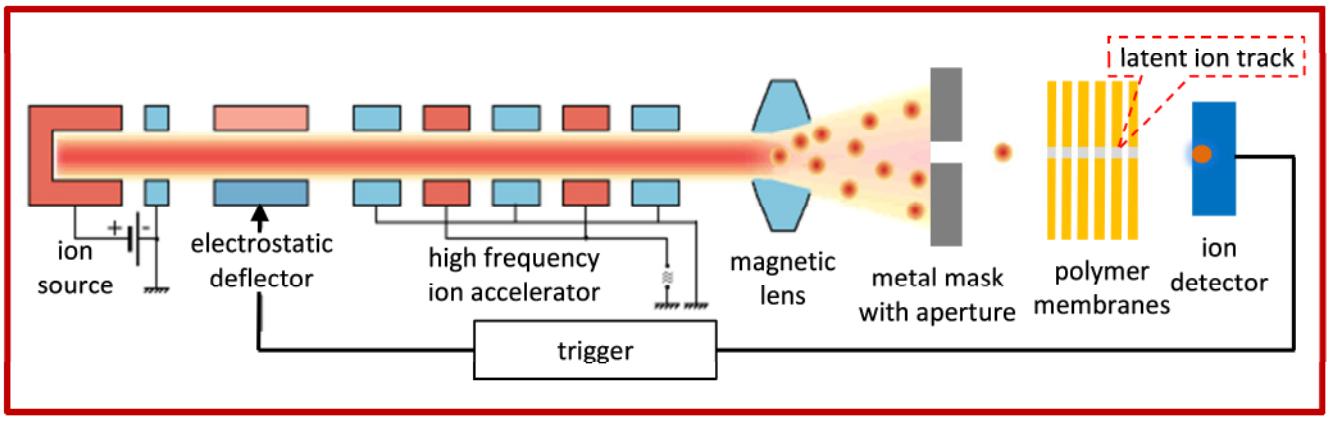

Figure 2.3: Scheme representing the setup for single ion irradiation experiments.

The experimental setup employed for single ion irradiation of polymer membranes[II] is different from that of high fluence irradiation (Figure 2.3). To this end, a metal mask with a centered aperture of diameter ~ 200 µm is placed in front of the membrane stack during the preparation of sample before irradiation (Figure 2.1d). Then the magazine packed with these holders is placed in the sample exchange system at cave X0 in such a way that the incident beam first hits the metal mask with small hole in front of membranes. Then a defocused pulsed ion beam having very low frequency (~ 1Hz) is employed to irradiate the sample in such a way that only one ion passes through the aperture. As soon as a single ion is registered by the detector placed behind the sample, the ion beam is immediately deflected electrostatically, thus avoiding the passage of a second one.

Irradiation of polymer membranes with swift heavy ions resulted in the generation of damaged zones which are given the name of latent tracks. These latent tracks are produced mainly due to the breakdown of chemical bonds, leading to the production of double and triple bonds via ionization and electric excitations during the interaction of high energy ions with the samples.[124] Moreover, outgassing of volatile fragments leads to a decrease in material density along the ion tracks. The amount of damage induced in the latent track depends on the energy loss dE / dx of the ions during their passage through the sample.

2.1.2 Chemical etching of latent ion tracks

Sensitization:

In heavy ion-track polymer membranes, the track core is mainly composed of chemically active polymer fragments, which can undergo post-irradiation reactions, such as oxidation, photo-oxidation, etc. Because of this reason, storage of the irradiated polymer membranes in air leads to a significant increase in track etch rate. Moreover, sensitization of tracks is carried out by exposing the samples to UV-light before etching. In case of PET, membranes are exposed to UV light (320 nm) for 15 minutes on each side, leading to photo-oxidative degration. This increases the surface polarity which facilitates the chemical (etchant) attack on the degraded polymer. It is well known that the energy deposited by UV light breaks additional chemical bonds along the track, thus increasing the track-etch rate (V_T) and selectivity by a factor of up to 10. It is realized that UV-light illumination not only increases the track-etching rate but also leads to a great improvement in the pore size distribution.[125] It is also considerable that illumination with the light at wavelengths longer than 320 nm showed strong enhancement in the track etching rates, whereas light with the wavelengths lower than this value causes large enhancement in both track-etch rates (V_T) and bulk-etching rates (V_B) even in the interior of the material. Moreover, heavy ion tracks in polymer membranes can also be effectively sensitized by the treatment with certain organic solvents.[126]

Ion track-etching:

Sensitized polymer membranes are exposed to a suitable etchant (chemical) solution. During the chemical etching process, the damaged zone (latent ion tracks) in polymer membrane is removed and converted into a hollow pore. The geometry of the nanopore depends on the ratio of track to bulk etching rate. Ion tracks are converted into pores because the track-etch rate (damaged material) is higher than the bulk-etch rate (undamaged material).[127] The track to bulk etch ratio (V_T / V_B) can be influenced by several parameters

[II] Materials Research Group and especially Prof. Dr. Christina Trautmann (GSI) is highly acknowledged for their support with the single heavy ion irradiation experiments.

employed in the etching process. For example, i) sensitivity and chemical nature of material, ii) energy loss of the ion in the material *dE* / *dx*, iii) concentration of the etching solution, iv) additives introduced in the etching solution, i.e., surfactants[128] v) sensitisation with UV light, vi) etching time and temperature, and vii) voltage applied during the etching process.

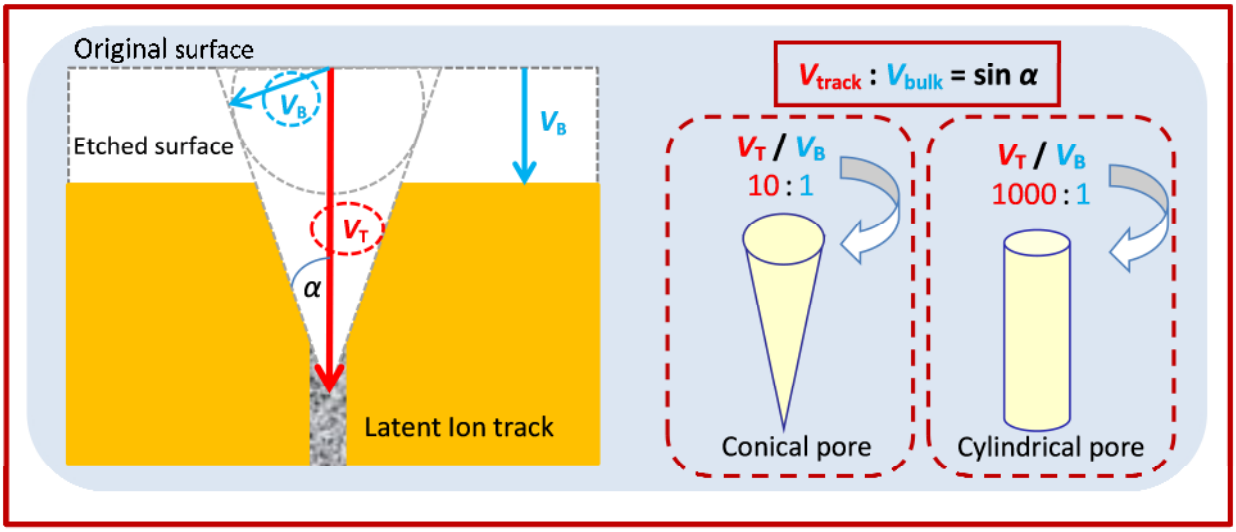

Figure 2.4: Schematic representation of chemical etching of latent track in heavy ion irradiated polymer membrane.

Figure 2.4 shows schematically the correlation of V_B and V_T, etching of the bulk material leads to a reduction of the foil thickness as well as widening of the nanopore, perpendicular to the surface of the "etch-cone". The breakthrough of the membrane is correlated with removal of the track material with speed V_T. The cone angle α can now be considered as a function of bulk etch rate V_B and track etch rate V_T, with $\sin \alpha = V_B / V_T$. The cone angle approaches to zero when track etch rate is much higher than bulk etch rate (V_T is >> V_B), which leads to a cylindrical geometry of the nanopore. The size of the latent track determines the minimal diameter of the resulting pores. The pores become more and more conical when bulk etch rate V_B becomes bigger with respect to track etch rate V_T.

2.1.2.1 Fabrication of conical nanopores

Asymmetrical etching of ion tracked polymer membranes is used to prepare conical nanopores and it is carried out in a conductivity cell, connected to a home- built current / voltage converter of *pA* sensivity, controlled by software written in Lab View 5.0 (National Instruments). The conductivity cell consists of three compartments made of polychlorotrifluoroethylene (PCTFE), also known as Neoflon. The side chambers contain only one hole, while middle chamber has two holes. The three chambers are separated from each other by placing a single-track and a multitrack polymer membrane in between them as shown in Figures 2.5a and 2.5c. The compartments are sealed mechanically by applying pressure with a clamp. Then the cell is placed in a metal case, which serves as an electrical as well as a thermal shield.

The asymmetric etching technique for the preparation of conical nanopores in ion tracked polymer membranes was developed by Apel and his co-workers.[41] In this method one single-shot membrane and one membrane irradiated with a higher fluence were etched at the same time. After fixing the membranes in the conductivity cell, the next step is to put the etching and stopping solution in the chambers. The middle chamber was filled with 9M NaOH sodium hydroxide (etchant), while the side chambers were filled with stopping solution containing a mixture of 1M formic acid (HCOOH) and 1M potassium chloride (KCl) as shown in Figure 2.5c. The stopping solution protects this side from etching to assure the conical geometry of the resulting

nanopore. The etching process was carried out at room temperature. For online monitoring (Figure 2.5b) of the etching process, two gold electrodes are placed in adjoining compartments containing the single-track membrane, and a potential of -1V was applied to monitor the current transported by the ions in the solution across the membrane. During the etching process, the voltage was applied in such a way that negatively charged hydroxyl (OH^-) ions of the etchant (NaOH) are drawn out from the pore tip. This is necessary for the preparation of the nanosized pores. For better reliability of the measurement, the current flowing through the single pore membrane is monitored. The current remains zero as long as the pore is not yet etched through. After the breakthrough of the pore (Figure 2.5d), the acid (HCOOH) neutralizes the base (NaOH) to protect the pore tip and to keep it small as much as possible. For PET membrane, the breakthrough usually occurs as a sudden increase in current with fluctuations. It was noticed that if the etching is interrupted during this time the pore can close again. Therefore, the etching process was stopped when the current reached a certain value and becomes stable to some extent. Then the etched pore was first washed with stopping solution in order to quench the etchant, followed by washing with deionized water. In order to remove the residual salts, the etched membranes were immersed in deionised water for minimum 10 hours. The time for the breakthrough in PET membrane is about 60 to 90 minutes, depending on the external condition such as laboratory temperature. The bulk-etch rate for the case of PET membrane is ~ 1.7 nm per minute.

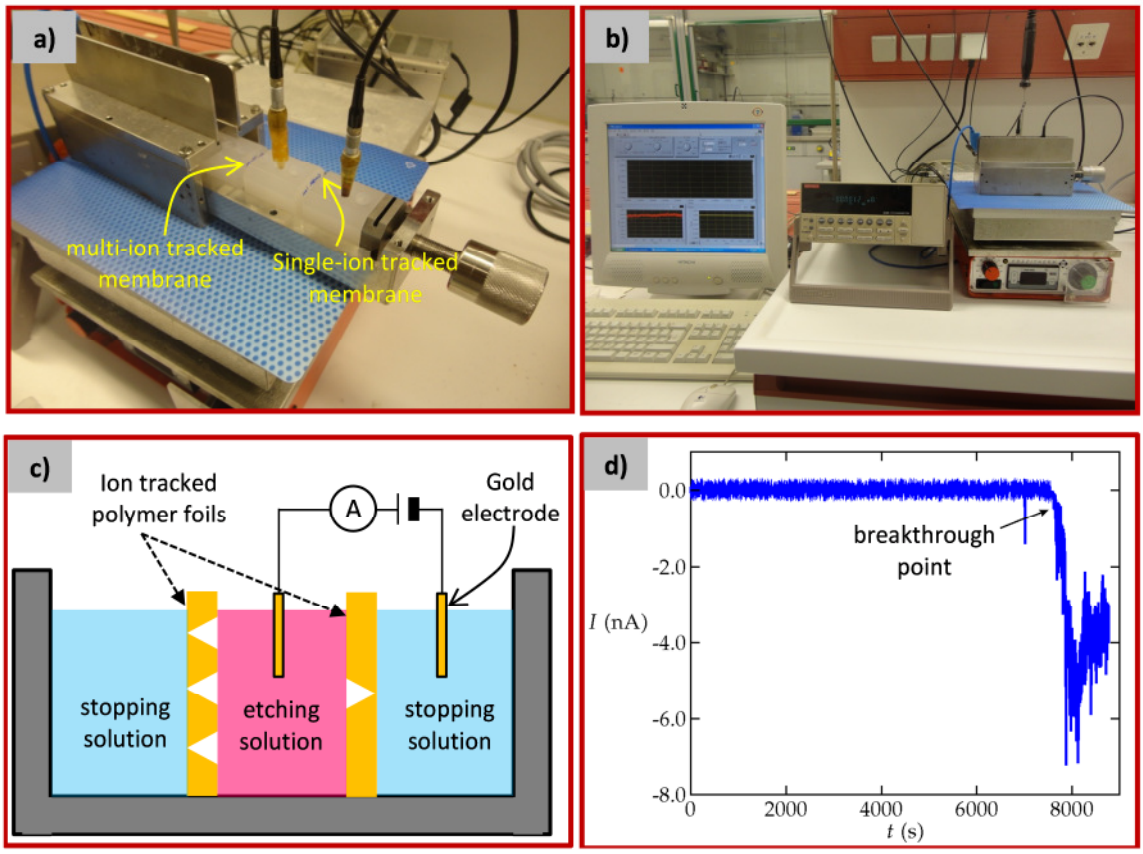

Figure 2.5: a) Conductivity cell with ion tracked PET polymer membranes. b) Experimental setup used for the asymmetric track-etching of polymer membranes. c) Scheme showing the fabrication process of conical nanopores. d) Current versus time curve recorded during asymmetric etching of single latent track in PET membrane.

The asymmetric track-etching procedure employed for the preparation of conical nanopore in PI membranes is the same as for PET membranes. In the case of PI membrane sodium hypochloride (NaOCl; 13% active chlorine content) is used as a chemical etchant to dissolve the ion tracks, while the stopping solution is potassium iodide (1M KI) to reduce the OCl^- into Cl^- ions. Secondly, the track-etching of PI membranes is

carried out at high temperature (50˚C). Moreover, the breakthrough in PI occurs in between 180 to 240 minutes and the bulk-etch rate is ~ 7 nm per minute.

After the etching process, the multipore membranes were used in permeation experiments. Moreover, pore size can be determined under field emission scaning electron microscope (FESEM). The single pore membranes obtained after asymmetric ion track-etching process can be used for quantitative current-voltage (*I-V*) measurements.

2.1.2.2 Fabrication of cylindrical nanopores

The fabrication of cylindrical nanopores in polymer membranes is a quite simple method. It is used to produce cylindrical nanopores in both single shot and high fluence membranes. The etching is carried out in a double walled isothermal bath, which is half-filled with 2M sodium hydroxide (NaOH) solution. The temperature of etching solution is maintained at 50˚C by a circuit of heated and cooling water flowing through the double walls of the beaker. The ion tracked polymer membranes were first fixed in the sample holders as shown in Figure 2.6a. Then this sample holder with membranes was immersed in the preheated etching bath (Figure 2.6b). The etching of the samples was carried out for a pre-set time according to the required pore diameter. Moreover, the concentration of the solution and the temperature in the vicinity of the ion tracked polymer membranes were kept approximately constant throughout the whole etching process due to constant stirring of the etchant. Figure 2.6c shows a simplified scheme for the fabrication of cylindrical nanopores in etching bath. Under these conditions the pore diameter scales linearly with etching time at a rate of ~ 5.4 nm per minute. After the etching, the sample holders along with polymer membranes are taken out from the etching bath and rinsed several times with deionized water. In this setup the etchant can attack and dissolve the latent ion tracks in polymer membrane from both sides. Therefore, this etching process is referred as symmetrical etching technique.

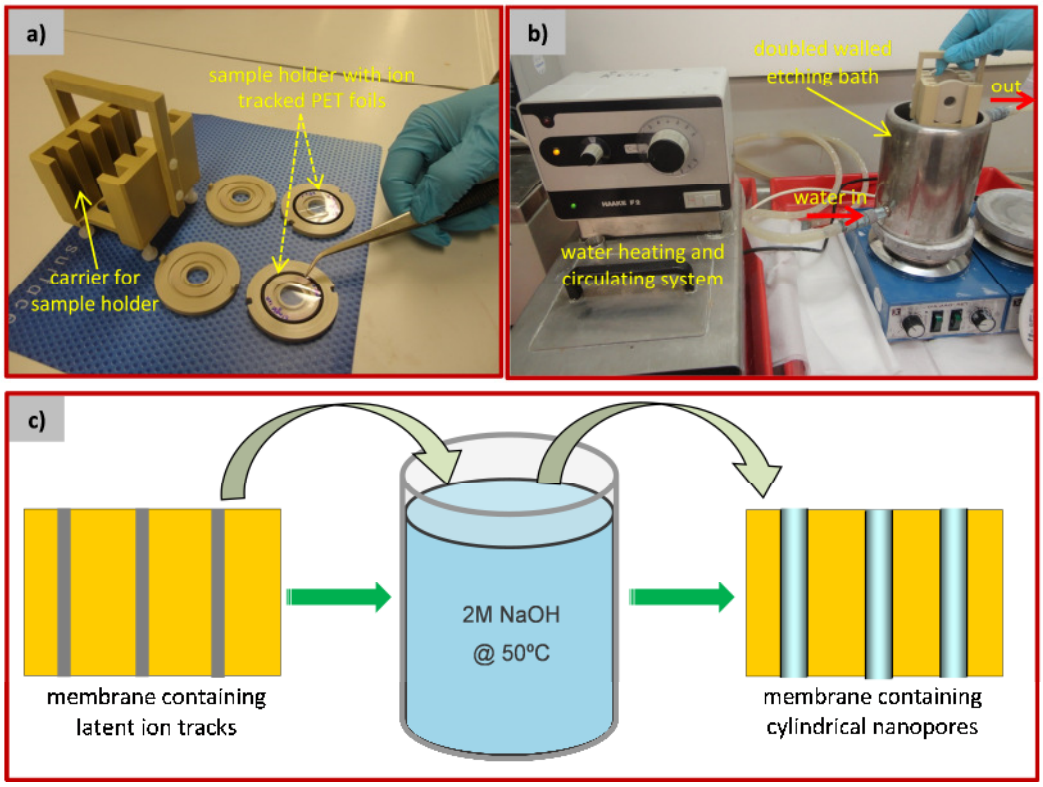

Figure 2.6: a) Sample holder with PET membranes used for the preparation of cylindrical nanopores. b) Experimental setup used for symmetric track-etching technique. c) Schematic representation of symmetric track-etching process.

2.2 Geometrical characterization of nanopores

After the successful fabrication of nanopores in polymer membranes the next step is to determine and investigate their shape, diameter as well as internal pore geometry. The analysts and engineers working in the field of nanopore are making attempts to develop new techniques or to invent new instruments to bring advancement in the characterisation of these nano-sized pores. The field emission scanning electron microscopy (FESEM), transmission electron microscopy (TEM) and atomic force microscopy (AFM) are the most frequently used instruments to carry out the geometrical characterization of nanopore. Moreover, size exclusion, conductometry and light scattering experiments can also be performed to calculate the nanopore dimensions. In addition to the above mentioned techniques, the internal shape and size of nanopores can also be confirmed by the replica method. In this method nanowires are electrochemically deposited inside the track-etched nanopores and then after dissolving the membrane in a suitable solvent, the nanowires can be imaged in FESEM.

In the present study, after track-etching the surface of multipore membranes is direct imaged in the field emission scaning electron microscope (FESEM-JEOL JMS-7401F, Japan). Additionally, the replica method together with FESEM is employed to investigate the internal geometry of the track-etched nanopores. For the case of single nanopore-membrane, conductivity method is used to determine the nanopore size. For the case of FESEM the samples must be electrically conductive in order to characterise the nanopore. The polymer membranes are non conductive. Therefore, the etched samples are usually coated with an ultrathin coating of an electrically conductive material. For this purpose, a piece of etched nanopore membrane is mounted on a sample holder with colloidal silver glue. The sample holder is made up of steel and it is a six inch (15 cm) semiconductor wafer named as stub. Then the sample is allowed to dry for about one hour. After that the sample is coated with a thin layer of gold (~3 nm) to make it conductive. To this end, the sample is placed in the chamber of a sputtering machine. After sputtering, mounting stub is screwed in mounting plate using special mounting plate holder. Then sample is loaded in FESEM, which produces clear, electrostatically less distorted images under vacuum.

FESEM images of track-etched PET membrane surface with conical and cylindrical nanopores fabricated via asymmetric and symmetric etching techniques, respectively, are shown in Figures 2.7(a) and 2.7(c). Moreover, the FESEM images of conical nanowires and cylindrical nanwires obtained by electrochemical deposition[III] of Au in conical and cylindrical track-etched nanopores are also shown in Figures 2.7(b) and 2.7(d).

[III] Dr. Q. H. Nguyen is highly acknowledged for the electrochemical deposition of Au wires inside the track-etched nanopores.

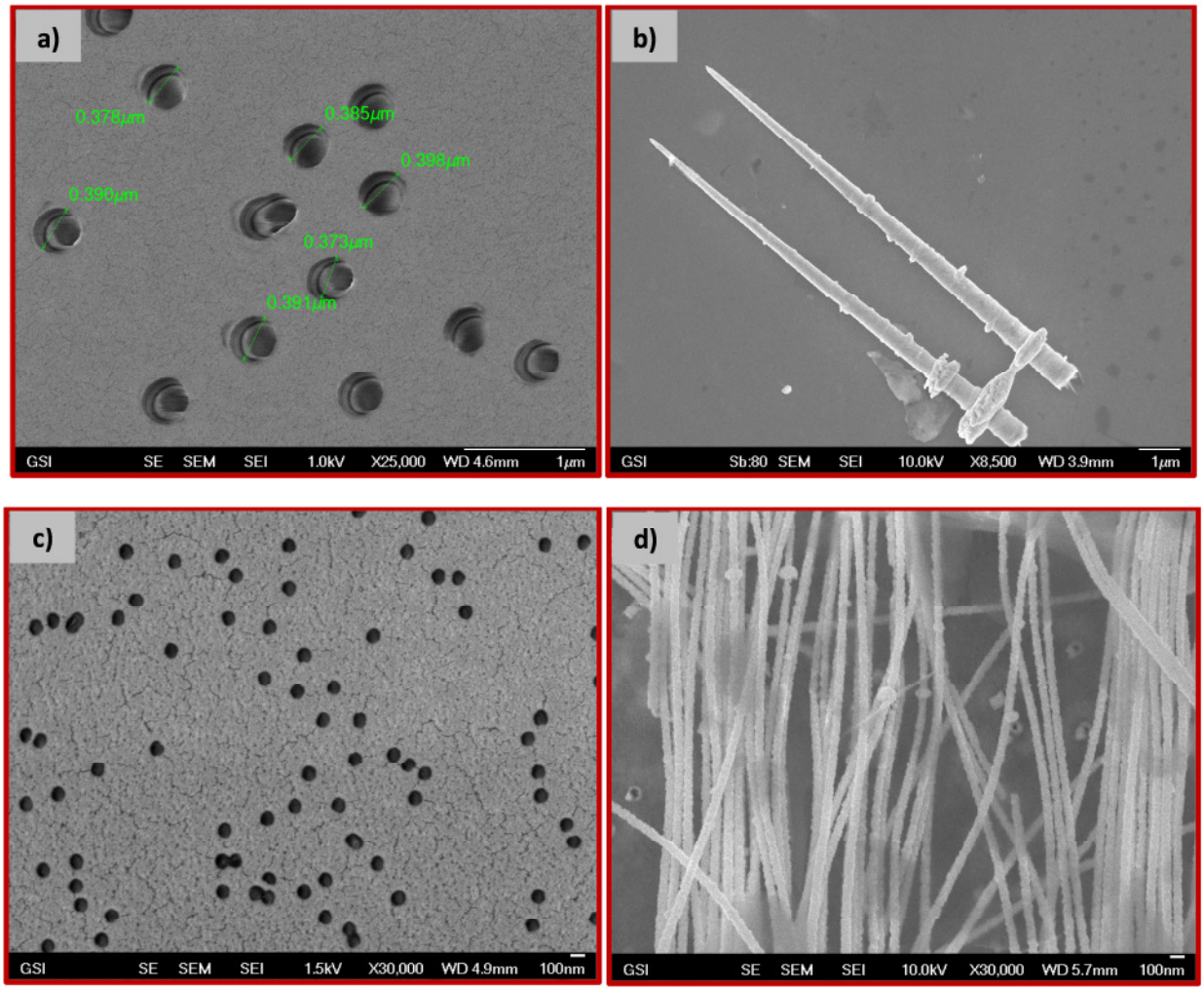

Figure 2.7: FESEM images of track-etched PET membrane surface with conical (a), and cylindrical nanopore (c). The FESEM images of conical nanowires (b) and cylindrical nanowires (d) formed by electrochemical deposition of Au in asymmetrically and symmetrically etched PET membranes, respectively.

2.3 Current-voltage (*I–V*) measurements

Ion track-etched single-pore membranes (with conical or cylindrical pore) are further characterized through the measurement of current-voltage (*I–V*) curves.[IV] In this method the ionic current flowing through the nanopore is measured in an electrolyte (KCl) solution. The experimental setup and conductivity cell is the same used for asymmetric track-etching process. In order to measure the *I–V* curve, a track-etched single-pore membrane is fixed between the two halves of the conductivity cell. Then both chambers of the conductivity cell are filled with KCl solution prepared in phosphate buffer (10 mM) solution. The pH of the electrolyte is adjusted with dilute HCl or KOH solution. Then a pair of Ag/AgCl electrodes is inserted in both chambers across the membrane. For the *I–V* measurements, a picoammeter/voltage source is used to apply a potential across the membrane. In this case a scanning triangle voltage with 100mV steps ranging from +2 to -2V is

[IV] *I–V* measurements are performed under the supervision of Dr. M. Ali

applied on the small opening (tip) side of the conical nanopore membrane. In order to assure that the system is in equilibrium a time span of ~ 1 second is introduced in between each step.

Figure 2.8 showed a typical *I–V* curve of a single conical nanopore and a single cylindrical nanopore fabricated through asymmetric and symmetric track-etching techniques, respectively. The ionic current flowing through the conical pore resulted in an asymmetric *I–V* curve. This means that conical nanopores have the ability to rectify the ionic current due to asymmetric geometry and negative pore surface charges. On the contrary, cylindrical nanopore showed ohmic behaviour due to the absence of asymmetry in the pore geometry. This means that the *I–V* curve of cylindrical nanopore is linear as shown in labview image (Figure 2.8b)

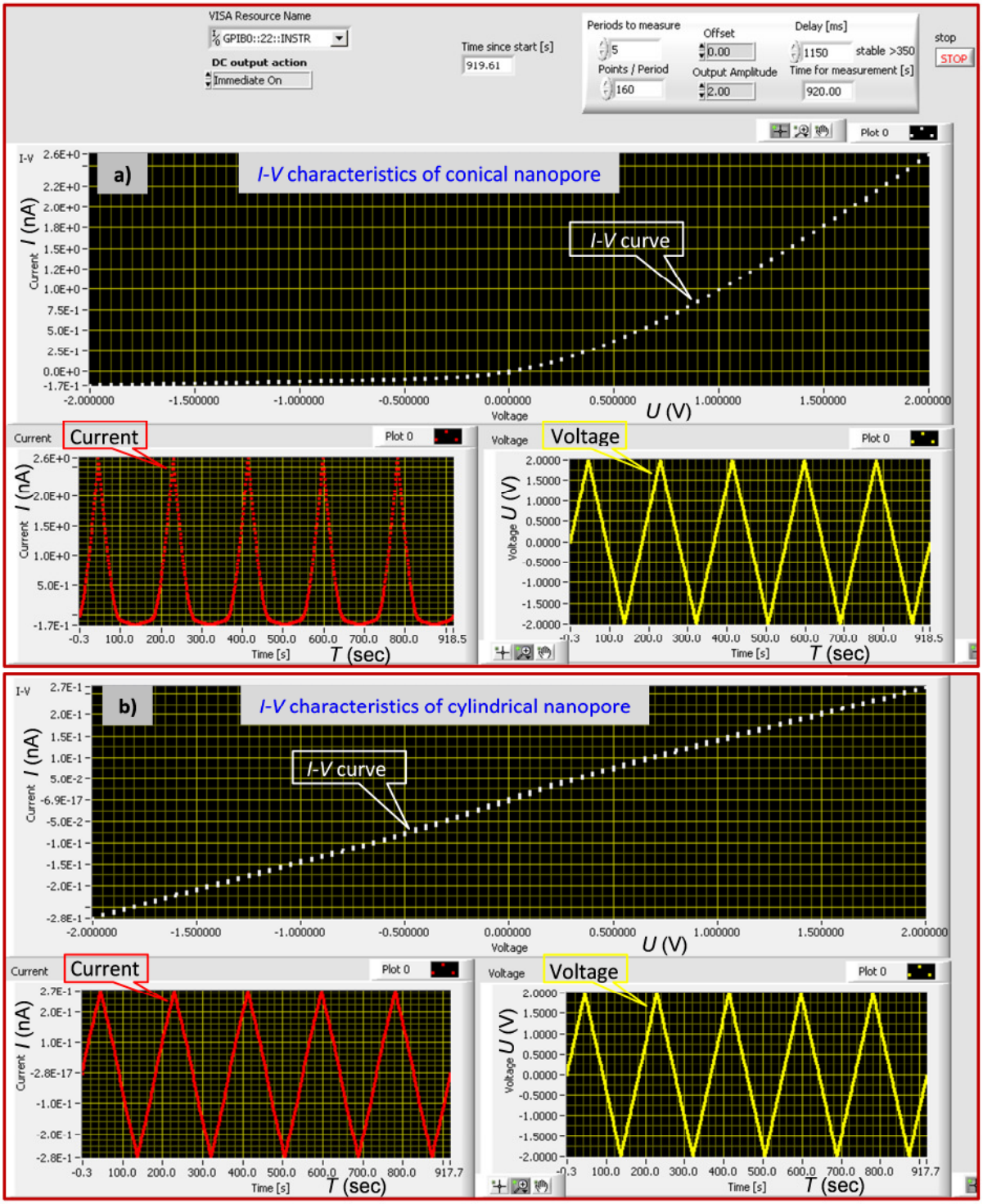

Figure 2.8: A labview window image showing current-voltage (*I–V*) characteristics of a single conical nanopore (a) and single cylindrical nanopore (b) in 100 mM KCl (pH 7.0) solution.

2.3.1 Estimation of single pore diameter

From the *I–V* curves it is possible to calculate the nanopore dimension by assuming certain geometry (conical or cylindrical), the pore diameter can be calculated by an electrochemical method. For this purpose, a properly washed single-pore membrane is placed between the two halves of a conductivity cell. Both compartments are then filled with 1 M KCl solution of known conductivity at room temperature.

Single conical nanopore:

Since the conical nanopore contain two openings, the small opening (*d*) is referred to as tip of the cone and the larger opening (*D*), is called base of the cone as shown in Figure 2.9a. The base opening diameter (*D*) of the conical nanopore is calculated separately from the multipore membrane FESEM images, which is etched along with the single-pore membrane under the same conditions. The tip of the conical pore is determined by conductometry method (*I–V* curve) by assuming the conical geometry of the pore. The following equation is employed to calculate the small opening diameter of the conical nanopore:[41]

$$d = \frac{4LI}{\pi\kappa UD} \qquad 2.4$$

where *L* is the length of the conical nanopore which is almost equal to the membrane thickness, *d* is the diameter of the small openig (tip), *D* is diameter of the large opening (base), κ is the specific conductivity of the electrolyte (11.377 S/m for 1 M KCl at 26 °C), *U* is the voltage applied across the membrane, and *I* is value of ionic current.

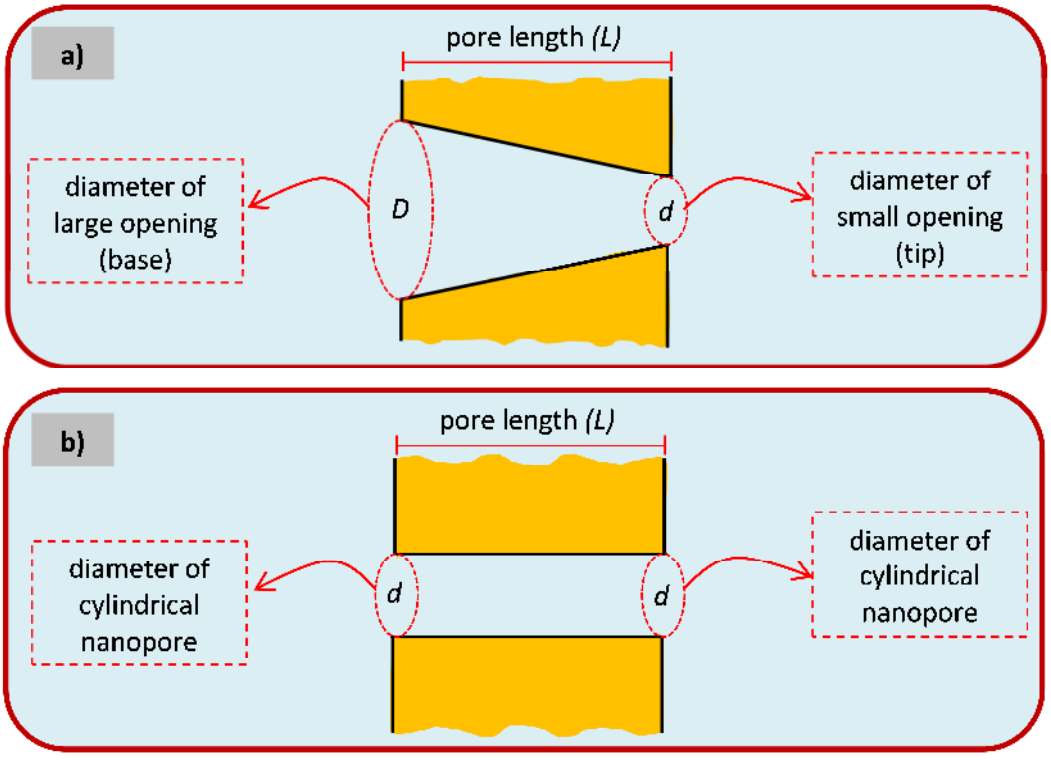

Figure 2.9: Schematic representation of the geometrical dimensions of a track-etched single conical nanopore (a), and cylindrical (b) nanopores.

Single cylindrical nanopore:

For the case of single cylindrical nanopore the conductance is measured from linear *I–V* curve and the diameter (*d*) is estimated by the following relation.

$$d = \sqrt{\frac{4LI}{\pi\kappa U}} \qquad 2.5$$

where *L* is the length of the pore which is almost equal to the membrane thickness (~12 µm), *d* is the diameter of the pore; κ is the specific conductivity of the electrolyte (11.377 S/m for 1 M KCl at 26 °C), *U* is the voltage applied across the membrane, and *I* is value of ionic current obtained from the *I–V* curve.

2.4 Tuning nanopore surface chemistry

The heavy ion irradiation and subsequent chemical etching process employed for production of track-etched nanopores resulted in the cleavage of chemical bonds in the polymeric material. As a result chemical groups are generated on the membrane surface and the channel. For the case of PET (also known as polyester) membrane, the polymer is formed through ester bonds via the condensation of terephthalic acid and ethylene glycol. These ester bonds are the main points for the chemical attack of the etchant (NaOH). The alkali easily hydrolyses these partially charged ester bonds in the polymer chain, leading to the production of carboxyl (-COOH) and hydroxyl (-OH) groups on the surface (Figure 2.10a). The reported results showed that the density of carboxyl groups on the inner pore (cylindrical and conical) walls was ~1 group nm^{-2}.[129]

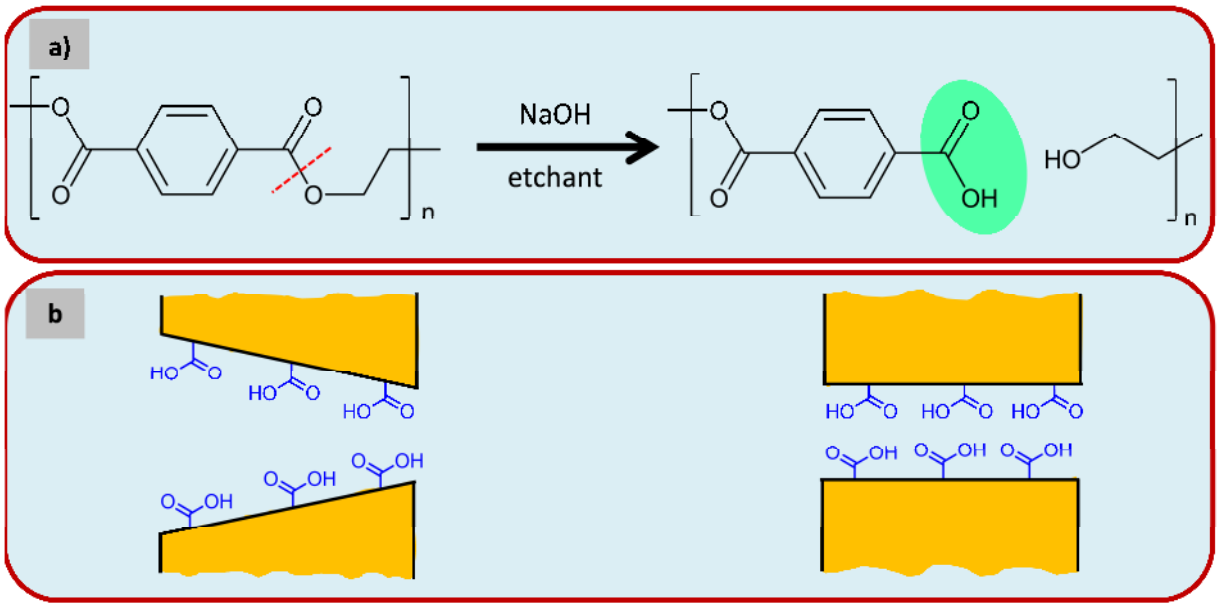

Figure 2.10: a) Scheme representing the hydrolysis of ester bonds via chemical etching of ion tracks in PET membrane. b) Track-etched nanopores with surface carboxylic acid groups on the inner pore walls.

The native –COOH groups on the inner pore walls (Figure 2.10b) can be used as a starting point to introduce other chemical groups and functionalities via carbodiimide coupling chemistry to tune the nanopore surface chemistry through the amide linkage between –COOH groups and amine-terminated molecules. The first step is

the activation of the pore surface –COOH groups, required for the chemical attachment of the primary amines of target molecules. The activation process should be carried out in mild condition, i.e., in water or ethanol medium. The activating agent used here is a water soluble carbodiimide known as *N*-(3-dimethylaminopropyl)-*N'*-ethylcarbodiimide HCl (EDC). The EDC first converted the –COOH groups into active ester functional groups, i.e., *o*-acylisourea intermediate as a leaving group. This intermediate is easily hydrolysed in aqueous medium. Therefore, it is further stabilized by reacting with *N*-hydroxysulfosuccinimide (sulfo-NHS) or pentafluorophenol (PFP).[130] The more stable sulfo-succinimidyl- and PFP-reactive esters are hydrophilic in nature and rapidly react with amine group of target molecule to form amide bond as shown in Figure 2.11.

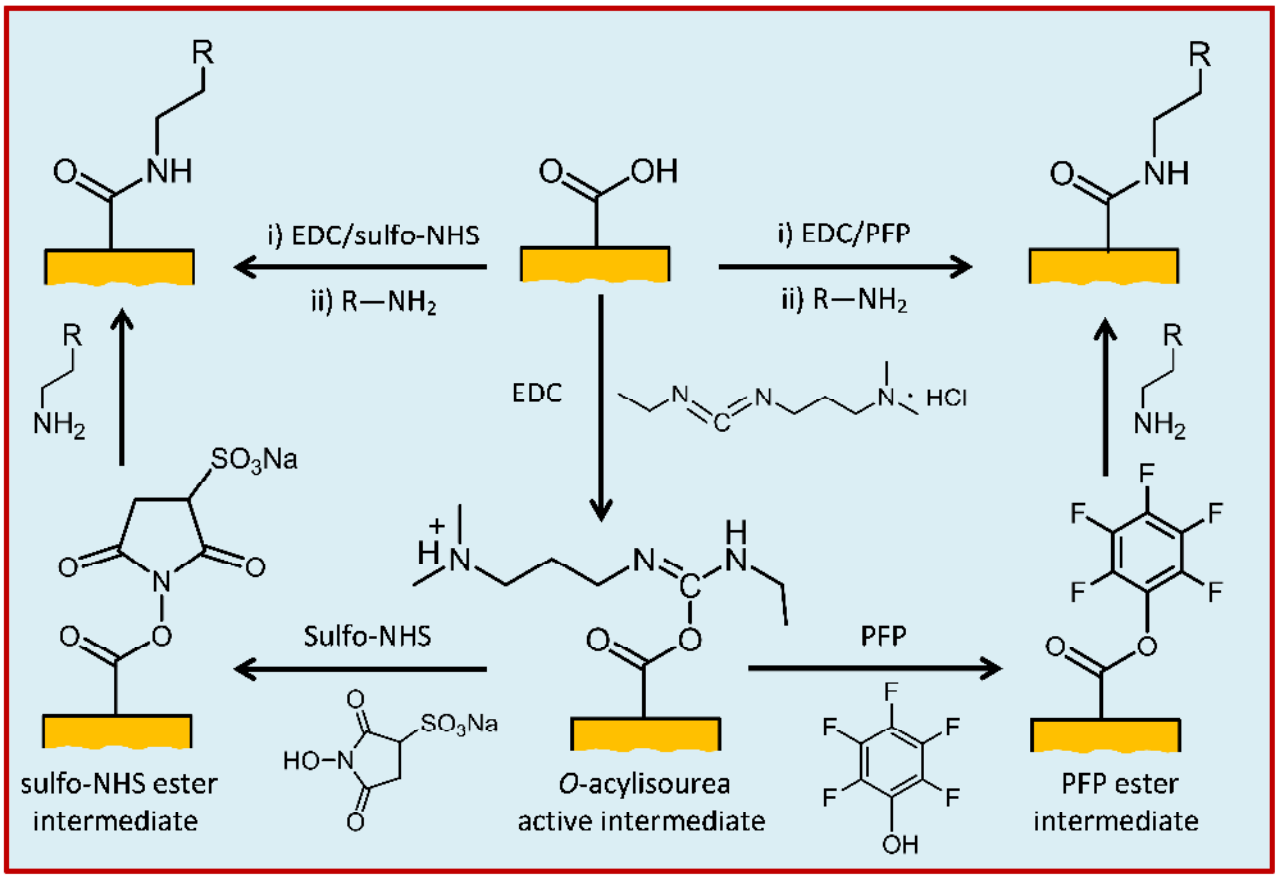

Figure 2.11: A general reaction scheme representing the tuning of nanopore surface functionalities via carbodiimide coupling chemistry. The terminal –R can be a primary amine, zwitterionic group or stimuli-responsive molecule / group.

2.5 Analyte permeation experiments

The permeation experiments are carried out in a transport cell having two chambers. The right and left chambers of the transport cell are known as feed cell and permeate cell, respectively. Each chamber contains a circular opening of diameter ~11.5 mm^2, representing the effective permeation area of the membrane. A maximum volume of ~3.4 ml can be filled in each chamber. The first step in the mass transport experiment is to fix the track-etched multipore membrane between these chambers (Figure 2.12). In the present work, three types of analyte molecules [methylviologen dichloride (MV^{2+}), 1,5-naphthalene disulfonate di-sodium salt (NDS^{2-}) and 2,2′-dipyridine (DPy)] with positive, negative and neutral charge are transported across the track-etched membrane in mass transport experiments. The analyte solution of known concentration is prepared in phosphate buffer solution. The left chamber is filled with analyte solution, while the right chamber contains only the buffer solution. Then the transport cell, filled with analyte and buffer solutions, is placed on the stirring plate and both the solutions are continuously stirred during the permeation experiment and allowed to transport the analyte molecules for pre-set time periods. By measuring the UV absorption of permeate solution by UNICAM UV-vis spectrophotometer, one is able to calculate the concentration of analyte molecules transported across the membrane.

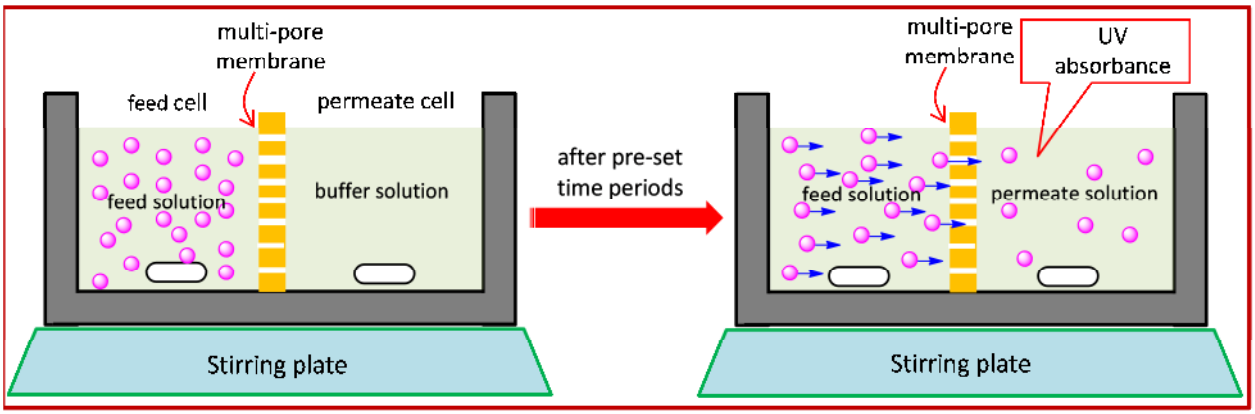

Figure 2.12: A simplified cartoon representing the process of analyte permeation across the track-etched nanoporous membrane.

The analyte molecules permeation across the porous membrane is based on several processes and mechanisms, e.g., diffusion, difference in concentration gradient and selective transport due to fixed charges on the inner pore walls. It is experimentally noticed that the main analyte permeation occurred via permselective transport. This means that negatively charged nanopores preferencially allow entering and transporting positive analyte molecules across the membrane and vice versa, while neutral molecules are passed through the charged pores without any hinderence. Moreover, uncharged nanopores are non-selective, i.e., both positive and negative analyte molecules are equally transported across the membrane.

Figure 2.13 shows the concentration-dependent absorption spectra of analytes used for the permeation experiments. To establish the linear relation of different analyte concentrations, the maximum absorption (λ_{max} at specific wavelength) values are obtained from the UV spectra. The λ_{max} for MV, NDS and DPy was taken at 258, 288 and 280 nm, respectively. The unknown concentration of permeate solution is estimated from the calibration curve of the respective analyte, as shown in Figure 2.13.

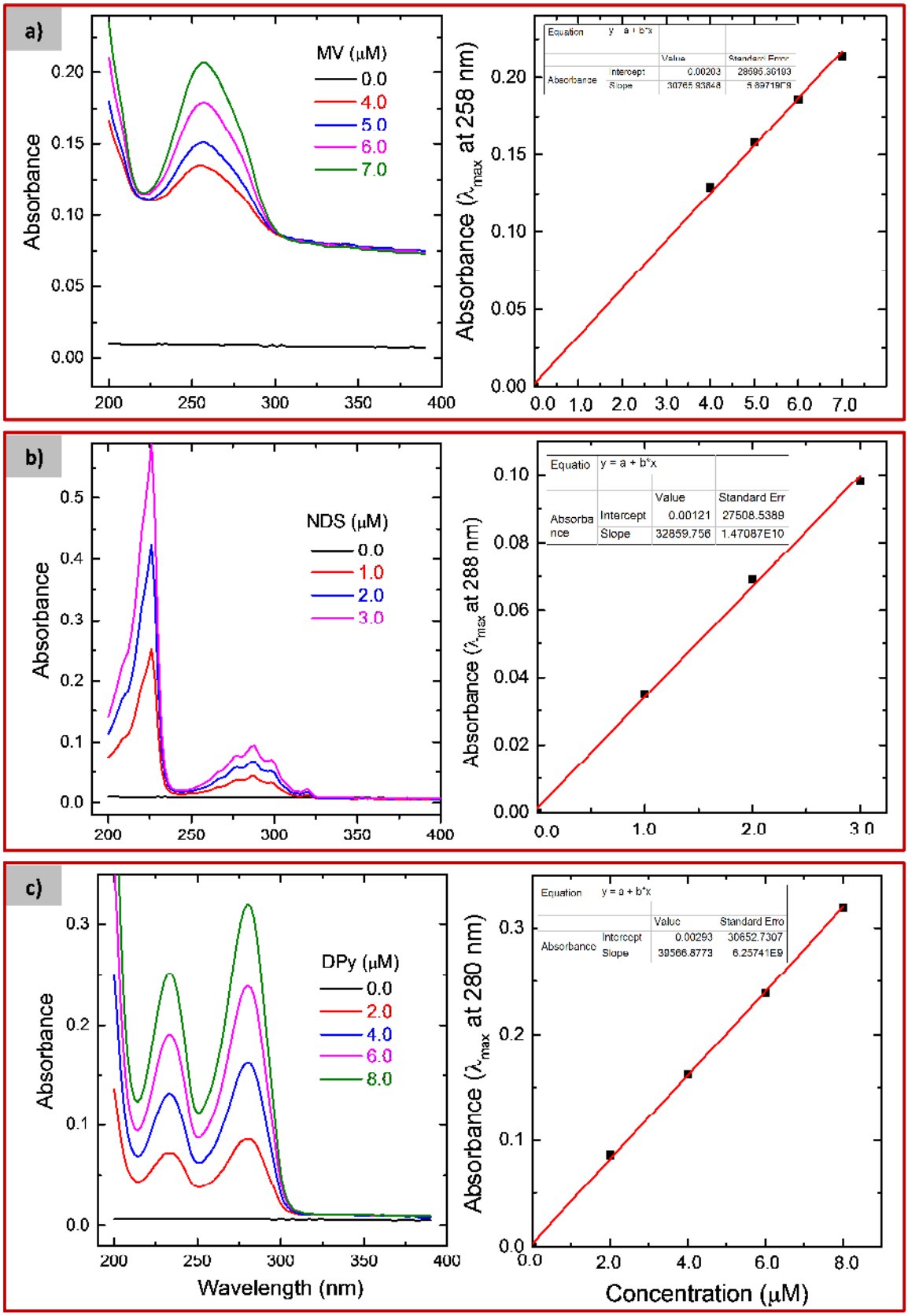

Figure 2.13: Concentration-dependent absorption spectra and linear fit for λ_{max} versus analyte concentration: a) methylviologen (MV), b) 1,5-naphthalene disulfonate (NDS), c) 2,2′-dipyridine (DPy). The different analyte concentrations are prepared in phosphate buffer solution.

2.6 Fabrication of stimuli-responsive nanopores

2.6.1 Materials and chemicals

In the present study heavy ion track-etched polymer (PET and PI) membranes containing a single conical nanopore and cylindrical nanopore arrays were used for the fabrication of the stimuli-responsive nanofluidic devices. During the track-etching process, carboxyl (–COOH) groups were generated on the surface and inner pore walls. These –COOH moieties served as starting points for the introduction of other responsive chemical functionalities onto the pore surface.

All the reagents used in the experimental work are of analytical grade and used as recieved without further purification. *N*-(3-dimethylaminopropyl)-*N′*-ethylcarbodiimide hydrochloride (EDC, 98%), ethylenediamine (EDA, 99+ %), pentafluorophenol (PFP, 99+ %) *N,N′*-dicyclohexylcarbodiimide (DCC, 98 %) 6-nitroveratryl alcohol, (99 %), 4,5-dimethoxy-2-nitrobenzyl chloroformate (97 %), 4-dimethylaminopyridine, *N*,*N*-diisopropylethylamine, 4-aminophenyl α-D-mannopyranoside (APMP), 1-pyrenemethanol (98%), piperidine, bovine serum albumin (BSA; fraction V), lactoferrin human (LFN), ferrous sulphate heptahydrate ($FeSO_4 \cdot 7H_2O$), dimethyl sulfoxide (anhydrous, DMSO) and 4′-chloro,2,2′,6′,2"-terpyridine, methylviologen dichloride (MV^{2+}), 1,5-naphthalene disulfonate di-sodium salt (NDS^{2-}), 2,2′-dipyridine (DPy), *N*-hydroxysulfosuccinimide (sulfo-NHS), 2-(2-aminoethoxyethanol) (AEE), succinic anhydride, Lysozyme and concanavalin A (ConA) were purchased from Sigma-Aldrich, Taufkirchen, Germany, and used without further purification.

Amine-terminated poly(*N*-isopropyl acrylamide) [P10405A-NIPAMNH$_2$, Mn = 82,000] was purchased from Polymer Source, Inc. 2-(*N*-morpholino)ethanesulfonic acid (anhydrous, MES) was purchased from SL Labor-Service GmbH, Germany. The solution ^{1}H-NMR spectra were measured on a Bruker Spectrospin 300 (300 MHz).

2.6.2 Preparation of thermo-sensitive nanopores

2.6.2.1 Functionalisation of PNIPAAM–NH$_2$ brushes

The functionalisation of amine-terminated polymer chains on the inner walls of the nanopores was achieved in the following way. The carboxyl groups of the pore walls were first converted into an amine reactive PFP-esters by immersing the track-etched membranes in an ethanolic solution containing a mixture of *N*-(3-dimethylaminopropyl)-*N′*-ethylcarbodiimide HCl (EDC, 100 mM) and pentafluorophenol (PFP, 200 mM). The activation of carboxyl groups was carried out for 60 minutes at room temperature. After the activation step, the foils were washed with ethanol. Subsequently, the activated membranes were exposed to an ethanolic solution of PNIPAAM-NH$_2$ (3 mg/ml). In this step, the amine-reactive PFP-esters were allowed to covalently couple with the terminal amine of the PNIPAAM chains in a reaction carried out overnight. Finally, the modified pores were washed thoroughly with ethanol followed by deionised water.

2.6.2.2 Characterization

I–V measurements:

As-prepared (carboxylated) and PNIPAAM-modified single pore-membranes were mounted between the two halves of the conductivity cell. Both halves of the cell were filled with an aqueous 0.1 M KCl solution prepared

in phosphate buffer (10 mM) with pH = 6.5. A Ag/AgCl electrode was placed into each half-cell solution, and a picoammeter/voltage source (Keithley 6487, Keithley Instruments, Cleveland, OH) was used to apply the desired transmembrane potential, and measure the ionic current across the single pore membrane. In the case of conical nanopores, the ground electrode was placed at the side of the membrane with the big opening of the pore. In order to record the *I–V* curves, a scanning triangle voltage signal from -2 to +2 V was used. The measurement of *I–V* curves was performed at low (23ºC) and high (39ºC) temperatures before and after the immobilisation of PNIPAAM chains onto the nanopore surface.

Analyte permeation:

The selective diffusion of doubly charged organic analytes: methyl viologen (MV^{2+}) and 1,5-naphthalenedisulfonate (NDS^{2-}) through the nanopore arrays in polymer membranes were performed before and after modification with PNIPAAM chains at low (23ºC) and high (39ºC) temperatures. The analyte solutions were prepared in phosphate buffer (pH 6.5). For the transport experiments, unmodified and PNIPAAM-modified membranes were mounted between the two halves of the conductivity cell. Each cell volume was 3.4 ml with an effective permeation area of the membrane of 1.15 cm^2. The feed half-cell contained a known concentration of 10 mM of each organic analyte in the buffer solution, while the permeate half-cell was filled with pure buffer solution. For the case of conical nanopore arrays, analyte solution was filled on the tip opening side of the membrane. Both solutions were continuously stirred during the whole transport experiment. After fixed time periods, the concentration of respective analyte in the permeate half-cell was determined by measuring the UV absorbance with a UNICAM UV/vis spectrometer.

2.6.3 Preparation of photosensitive nanopores

2.6.3.1 Synthesis of 4-oxo-4-(pyren-4-ylmethoxy) butanoic acid[V]

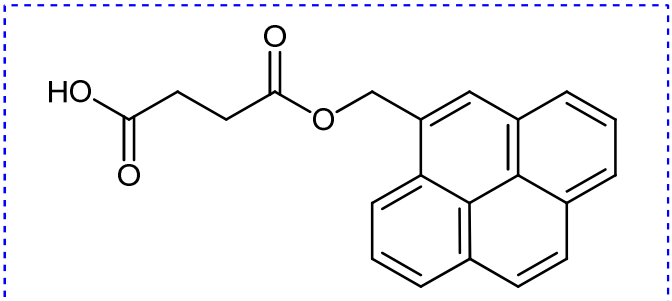

4-oxo-4-(pyren-4-ylmethoxy) butanoic acid (PYBA)

The synthesis of 4-oxo-4-(pyren-4-ylmethoxy) butanoic acid (PYBA) was carried out following the method reported in reference [37]. 1-pyrenemethanol (2.15 mmol, 500 mg) was added to a solution of succinic anhydride (2.80 mmol, 280 mg) in dichloromethane (80 mL). After complete dissolution of 1- pyrenemethanol, pyridine (266.6 mmol, 21.5 mL) was added into the solution dropwise. The reaction mixture was stirred at 50 °C for 18 h and a 30% (v/v) aqueous solution of hydrochloric acid (100 mL) was added to remove excess of pyridine. The reaction mixture was then extracted three times with dichloromethane (50 mL). The combined

[V] Dr. I. Ahmed (Karlsruhe Institute of Technology, Karlsruhe) is highly acknowledged for the synthesis of PYBA.

organic layers were collected, washed three times with water (50 mL), and dried over anhydrous sodium sulfate. After filtration, the solvent was evaporated under reduced pressure to afford 4-oxo-4-(pyren-4-ylmethoxy) butanoic acid (PYBA) as a light yellow powder (465 mg, 65%). ^{1}H-NMR (200 MHz, $CDCl_3$): δ = 8.17–7.88 (m, 9H, H-atom), 5.77 (s, 2H, -CH_2-), 2.59 (s, 4H, -CH_2CH_2-).

2.6.3.2 Functionalisation of 4-oxo-4-(pyren-4-ylmethoxy) butanoic acid

The covalent immobilisation of photolabile protecting molecules onto the channel surface was accomplished in two steps. Firstly, the carboxyl groups on the channel surface were converted into amine reactive PFP-esters by immersing the track-etched membranes in an ethanolic solution containing a mixture of EDC (100 mM) and PFP (200 mM). The activation process was carried out for one hour. After washing with ethanol, the activated membranes were treated with ethylenediamine (EDA, 50 mM) solution prepared in ethanol for the amination of channel surface. Subsequently, the aminated membranes were washed first with ethanol and finally with deionised water. Secondly, the aminated membranes were exposed to a solution of 4-oxo-4-(pyren-4-ylmethoxy) butanoic acid (PYBA, 10 mM) along with an activating agent (EDC, 50 mM) in ethanol. In this step, the amine groups on the channels surface were allowed to covalently couple with the carboxyl group of PYBA in a reaction carried out for two hours. Finally, the modified membranes were thoroughly washed with ethanol.

It should be cited that alternative photo-removable groups have been studied previously for protecting carboxylic acids. In particular, benzyl, nitrophenyl and nitobenzyl groups were employed successfully for the surface modification of different materials in order to tune their wettability upon UV irradiation. However, the fact is that some of the photo-labile groups behave differently when we switched from surface to nanoconfined geometries. Moreover, our choice of pyrene is based on the previous study,[131] which demonstrated that, after UV irradiation, the recovery of carboxylic acid moieties is maximum when they are protected with pyrenemethyl ester groups in mild conditions.[132]

2.6.3.3 UV light irradiation[VI]

The PYBA-modified membranes were irradiated with UV light of wavelength 365 nm for 10 minutes on each side in dry state. For UV light irradiation, an Oriel Instruments 500 W mercury lamp was used with a 365 nm filter. After irradiation, membranes were washed first with ethanol followed by deionised water in order to remove the photocleaved groups from the interior of the nanochannels.

Following a previous study,[131] we selected a minimum exposition time of 10 minutes on each side of the polymeric membrane containing the nanochannels. This time is enough to remove most of the photo-labile moieties from the channel surface, as confirmed by the subsequent transport experiments. The successful cleavage of pyrene moieties was further confirmed by the *I–V* curves in the case of the single nanopore.

[VI] Dr. M. N. Tahir (Johannes Gutenberg-Universität, Mainz) is highly acknowledged for his help in the UV light irradiation experiments.

2.6.3.4 Characterization

I–V measurements:

The membrane with a single channel was characterised by measuring the *I-V* curves. To this end, a single-channel membrane was mounted between the two halves of the conductivity cell. An electrolyte solution (0.1M KCl, pH 6.0) was filled on both sides of the membrane. An Ag/AgCl electrode was placed into each half-cell solution and the ionic current flowing through the single channel membrane was measured with a picoammeter/voltage source (Keithley 6487, Keithley Instruments, Cleveland, OH). The ground electrode was placed on the base opening side of the conical nanochannel and the *I–V* curves were recorded by applying a scanning triangle voltage signal from -2 to +2 V across the membrane.

Analyte permeation:

The multi-channel membrane was placed between the two halves of the conductivity cell. Each cell volume was 3.4 ml with an effective membrane permeation area of 1.15 cm^2. The feed half-cell contained a known concentration (10 mM) of each organic analyte (MV^{2+} and NDS^{2-}) prepared in the buffer solution. The permeate half-cell was filled with a pure buffer solution. Both solutions were continuously stirred during the experiment. After fixed time periods, the concentrations of respective analytes in the permeate half-cell were estimated from the UV absorbance values. Similar transport experiments were performed after UV_{365} light irradiation of the PYBA-modified membrane.

2.6.4 Preparation of photo-triggered pH-sensitive nanopores

2.6.4.1 Synthesis of "caged" lysine amino acid (7)[VII]

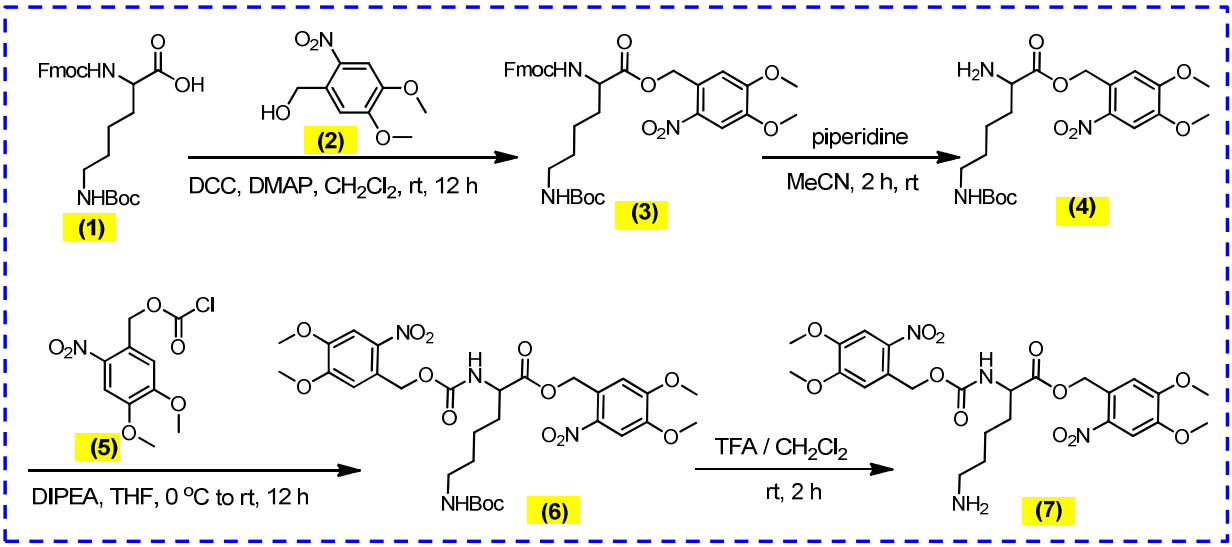

Figure 2.14: Reaction scheme for the synthesis of photosensitive "caged" lysine amino acid (7).

[VII] Dr. I. Ahmed (Karlsruhe Institute of Technology, Karlsruhe) is highly acknowledged for the synthesis of "caged" lysine amino acid.

Synthesis of *compound **(3)**:*

Fmoc-Lys(Boc)-OH (**1**) (2.0 g, 4.27 mmoles) is added to an oven dried round bottom flask and the flask is purged with argon. The sample is diluted with CH_2Cl_2 (20 mL), *N*,*N*-dicyclohexyl carbodiimide (DCC, 1.77 g, 8.54 mmoles), 4-(dimethyl amino)-pyridine (DMAP, 1.04 g, 8.54 mmoles), and 6-nitroveratryl alcohol (**2**) (1.4 g, 6.83 mmoles) are added to the flask. The reaction is allowed to proceed overnight. The reaction mixture is rinsed with 1 M HCl (25 mL). The organic layer is dried over sodium sulfate, concentrated to give yellow residue which is purified by silica gel column chromatography eluting with cyclohexane to cyclohexan/ ethyl aceate (5:1) to afford product **3** in 73% yield (2.06 g, 3.11 mmol) as yellow solid.

^{1}H-NMR (300 MHz, $CDCl_3$): δ ppm = 1.35 (s, 9 H), 1.40-1.42 (m, 2 H, overlapped), 1.52-1.63 (m, 1 H), 1.65-1.73 (m, 1 H), 1.82-1.85 (m, 2 H), 2.99-3.05 (br 2 H), 3.84 (s, 6 H), 4.09 (t, 1 H, *J* = 6.8 Hz), 4.23-4.36 (m, 3 H), 4.59 (br, 1 H), 5.48 (m, 2 H, CH_2-Ph), 6.90 (br, 1 H, Ar-H), 7.16-7.22 (m. 2 H, Ar-H), 7.24-7.32 (m, 2 H, Ar-H), 7.48 (d, *J* = 7.3 Hz, 2 H, Ar-H), 7.61 (s, 1 H, Ar-H), 7.65 (d, *J* = 7.4 Hz, 2 H, Ar-H)

^{13}C-NMR (75 MHz, $CDCl_3$): δ = 22.4, 26.9, 28.4, 29.7, 33.9, 39.4, 47.1, 54.1, 56.3, 56.7, 64.1, 67.0, 79.2, 108.2, 110.4, 119.2, 125.0, 127.0, 127.7, 139.7, 141.2, 143.6, 148.3, 153.7, 156.2, 172.2

FT-IR (ATR) υ_{max}: 3315, 2934, 2857, 1748, 1694, 1677, 1618, 1580, 1519, 1449, 1365, 1324, 1273, 1221, 1196, 1086, 931, 731 cm^{-1}.

MS (+FAB): *m/z* (%) = 686.3 (10) [M+Na], 664.3 (28) [M+H], 564.3 (35), 336 (20), 195.9 (40), 177.9 (62), 165 (21), 153.9 (100)

HRMS (FAB) calcd for $C_{35}H_{41}N3O_{10}$ $[M + H]^+$: 664.2870; found: 664.2872

*Synthesis of compound **(6)**:*

Lysine derivative **3** (2.0 g, 3.01 mmol) is dissolved in acetonitrile (30 mL) and piperidine (10 mL) is then added. The mixture is stirred at room temperature for 2 h. The solvent (acetonitrile) and piperidine are removed at reduced pressure to give fmoc-deprotected lysine **4** as brown sticky residue which is used in the next step without further purification.

To a stirred solution of fmoc-deprotected lysine **4** (1.50 g, 3.40 mmol) in anhydrous THF (50 mL) is added *N*,*N*-diisopropylethylamine (DIPEA) (1.18 mL, 6.80 mmol, 2 eq.). The mixture is stirred at room temperature for 10 min. The reaction mixture is cooled to 0^{o}C and 4,5-dimethoxy-2-nirobenzyl chloroformate (**5**) (0.935 g, 3.40 mmol) is added at 0^{o}C. The reaction mixture is allowed to warm at room temperature and is stirred overnight. The mixture is neutralized by dilute HCl and extracted three times by ethyl acetate (3 x 60 mL). The organic layers are combined, washed with water (50 mL) and dried over anhydrous sodium sulfate. After filtration, the solvent is evaporated under reduced pressure to give brown residue which is purified by silica gel chromatography eluting with cyclohexane to cyclohexan/ ethyl aceate (5:1) to afford **6** in 71% yield (1.64 g, 2.41 mmol) as pale yellow solid.

^{1}H-NMR (300 MHz, $CDCl_3$): δ ppm = 1.16 (m, 2 H), 1.33 (s, 9 H), 1.41 (m, 2 H, overlapped), 1.57-1.71 (m, 1 H), 1.74-1.83 (m, 1 H), 3.03 (br 2 H), 3.84 (s, 12 H), 4.33 (m, 1 H), 4.82 (m, 3 H), 5.30-5.52 (m, 4 H), 6.90 (br, 2 H), 7.59 (br. 2 H).

^{13}C-NMR (75 MHz, $CDCl_3$): δ = 22.4, 28.2, 29.5, 31.0, 39.6, 54.2, 56.2, 56.3, 56.4, 60.3, 63.6, 64.0, 79.1, 107.9, 108.1, 109.4, 110.1, 126.5, 128.1, 139.3, 139.5, 147.9, 148.2, 153.6, 155.8, 172.2.

FT-IR (ATR) υ_{max}: 3332, 2932, 2854, 1752, 1692, 1674, 1618, 1579, 1516, 1323, 1273, 1219, 1167, 981, 868, 795, 754, 599 cm^{-1}.

MS (+FAB): *m/z* (%) = 703.1 (3) [M+Na], 581.1 (10) [M-Boc], 520.4 (5), 415 (22), 316.2 (38), 95 (100)

HRMS (FAB) calcd for $C_{30}H_{40}N_4O_{14}$ $[M + H]^+$: 681,2541; found: 681.2536

*Synthesis of compound **(7)**:*

Trifluoroacetic acid (5 mL) is added to a solution of the *tert*-boc protected lysine **6** (520 mg, 0.76 mmol) in dry CH_2Cl_2 (15 mL). The reaction mixture is stirred for 2 h at room temperature and the volatiles are removed on rotary evaporator. Dichloromethane (15 mL) is again added and the solvent is removed under reduced pressure. The procedure is repeated thrice to remove traces of trifluoroacetic acid to afford amine **7** in 88% yield (390 mg, 0.67 mmol) as yellow semi-solid.

^{1}H-NMR (300 MHz, $CDCl_3$): δ ppm = 1.17 (m, 2 H), 1.44 (m, 2 H), 1.66 (m, 2 H), 2.97 (br 2 H), 3.81 (s, 12 H), 4.28 (m, 1 H), 5.25-5.48 (m, 4 H), 6.88 (br, 2 H), 7.51 (br. 2 H), 7.60 (br. 2 H), 8.06 (br. 1 H).

^{13}C-NMR (75 MHz, $CDCl_3$): δ = 22.1, 26.6, 29.6, 31.0, 39.7, 54.0, 56.2, 56.2, 56.3, 56.4, 63.9, 64.4, 108.0, 108.1, 109.8, 110.9, 125.9, 127.6, 139.2, 139.7, 148.0, 148.4, 153.7, 153.7, 156.1, 160.9, 161.4, 172.1.

FT-IR (ATR) ύmax: 3307, 2923, 2851, 1738, 1680, 1581, 1518, 1457, 1436, 1324, 1268, 1063, 983, 877, 794, 720 cm-1.

MS (+FAB): *m/z* (%) = 581.1 (10) [M+H], 551.6 (5), 503 (22), 383.4 (38), 109.4 (62) 95 (100)
HRMS (FAB) calcd for $C_{25}H_{32}N_4O_{12}$ $[M + H]^+$: 581,2016; found: 581.2093

2.6.4.2 Functionalisation of "caged" lysine chains

The above-described etching procedure results in the generation of carboxyl groups on the surface and inner wall of the nanopore. These carboxyl groups are converted into amine-reactive pentafluorophenyl esters via EDC/PFP coupling chemistry. For activation, the track-etched membranes are immersed in an ethanolic solution containing a mixture of 0.1 M EDC and 0.2 M PFP at room temperature for one hour. After washing the activated membrane with ethanol several times, the samples are further dipped in a solution of "caged" lysine (10 mM) prepared in anhydrous ethanol and left for overnight. During this reaction period, amine-reactive PFP-esters are covalently coupled with terminal amine group of lysine**.** Then, the modified membranes are washed thoroughly first with ethanol followed by careful rinsing with deionized water and kept in darkness until further measurements.

2.6.4.3 UV light irradiation[VIII]

The membranes modified with "caged" lysine chains are irradiated with UV light of wavelength 365 nm for 15 minutes on each side in dry state. For UV light irradiation, an Oriel Instruments 500 W mercury lamp is used with a 365 nm filter. After irradiation, the membranes are washed first with ethanol followed by deionized water in order to remove the photocleaved groups from the interior of the nanopores.

[VIII] Dr. M. N. Tahir (Johannes Gutenberg-Universität, Mainz) is highly acknowledged for his help in the UV light irradiation experiments.

2.6.4.4 Characterization

I–V measurements:

The single-pore membrane is characterized by measuring the *I–V* curves. To this end, the membrane is clamped between the two halves of the conductivity cell. An electrolyte (0.1M KCl,) prepared in a phosphate buffer (10 mM) solution is filled on both sides of the membrane. The *pH* of the solution is adjusted with dilute HCl or NaOH to the desired values: 3.0, 5.0 and 9.5. An Ag/AgCl electrode is placed into each half-cell solution and the ionic current flowing through the single pore membrane is measured with a picoammeter/voltage source (Keithley 6487, Keithley Instruments, Cleveland, OH). The ground electrode is placed on the base opening side of the conical pore and the *I–V* curves are recorded by applying a scanning triangle voltage signal from -2 to +2 V across the membrane.

Analyte permeation:

The membrane with conical nanopore arrays is fixed between the two halves of the conductivity cell. Each cell volume is 3.4 ml with an effective membrane permeation area of 1.15 cm^2. The analyte MV^{2+} and NDS^{2-} solutions of known concentration (10 mM) are prepared in the phosphate buffer at different pH values (3.0, 5.0, and 9.5). The feed half-cell facing the tip opening of the conical nanopores is filled with analyte solution. The permeate half-cell on the side facing to the base opening of the conical pores is filled with a pure buffer solution. Both solutions are continuously stirred during the experiment. After fixed time periods, the concentrations of respective analyte in the permeate half-cell are estimated from the UV absorbance values. The mass transport experiments are performed separately for each analyte at specific pH conditions. Similar transport experiments are performed after UV light irradiation of the modified membrane.

2.6.5 Lactoferrin protein sensitive nanopore

2.6.5.1 Synthesis of 1-amino-5-(2,2′:6′,2″-terpyrid-4′-yl-oxy)pentane (terPy–DEG-NH_2) [IX]

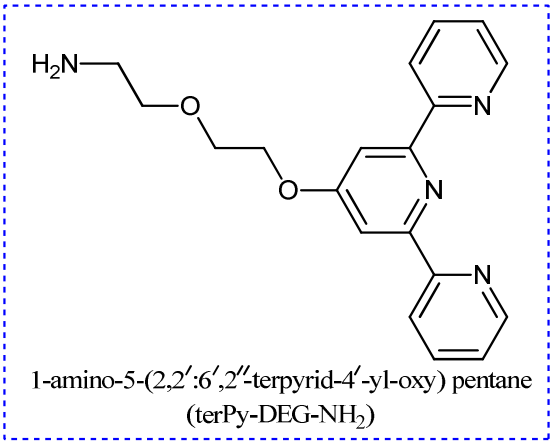

1-amino-5-(2,2′:6′,2″-terpyrid-4′-yl-oxy) pentane
(terPy-DEG-NH_2)

The synthesis of 1-amino-5-(2,2′:6′,2″-terpyrid-4′-yl-oxy)pentane (terPy–DEG-NH_2) ligand was carried out by following the reported method.[133] In order to synthesize this compound, 1.6 mg (in excess) of ground KOH flakes was added to a three-neck round-bottomed flask, and dispersed in anhydrous DMSO at 60°C for 15 minutes, followed by the addition of diethylene glycolamine (DEG-NH_2, 1 mM) to the reaction chamber. The reaction was allowed to proceed for 30 minutes before the addition of 4′-chloro,2,2′:6′,2″-terpyridine (1 mM) into the reaction chamber. The reaction was carried out at 70°C for 6 hours. When the reaction was completed, the flask was allowed to cool down to room temperature. Then 120 ml of Millipore water was added in the flask. The reaction mixture was extracted in dichloromethane (3 x 30 ml). The organic fraction was collected and dried in anhydrous sodium sulphate, followed by evaporating the solvent in a rotary evaporator. The crude product was purified by column chromatography (DCM : methanol, 9:1). The purified compound was further characterised by ^{1}H NMR and FD-MS techniques.

^{1}H NMR (400 MHz, DMSO-d_6): 2.7 (t, 2H, CH_2, H_d), 3.2 (s, broad, NH_2), 3.5 (t, 2H, CH2, H_c), 3.82 (t, 2H, CH2, H_b), 4.35 (t, 2H, CH_2, H_a), 7.5 (ddd, 2H, CH_{terpy}, $H_{5,5''}$), 7.98 (s, 2H, CH_{terpy}, $H_{3',5'}$), 8.00 (m, 2H, CH_{terpy}, $H_{4,4''}$), 8.62 (d, 2H, CH_{terpy}, $H_{3,3''}$), 8.72 (dd, 2H, CH_{terpy}, $H_{6,6''}$).

FD-MS : [M+H] = 337 g/mol

2.6.5.2 Functionalisation of terPy–DEG-NH_2

The functionalisation of terpyridine ligand on the inner walls of the nanopore was achieved by the following method. The carboxyl groups of the pore walls were first converted into an amine reactive sulfo-NHS-esters by immersing the track-etched membranes in a solution containing a mixture of EDC (10 mM) and sulfo-NHS (20 mM) dissolved in 0.1M MES buffer 2-(*N*-morpholino)ethanesulfonic acid, pH = 5.5. The activation of carboxyl groups was carried out for 50 minutes at room temperature. After the activation step, the foil was washed with the same buffer. Subsequently, the activated membranes were exposed to 10 mM solution of terPy–DEG-NH_2 prepared in the same buffer. In this step, the amine-reactive sulfo-NHS-esters were allowed to covalently couple with the terminal amine of the ligand in a reaction carried out overnight. Finally, the modified pore was washed

[IX] Dr. M. N. Tahir (Johannes Gutenberg-Universität, Mainz) is highly acknowledged for the synthesis of terPy-DEG-NH_2.

thoroughly with buffer followed by deionised water. The same procedure was used for the modification of the multi-nanopore membrane.

2.6.5.3 Formation of iron–terpyridine complexes

A solution of ferrous sulphate (100 µM) was prepared in 50% aqueous ethanol (C_2H_5OH/H_2O, 1:1 by volume). Polymer membranes (single / multi-pore) modified with terpyridine amine (metal chelating ligand) were exposed to a solution of ferrous sulphate for 60 min at room temperature. Subsequently, the membranes were washed first with ethanol followed by deionized water.

2.6.5.4 Characterization

I–V measurements:

As-prepared (carboxylated) and ligand modified (iron–terPy complexed) single pore-membranes were mounted between the two halves of the conductivity cell. Both halves of the cell were filled with an aqueous 0.1 M KCl solution prepared in phosphate buffer (10 mM) with pH = 7.0. An Ag/AgCl electrode was placed into each half-cell solution, and a picoammeter/voltage source (Keithley 6487, Keithley Instruments, Cleveland, OH) was used to apply the desired transmembrane potential, and measure the ionic current across the single pore membrane. In the case of conical nanopores, the ground electrode was placed at the side of the membrane with the big opening of the pore. In order to record the *I–V* curves, a scanning triangle voltage signal from -1 to +1 V was used. The small opening of the conical nanopores was determined through the *I–V* recording in 1 M KCl solution.

Various concentrations of lactoferrin (LFN) protein are prepared in the same electrolyte solution, used for the measurement of respective *I–V* curve.

Analyte permeation:

The selective diffusion of doubly charged organic analytes: MV^{2+} and NDS^{2-} through polymer membranes were performed before and after modification with iron–terPy ligand on the pore surface. The analyte solutions were prepared in phosphate buffer (pH 7.0). For the transport experiments, membranes were mounted between the two halves of the conductivity cell. Each cell volume was 3.4 ml with an effective permeation area of the membrane of 1.15 cm^2. The feed half-cell contained a known concentration of 10 mM of each organic analyte in the buffer solution, whereas the permeate half-cell was filled with pure buffer solution. Both solutions were continuously stirred during the whole process. Similarly, transport experiments were performed through the membranes bearing terPy–Fe(II) complex on the inner walls of the nanopores. For this purpose, lactoferrin (100 nM) was dissolved in 10 mM solution of each MV^{2+} and NDS^{2-}, respectively. After fixed time periods, the concentration of respective analyte in the permeate half-cell was determined by measuring the UV absorbance with a UNICAM UV/vis spectrometer.

2.6.6 Lectin (ConA) protein sensitive nanopores

2.6.6.1 Functionalisation of p-aminophenyl α-D-mannopyranoside

For the covalent attachment of the p-aminophenyl α-D-mannopyranoside (APMP) molecules with the channel surface carboxylic acid groups a two-step reaction procedure is followed.[40] For this purpose, carboxyl groups are first converted into amine reactive PFP-esters by exposing the track-etched channel to the solution containing a mixture EDC (100 mM) and PFP (200 mM) prepared in anhydrous ethanol. The activation process is carried out for one hour. The activated nanochannel membranes are washed several times with ethanol. Then activated membranes are dipped in a solution of APMP (40 mM) prepared also in ethanol. These membranes remained in the APMP solution for overnight. During this time, the amine-reactive PFP-esters are covalently coupled with the terminus amine groups of the APMP molecules. Then the APMP-modified membranes are washed first with ethanol and finally with deionized water.

2.6.6.2 Characterization

I–V measurements:

In order to obtain *I–V* characteristics, the single channel-membrane is mounted in between the two compartments of the conductivity cell. An aqueous 0.1 M KCl solution prepared in 10 mM HEPES buffer (pH 7.2) containing 0.1mM $CaCl_2$ and 0.1 mM $MnCl_2$ is filled in both compartments of the cell. The Ag/AgCl electrode is placed into each half-cell solution, and a picoammeter/voltage source (Keithley 6487, Keithley Instruments, Cleveland, OH) is used to apply the desired transmembrane potential and measure the ionic current across the single-channel membrane. The ground electrode is placed at the side of the membrane with the big opening (base) of the asymmetric nanochannel. To record the *I–V* curves, a scanning triangle voltage signal from -1 to +1 V is used.

Different concentrations of nonspecific proteins (lysozyme and BSA) and concanavalin A (ConA) protein are prepared in the same electrolyte solution employed for the measurement of the *I–V* curves.

Analyte permeation:

The PET membrane with cylindrical nanochannel arrays is fixed between the two halves of the conductivity cell. Each cell volume contains 3.4 ml of solution facing a 1.15 cm^2 effective permeation area of the membrane. The analyte solution contains a mixture of dipyridine (10 mM), $CaCl_2$ (0.1 mM) and $MnCl_2$ (0.1 mM) prepared in the HEPES buffer (pH 7.2). The feed half-cell is filled with analyte solution. The permeate half-cell contains a pure buffer solution. Both solutions are continuously stirred during the experiment. After fixed time periods (60 min), the concentration of DPy in the permeate half-cell is estimated from the UV absorbance at maximum wavelength λ_{max} = 280 nm. The DPy permeation experiments are performed separately for non-bioconjugated, bioconjugated and mannose treated membranes under the same conditions.

3. Results and discussion

3.1 Thermally Controlled Permeation of Ionic Molecules through Synthetic Nanopores Functionalized with Amine–Terminated Polymer Brushes [x]

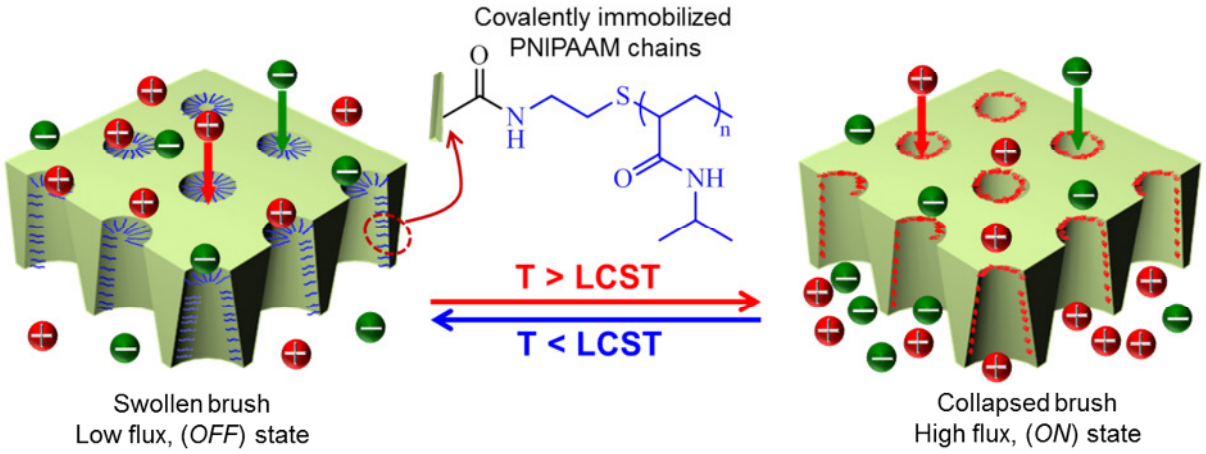

The work presented in this section describes the temperature-dependent ionic transport through an array of nanopores (cylindrical and conical) and a single conical nanopore. End-functionalised polymer chains are immobilised onto the inner pore walls via "grafting-to" approach through the covalent linkage of surface COOH moieties with the terminal amine groups of the PNIPAAM chains via carbodiimide coupling chemistry. The success of chemical modification reaction is corroborated by measuring the permeation flux of charged analytes across the multipore membranes in an aqueous solution, and for the case of single conical pore by measuring the current–voltage (I–V) characteristics, which are dictated by the electrostatic interaction of the charged pore surface with the mobile ions in an electrolyte solution. The effective nanopore diameter is tuned by manipulating the environmental temperature due to the swelling / shrinking behaviour of polymer brushes attached to the inner nanopore walls, leading to a decrease / increase in the ionic transport across the membrane. This process should permit the thermal gating and controlled release of ionic drug molecules through the nanopores modified with thermoresponsive polymer chains across the membrane.

[x] Published work:

Nasir, S.; Ali, M.; Ensinger, W. "Thermally controlled permeation of ionic molecules through synthetic nanopores functionalized with amine-terminated polymer brushes" *Nanotechnology* **2012,** 23, (22), 225502.

DOI: 10.1088/0957-4484/23/22/225502

3.1.1 Introduction

Membrane science and technology,[134] in particular, stimuli-responsive nanoporous membranes, is attracting an increasing attention because of their broad applications for selective separation, biochemical sensing, and controlled release and drug delivery processes.[13,15,19,85,135,136] In nature, the ion channels facilitate the selective transport of ions and small organic molecules across the cell membrane. Under the influence of external stimuli, these channels change their conformation states in order to enhance or inhibit the transport across the membrane, allowing functions such as communication between cells, nerve conduction and signal transmission.[1,5,28]

Bio-inspired designs have produced artificial responsive-nanoporous systems based on organic and inorganic materials with the ability to mimic the functionality of ion channels.[6,8,10,11] To achieve this goal, the internal architecture of the nanoporous membrane is chemically modified with stimuli-responsive molecules. The molecules are immobilised on the pore surface and their conformation is changed in response to external stimuli (pH, ionic concentration, temperature, light, electric potential). These changes permit to tune the ionic and molecular transport through the "smart" membrane.[14]

Polymeric membranes produced by ion-track technology have attracted interest because of their uniform pore size and length, tunable pore geometry, and surface functionalisations.[42] In particular, native chemical groups generated on the pore surface during the track-etching process allow the subsequent introduction of self-assembled monolayers[53,63,65,67,100,101,104,115]and polymer brushes to tune the transport properties of the membrane.[70-76,86,137] Different macromolecules can be arranged in polymer brushes[78] that undergo phase transitions under the action of environmental factors such as *pH*, light, and temperature. The poly(*N*-isopropylacrylamide) [PNIPAAM] brushes exhibit rapid and highly sensitive conformational transitions triggered by temperature changes in the physiological range.[138] Much attention has recently been paid to the preparation of thermoresponsive nanoporous membranes modified with PNIPAAM brushes for bioseparation and drug delivery processes.

The covalent attachment of polymer brushes can be accomplished by the “grafting-from” (polymerisation reaction initiated from the substrate surface by covalently immobilised initiator groups) or the “grafting-to” (end-functionalised polymer molecules react with reactive surface functional groups) experimental approaches .[138] To date, most studies have considered the grafting of polymer brushes onto the surface and inner walls of the track-etched single nanopore-membrane and multipore-membranes containing an array of nanopores using the "grafting from" technique.[70-75,86,137] Here, the direct immobilisation of amine-terminated PNIPAAM chains on the nanopore (cylindrical and conical) surface using a “grafting-to” approach allows also thermal gating (Figures 3.1 and 3.4) is demonstrated. Emphasis is made on the chemically and pharmaceutically relevant case of ionic transport (note that most biomolecules and drugs are ionised when immersed in an aqueous solution).

3.1.2 Immobilzation of polymer chains

Swift heavy ion irradiated polyethylene terephthalate (PET) membranes of thickness 12 µm were used for the fabrication of the cylindrical nanopore array (5×10^8 pores cm^{-2}) by symmetric track-etching technique.[139] The cylindrical geometry of the resulting nanopore has been confirmed by the electrochemical deposition of gold wires inside the nanopores.[139] The fabrication of an array of conical nanopores (5×10^7 pores cm^{-2}) and a single conical nanopores was achieved by well-established asymmetric chemical track-etching techniques developed by Apel *et al.*[41] As a result of heavy ion irradiation and subsequent chemical etching, native carboxylic acid (COOH) groups were exposed on the external surface and inner walls of the nanopores. The surface COOH moeities were exploited for the attachment of amine-terminated PNIPAAM chains onto the pore surface. For this purpose, the COOH groups were first converted into amine-reactive ester molecules by reacting with an ethanolic solution containing a mixture of *N*-(3-dimethylaminopropyl)-*N'*-ethylcarbodiimide (EDC) and

pentafluorophenol (PFP).[101] After washing with ethanol, the PFP-ester molecules were subsequently covalently coupled with the terminal amine groups of the PNIPAAM molecules through amide-bond formation (Figure 3.1).

The selection of the PNIPAAM–amine and the "grafting to" technique for the preparation of the thermoresponsive membranes is based on the following facts: 1) the attachment of the PNIPAAM chains on the pore surface is very simple and can be achieved under mild reaction conditions and 2) the properties of the pre-synthesised polymer molecules are well-known compared to those of different brushes grown by other polymerisation techniques.

3.1.3 Analyte permeation

Permeation experiments were conducted at low (23 ± 1)ºC and high (39 ± 1)ºC temperatures to show the responsiveness behaviour of the PNIPAAM molecules attached to the surface and inner walls of the nanopore. The mass transport experiments were performed in the following way: The nanoporous membrane was clamped between the two compartments of the conductivity cell in which the membrane is served as a dividing wall between the compartments. The feed compartment was filled with an analyte 10 mM solution of either methylviologen (MV^{2+}) or 1,5-naphthalenedisulfonate (NDS^{2-}) prepared in phosphate buffer at pH 6.5. For the case of conical multipore membrane, the analyte solution was filled on the tip opening side of the membrane. The permeate compartment was filled with the buffer solution only. After a preset time, the concentration of analyte in the permeate compartment was determined by measuring the UV absorbance.

For the mass transport experiments, the MV^{2+} and NDS^{2-} molecules were selected because of the following reasons: (i) they have similar molecular volumes (0.637 and 0.680 nm^3, respectively), (ii) the molecular structures of both MV^{2+} and NDS^{2-} contain two benzyl rings which should give similar hydrophobic behaviour within the nanopores, and (iii) the molecules have the same charge number (in absolute value; they are oppositely charged). Hence, the channel surface charges dictate the ionic permeation via electrostatic interactions.

3.1.3.1 Cylindrical nanopore arrays

Figure 3.2 shows the permeation data for the unmodified and PNIPAAM-modified membrane at low and high temperatures. As-prepared membrane composed of an array of cylindrical nanopores (45 ± 3 nm) exhibits cation selectivity due to the presence of ionised $–COO^-$ groups on the pore surface. Therefore, the permeation of MV^{2+} (206 nanomoles) is higher when compared to NDS^{2-} (54 nanomoles) molecules across the membrane after 160 min of diffusion time at low (23ºC) temperature. Figure 3.2a shows that at 39ºC a small increase in the nanomoles of MV^{2+} (from 206 to 271) and NDS^{2-} (from 54 to 70) transported through the nanopores of unmodified membrane has occurred due to the increase in the diffusion coefficient.[84]

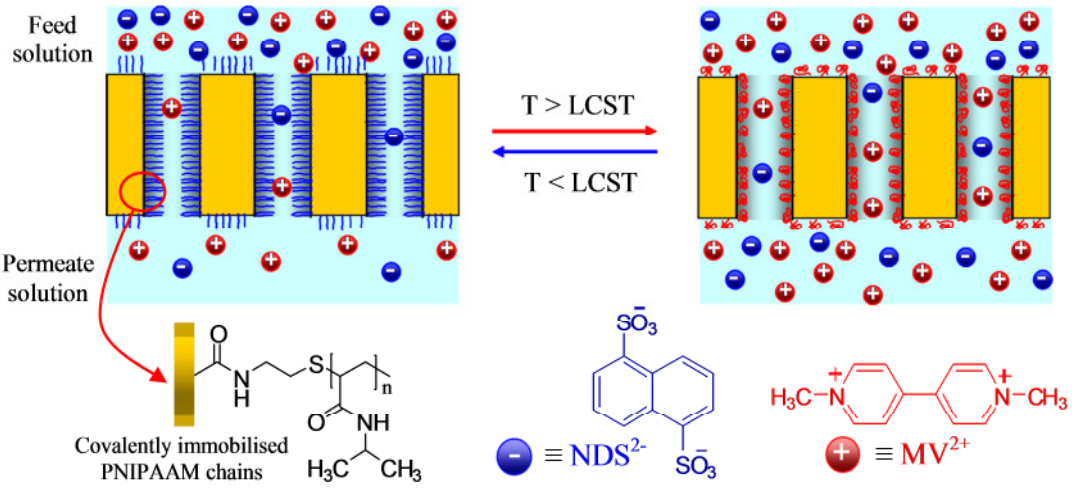

Figure 3.1: The thermally-driven conformational transitions of the attached polymer brushes and respective transport of ionic molecules through an array of cylindrical nanopores across the modified membrane below (left) and above (right) the lower solubility temperature (LCST) of the PNIPAAM chains.

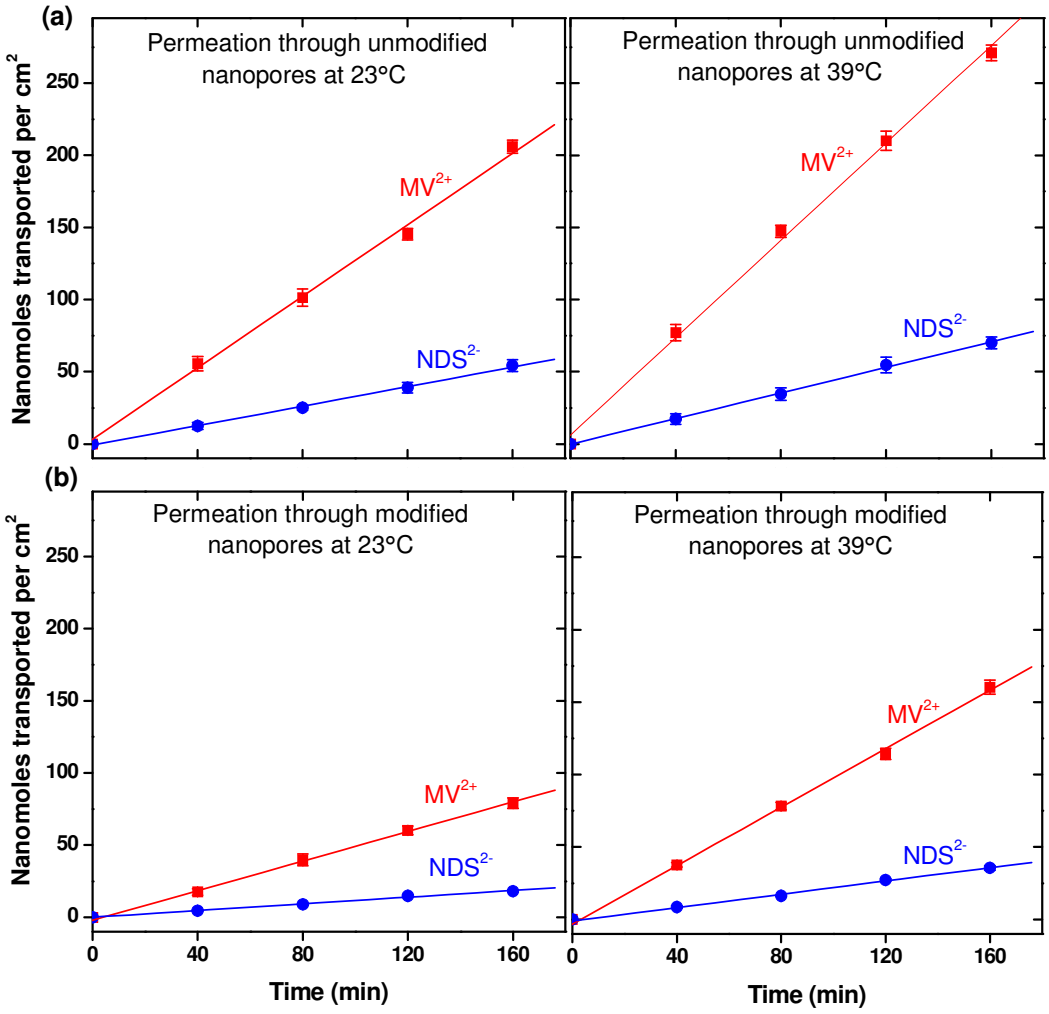

Figure 3.2: Thermally controlled permeation of MV^{2+} and NDS^{2-} molecules through cylindrical nanopore arrays before (a) and after (b) modification with PNIPAAM brushes at low and high temperatures.

Functionalisation of PNIPAAM brushes onto the nanopore surface leads to an about three-fold decrease in the permeation of MV^{2+} (from 206 to 78 nanomoles) and NDS^{2-} (from 54 to 18 nanomoles) at 23ºC compared to that of unmodified membrane (Figure 3.2b). This clearly indicates the success of modification reaction, because PNIPAAM brushes are swollen at 23ºC, thus decreasing the effective pore diameter (Figure 3.1). When the temperature of the system is raised from 23 to 39ºC, PNIPAAM brushes suffer a transition from swollen to collapsed state, leading to an increase in the effective nanopore diameter available for analyte permeation. Therefore, at 39ºC the thermal gating (Figure 3.2b) yields significant increase in the nanomoles of each analyte (from ~78 to 160 for MV^{2+} and from ~17 to 36 for NDS^{2-}) transported across the modified-membrane. The analyte permeation rates (number of moles transported per unit time) are also calculated from the slopes of the plots shown in Figure 3.2. It is evident from the data shown in Table 3.1 that permeation rate of both analytes is almost doubled at 39ºC for the case of the modified membrane. On the contrary, for the unmodified membrane we observed an increase of only ~37 and ~33% in the permeation rates of MV^{2+} and NDS^{2-} molecules, respectively. Importantly, reversible switching of the thermal gating for the modified membrane can be demonstrated by cycling the temperature between 23 and 39ºC (Figure 3.3).

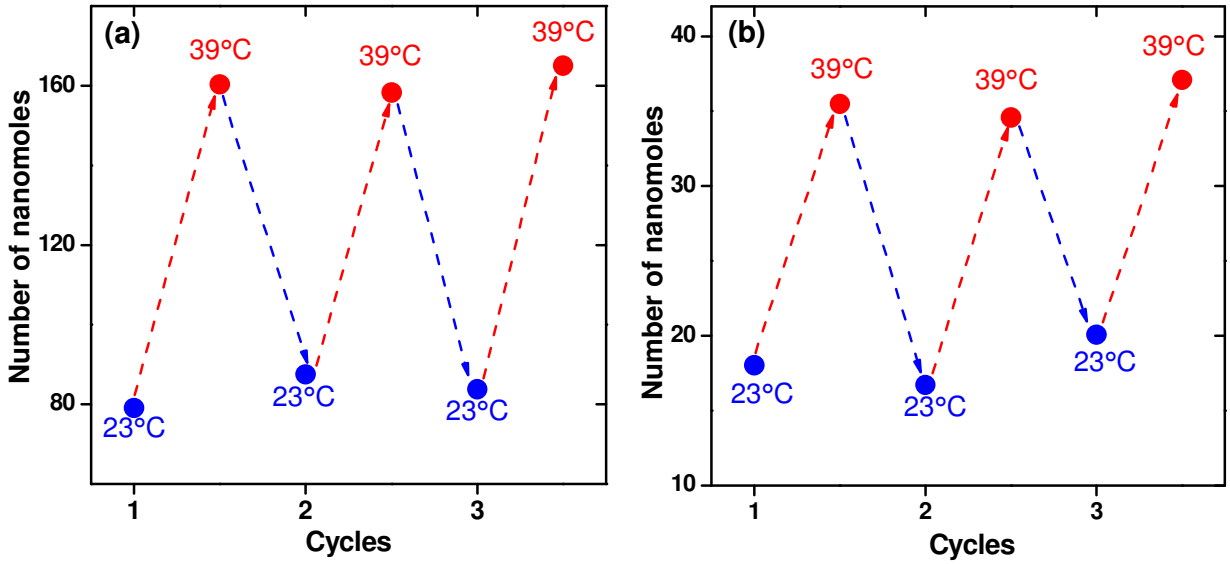

Figure 3.3: Reversible switching of thermal gating of the modified membrane; (a) for the transport of MV^{2+} and (b) NDS^{2-} molecules through the cylindrical nanopore arrays at low and high temperature.

Table 3.1: Analyte permeation rates (nanomoles cm^{-2} min^{-1}) before and after modification through cylindrical nanopore arrays at low and high temperature.

	MV^{2+} permeation rate			*NDS^{2-} permeation rate*		
Cylindrical nanopores	23ºC	39ºC	Increase (%)	23ºC	39ºC	Increase (%)
Unmodified	1.27	1.74	37	0.33	0.44	33
Modified	0.50	0.98	97	0.12	0.23	92

Here, it should be pointed out that for the case of cylindrical nanoporous membrane, we are expecting the removal of fixed surface charges after immobilisation of uncharged PNIPAAM chains onto the pore walls, leading to the loss of permselective behaviour of the modified membrane. But the observed concentration of MV^{2+} (78 nanomoles) in the permeat half-cell is higher than that of NDS^{2-} (17 nanomoles) after 160 min of diffusion time (Figure 3.2b). A plausible explanation for the diminished NDS^{2-} permeation is the following: 1)

The modification reaction occurs everywhere on the track-etched membrane, and the PNIPAAM chains attached on the surface and pore entrance cause hinderence to the diffusion of polymer chains inside the interior of the nanopore. 2) Due to narrow size and longer length (L = 12 µm) of the cylindrical nanopore, the covalent immobilisation of PNIPAAM chains might not be achieved completely throughout the whole length of the pore. Especially, the middle portion of the cylindrical nanopores was partially modified because swollen uncharged polymer chains can not diffuse freely into the interior of the hydrophilic nanopore,[95] leaving some of COOH groups unmodified. Under our experimental condition these groups are ionised (–COO^-), facilitating the transport of cationic (MV^{2+}) species and diminishing the anionic (NDS^{2-}) transport.

3.1.3.2 Conical nanopore arrays

Furthermore, mass transport experiments were also performed with multipore membranes containing an array of conical nanopores in order to support our finding. At room temperature (23 °C), the immobilised PNIPAAM chains remain swollen, thus decreasing the effective cross-section (tip opening) of the conical nanopores, resulting in reduced analyte permeation rates. Increasing the temperature above LCST promotes drastic changes of the conformational state of the PNIPAAM chains. In this case, the polymer chains undergo a transition into a collapsed state which has also an impact on the effective nanopore diameter as shown in Figure 3.4. The conformational transition into a more compact state promotes the widening of the nanochannel which is evidenced as an increase in the ionic analyte permeation rates at 39 °C.

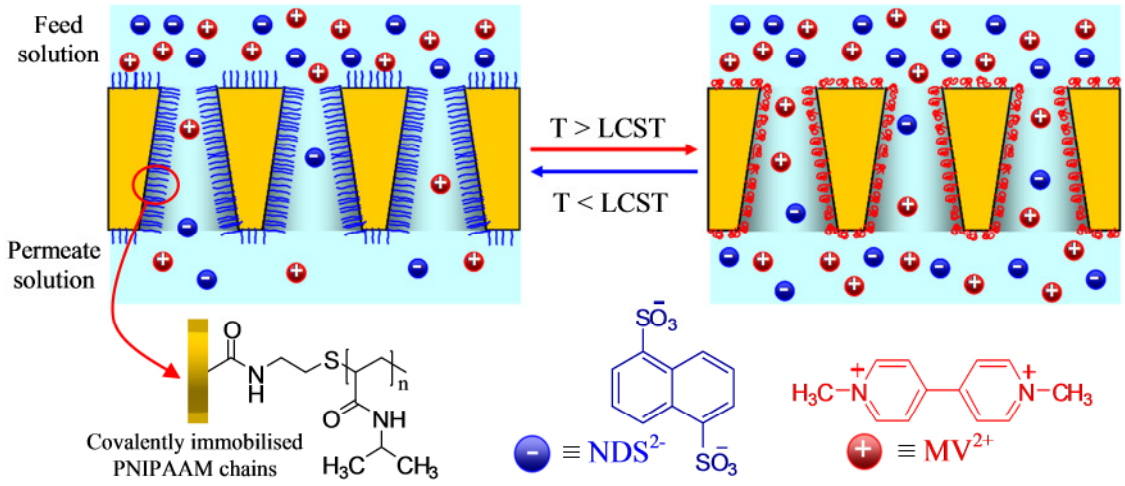

Figure 3.4: The thermally-driven conformational transitions of the attached polymer brushes and respective transport of ionic molecules through an array of conical nanopores across the modified membrane below (left) and above (right) the lower critical solubility temperature (LCST) of the PNIPAAM chains.

Figure 3.5 shows the permeation of charged analyte molecules as a function of time through the conical nanopores before and after modification of the surface with PNIPAAM chains. It is well-known that for the case of conical nanopore, the tip region mainly controls the permselective ionic transport across the membrane.[46,140-143] From the permeation data shown in Figure 3.5a, it is obvious that the as-prepared (unmodified) membrane selectively transports MV^{2+} molecules due to the presence of ionised –COO^- groups on the pore surface, while the co-ions (NDS^{2-}) are electrostatically excluded from entering the conical nanopores. A minor increase was observed in the number of the MV^{2+} nanomoles transported across the unmodified membrane when the temperature of the system was increased from 23 to 39°C due to viscosity change of the solution. This increase is most commonly due to the following reasons: 1) Decrease in viscosity of the feed solution, and 2) higher

diffusion rates or increased solubility of the permeating analyte molecules. We did not observe any detectable amount of NDS^{2-} molecules in the permeate-half cell even at high temperature (Figure 3.5a).

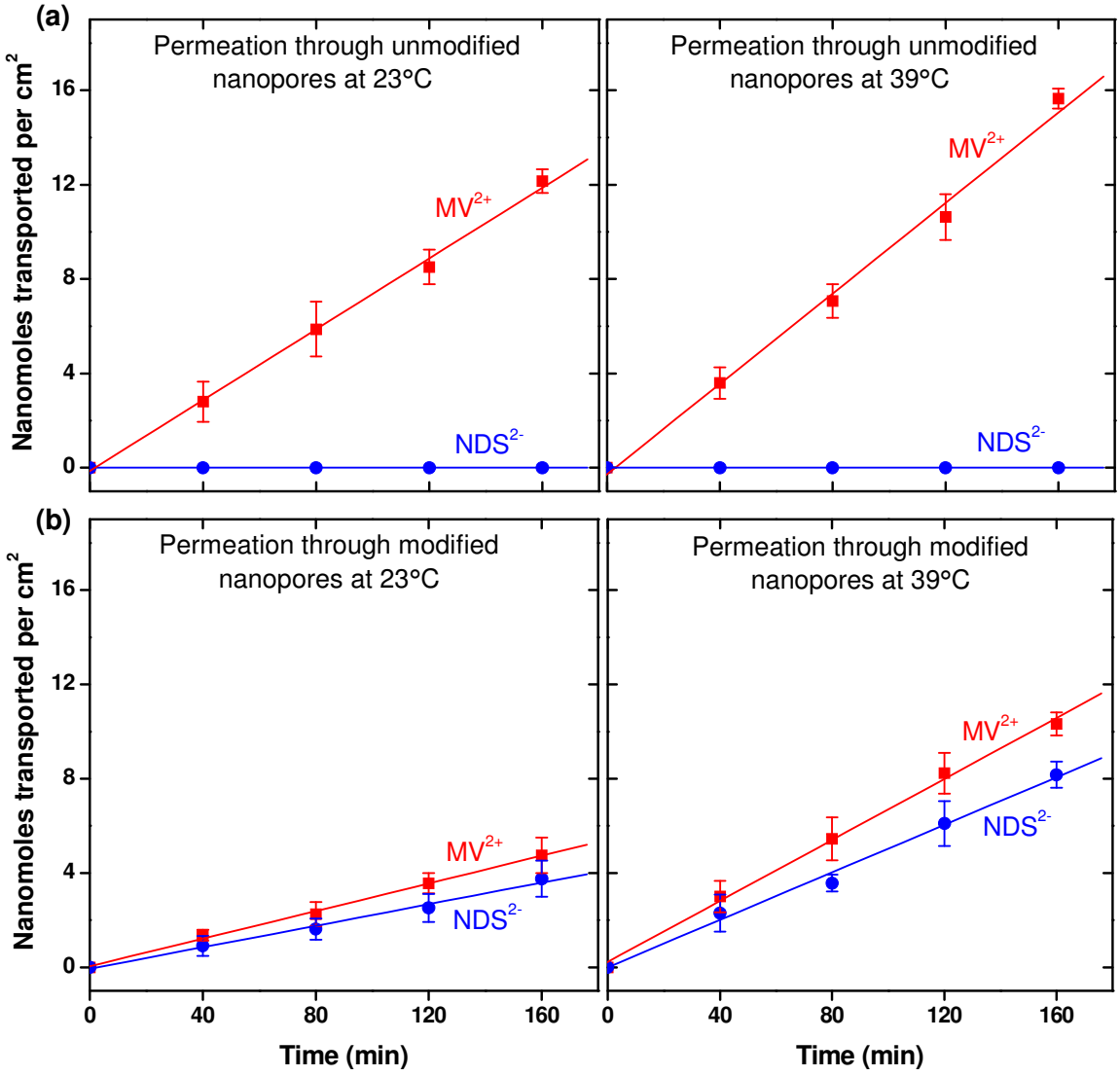

Figure 3.5: Temperature-dependent permeation of NDS^{2-} and MV^{2+} molecules prior to (a) and after (b) modification of an array of conical nanopores (5×10^7 pores cm^{-2}) with tip and base openings of ~18±3 and 500±5 nm in diameters, respectively.

Figure 3.5b shows the permeation data for the case of the modified membrane at low and high temperatures. After functionalisation, the inner walls of the nanoporous membrane (especially the tip region of the conical nanopores) become approximately neutral due to the presence of the uncharged PNIPAAM chains. After 160 min of diffusion time, the transport of MV^{2+} (~4.7 nanomoles cm^{-2}) and NDS^{2-} (~4 nanomoles cm^{-2}) at low temperature is almost the same in spite of their opposite charge (Figure 3.5b). At 39ºC, the thermal gating (Figure 3.4) yields an increased transport (from 4.7 to 10.3 nanomoles cm^{-2} for MV^{2+} and from 3.8 to 8.0 nanomoles cm^{-2} for NDS^{2-}). Table 3.2 shows the permeation rates (calculated from the slopes of the plots in Figure 3.5) of the charged molecules through the conical nanopore arrays before and after modification of the membrane. For the unmodified membrane we observed an increase of only ~27% in the MV^{2+} permeation rate. After modification, a significant increase was observed in the permeation rates of both analytes when the temperature of the system increased from 23 to 39ºC due to the transition of immobilised PNIPAAM chains

from swollen to collapsed state (Figure 3.5b). Moreover, modified conical nanoporous membrane exhibits reversiblity in gating performance (Figure 3.6).

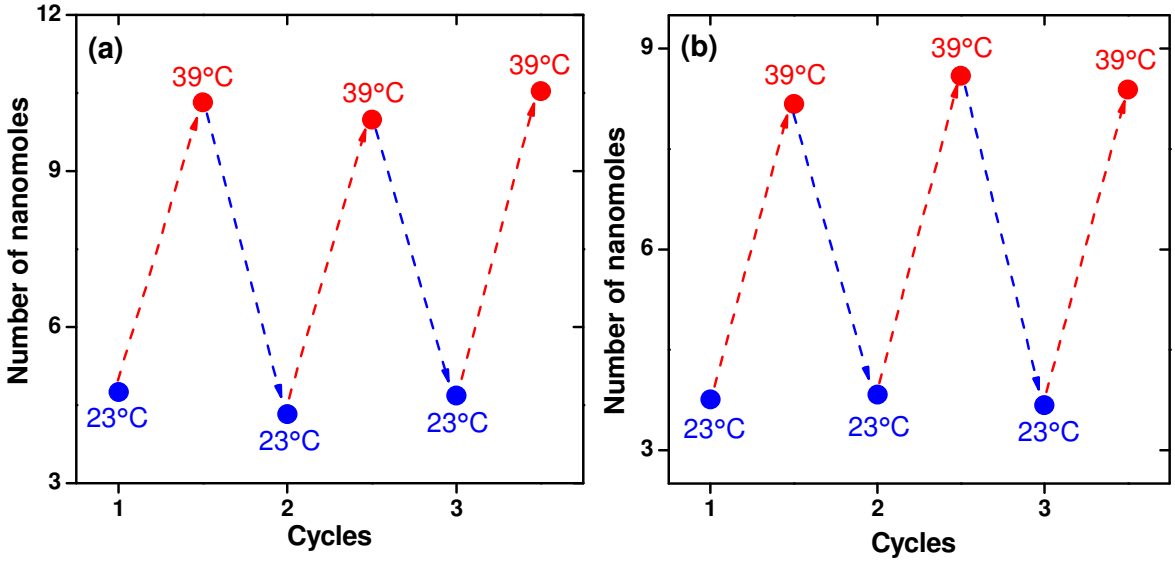

Figure 3.6: Reversible switching of thermal gating of the modified membrane; (a) for the transport of MV^{2+} and (b) NDS^{2-} molecules through arrays of conical nanopores at low and high temperature.

Table 3.2: Analyte permeation rates (nanomoles cm^{-2} min^{-1}) before and after modification through conical nanopore arrays at low and high temperature.

	MV^{2+} permeation rate			*NDS^{2-} permeation rate*		
Conical nanopores	23ºC	39ºC	Increase (%)	23ºC	39ºC	Increase (%)
Unmodified	0.074	0.094	27	–	–	–
Modified	0.029	0.066	128	0.023	0.05	117

On the basis of above-mentioned results we conclude that the gating performance of arrays of conical nanopores (Figure 3.5b) is much better when compared to that of cylindrical nanopore arrays (Figure 3.2b) after immobilisation of polymer chains due to the following reasons: (1) Polymer molecules diffuse freely into the pore and are immobilised throughout the whole length of the conical nanopore. (2) The tip of the cone is considered as the most sensitive part of the conical nanopores. Therefore, the pore tip with immobilised polymer chains acted as a gate-keeper, and controls the trafficking of ionic species flowing through the conical nanopores across the modified membrane. Moreover, the pore tip also has the ability to sense a minor change in the pore surface charge upon chemical modification, and/ or effective pore diameter in response to external stimulus, i.e., environmental temperature.

3.1.4 Single conical nanopore

To check further the gating mechanism at the nanoscale level experiments with a single nanopore were carried out. Figure 3.7 shows the *I-V* curves of a single conical nanopore before and after PNIPAAM functionalization. It is well-known that conical polymeric nanopores exhibit ion selectivity and current rectification phenomena similar to those of biological ion channels.[3] The unmodified nanopore rectifies the current because of the asymmetrical distribution of the negative surface charges (see the nanofluidic “diode” of

Figure 3.7a). After PNIPAAM immobilisation, however, the surface charge is switched from negative to approximately neutral, and consequently the modified nanopore exhibits a linear *I–V* curve (see the "resistor" of Figure 3.7b). Additional evidence of the thermal gating is provided by an increase in the ionic current through the modified nanopore at potentials of +2 and -2V observed upon heating from 23 to 39ºC (Figure 3.7b). Under these conditions, the unmodified nanopore exhibits only a minor change in the rectified ion current at positive potential (Figure 3.7a). Figure 3.7b clearly shows that the attachment of PNIPAAM chains inside confined geometries via the "grafting to" approach is feasible and allows thermally controlled ionic transport through the conical nanopore. This question is significant for potential applications since brush layers grafted on open surfaces tend to swell to a larger extent than those geometrically confined within the nanopore.

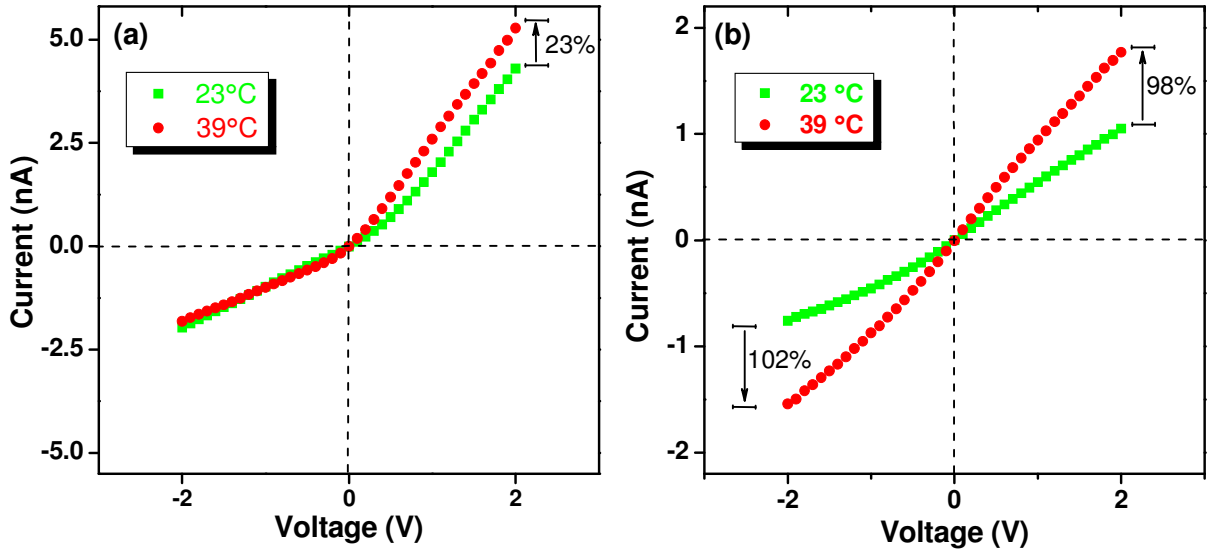

Figure 3.7: Temperature-dependent current–voltage (*I–V*) curves of a single conical nanopore prior to (a) and after (b) modification with PNIPAAM molecules. The tip diameter of the conical pore is ~15 nm.

3.1.5 Conclusions

In conclusion, reversible temperature-dependent ionic transport through an array of nanopores (cylindrical and conical), and also through a single conical nanopore functionalised with amine-terminated PNIPAAM brushes was demonstrated. The effective nanopore diameter for the permeation of ionic species is externally controlled by the swelling/ shrinking of the polymer brushes attached to the nanopore surface upon manipulating the environmental temperature. While pH and temperature-tunable asymmetric ionic transport through single nanopore has recently been demonstrated with similar temperature-responsive polymers. Up to now, the questions of the ionic analyte permeation through thermo-responsive PET membranes containing arrays of cylindrical (Figure 3.2) and conical nanopores (Figure 3.5) were not considered. These findings will further broaden the range of possibilities to design nanoporous systems which respond to a variety of stimuli such as pH, light, and dual-responsive stimuli (pH and temperature or pH and light) on the way to applications in directed molecular transport and separation, and targeted drug delivery at the nanoscale level. For example, a solution containing a mixture of hydrophobic and hydrophilic molecules can be resolved based on the hydrophilicity of the modified pore surface which can be tuned by the temperature change. Below the LCST, pore walls become hydrophilic, allowing the permeation of hydrophobic molecules, while above the LCST, the hydrophilic pore surface allows only the transport of hydrophobic molecules across the modified membrane. Moreover, thermoresponsive membranes modified with copolymers of NIPAAM containing cationic/anionic monomers can be employed for the separation of biomolecules based on their isoelectric points.

A previous study with poly(vinylidene fluoride) membranes graft modified with poly(acrylic acid) chains by radiation-induced grafting[144] showed that the ionic selectivity can also be tuned with variable permeability membranes. Our results suggest that both thermal and electrical effects could be combined at the nanoscale in order to modify the permeation rates of ionic drugs. The gating effect is significant at the single nanopore level as well as the nanopore array level, which is most relevant for chemical and pharmaceutical processes involving charged biomolecules and drugs in aqueous solutions.

3.2 Optical Gating of Photosensitive Synthetic Ion Channels [XI]

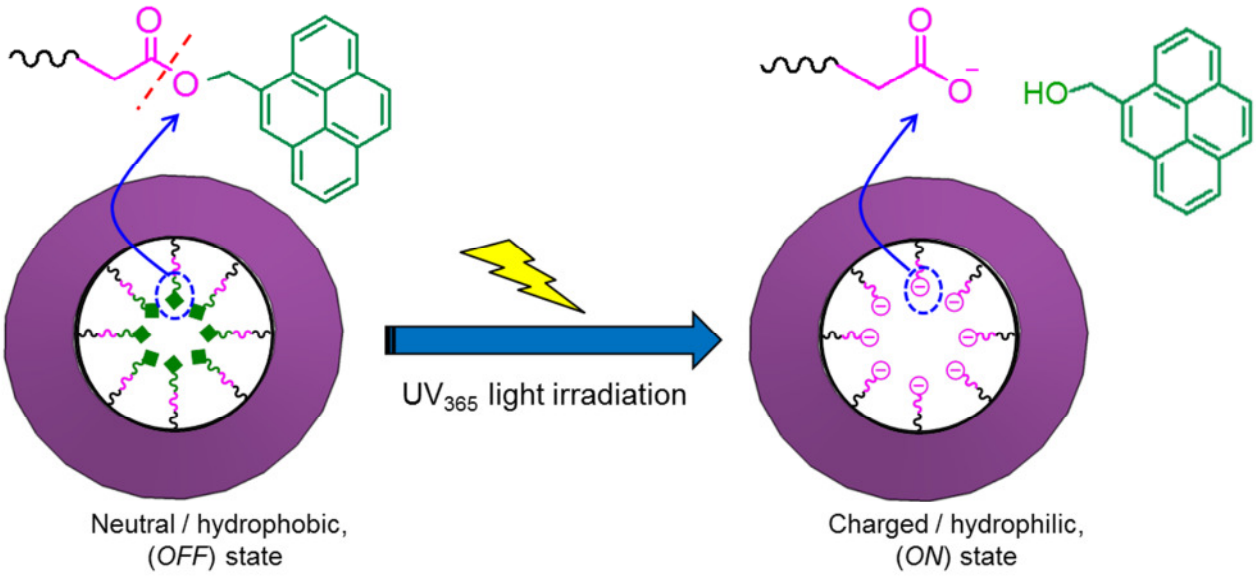

In this section the use of 4-oxo-4-(pyren-4-ylmethoxy) butanoic acid as a photo-labile protecting group is described to show the optical gating of nanofluidic devices based on synthetic ion channels. The inner surface of the channels is decorated with monolayers of photo-labile hydrophobic molecules that can be removed by irradiation, which leads to the generation of hydrophilic groups. This process can be exploited in the UV light-triggered permselective transport of ionic species in aqueous solution through the channels. The optical gating of a single conical nanochannel and multichannel polymeric membranes is evaluated experimentally and theoretically by means of current–voltage and selective permeation measurements, respectively. One can anticipate that the integration of nanostructures into multifunctional devices is feasible and will readily find applications in light-induced controlled release, sensing, and information processing.

[XI] Published work:

Ali, M.; Nasir, S.; Ramirez, P.; Ahmed, I.; Nguyen, Q. H.; Fruk, L.; Mafe, S.; Ensinger, W. "Optical gating of photosensitive synthetic ion channels" *Advanced Functional Materials* **2012,** 22, (2), 390-396.

DOI: 10.1002/adfm.201102146

3.2.1 Introduction

The miniaturisation of fluidic devices that may respond to external triggering is crucial to mimic and exploit the functionality of biological ion channels in health sciences and biotechnology.[5,145] In nature, ion channels regulate the flow of permeants across the cell membrane, allowing physiological functions such as energy storage and signal transduction.[1] Natural ion channels and pores such as α-hemolysin provide structures whose interfacial chemistry can be controlled with high precision.[29] However, these nanostructures are not suitable for practical applications due to their fragility and the sensitivity of the embedding lipid bilayer to external parameters such as pH, temperature, and salt concentration. Synthetic nanochannels show some advantages over their biological counterparts such as stability, tunable channel diameter and shape, possibility of integration into nanofluidic devices, and tailored surface properties.[6,10] Furthermore, these nanochannels exhibit transport properties similar to those of biological ion channels, such as current rectification, voltage-dependent current gating, and permselectivity to ionic species.[41,141-143] In particular, current rectification in conical nanochannels and nanopipettes occurs due to the combined effect of the surface charge and the conical geometry under an applied voltage.[146-148]

Several approaches have been pursued to achieve active control over ion transport in nanoconfined geometries. To this end, the channel surface was decorated with a variety of chemical functionalities that responded to external stimuli such as ions in solution,[107,108] biomolecules,[64,67,69,113,115] light,[55,56] pH,[34,65,72,100,102,104] temperature[73,137] or both pH and temperature.[76,86] The design of nanochannels sensitive to ultraviolet (UV) light still constitutes a challenge for current techniques. Unlike a chemical stimulus, UV light is non-invasive and the whole process can easily be tuned by manipulating the light wavelength. Moreover, UV light can be used to induce a wide range of photochemical changes, *e.g.* triggering molecular rearrangements and leading to the cleavage of chemical bonds.[149]

Numerous photo-labile protecting groups (PPGs) have been reported which are based on different mechanisms involving the excitation of chromophores.[93,94,132] PPGs have been widely used in organic synthesis,[150] for protecting carbohydrates,[151] in biochemistry (*e.g.* as "caged compounds"),[152] and in solid phase and combinatorial synthesis.[153] The most interesting feature of PPGs is that they can be cleaved upon exposure to long UV wavelength (UV_{365}) without causing any damage to the rest of the molecule directly attached to the substrate. Photoremovable protecting molecules have also been successfully employed in the polymer backbone and self-assembled monolayers to control the surface wettability as well as in controlled release processes.[96,131,154] Seminal work by Moore and co-workers involved the design and fabrication of microfluidic devices to regulate liquid flow inside the microchannels modified with photocleavable self-assembled monolayers through UV light irradiation.[155]

Here a novel technique in which photoremovable protecting molecules were used to construct photosensitive nanofluidic devices based on synthetic ion channels is described. For this purpose, the inner walls of the nanochannels are decorated with monolayers of photo-labile protecting molecules. Subsequently, the targeted hydrophobic PPGs are removed by using UV light as an external stimulus, leading to the generation of hydrophilic groups which are responsible for the permselective transport of ionic and molecular species through the channels. First, experimentally and theoretically the UV light-operated conical nanochannel is demonstrated. Second, a collection of nanochannels in a polymeric membrane to obtain a multifunctional nanofluidic device is integrated. It shows that optical gating allows the permselective transport of charged species through the membrane nanochannels. Potential applications of the nanochannel and the multichannel membrane are light-induced controlled release, sensing, and information processing. In particular, most experimental systems proposed previously are based on chemical signals as *inputs* and optical (e.g., fluorescence) signals as *outputs*. The system characterised here could be employed with optical and electrical signals as the inputs and electrical and chemical signal as the outputs.

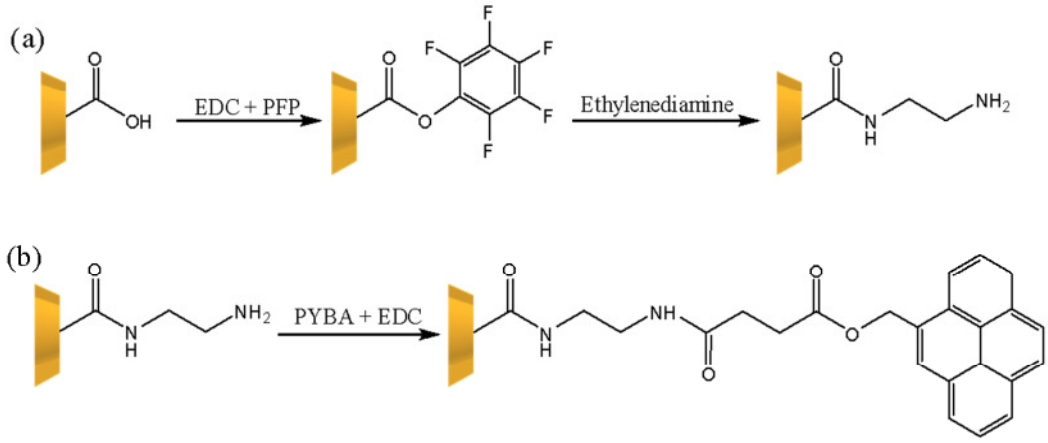

Scheme 3.1: Scheme of the chemical functionalisation of the inner nanochannel surface.

3.2.2 Immobilization of photo-labile PYBA molecules

Ion track-etched polyethylene terephthalate (PET) membranes containing a single conical nanochannel and cylindrical nanochannel arrays (5×10^8 channels cm^{-2}) were used for the fabrication of the photosensitive nanofluidic devices. During the track-etching process, carboxyl (–COOH) groups were generated on the surface and the inner channel walls.[156] These moieties served as starting points for the introduction of other responsive chemical functionalities onto the channel surface. The immobilisation of PPGs onto the inner channel walls was accomplished in a two-step process (Scheme 3.1),[101] as described in the experimental section 2.6.3 (Chapter 2).

3.2.3 Single conical nanochannels

For the case of a single conical nanochannel, the success of surface modification reactions was corroborated by measuring the current–voltage (*I–V*) characteristics,[69,100,110,120] which are dictated by the electrostatic interaction of the charged channel surface with the mobile ions in the inside solution.

Figure 3.8a shows the *I–V* curves prior to and after EDA functionalisation. The recordings were obtained under symmetric electrolyte conditions using a 0.1M KCl solution prepared in a 10 mM phosphate buffer (pH = 6.0). The current rectification of the single conical nanochannel is due to the surface charge and polarity.[147,148,157] Before modification, the nanochannel is cation selective and thus rectifies the cation flux. The preferential direction of the flux is from the narrow cone opening to the wide opening because of the negative $–COO^-$ groups.[135] After amidation, the nanochannel surface charge was switched from negative to positive, resulting in an anionic selectivity and the concomitant inversion in the rectification characteristics.[58,67,68,101,115]

Figure 3.8b shows the *I–V* curves of the same conical nanochannel, modified now with monolayers of photo-labile PYBA molecules, before and after UV_{365} light irradiation. As expected, immobilisation of PYBA resulted in the loss of channel surface charge due to the presence of uncharged terminal pyrene moieties. Eventually, the PYBA-modified channel behaved like an ohmic resistor (the net surface charge on the channel walls was zero). Upon UV_{365} light irradiation of the PYBA-modified channel, the ester bond adjoining the pyrene chromophore was cleaved,[131,154] resulting in the generation of –COOH functionalities on the channel surface (Figure 3.9). Under our experimental conditions, the exposed carboxyl groups are ionised ($–COO^-$),[135] which restores the cation-selective behaviour of the channel. This reveals that upon UV light irradiation the inner environment of the nanochannel was switched from a hydrophobic, nonconducting (*off*) state to a hydrophilic, conducting (*on*) state (Figure 3.9). Thus, the UV light-induced change in the surface charge modulates the permselective behaviour of the channel: the *I–V* curve shows an eight-fold increase in the rectified ionic current (from 100 to

800 pA approximately; see Figure 3.8b) after irradiation. Moreover, the *I-V* curves show a significant recovery of most of the protected carboxyl groups (compare the NH_3^+ curve at $V < 0$ of Figure 3.8a with the PYBA curve at $V > 0$ after irradiation of Figure 3.8b.) Light-controlled modulation provides then a feasible tool to externally tune the electrical behaviour of the nanochannel by exploiting the interactions between the charged inner walls and the mobile ionic species in solution.

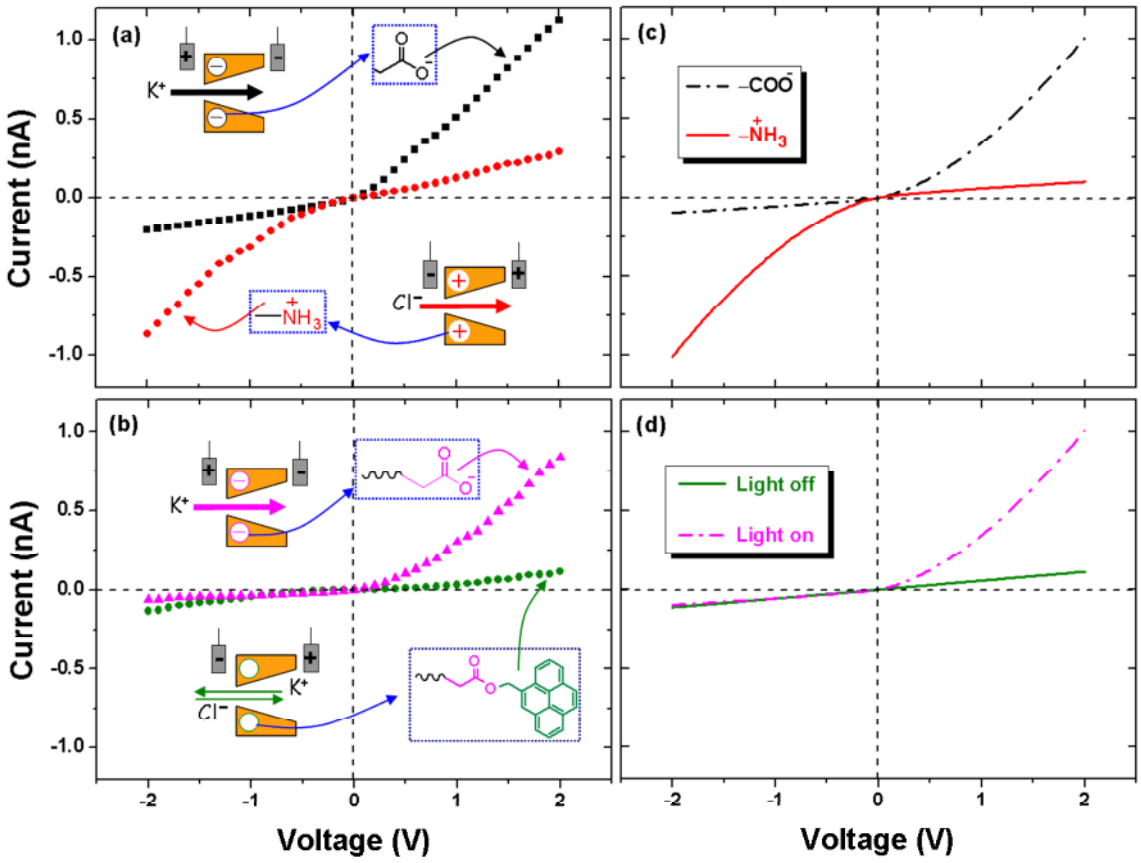

Figure 3.8: (a) *I–V* curves of single conical nanochannels bearing ionised carboxyl and amine groups in a 0.1 M KCl (pH = 6.0) aqueous solution. (b) *I–V* characteristics of the same nanochannel modified with photosensitive PYBA molecules before and after UV light irradiation. (c) and (d) *I–V* theoretical curves corresponding to the experimental curves (a) and (b) respectively. The approximate radii are a_B = 140 nm for the channel base and a_T = 2 nm for the channel tip (COO^- and NH_3^+ pores). For the PYBA pore, a_B = 139 nm and a_T = 1 nm.

3.2.4 Theoretical Modeling [XII]

The experimental results of Figures 3.8a and 3.8b can be described theoretically (by theoretician collaborators in Spain) in terms of a continuous model based on the Poisson and Nernst-Planck (PNP) equations.[147]

[XII] Prof. Dr. P. Ramirez (Universitat Politècnica de València, Spain) and Prof. Dr. S. Mafe (Universitat de València, Spain) are highly acknowledged for the theoretical modelling of experimental results.

$$\nabla^2\phi = \frac{F^2}{\varepsilon RT}\left(c_{Cl^-} - c_{K^+}\right) \tag{1}$$

$$\nabla \cdot \vec{J}_i = -\nabla \cdot \left[D_i \left(\nabla c_i + z_i c_i \nabla \phi \right) \right] = 0 \, , i = K^+, Cl^- \tag{2}$$

where $\vec{J}_i$, c_i, D_i and z_i are the flux, the local concentration, the diffusion coefficient and the charge number of ion i (i = K^+ and Cl^-), with ϕ and ε being the local electric potential and the dielectric permittivity of the solution within the pore, respectively. F is the Faraday constant, R is the gas constant, and T is the temperature.

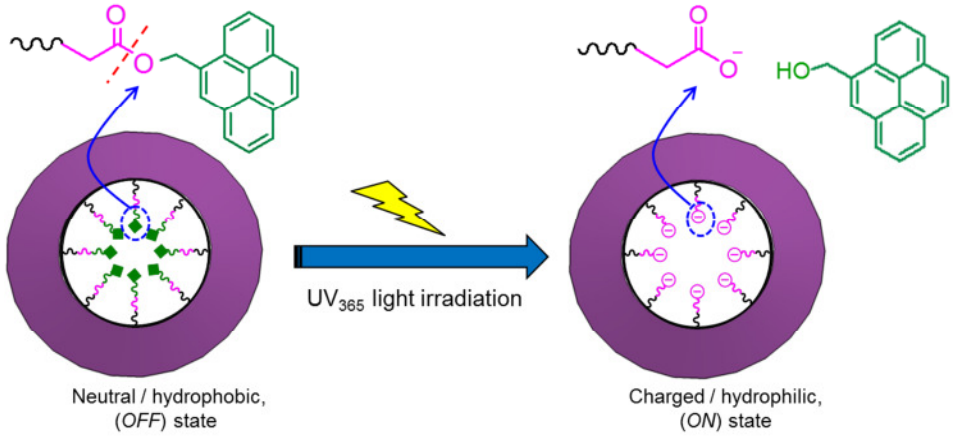

Figure 3.9: Schematic illustration of the wettability changes produced by UV light irradiation of a single conical nanochannel modified with photoremovable protecting molecules.

The theoretical results obtained using the above model are shown in Figures 3.8c and 3.8d and correspond to the experimental *I–V* curves of Figures 3.8a and 3.8b. The nanochannel radii and the surface concentrations of negative ($–COO^-$) and positive ($–NH_3^+$) fixed charge groups before the functionalisation of the UV-sensitive moiety were estimated as follows. Microscopy techniques give the approximate value a_B = (140 ± 5) nm for the radius of the conical channel base. Introducing this value in the theoretical model gives the fitting parameters a_T = 2 nm and σ = 0.1 e/nm^2 for the radius of the channel tip and the channel surface charge density, respectively (Figure 3.8a). These values agree with those previously found in similar nanochannels[68] and give theoretical curves (Figure 3.8c) that can describe the experimental data (Figure 3.8a) without invoking particular channel shape effects.[148] We use later the same parameters for the charged nanochannel of Figure 3.8b in the theoretical fitting of Figure 3.8d. Again, the agreement between the theoretical and experimental curves indicates that the substitution of the original charged groups by the UV-sensitive moieties is almost complete. For the neutralised nanochannel, the a_B = 139 nm, a_T = 1 nm, and σ = 0.1 e/nm^2 is obtained, which is consistent with the fact that the channel with the attached UV-sensitive moiety should have a lower effective radius than the original channel.

3.2.4 Multichannel membranes

UV light-induced changes in the channel surface properties were further investigated by transport experiments using a PYBA-modified nanoporous membrane containing an array of cylindrical nanochannels containing an aerial density of 5 × 10^8 channels cm^{-2} with an average diameter of (20 ± 3) nm. Ionic species carrying opposite charge to that of the channel surface will be attracted to and transported selectively through

the channel. On the contrary, species with charge of the same sign as that of the surface charge will be repelled and prevented from entering the channel.[51,136] Finally, neutral channels are non-selective, *i.e.*, both cationic and anionic species are equally transported across the membrane (Figure 3.10).

For the transport experiments, the PYBA-modified nanoporous membrane was mounted between the two compartments of a conductivity cell and the feed compartment was filled with a 10 mM aqueous solution of methylviologen (MV^{2+}) or 1,5-naphthalenedisulfonate (NDS^{2-}) in a phosphate buffer (pH = 6.0).

There are three major effects dictating the transport through nanochannels: (a) volume exclusion, (b) hydrophobic, and (c) electrostatic interactions. The transport of the MV^{2+} and NDS^{2-} molecules is studied because of the following reasons: (i) they have similar molecular volumes (0.637 and 0.680 nm^3, respectively),[17] (ii) the molecular structures of both MV^{2+} and NDS^{2-} contain two benzyl rings giving similar hydrophobic behaviour within the nanopores, and (iii) the molecules have the same charge number in absolute value (they are oppositely charged). Hence, only the surface charges dictate the ionic permeation via electrostatic interactions. Because an electrical double layer is formed in the channel, the inside solution has a higher concentration of counter-ions (MV^{2+}) than co-ions (NDS^{2-}).

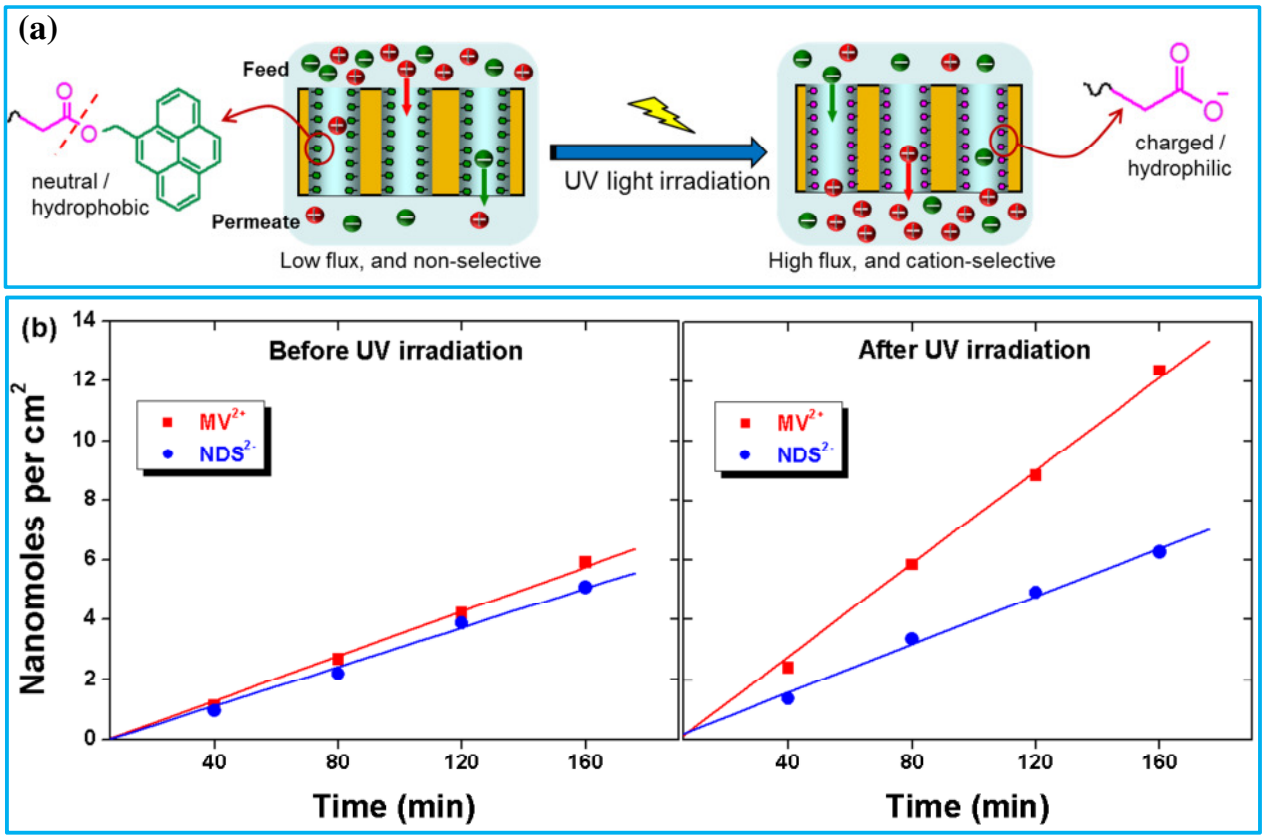

Figure 3.10: (a) Schematic illustration of the transport of ionic species through the multi-channel membrane before and after UV irradiation. (b) Permeation data for MV^{2+} and NDS^{2-} prior to and after UV treatment of the PYBA-modified membrane. The fluxes are obtained for an array of cylindrical nanochannels with an average diameter (20 ± 3) nm in a multipore membrane.

Figure 3.10b shows the number of moles for the charged analytes MV^{2+} and NDS^{2-} transported per cm^2 of the PYBA-modified membrane *versus* time before and after UV light irradiation. The order of magnitude of the MV^{2+} permeation flux (number of moles transported per cm^2 per second) can be estimated from Figure 3.10b as $J = (8 \times 10^{-9}$ mol/$cm^2)/6000$ s ~ 10^{-12} mol cm^{-2} s^{-1}. Comparison of this flux with the theoretical estimation $J = \varepsilon Dc/d$ where ε is the porosity, D is the effective diffusion coefficient, c is the feed concentration, and d is the membrane thickness, leads to the effective value $\varepsilon D = 10^{-10}$ cm^2 s^{-1} for $c = 10^{-5}$ mol cm^{-3} and $d = 10^{-3}$ cm.

Before the irradiation, the inner walls of the multichannel membrane are neutral due to the presence of the uncharged photo-labile pyrene moieties. These moieties were responsible for the absence of permselective characteristic of the membrane channels. The permeation of both MV^{2+} and NDS^{2-} molecules is similar despite their opposite charges (see Figure 3.10b) before the UV treatment. After 160 minutes of analyte diffusion, 5.9 and 5.1 nanomoles of MV^{2+} and NDS^{2-} were transported through the membrane, respectively. However, these quantities were very different after light irradiation. The permeation of MV^{2+} was remarkably increased with respect to the permeation of NDS^{2-} (see Figure 3.10b): the light-induced gating led to an increase of ~110% in the number of moles of MV^{2+} transported (from 5.9 to 12.4 nanomoles) while this increase was only of ~23% in the case of NDS^{2-} (from 5.1 to 6.3 nanomoles). Upon UV irradiation of the PYBA-modified channels, the targeted photo-labile pyrene moieties were removed leading to exposed carboxylate ($–COO^-$) groups. These moieties transformed the neutral and hydrophobic inner channel walls into the negatively charged and hydrophilic channel walls. Therefore, UV irradiation acted as an optical gating, allowing the PYBA-modified membrane to select the cationic MV^{2+} species over the anionic NDS^{2-} ones. Note finally that we should expect the selectivity of the membranes to change also with the solute size in experiments with other bulky analytes because the pore radius is close to 10 nm.

Table 3.3: YES logic function for the single nanochannel with an optical input and an electrical output.

Input	Output
UV light	I(nA) at V = +2 V
Off (0)	0.11 (0)
On (1)	0.84 (1)

Table 3.4: YES logic function for the multichannel membrane with an optical input and a chemical output.

Input	Output
UV light	Ionic selectivity S
Off (0)	0.07 (0)
On (1)	0.32 (1)

Table 3.5: AND logic function for single nanochannel with electro-optical inputs and an electrical output.

Input		Output
V (V)	UV light	G (nS)
-2 (0)	Off (0)	0.03 (0)
-2 (0)	On (1)	0.05 (0)
2 (1)	Off (0)	0.06 (0)
2 (1)	On (1)	0.42 (1)

3.2.5 Logic functions and controlled release

Logic functions using different combinations of chemical species and electrical potentials as inputs have been proposed.[158] We demonstrated theoretically and experimentally that single-track conical nanochannels functionalised with polyprotic acid chains show three levels of conductance that could be tuned externally because of the pH-sensitive fixed charges.[100] Binary and multivalued logical functions were implemented using chemical and electrical inputs.[100] Other logical gate schemes with nanochannels have recently been proposed.[110,120,140] Potential applications of nanofluidics-based logical functions involve information processing, sensing, and controlled release of chemicals in liquid media. In particular, integration of microchannels and nanochannels in chip-based ionic circuits[159] should be useful for analytical and pharmaceutical applications.

Light-based molecular systems for information processing typically use chemical signals as inputs and optical (e.g. fluorescence) signals as outputs.[160,161] Alternatively, the light-gated nanochannel studied here could be used to implement a variety of logic functions using optical and electrical signal as the inputs and electrical and chemical signals as the outputs. Some examples are given in Tables 3.3–3.5 where the multichannel membrane selectivity was quantified by the ratio of ionic fluxes $S = \left(J_{MV^{2+}} - J_{NDS^{2-}}\right) / \left(J_{MV^{2+}} + J_{NDS^{2-}}\right)$. From the experimental data of Figure 3.10b, S = 0.067 before the UV irradiation while S = 0.320 after irradiation. Future implementation of reset functions could be achieved by light-induced conformational changes in the functionalised molecules, thus avoiding the irreversible molecular detaching employed here.

Irreversibility phenomena and accumulation of chemical waste could be serious problems for chemically driven molecular logic devices. While in this case the reset function could be provided by light-induced conformational changes in the functionalised molecules,[162] the fact is that for controlled release applications based on the optical gating of the multichannel membrane (see Figure 3.10), the irreversibility should not be a serious issue because the chemical drug is intended to be absorbed by the external solution after release.

3.2.6 Conclusions

In this study 4-oxo-4-(pyren-4-ylmethoxy) butanoic acid was used as the photo-labile protecting group to design a light-gated nanofluidic device based on synthetic ion channels. The inner walls of the channels were decorated with monolayers of photo-labile molecules that can be removed by irradiation with UV light. This process leads to the generation of hydrophilic groups and the concomitant perm-selective transport of the ionic species in aqueous solution through the channels. In particular, experimentally and theoretically the optical gating of a conical nanochannel and a multichannel polymeric membrane was characterized by means of current–voltage and selective permeation measurements. It is anticipated that the integration of nanostructures into multifunctional devices is feasible, and should readily find applications in light-induced controlled release, sensing, and information processing. In particular, the nanofluidic devices should allow different optical, chemical and electrical signals to be used as inputs and outputs.

3.3 Nernst-Planck Model of Photo-Triggered, *pH*–Tunable Ionic Transport through Nanopores Functionalized with "Caged" Lysine Chains [XIII]

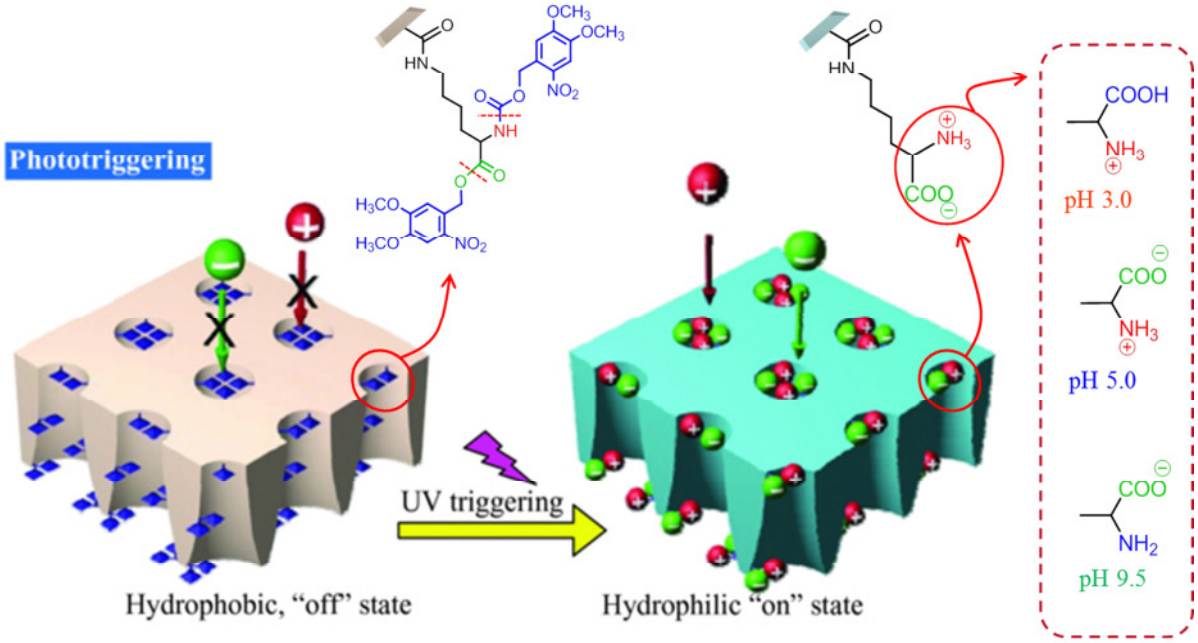

The fabrication of asymmetric nanopores sensitive to ultraviolet (UV) light and a detailed account of the divalent ionic transport through these pores using a theoretical model based on the Nernst-Planck equations is described in this section of the thesis. Central to this work is to decorate the pore surface with lysine chains having pH-sensitive (amine and carboxylic acid) moieties that are caged with photo-labile 4,5-dimethoxy-2-nitrobenzyl (NVOC) groups. The uncharged hydrophobic NVOC groups are removed using UV irradiation, leading to the generation of hydrophilic "uncaged" amphoteric groups on the pore surface. It is demonstrated experimentally that polymer membranes containing single pore and arrays of asymmetric nanopores can be employed for the pH-controlled transport of ionic and molecular analytes. Comparison between theory and experiment allows for understanding the individual properties of the phototriggered nanopores and provides also useful clues for the design and fabrication of multipore membranes to be used in practical applications.

[XIII] Published work:

Nasir, S.; Ramirez, P.; Ali, M.; Ahmed, I.; Fruk, L.; Mafe, S.; Ensinger, W. "Nernst-Planck model of photo-triggered, pH-tunable ionic transport through nanopores functionalized with "caged" lysine chains" *Journal of Chemical Physics* **2013,** 138, (3), 034709.

DOI: 10.1063/1.4775811

3.3.1 Introduction

Nanoscale pores have been studied extensively in the last decade due to the new basic phenomena involved and the potential applications in medicine,[118,145] nanofluidics,[163,164] membrane science[165] and biotechnology.[6] Polymer samples containing single asymmetric nanopores and multipore arrays obtained by track-etching[41] are of particular interest because they mimic some of the transport properties of biological ion channels.[10,11,66,79,142] Recent advances concerning the fabrication processes and the tailoring of the surface properties have permitted to control the pore geometry[99,166,167] and the response to external stimuli such as voltage,[168] temperature,[77,86] *pH*[65,75,100] or the presence of a given analyte in the pore solution.[63,64,76,120] These features have allowed the fabrication of nanofluidic devices[65,67,103] with potential applications in sensing,[8,11] energy harvesting[86,140] and information processing.[140,169]

Recently, synthetic nanopores sensitive to ultraviolet (UV) light have been reported.[61,92] The pores use photo-labile protecting groups (PPGs) or photosensitive active groups, initially in hydrophobic state, that switch to a hydrophilic form after UV light irradiation. UV light constitutes a facile way to change the pore functionalities externally, without causing further damage to the active groups attached to the pore wall.

In this work a technique to obtain asymmetric nanopores sensitive to UV light is described. To achieve this goal, the "caged" lysine amino acid is chemically synthesized with an unprotected amine group at the terminus of alkyl chain. Then the pore surface and inner pore walls are functionalized with monolayers of amino acid "caged" lysine chains through carbodiimide coupling chemistry. The immobilized lysine chains contain photolysable 4,5-dimethoxy-2-nitrobenzyl (NVOC) moieties attached to the $-NH_2$ and –COOH groups at α–carbon of lysine. Upon UV treatment, the uncharged hydrophobic aromatic chromophore NVOC moieties are removed and hydrophilic "uncaged" amphoteric groups sensitive to environmental pH are exposed on the pore surface. The UV treated asymmetric nanopore displays a broad range of *pH*-controlled rectifying properties. Firstly, we demonstrate experimentally that polymer samples containing single and multiple UV light-operated pores can be employed for the *pH*-controlled transport of divalent anionic and cationic analytes across the membrane. Secondly, we present a detailed account of the experimental findings using a theoretical model based on the Nernst-Planck (NP) equation. The systematic comparison of the model predictions with the experimental data allows for the estimation of the pore characteristics and the diffusion coefficients of the divalent analytes. The approach provides an understanding of the properties of a single pore that should be useful in the design of multipore membranes for sensing, controlled release, and information processing.

3.3.2 Synthesis and immobilization of Photosensitive "caged" amino acid lysine

Single asymmetric nanopores (Figure 3.11a) as well as multipore membranes containing arrays of pores were fabricated from heavy ion tracked polyethylene terephthalate (PET) membranes of thickness 12 µm by well-established track-etching techniques.[41] During the chemical etching process, the carboxylic acid groups generated on the pore surface act as sites for the covalent attachment of functional molecules containing primary amine in their backbone.

The photosensitive "caged" lysine amino acid with a free amine group at ε-position was synthesized following the chemical reactions shown (see experimental section 2.6.5 for details in chapter 2) in the scheme of Figure 3.11b. The compound 3 was obtained in high yield by the esterification reaction between Fmoc-Lys(Boc)-OH (1) and 6-nitroveratryl alcohol (2) using dicyclohexyl carbodiimide (DCC) and 4-(dimethyl amino)-pyridine (DMAP) in dichloromethane at room temperature. The deprotection of Fmoc-group in 3 yields compound 4 (Figure 3.11b), which was used without purification in the next reaction step. The compound 6 was synthesized by the direct coupling reaction between deprotected amine of compound 4 with reactive 4,5-

dimethoxy-2-nirobenzyl chloroformate 5 (NVOC-Cl). Finally, the deprotection of Boc-group in 6 afforded the desired lysine (7).

The "caged" lysine chains (7) of Figure 3.11b were immobilized on the pore surface and inner walls through carbodiimide coupling chemistry (see experimental section 2.6.5 for details). To this end, the track-etched membranes were treated with an activation solution containing *N*-(3-dimethylaminopropyl-*N'*-ethylcarbodiimide (EDC) and pentafluorophenol (PFP) to convert the native –COOH groups into amine-reactive ester molecules. Subsequently, the activated PFP-ester molecules were covalently coupled with the terminal ε-amine group of photosensitive lysine molecules.

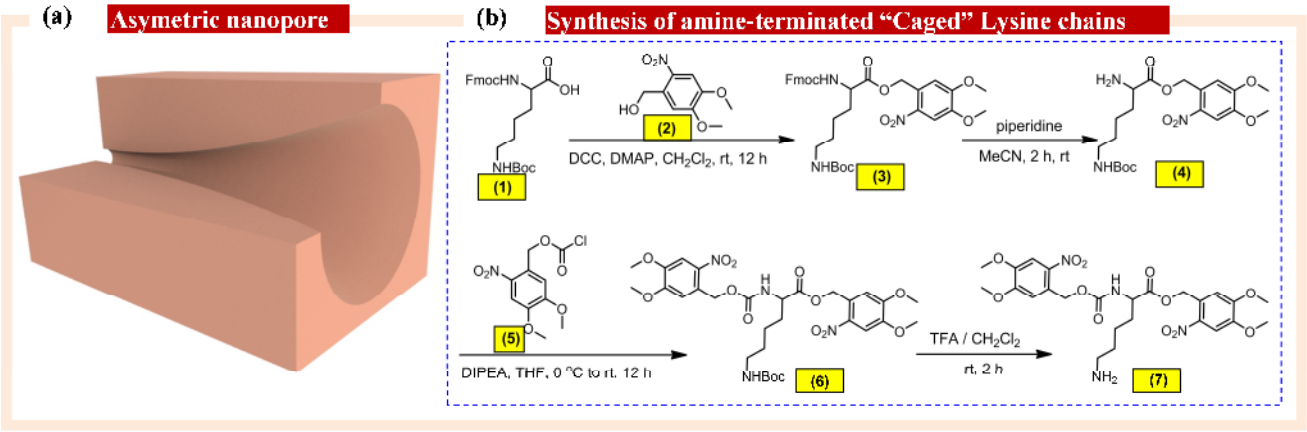

Figure 3.11: a) Scheme (not to scale) of the asymmetric nanopore. b) Reaction scheme for the synthesis of "caged" amino acid lysine (7) with caged amine and carboxylic acid groups attached to the α-carbon.

3.3.3 Single asymmetric nanopore

The success of the pore surface modification reaction was confirmed by measuring the current–voltage (*I–V*) characteristics of a single nanopore prior to and after the immobilization of "caged" lysine chains (Figure 3.12). For the case of as-prepared nanopores, native ionized carboxylate ($–COO^-$) groups impart negative charge to the pore walls under neutral and basic *pH* conditions. Therefore, the asymmetric single pore shows rectification characteristics that depend on the surface charge of the pore walls, which can be tuned by the *pH* value of the external solutions. By changing the solution *pH* from basic to acidic values, a significant decrease in positive currents (from the pore tip to the pore basis) is observed, suggesting a decrease in the surface charge density due to the protonation of –COOH groups (Figure 3.12a).

After functionalization, the hydrophobic and uncharged photolabile NVOC groups in the immobilized lysine chains drastically reduce the ionic current and rectification, as it is shown in the *I–V* curve of Figure 3.12b. This experimental fact confirms the successful anchoring of "caged" lysine chains onto the surface and walls of the pore.

Upon UV light irradiation of the pore, the NVOC groups are detached from the immobilized lysine chains and the amphoteric groups are exposed on the pore surface. This switches the chemical characteristics of the pore from hydrophobic to hydrophilic, which in turn changes the ion transport behavior (Figure 3.12c) from non-selective ("off" state) to perm-selective ("on" state).

Due to the amphoteric nature of the resulting end groups, the *pH* of the surrounding solutions dictates the pore net charge and permselectivity. The *I–V* curves of Figure 3.12c confirm the successful uncaging of the $–NH_2$ and –COOH groups of lysine chains immobilized on the pore surface. At *pH* = 9.5, both groups are deprotonated and the net charge on the pore surface is negative due to the presence of ionized $–COO^-$ groups.

The pore is cation-selective and rectifies the ionic current flowing across the membrane. On the contrary, at acidic conditions (*pH* = 3.0) both groups are protonated and the $-NH_3^+$ groups impart positive charge to the pore. Due to the switching of the pore net charge from negative to positive, the permselectivity and rectification behavior is also reversed (the pore is now anion-selective). Finally, at the intermediate *pH* = 5.0, the pore behaves like an ohmic resistor because the net pore charge is zero due to the ionization of the $-COO^-$ and $-NH_3^+$ groups (Figure 3.12c). It is interesting to note that this behavior is present to some degree in the case of the *I–V* curves corresponding to the pore with "caged" lysine chains (Figure 3.12b). This fact reveals the presence of a small amount of residual "uncaged" amphoteric groups in the pore surface before UV irradiation.

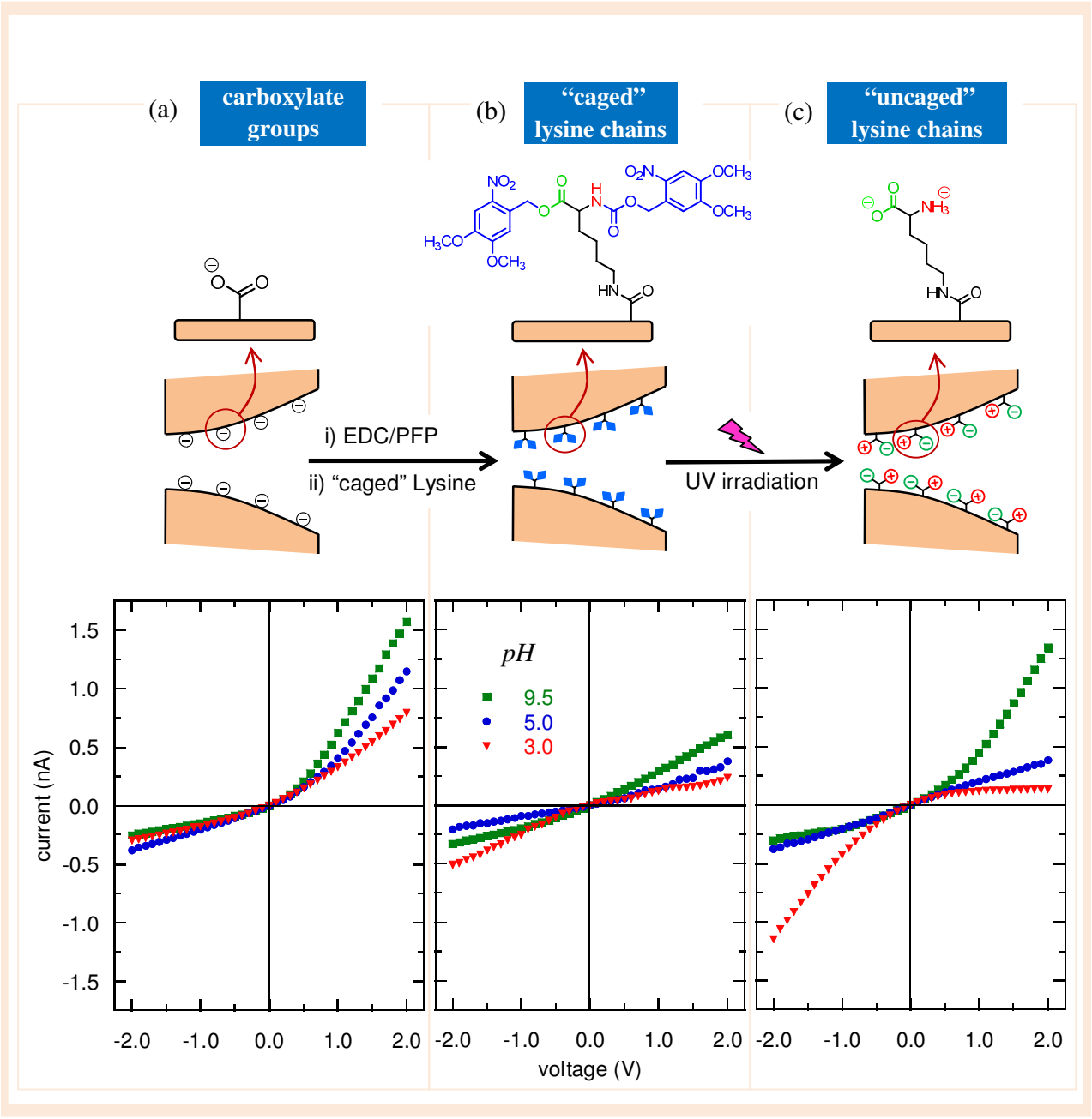

Figure 3.12: Schematic pore and *pH*-dependent *I–V* curves of a single asymmetric nanopore with carboxylate groups (a), "caged" (b), and "uncaged" amphoteric lysine chains (c). The *I–V* curves are measured in a 0.1 M KCl solution prepared in a phosphate buffer at different *pH* values.

3.3.4 Multipore membranes

It has also been investigated the UV-light-induced transport of divalent analytes across the nanoporous membrane containing 5×10^7 pores cm^{-2} functionalized with "caged" lysine chains (Figure 3.13), prior to and after UV treatment (see experimental section 2.6.5 for detail). The membrane sample separated the feed compartment filled with an aqueous solution of either cationic or anionic analyte and the permeate compartment contained a buffer solution only. The results obtained are presented in Figures 3.14 (methylviologen ion, MV^{2+}) and 3.15 (1,5-naphthalene disulfonate ion, NDS^{2-}). The flux of analyte through the membrane sample (Figures 4d and 5d) was obtained by monitoring the time-dependent concentration of analyte in the permeate chamber (Figures 3.14a, 3.14b, 3.15a and 3.15b) from UV absorbance measurements with a UV/Vis spectrophotometer (Figures 3.14c and 3.15c). The experiments clearly suggest that the transport of analyte is governed by the interaction of the permeate ions with the groups fixed on the pore surface.

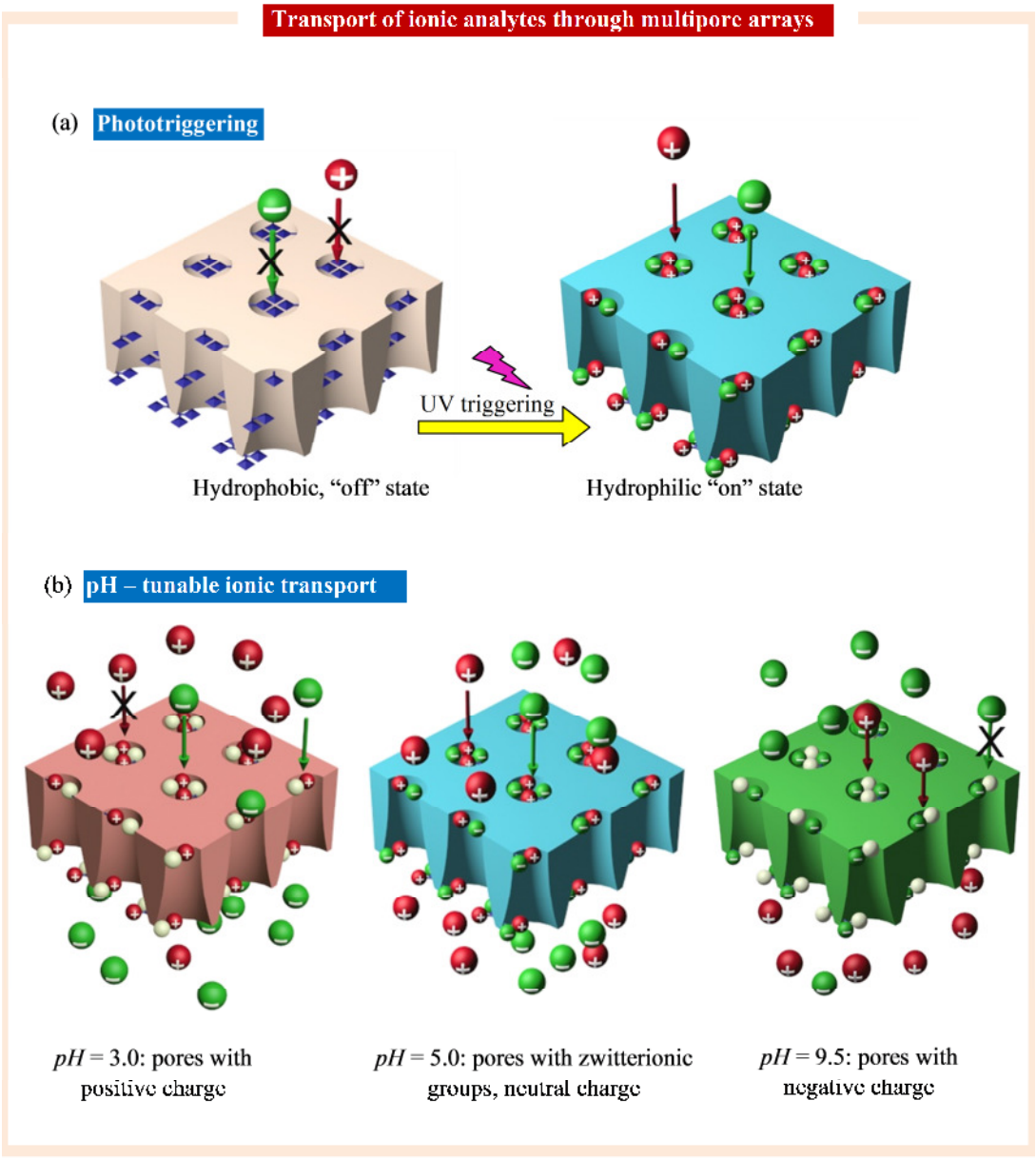

Figure 3.13: Schematic cartoon describing the (a) phototriggered permeation through the asymmetric nanopore arrays bearing "caged" lysine chains ("off" state) and "uncaged" lysine chains ("on" state) on the inner pore walls. (b) The *pH*-tunable permselective transport of ionic analytes across the multipore membrane containing "uncaged" amphoteric lysine chains.

Before UV irradiation (Figure 3.13a, left), the pore is in hydrophobic ("off") state and the divalent ions in the external solutions can hardly enter and pass through the nanopores. The resulting analyte fluxes are therefore relatively small at all *pH* values (Figures 3.14d and 3.15d). After UV irradiation (Figure 3.13a, right) the pore switches to a hydrophilic ("on") state and the analyte fluxes depend markedly on the environmental *pH* (Figure 3.13b). Ionic species with the same sign as that of the pore charge are prevented from entering the membrane while species with opposite charge to that of the pore permeate through the pore. Finally, in the case of neutral pores both positive and negative species are almost equally transported across the pores, and the membrane is non-selective. Note that the pore with "caged" lysine chains (Figures 3.14a and 3.15a) shows qualitatively similar *pH*-controlled transport properties as the pore with "uncaged" lysine groups (Figures 3.14b and 3.15b), which suggests again that some residual "uncaged" amphoteric groups are present in the pore surface before UV irradiation.

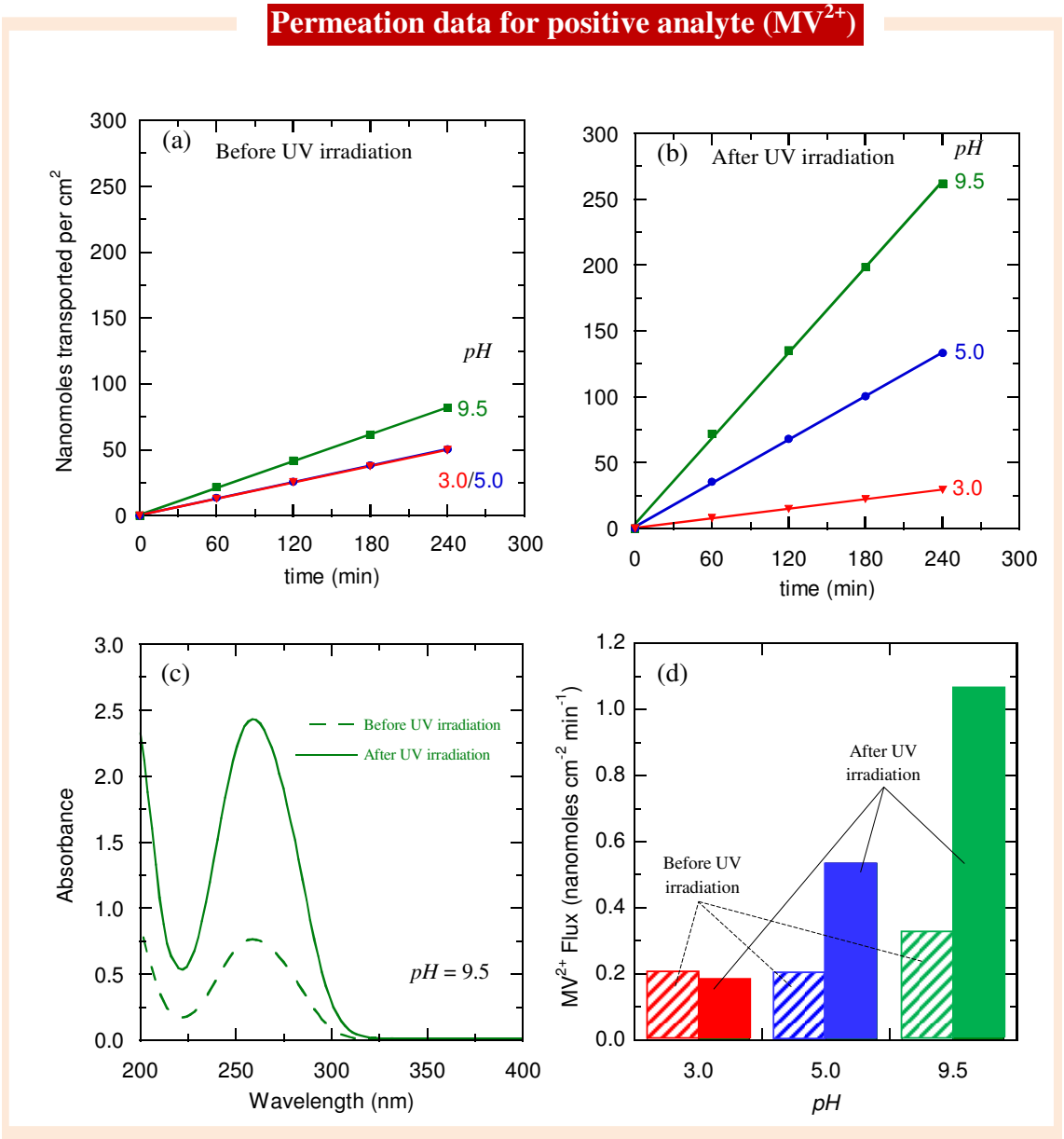

Figure 3.14: pH-dependent permeation of MV^{2+} through the multipore membrane prior to (a) and after (b) UV irradiation. (c) Absorption spectra recorded for MV^{2+} in the permeate solution obtained after 4 hours of analyte transport at *pH* = 9.5 before and after UV irradiation of the membrane. (d) MV^{2+} permeation rates through the multipore membrane before and after UV treatment, respectively.

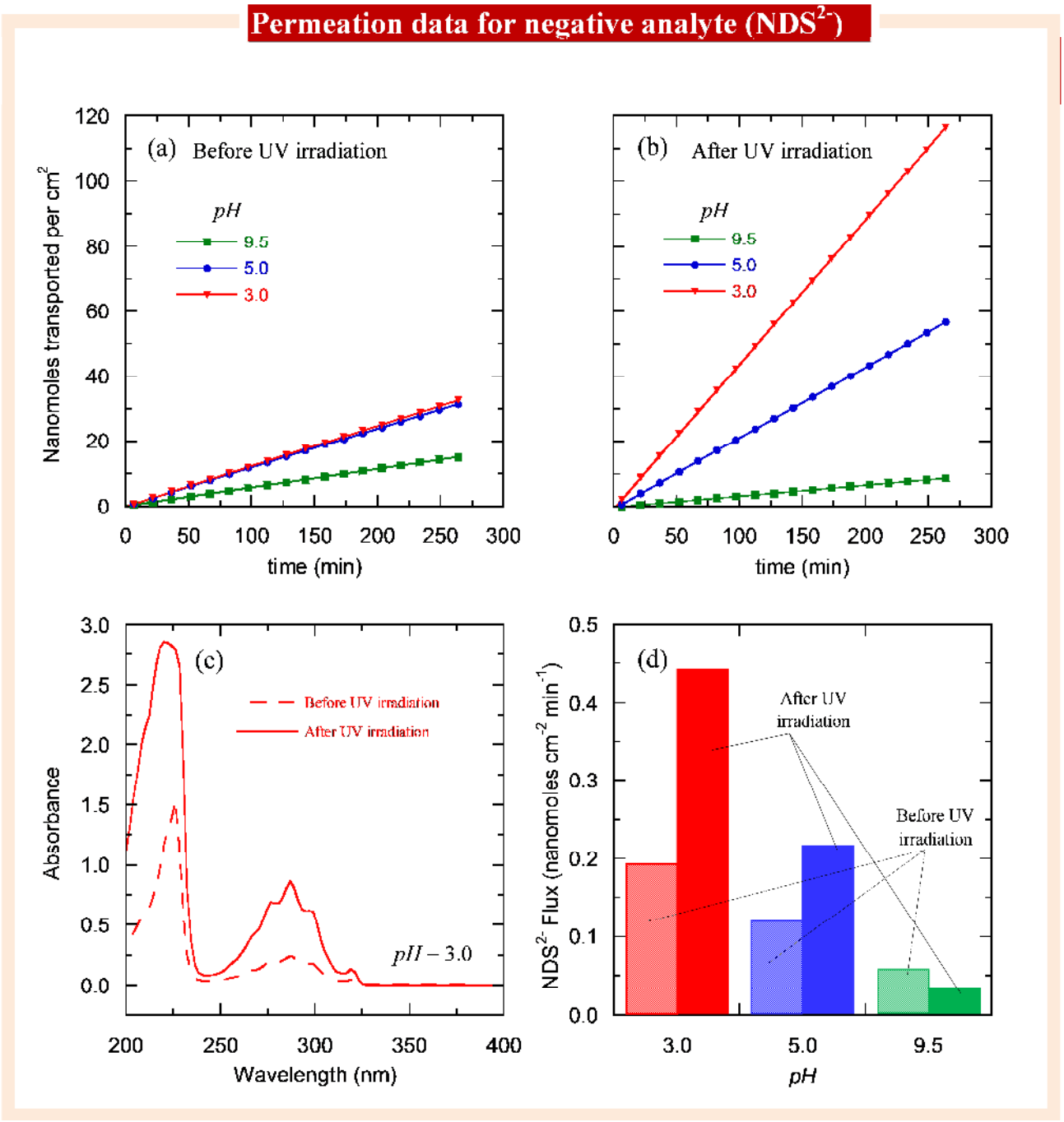

Figure 3.15: pH-dependent permeation of NDS^{2-} through the multipore membrane prior to (a) and after (b) UV irradiation. (c) Absorption spectra recorded for NDS^{2-} in the permeate solution obtained after 4 hours of analyte transport at pH = 3.0 before and after UV irradiation of the membrane. (d) NDS^{2-} permeation rates through the multipore membrane before and after UV treatment, respectively.

3.3.5 Theory [XIV]

The scheme of Figure 3.16 where a polymeric film of thickness d containing a single asymmetric nanopore separates two electrolyte solutions is considered. The pore radius $a(x)$ has symmetry of rotation around the axis x and can be described by the equation:[68,148]

$$a(x) = \frac{a_R - a_L \exp\left[-(d/h)^n\right] - (a_R - a_L)\exp\left[-(x/d)^n (d/h)^n\right]}{1 - \exp\left[-(d/h)^n\right]} \quad (n > 0), \qquad (1)$$

where a_L and a_R are, respectively, the radii at the left (tip) and right (base) pore openings. Typical nanopores obtained using the track-etching procedure show pore openings ranging from a few or tens of nanometers (pore tip) to a few hundreds of nanometers (pore base), while the pore length d is of the order of 10 µm.[41] Therefore, the pores can be assumed to be long and narrow, $d >> a(x)$. The radius profiles generated by Eq. (1) are in agreement with the typical tip shapes obtained by using recent improvements of the track-etching procedure.[68,99,105,166,167] The pore shape can be controlled by changing the values of the geometrical parameters n and d/h in Eq. (1).[148] For instance, $n = 1$ and $d/h > 0$ give profiles showing concave, bullet-like pore tips (the limit $d/h \rightarrow 0$ corresponds to the case of a conical pore). Using $d/h \rightarrow 0$ and $n > 1$ lead to pores with convex, trumpet-like profiles. Finally, the values $d/h > 0$ and $n > 1$ produce profiles showing pore tips and lumens of variable length.[148]

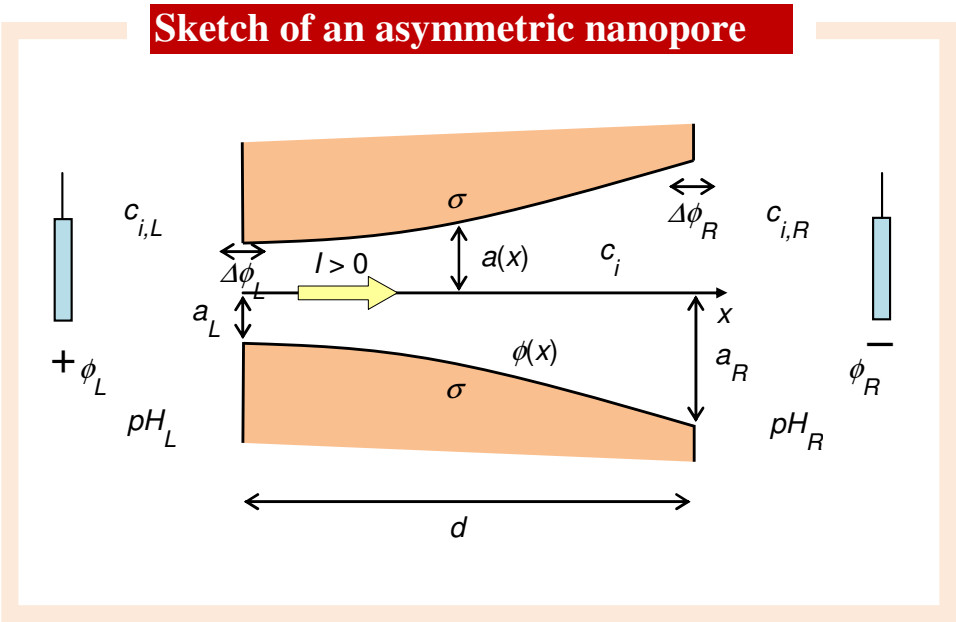

Figure 3.16: Sketch of the asymmetric nanopore (not to scale).

[XIV] Prof. Dr. P. Ramirez (Universitat Politècnica de València, Spain) and Prof. Dr. S. Mafe (Universitat de València, Spain) are highly acknowledged for the theoretical modelling of experimental results.

In Figure 3.16, pH_j refers to the pH value of solution j ($j = L$ for the left and $j = R$ for the right external solutions). In the following calculations, we assume $pH_L = pH_R \equiv pH$. Also, $c_{i,j}$ is the concentration of ion i in the bulk of solution j and ϕ_j denotes the dimensionless electric potential (normalized to RT/F, where R, T anf F have their usual meaning[148]) in the bulk of the solution j, respectively. Finally, c_i and ϕ refer to the local concentration of species i and dimensionless electric potential, respectively. The potential drops $\Delta\phi_L = \phi\ (0) - \phi_L$ and $\Delta\phi_R = \phi_R - \phi(d)$, are the Donnan potential differences through the left and right interfaces, respectively. Finally, σ is the surface charge density, assumed to be constant and related to the volume concentration of fixed charges X_F as

$$X_F = \frac{2\sigma}{aF}. \tag{2}$$

The external solutions are considered to be ideal and perfectly stirred (the effect of the diffusion boundary layers is ignored because the resistance to flow is due to the single nanopore) and the system is isothermal and at steady state. Finally, convective flows are ignored (note that the experiments of Figures 3.14 and 3.15 are conducted under zero electric current).

It is assumed that the ionic transport through the pore can be described by the Nernst-Planck equation

$$\vec{J}_i = -D_i\left(\vec{\nabla}c_i + z_i c_i \vec{\nabla}\phi\right), \tag{3}$$

the continuity equation at steady state

$$\nabla \cdot \vec{J}_i = 0, \tag{4}$$

and the Poisson equation

$$\nabla^2\phi = -\frac{F^2}{\varepsilon RT}\left(\sum_i z_i c_i + X_F\right). \tag{5}$$

In Eqs. (3) – (5), D_i, z_i and $\vec{J}_i$ are the diffusion coefficient, the charge number and the ionic flux density of ion i, respectively, and ε is the electric permittivity of the aqueous solution (approximately equal to that of water).

As stated above, the pore is long and narrow, and the ionic fluxes can be assumed to have only axial component

$$\vec{J}_i \approx J_i \hat{u}_x. \tag{6}$$

According with this approximation,

$$j_i \approx -\pi a^2 D_i\left(\frac{dc_i}{dx} + z_i c_i \frac{d\phi}{dx}\right), \tag{7}$$

where

$$j_i = \pi a^2 J_i \tag{8}$$

is the total flux of ion *i* through an arbitrary section of the pore (Eq. (1)). Equation (4) is then approximated as

$$\frac{dj_i}{dx} = 0 . \tag{9}$$

Finally, the local electroneutrality condition

$$\sum_i z_i c_i + X_F = 0 \tag{10}$$

can be used instead of the Poisson equation in the case of long pores. Indeed, for one-dimensional problems where averaging to the longitudinal channel axis is assumed, Eq. (10) can replace the Poisson equation when the axial pore length is much greater than the Debye length,[170,171] which is the region where significant deviations from electroneutrality occur. The Debye length is typically 3 – 30 nm thick for most aqueous electrolyte solutions. Our pore is 12000 nm long while the pore tip radii are in the 5 nm range. Therefore, Eq. (10) constitutes a useful approximation to the complex transport phenomena studied here.

The values of the electric potential and the ionic concentrations at the pore limits $x = 0$ and $x = L$ are unknown and must be calculated in terms of those in the external solutions. Again, the influence of the access resistance can be neglected, because the pore is long and narrow, and we can assume the Donnan equilibria[16,170,171] at the interfaces at $x = 0$ and $x = d$ (Figure 3.16):

$$c_i(0) = c_L \exp\left(-z_i \Delta\phi_L\right), \tag{11a}$$

$$c_i(d) = c_R \exp\left(z_i \Delta\phi_R\right). \tag{11b}$$

Combining Eqs. (10) and (11) with the electroneutrality condition in the bulk of the external solutions

$$\sum_i z_i c_{i,j} = 0 , \; j = L, R \tag{12}$$

allows for the calculation of the concentrations of all mobile ionic species at the pore limits, $c_i(0)$ and $c_i(d)$, and the interfacial Donnan potential differences (Figure 3.16) at any value pH_j. Finally, Eqs. (7)-(10), together with the boundary conditions given in Eqs. (11) – (12), can be integrated using iterative schemes to obtain the concentrations and electric potential profiles, as well as the total fluxes, for any applied voltage $V \equiv RT(\phi_L - \phi_R)/F$. From the ionic fluxes, the total electric current passing through the pore is

$$I = \sum_i z_i F j_i \tag{13}$$

Note that Figure 3.16 shows the sign criteria used for *V* and *I*. Mathematically, the solution to the above transport equations could be obtained as an inverse problem where the structural characteristics of the nanopore should be determined from measurements of its function.[172]

However, we will use simple, approximate models that address the phenomenological basis of the observed phenomena.

3.3.5.1 A single pore with COOH groups

In the case of the as-prepared single nanopore with native –COOH groups, we have considered the following equilibrium between the neutral and ionized carboxylate groups

$$\mathrm{COOH} \underset{\longleftarrow}{\overset{K_C}{\longrightarrow}} \mathrm{COO^-} + \mathrm{H^+}, \tag{14}$$

The local fixed charge concentration in Eq. (2) can be written as

$$X_F = -X_C^- = -\frac{X_C^T}{1 + c_{H^+}/K_C}, \tag{15}$$

where

$$K_C = 10^{-pK_C} = \frac{X_C^- c_{\mathrm{H^+}}}{X_C^0}, \tag{16}$$

is the equilibrium constant of Eq. (14), X_C^- and X_C^0 are the volume concentration of carboxylic groups in ionized and neutral forms, respectively, and

$$X_C^T = X_C^- + X_C^0 \tag{17}$$

is the total volume concentration of carboxylic groups.

3.3.5.2 A single pore with amphoteric groups

For a pore containing amphoteric groups, we have considered the equilibria

$$\mathrm{NH_3^+ - A - COOH} \underset{\longleftarrow}{\overset{K_{A,1}}{\longrightarrow}} \mathrm{NH_3^+ - A - COO^- + H^+}, \tag{18}$$

$$\mathrm{NH_3^+ - A - COO^-} \underset{\longleftarrow}{\overset{K_{A,2}}{\longrightarrow}} \mathrm{NH_2 - A - COO^- + H^+}, \tag{19}$$

and the local volume fixed charge concentration of Eq. (2) is now

$$X_F = X_A^+ - X_A^- = \frac{X_A^T\left[c_{H^+}^2/(K_{A,1}K_{A,2}) - 1\right]}{1 + c_{H^+}/K_{A,2} + c_{H^+}^2/(K_{A,1}K_{A,2})}, \tag{20}$$

where

$$K_{A,1} = 10^{-pK_{A,1}} = \frac{X_A^{\pm} c_{H^+}}{X_A^+}, \quad (21)$$

$$K_{A,2} = 10^{-pK_{A,2}} = \frac{X_A^- c_{H^+}}{X_A^{\pm}}, \quad (22)$$

are the equilibrium constants in Eqs. (18) and (19), $X_A^{\pm}$, X_A^- and X_A^+ are the volume concentration of amphoteric groups in zwitterionic, negatively charged, and positively charged forms, respectively, and $X_A^T = X_A^- + X_A^+ + X_A^{\pm}$ is the total volume concentration of amphoteric groups in the pore. For the sake of simplicity, we have assumed that the surface charge concentration in the pore is constant and equal to that calculated for the pore tip.

3.3.5.3 Estimation of the pore parameters

The pore parameters involved in the transport process were estimated according to the following protocol. The radius of the pore base was measured directly using AFM techniques in polymer samples with a high number of pores etched simultaneously with the sample containing the single nanopore. In our case, we obtained $a_R \approx 300$ nm. Because small variations in a_R lead to negligible changes in the calculated *I–V* curves, we employed this value in all calculations. We used also the free solution diffusion coefficients. D_{K^+} = 1.95 10^{-5} cm^2/s, D_{Cl^-} = 2.03 10^{-5} cm^2/s, D_{H^+} = 9 10^{-5} cm^2/s and D_{OH^-} = 4.5 10^{-5} cm^2/s.[173]

When the pore is uncharged (X_F = 0 and σ = 0 in the model), the *I–V* curves depend only on the concentrations of mobile ions in the surrounding solutions and the geometrical characteristics of the pore. Under these conditions, the concentrations of mobile ions within the pore are constant,

$$c_i = c_{i,L} = c_{i,R} \equiv c_{i,B}, \quad (23)$$

and integration of Eqs. (6)–(10) gives the linear *I–V* curve

$$I = \frac{\kappa}{g_m} V, \quad (24)$$

where

$$\kappa = \frac{F^2}{RT} \sum_i z_i^2 D_i c_{i,B} \quad (25)$$

is the conductivity of the solution inside the pore and

$$g_m = \int_0^d \frac{dx}{\pi a^2} \quad (26)$$

is a geometrical factor depending exclusively on the pore shape (see Eq. (1) for $a(x)$). In the case of a conical pore, this factor gives

$$g_m = \frac{d}{\pi a_L a_R}. \qquad (27)$$

Note that for $a_L = a_R$, Eq. (27) gives the well-known result corresponding to the cylindrical pore (Figure 3.11). For geometries other than cylindrical (or conical), Eq. (26) must be solved numerically taken into account the radius profile of Eq. (1).

In the experiments of Figure 3.12, the obtained quasi-linear *I–V* curves for the case of the pores containing "uncaged" and "caged" lysine groups when these chains are mostly in zwitterionic form (Figures 3.12b and 3.12c at *pH* = 5.0). A linear fitting using the least square method provides the slopes (pore conductances) of the *I–V* curves. Because the concentrations of all ionic species can be calculated from the electrolyte concentration and the *pH* of the external solutions, the only free parameter in the slope of the straight line is the geometrical factor g_m. The results obtained for the experimental data in Figures 3.12b and 3.12c are summarized in Table 3.6. Once the value of *gm* has been determined, the radius of the pore tip can be calculated from Eq. (26) assuming a particular geometry in Eq. (1). Table 3.6 shows the values of a_L obtained using this procedure. We have considered the cases of a perfectly conical pore and an asymmetric pore showing a convex profile that deviates slightly from the conical geometry ($d/h \rightarrow 0$ and $n = 1.5$ in Eq. (1); see Figure 3.16).

Table 3.6: Estimation of pore parameters from least-square fittings of linear *I–V* curves in Figures 3.12b and 3.12c.

	Conductance (nS)	$10^{-9}\, g_m$ (m^{-1})	a_L (nm) conical geometry	a_L (nm) convex tip ($n = 1.5$)
Figure 3.12b	0.1335	11.40	1.1	3.9
Figure 3.12c	0.1936	7.86	1.6	5.1

It is concluded that the assumption of conical geometry gives unrealistically low values of a_L for pores fabricated using the track-etching method.[68,146,147,157] If we assume convex pores, the values of a_L in Table 3.6 are now within the range of those estimated in previous studies. [68,146,147,157] Otherwise stated, we will assume thus that the pore tip is convex and deviates slightly from the conical geometry. As expected, the effective pore radii obtained for the pores with "caged" lysine chains are significantly lower than those corresponding to the "uncaged" chains (Table 3.6), in agreement with the bulky terminal ends and its hydrophobic character (Figure 3.12a).

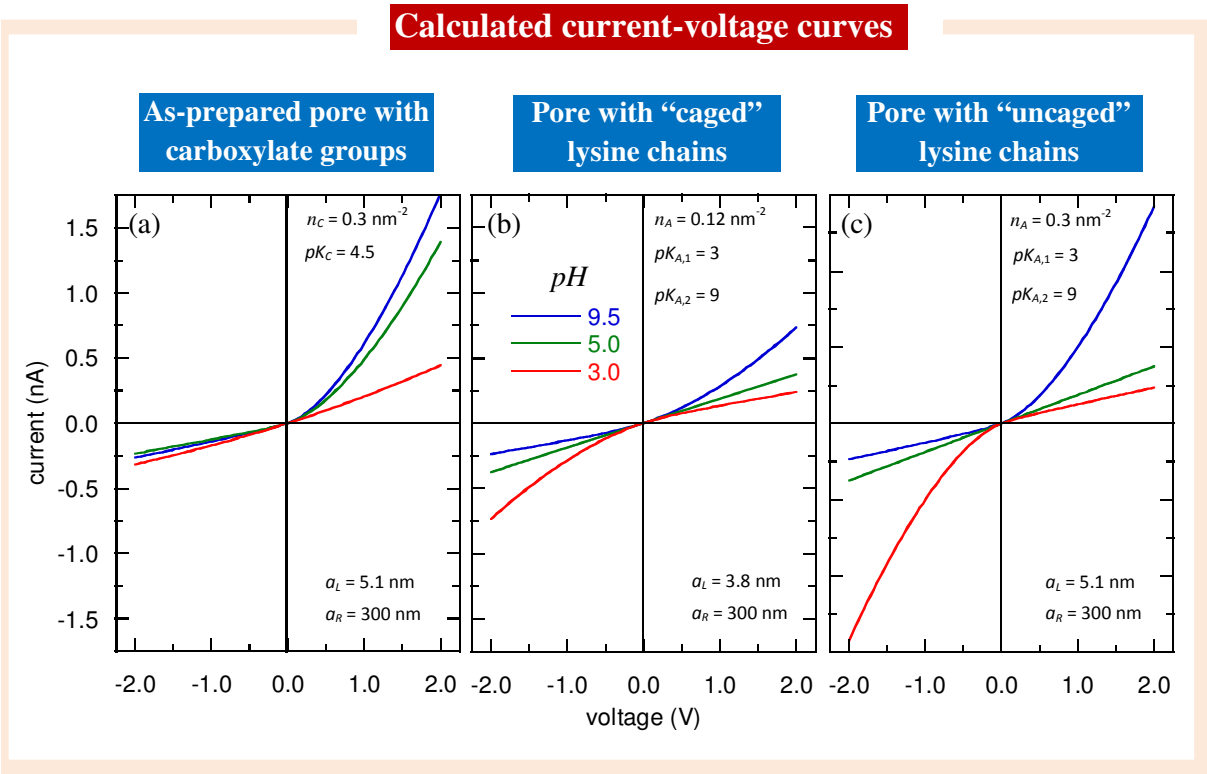

Figure 3.17: Calculated *I–V* curves of a single asymmetric nanopore with carboxylate groups (a), "caged" lysine chains (b), and "uncaged" lysine chains (7c), for the same experimental conditions as in Figure 3.12. The nanopore parameters used in the calculations are shown in the insets.

Now the case of charged pores is considered. The results obtained for the as-prepared pore with carboxylate groups (Figure 3.12a) show non-linear curves at the *pH* values measured and thus the above procedure cannot be applied directly. Since the value obtained for a_L in the case of the pores with "uncaged" lysine reveals a relatively wide tip opening, we can assume that the pore tip radius of the as-prepared nanopore is the same as that calculated from Figure 3.12c, a_L = 5.1 nm. With this assumption, the only free parameters in the NP model are the surface charge density σ and the pK_a value of the carboxylate groups, pK_C. The best fit for the as-prepared pore (Figure 3.17a) gave a surface charge density σ = -0.3e nm^{-2} at pH = 9.5, where e is the elementary charge, and pK_C = 4.5. Because at pH = 9.5 all the carboxylate groups are in charged form, it can be concluded that the surface density of groups attached to the pore walls is approximately n_C = 0.3 groups/nm^2. The values of n_C and pK_C are in agreement with those found in previous studies for the case of pores functionalized with carboxylate groups.[146]

It must also be mentioned that similar calculations assuming a perfect conical geometry instead of a convex tip geometry lead to unrealistically low values of the surface charge density (σ = -0.07e nm^{-2} at pH = 9.5 in the case of the experiments of Figure 3.12a). Also, the rectification ratios (defined as the absolute value of the ratio between the electric current in the "on" and "off" states at a given voltage) calculated assuming a perfect conical geometry are much higher than those obtained using the experimental data of Figure 3.12a. These two facts give further support to our assumption that the pore with a convex tip deviates slightly from the conical geometry.

Next, the experiments with the pore functionalized with "uncaged" lysine chains (Figure 3.12c) are considered. Because the axial pore profile and the values of the pore radii at the tip and base have already been determined, the unknown parameters in the NP model are the surface density nA and the two pK_a values of the amphoteric lysine groups, $pK_{A,1}$ and $pK_{A,2}$. Figure 3.17c shows the theoretical results obtained for this pore using n_A = 0.3 groups/nm^2, $pK_{A,1}$ = 3 and $pK_{A,2}$ = 9. The value for n_A assumes a 100% substitution of the original

carboxylate groups by the amphoteric groups. The values for $pK_{A,1}$ and $pK_{A,2}$ provide the best fit to the experimental data of Figure 3.12c and are close to the pK_a values of lysine in free solution (2.18 and 8.95),[174] which gives support to the pore characterization procedure followed here.

Finally, Figure 3.17b shows the results provided by the NP model for the pore functionalized with "caged" lysine. Using the $pK_{A,1}$ and $pK_{A,2}$ values calculated above, the best fit to experimental data was obtained assuming n_A = 0.12 groups/nm^2. This value suggests that approximately one third of the supposedly "caged" lysine groups were actually in ionized form, which explains the residual *pH*-controlled transport shown in Figures 3.12b and 3.17b.

3.3.5.4 Permeation of MV^{2+} and NDS^{2-}

The ionic analyte molecules used in the transport measurements through the multipore membranes of Figures 3.14 and 3.15 were methylviologen dichloride ($MVCl_2$) and 1,5-naphthalene disulfonate di-sodium salt (Na_2NDS). The ionic species involved in the permeation process were MV^{2+} and Cl^- in the case of the $MVCl_2$ and NDS^{2-} and Na^+ for the Na_2NDS. For the sake of simplicity, we have neglected the influence of the ionic species present in the buffer solutions used to control the external *pH*. Also, we restrict our calculations to the case of the membrane in the "on" state (after UV irradiation) when all the lysine groups are "uncaged".

In the case of $MVCl_2$ again the case X_F = 0 (*pH* = 5.0) is considered. When the membrane is uncharged, integration of the Nernst-Planck equation gives the total flux

$$j_{MV^{2+}} n_p A_{sample} = \frac{3c_{MV^{2+}}(0)}{g_m\left(1/D_{MV^{2+}} + 2/D_{Cl^-}\right)} n_p A_{sample}, \qquad (28)$$

where n_p is the number of pores per unit of area and A_{sample} is the membrane area used in the experiments. Equation (28) is obtained with the condition of zero electric current through the membrane

$$2j_{MV^{2+}} - j_{Cl^-} = 0. \qquad (29)$$

Because the multipore membrane sample was etched at the same time as the single nanopore sample, we can assume that the geometrical factor g_m is the same for the two samples. With this assumption, the only free parameter in Eq. (28) is the diffusion coefficient of the analyte. Using the experimental data of Figure 3.14 for *pH* = 5.0, we obtain $D_{MV^{2+}}$ = 5.1 10^{-7} cm^2/s. Similar calculations for the NDS^{2-} experimental data of Figure 3.15d at *pH* = 5 give $D_{NDS^{2-}}$ = 2.5 10^{-7} cm^2/s. These values are in good agreement with those found in previous studies of $MVCl_2$ and Na_2NDS diffusion through nanoporous membranes.[17]

In the case of acidic or basic *pH*, the membrane is charged and the Nernst-Planck equation must be solved using numerical procedures. In order to find an approximate analytical solution, the following is assumed

$$\pi a^2 \frac{d\phi}{dx} = \text{constant}. \qquad (30)$$

Equation (30) is a generalization of the Goldman constant field assumption commonly used in the study of biological ion channels and synthetic membranes. With this assumption, the integration of the Nernst Planck equation yields

$$j_{MV^{2+}} n_p A_{sample} = \frac{2D_{MV^{2+}} c_{MV^{2+}}(0) u^2 \log(1/u)}{g_m (1-u^2)} n_p A_{sample}, \quad (31)$$

where

$$u = \frac{f_c + \sqrt{f_c^2 + 4f_c}}{2}, \quad (32)$$

and

$$f_c = \frac{D_{Cl^-}}{4D_{MV^{2+}}} \frac{c_{Cl^-}(0)}{c_{MV^{2+}}(0)}. \quad (33)$$

Similar calculations allow the estimation of the total NDS^{2-} flux through the multipore membrane.

Because the concentration of the mobile species at the pore tip can be calculated from the external concentrations in the feeding compartment using Eqs. (10)-(12), the simplified model of Eqs. (30)-(33) contains no additional free parameters, and can then be used to check further the validity of the theoretical approach proposed here. The comparison between the model predictions and the experiments of Figures 3.14 and 3.15 is given in terms of the ratio between the analyte fluxes in Table 3.7. In spite of the rough approximations introduced, the agreement between theory and experiment is good for analytes with charge of the same sign as that of the pore surface charge. However, the theoretical model overestimates the fluxes if the analyte and surface charges have opposite signs. This result suggests that other effects in addition to those characteristic of the simple point ion models could be important for the relatively bulky divalent ions used in the permeation experiments.

Table 3.7: The flux ratios at different pH values obtained with the NP model and the experimental ratios for the permeation of MV^{2+} and NDS^{2-} through the multipore membrane.

Flux ratio	Experiment	Theory
MV^{2+}		
$\frac{\text{Flux at } p\text{H} = 9.5}{\text{Flux at } p\text{H} = 5.0}$	1.97	4.01
$\frac{\text{Flux at } p\text{H} = 5.0}{\text{Flux at } p\text{H} = 3.0}$	3.07	3.67
NDS^{2-}		
$\frac{\text{Flux at } p\text{H} = 3.0}{\text{Flux at } p\text{H} = 5.0}$	2.05	5.45
$\frac{\text{Flux at } p\text{H} = 5.0}{\text{Flux at } p\text{H} = 9.5}$	6.48	5.72

3.3.6 Conclusions

Photochemical gating of nanoscale pores constitutes a subject of current interest because of the potential applications.[55,56,61,92] The transport properties of asymmetric nanopores functionalized with photosensitive amphoteric lysine groups were demonstrated. The experiments concern the *I–V* curves of polymer samples containing the as-prepared single asymmetric nanopore with carboxylate groups acting as fixed charges, the *I–V* curves of the single nanopore functionalized with "caged" and "uncaged" lysine groups, and the fluxes of divalent positive and negative analytes through multipore membranes. A detailed theoretical study based on the NP equation allows for obtaining the key parameters involved in the transport processes (pore tip shape and dimensions, surface charge concentrations, and pK_a values of the functional groups fixed on the pore walls). In this work, a relatively simple continuum model is employed, similar to those previously introduced to describe transport in ion channels. The model involves a reduced number of basic concepts and approximately describes the observed transport phenomena in terms of the electrostatic, *pH*-tunable interaction of the mobile ions with the pore surface charges.

3.4 Metal Ion Affinity-based Biomolecular Recognition and Conjugation inside Polymer Nanopores Modified with Iron–Terpyridine Complexes [XV]

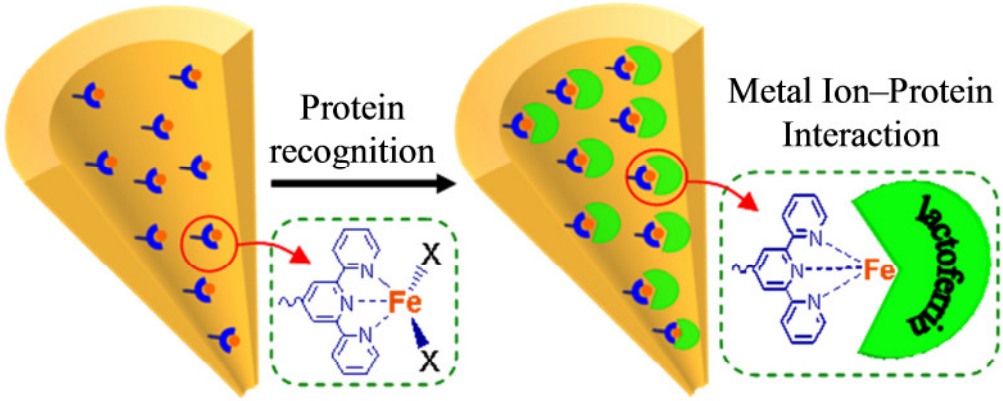

In this section a nanopore-based biosensing system for the detection of lactoferrin (LFN) via metal–organic frameworks is demonstrated. Firstly, a monolayer of amine-terminated terpyridine (metal–chelating ligand) is covalently immobilized on the inner walls of the nanopore via carbodiimide coupling chemistry. Secondly, iron–terpyridine (iron–terPy) complexes are obtained by treating the terpyridine modified-nanopores with ferrous sulphate solution. The immobilized iron–terPy complexes can be used as recognition elements to fabricate a biosensing nanodevice. The working principle of the proposed biosensor is based on specific noncovalent interactions between LFN and chelated metal ions in the immobilized terpyridine monolayer, leading to the selective detection of analyte protein. In addition, control experiments proved that the designed biosensor exhibits excellent biospecificity and non-fouling properties. Furthermore, complementary experiments are conducted with multipore membranes containing an array of cylindrical nanopores. It is demonstrated that in the presence of LFN in the feed solution, permeation of methyl viologen (MV^{2+}) and 1,5-naphthalenedisulfonate (NDS^{2-}) is drastically suppressed across the iron–terPy modified membranes. Based on these findings, the designing and immobilization of functional ligands inside the synthetic nanopores would extend this method for the construction of new metal ion affinity-based biomimetic systems for the specific binding and recognition of other biomolecules.

[XV] Published work:

Ali, M.; Nasir, S.; Nguyen, Q. H.; Sahoo, J. K.; Tahir, M. N.; Tremel, W.; Ensinger, W. "Metal ion affinity-based biomolecular recognition and conjugation inside synthetic polymer nanopores modified with iron-terpyridine complexes" *Journal of the American Chemical Society* **2011,** 133, (43), 17307-17314.

DOI: 10.1021/ja205042t

3.4.1 Introduction

During the recent years, solid-state nanopores have gained considerable attention of the scientific community because of their unique ionic transport properties, providing an excellent platform for potential applications such as biosensing,[63,69,111,115,117,119] molecular separation,[15,19,51,136,175] and targeted drug delivery[85,176] at the nanoscale level. Biological ion channels in living organisms facilitate the diffusion of ions, water or small organic molecules across the cell membrane, portray a perfect example from nature.[1] However, because of fragility and sensitivity of the embedding lipid bilayer, biological pores are not suitable for practical applications. On the contrary, synthetic nanopores display several advantages over their biological counterparts, especially: stability, control over pore shape and diameter, possibility of integration into nanofluidic devices, and modifiable surface properties for interaction with molecules of interest.[6,8,10,11,66]

To date, different strategies have been developed for the fabrication of nanoscale architectures to maintain a natural environment in an artificial device that closely mimic biological system.[6,8,10,66] Compared with other techniques, ion-track-technology[42] offers a unique possibility to fabricate single pore as well as multi-pore membranes, depending on the number of heavy ions penetrated. Secondly, it also provides flexibility to control over both pore shape (*e.g.*, conical, cylindrical or biconical) and size down to a few nanometers. Track-etched nanopores also display transport properties similar to that of biological ion channels, such as ion current rectification, voltage-dependent current gating, and selective ion permeation.[41,142,156,177] The chemical functionalities on the pore surface are crucial for the above mentioned applications, since they strongly influence the ionic transport through the nanopore.[65,101,102] The immobilized ligands onto the surface and inner walls of the nanopores would serve as binding or sensing sites for different analytes as well as interact with molecules passing through the pore.[7,69,111,113,115,178]

The immobilization of bio-recognizable elements into these nanoscale architectures has been achieved mainly through covalent attachment and electrostatic self-assembly of functional polyelectrolytes onto the interior of the nanopore by exploiting the existing chemical groups on the pore surface. Seminal work of Martin *et al.* demonstrated the covalent immobilization of thiol-terminated organic/biomolecules on the inner wall of gold coated nanopores inside polymeric membrane for protein sensing and permselective ionic transport.[15,51,113,136,175,] More importantly, track-etched nanopores in polyethylene terephthalate (PET) membranes possess carboxylic acid functionalities on the surface and inner walls.[58,63,156,179] We and others have also reported the direct covalent attachment amino-terminated molecules onto the inner pore surface.[100,101,104,108,115,120] Moreover, biomolecular immobilization has also been achieved *via* electrostatic interactions onto the surface and inner walls of the nanopore.[58,68,69] Recently, our group have also demonstrated biomolecular immobilization onto the interior of the nanopore through sugar–lectin biospecific interactions.[110] However, previously developed biosensing nanodevices were mainly based on conventional ligand–receptor interactions, such as protein–protein,[110] biotin–streptavidin/avidin,[69,113,115] antigen–antibody binding[112,113] and peptide nucleic acid–DNA interactions,[63] leading to the blockage of the pore opening and/ or modulation of pore surface charge. In order to further expand the potentialities of these nanosized systems, decorating nanopore interior with metal chelating organic ligands would also provide another biosensing platform for the immobilization and detection of biomolecules which display affinity towards specific metal ions.

Among the various organic metal–chelating ligands, terpyridine (terPy) is quite attractive because of its ability to form stable complexes with different metallic ions (Fe, Co, Ni, Zn, etc.).[180] Based on metal ion affinity approach, Tuccitto *et al.* have already been demonstrated the successful immobilization of lactoferrin (LFN) onto the gold surface *via* a patterned self-assembled monolayer containing of iron–terpyridine complexes.[181] Lactoferrin is widely distributed in mammalian physiological secretions such as milk, saliva, tears and seminal fluids.[182] LFN is also recognized as iron–binding glycoproteins which play a key role in the transport of iron in biological systems. In recent years, LFN is successfully used as a carrier for drugs to target brain tumer.[183] Moreover, LFN also play an important role in the host defence system against microbial and viral

infections.[184,185] Naturally, LFN molecule possesses two specific iron-binding sites. These binding sites are localized in each of the two homologous globular domains named N-and C-lobes. Each LFN molecule can reversibly bind with two ions of iron. The coordination of iron cation involves four amino acid residues in each lobe: two tyrosine residues, one histidine residue and one aspartic acid residue.[182]

Herein, a biosensing platform based on the specific noncovalent interactions between LFN and metallic ion chelated in terPy monolayer, immobilized on the inner walls of track-etched nanopores is demonstrated. For this purpose, the interior of the nanopore is tailored with terpyridine ligand. Subsequently, modified nanopores are treated with a solution of iron(II) salt in order to form iron–terPy complexes, which acted as recognition elements for the capturing of LFN molecules. The success of chemical reactions and biorecognition events are confirmed *via* ionic current passing through the nanopore by measuring the current–voltage (*I–V*) characteristics of the single-pore membranes. The modified nanopores are successfully used as nanobiosensor for the specific detection of LFN. In addition, complementary experiments are performed by using multi-pore polymer membranes. In this case, after immobilization of iron–terPy complexes onto the pore surface, permeation of doubly charged organic analyte through a cylindrical nanopore array is suppressed by the co-addition of LFN in the feed solution.

3.4.2 Immobilization of amine-terminated terpyridine ligand

Polyethylene terephthalate (PET) membranes containing single conical nanopores, and cylindrical nanopore arrays (10^8 pores cm^{-2}) were used in this study. Single conical nanopores were fabricated *via* asymmetric chemical etching of the latent track of a single energetic heavy ion.[41] On the other hand, multi-track array membranes were etched symmetrically for the fabrication of cylindrical nanopores.[72,139] PET is a polyester, and the etchant (NaOH) species preferentially attack on the partially charged ester groups. As a result of track-etching process, approximately one carboxyl (–COOH) group per nm^2 is exposed on the nanopore surface due to the cleavage of polymeric chains.[129] These groups can act as sites for the covalent attachment of desired ligand molecules on the interior of the nanopore surface.

The metal–chelating ligand used in this study is 1-amino-5-(2,2′:6′,2″-terpyrid-4′-yl-oxy) pentane (terPy–DEG-NH_2). The ligand was synthesized by the direct coupling of diethylene glycolamine (DEG-NH_2) with 4′-chloro,2,2′:6′,2″-terpyridine (terPy) molecule.[133] The synthesis of terPy–DEG-NH_2 is described in chapre 2, section 2.6.5. The primary amine on one terminus of the ligand (terPy–DEG-NH_2) was exploited for the covalent linkage with surface –COOH groups, while terpyridine moiety on the other terminus used for metal ion complexation.

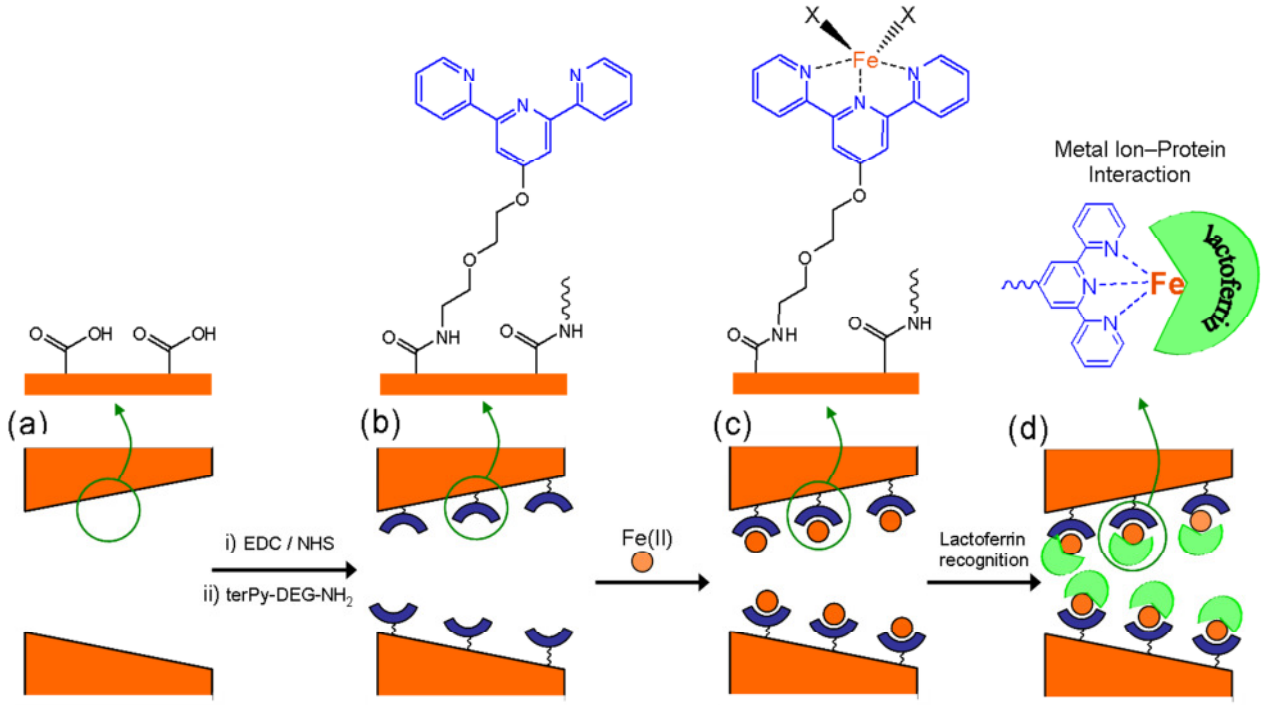

Figure 3.18: Schematic representation of (a) as-prepared single conical nanopore containing surface carboxylic acid groups , (b) covalent immobilization of amine-terminated terpyridine ligand with carboxyl groups via carbodiimide coupling chemistry, (c) subsequent treatment with iron(II) salt solution to obtain iron–terPy complexes (X represents any counter-ion or coordinating solvent molecule), and (d) biorecognition of lactoferrin molecules.

The covalent attachment of surface –COOH groups with terminal amine of the ligand (terPy–DEG-NH_2) is demonstrated in Figure 3.18. The detailed experimental procedure is provided in chapter 2, section 2.6.5. To achieve this, carboxyl groups were first activated into amine-reactive sulfo-NHS ester molecules by using an aqueous solution of *N*-(3-dimethylaminopropyl)-*N'*-ethylcarbodiimide HCl (EDC) and *N*-hydroxysulfosuccinimide (sulfo-NHS).[130] Subsequently, the succinimidyl intermediate was covalently coupled with the amine of the ligand *via* stable amide linkage. After modification, the iron–terpyridine (iron–terPy) complex was achieved by treating the modified pore with an aqueous ethanolic solution of ferrous sulphate (Figure 3.18).[181]

3.4.3 Single conical nanopore

Before modification, pore walls are negatively charged at neutral pH due to the presence of ionised carboxyl ($–COO^-$) groups. Therefore, the nanopore volume in an aqueous solution is mainly filled with ions of charge opposite to that of the fixed charged groups on the pore surface. In the present case, the unipolar solution of positive ions inside the nanopores is responsible for the observed electrical conductance at each potential difference applied externally. It is well known that single conical nanopores rectify the ionic current due to an asymmetry in the intrinsic electrostatic potential along the pore axis.[45,46,102,141-143,148,157,177]

I–V characteristics of single conical nanopores in PET membranes were recorded in symmetric electrolyte conditions on both sides of the membrane using 0.1M KCl solution as an electrolyte at neutral pH. The direction of rectification in conical channels is solely based on surface charge. Before modification, the pore rectifies the cation current with the preferential direction of the cation flow from the narrow opening to the wide opening of a cone due to the presence of inherent $–COO^-$ groups (Figure 3.19). Based on the electrode configuration in our system, higher currents are recorded for positive voltages, while lower value of negative ionic currents is

observed due to the cations flow from the wide opening towards the narrow tip of the cone at reversed voltages. After modification, monolayers of iron–terPy complexes switched the surface charge from negative to neutral, resulting in the loss of rectification behaviour as exhibited from the current–voltage (*I–V*) curve shown in Figure 3.19. This clearly confirmed the successful anchoring of chelated metal ions onto the inner walls of the nanopore.

3.4.3.1 Bioconjugation inside a confined environment

The bioconjugation process confined into a nanopore would lead to volume exclusion and/ or electrostatic-based effects, which govern the ionic mass transport across the nanopore. Here, our main concern is with the volume exclusion principle because the molecular size of analyte is comparable to the tip opening of the nanopore.[69,113] Thus, the binding of biomolecular analyte to the pore walls would lead to the partial or complete occlusion of the pore opening and would hinder the flow of ions across the membrane. Consequently, the molecular recognition process would promote a sensitive change in the magnitude of the ionic current passing through the nanopore.

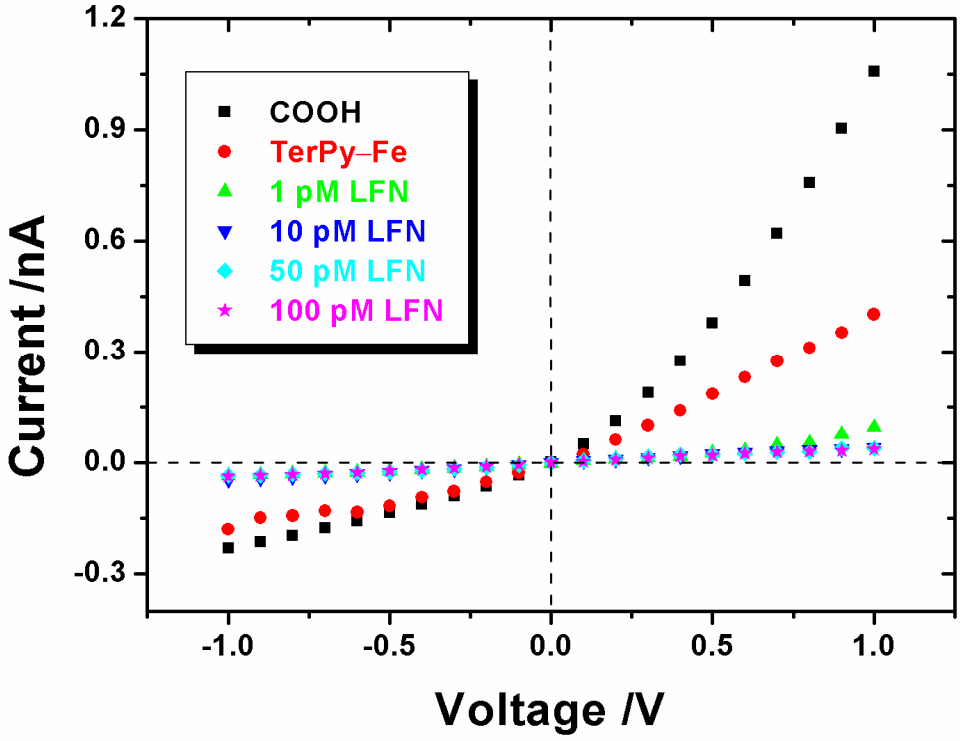

Figure 3.19: *I–V* characteristics of a single conical nanopore with tip $d \approx 13$ nm measured in 0.1 M KCl (pH 7.0) solutions corresponding to pore surfaces with carboxylate groups (black square), and iron–terpyridine complexes (red filled circle); and upon exposing the modified pore to different concentration of lactoferrin prepared (separately) in the same electrolyte solution, respectively.

3.4.3.2 Sensitivity and specificity of the nanopore biosensor

Analytical parameters such as sensitivity and selectivity (specificity) should also be taken into account, when designing a biosensing platform. The sensitivity of the designed biosensor was evaluated by exposing the modified pore to different concentrations of analyte (LFN) protein, prepared in the working electrolyte solution.

Figure 3.19 shows the change in the *I–V* characteristics upon exposing the iron chelated nanopore to different concentrations of LFN protein in electrolyte solution. As expected, the presence of LFN in the background electrolyte, even at very low concentrations, resulted in a drastic decrease in the ion flux across the nanopore. From the *I–V* curve, the ionic transport across the modified nanopore was 400 pA at a potential of +1 V. The binding of LFN to chelated iron ion inside the nanopore led to a significant decrease in the effective diameter which in turn affects the ionic flux through the nanopore. Upon exposure to a LFN solution of only 1pM, the observed value of ionic current for +1 V was dropped from 400 to 95 pA. Similarly, the ion current measured at the reverse bias, *i.e.,* -1 V, also decreased from 180 to 35 pA. This means that 1pM solution of LFN promoted a ~76% and ~80% decrease in the ion flux through the pore at +1 V and -1 V, respectively. The observed decrease in the ionic current was due to the formation of bioconjugates on the inner pore surface. With 10 pM LFN solution, ionic current was further decrease to 41 pA at positive potential which correspond to ~90% reduction in ionic flux, compared to the modified pore without bioconjugation. From the *I–V* data shown in Figure 3.19 it is evident that the modified pore became saturated with bioconjugates with 10 pM LFN solution. Further an increase in LFN concentration did not induce any significant change in the ionic current flowing across the nanopore at both positive and negative voltages. It has already been reported that bioconjugation of protein analytes in conical shaped gold nanotubes and nanopores through ligand–receptor interactions onto the inner walls clogged the tip opening, leading to the permanent blockage of the ion current.[69,113] The above experimental results provide clear evidence that the metal ions in the immobilized ligand (iron–terPy) are able to biorecognize receptors (LFN) even at very low concentrations in the surrounding environment, and this biorecognition can be transduced in an electronic signal originating from the ionic transport through the nanopore.

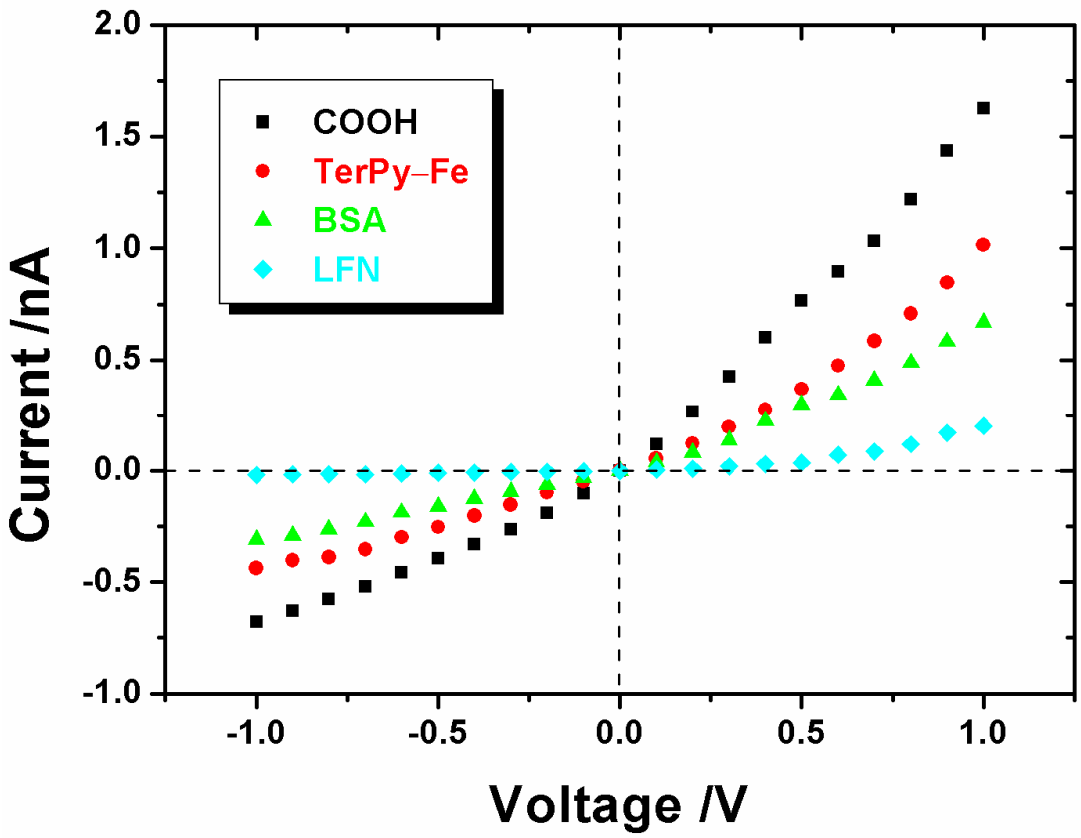

Figure 3.20: Current-voltage characteristics of a single conical nanopore with tip $d \approx 11$ nm and base $D \approx 575$ nm in 0.1 M KCl prior to and after the covalent immobilization of iron–terPy ligand followed by the addition (separately) of 100 nM of each, bovine serum albumin (BSA) and lactoferrin (LFN) protein in the electrolyte solution, respectively.

Secondly, selective (specific) recognition of the target analyte is also a most desirable characteristic of a biosensor, *i.e.* biosensors should also exhibit selectivity for the detection and transduction of specific events upon the binding of analyte molecules. In other words, in order to demonstrate that this approach is valid to create a biosensing platform inside the nanoconfined geometry, it is important to show that the changes in the ionic current are mainly due to the biorecognition events, and not to the mere physical adsorption of protein analyte onto the pore surface. To verify the selectivity/specificity of the iron–terPy-modified nanopore, we repeated the same experiment using bovine serum albumin (BSA) and lactoferrin (LFN) protein analytes, respectively. Figure 3.20 shows that the presence of BSA in the background electrolyte in contact with modified nanopore could not led to the blockage of the ionic flux across the nanopore. This confirmed the lack of binding capability of BSA towards chelated metal ion, leaving the original surface remain undisturbed with free coordination sites of metal cations in the iron–terPy monolayers. Subsequently, when the same pore was exposed to lactoferrin (LFN) protein, bioconjugation occurred due to the specific metal ion–protein binding interactions, leading to a decrease of ~80% at +1 V and ~95% at reversed voltage bias (-1 V) in the ionic current, compared to the modified pore without bioconjugation (Figure 3.20). From the *I–V* characteristics, we can infer that the presented sensor exhibits a remarkable selectivity and specificity towards LFN because of natural possession of iron–binding sites in the globular domain of that protein.

3.4.3.3 Control experiment

Additionally, a negative control experiment was also performed in the same set of experimental conditions with unmodified (carboxylated) and terPy-modified (Figure 3.18b) single conical nanopore without iron complexation. It is evident from the *I–V* characteristics shown in Figure 3.21 that even working with higher concentration of LFN in the background electrolyte, we did not observe any significant change in the ionic current passing through the as-prepared (carboxylated) and terPy-modified nanopore. These experimental results further supported our finding that LFN can only specifically bind with chelated metal ion in the terPy-iron complexes immobilized on the inner walls of the pores.

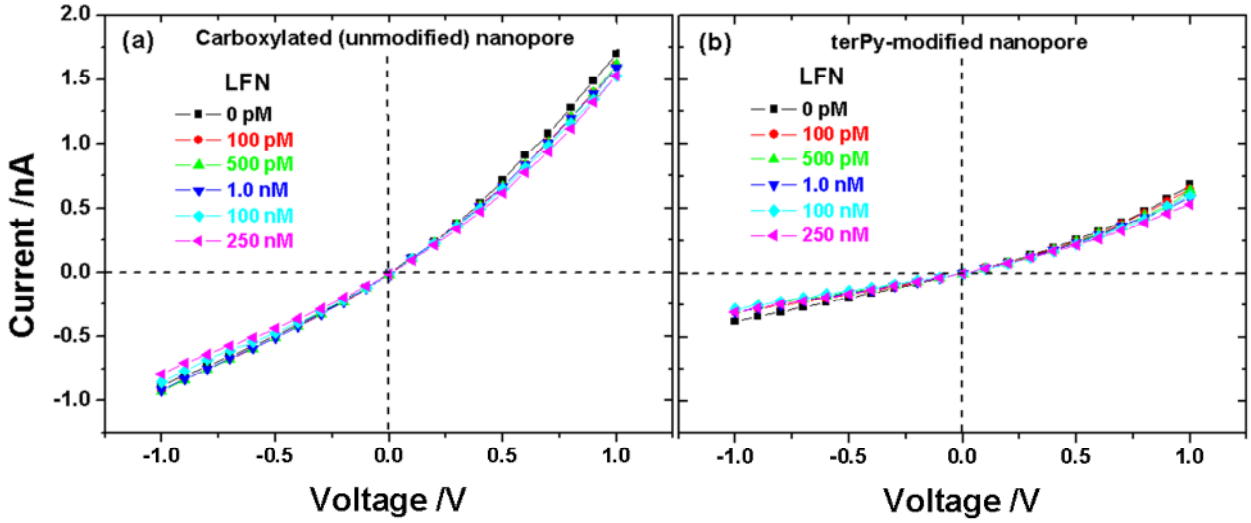

Figure 3.21: Current–voltage (*I–V*) characteristics of a single conical nanopore with tip d ≈ 10 nm in 0.1M KCl solution (a) before, and (b) after the covalent attachment of terpyridine followed by the addition of various concentration of lactoferrin the background electrolyte solution.

3.4.3 Multipore membranes

Moreover, in order to support and confirm the proposed ligand-receptor interaction based on metal ion affinity approach, complementary experiments were conducted using multipore membranes containing an array of cylindrical nanopores with an areal density of 10^8 pores cm^{-2}. The influence of lactoferrin on the selective permeability was investigated by monitoring the ionic permeation of doubly charged organic analytes across the nanoporous membrane. The membrane was clamped between the two halves of the conductivity cells. The feed half-cell contained a known concentration of methylviologen (MV^{2+}) or 1,5-naphthalenedisulfonate (NDS^{2-}) analyte (separately). The permeate half-cell was filled with pure buffer solution. At fixed periods of time, the concentration of analyte in the permeate half-cell was obtained by measuring the UV absorbance with a UV/Vis spectrometer.

Figure 3.22 shows the permeation data *versus* time of charged analytes (MV^{2+} and NDS^{2-}) across the nanoporous membrane before modification and after iron–terPy immobilization followed by the bioconjugation onto the pore surface. The diffusion data reveals the number of moles of the charged molecules transported per cm^2 area of the membrane. Both MV^{2+} and NDS^{2-} molecules have quite similar molecular volumes of 0.637 and 0.680 nm^3, respectively.[17] Furthermore, the molecular structures of both MV^{2+} and NDS^{2-} analytes contain two benzyl rings which determine their same hydrophobic behaviour within the nanopores.[139] Therefore, the volume exclusion and hydrophobic interaction mechanisms can be neglected in the case of as-prepared (unmodified) multi-pore membranes. Hence, in our system, the electrostatic interaction between charged analytes (MV^{2+} and NDS^{2-}) in solution and fixed negative ($–COO^-$) charges on the inner walls of the pore was the main driving force, responsible for the permeation variation across the membrane (Figure 3.22a). Initially, an electrical double layer was generated inside the nanopore which contains a higher concentration of MV^{2+} cations, compared to NDS^{2-}analyte anions. Therefore, MV^{2+} ions selectively diffused across the membrane, while co-ions (NDS^{2-}) are electrostatically prohibited from entering the nanopore. Therefore, diffusion of MV^{2+} is much higher than that of the NDS^{2-} molecules in the permeate compartment (Figure 3.22a).[139]

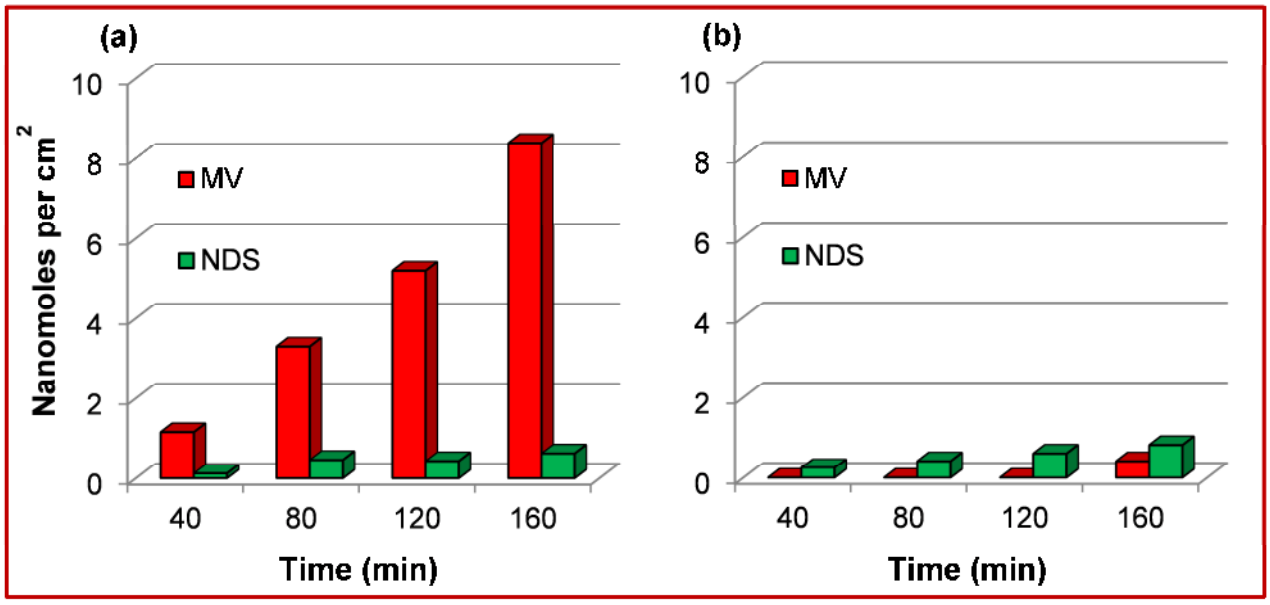

Figure 3.22: Diffusion of doubly charged organic analytes (MV^{2+} and NDS^{2-}) through nanoporous membrane containing an array of cylindrical nanopores (10^8 pores cm^{-2}) of ~18 nm in diameter, (a) before modification (carboxylated pore surface) without lactoferrin in the feed solution, and (b) after the immobilization of iron–terPy complexes in the presence of lactoferrin (100 nM) in the feed solution.

Figure 3.22b shows that after the immobilization of iron–terPy complexes onto the pore surface, the diffusion of MV^{2+} molecules was also drastically decreased in the presence of LFN in the feed solution. A plausible explanation for the observed decrease in permeation is that the LFN bioconjugate inside the pore significantly reduced the effective pore diameter available for the ionic transport. This in turn hindered the flow of analyte molecules across the membrane. Therefore, selective permeation of analyte was lost after LFN conjugation, and now the volume exclusion principle mainly governs the ionic transport across the membrane. The permeation data shown in Figure 3.22b indicated that the permeation of MV^{2+} ions was almost blocked, *i.e.,* no detectable amount of these ions was transported across the membrane up to 120 minutes of diffusion time. However, the permeation of MV^{2+} ions after 160 min was only 0.42 nanomoles which is negligible when compared with 8.4 nanomoles corresponding to as-prepared (unmodified) membrane.

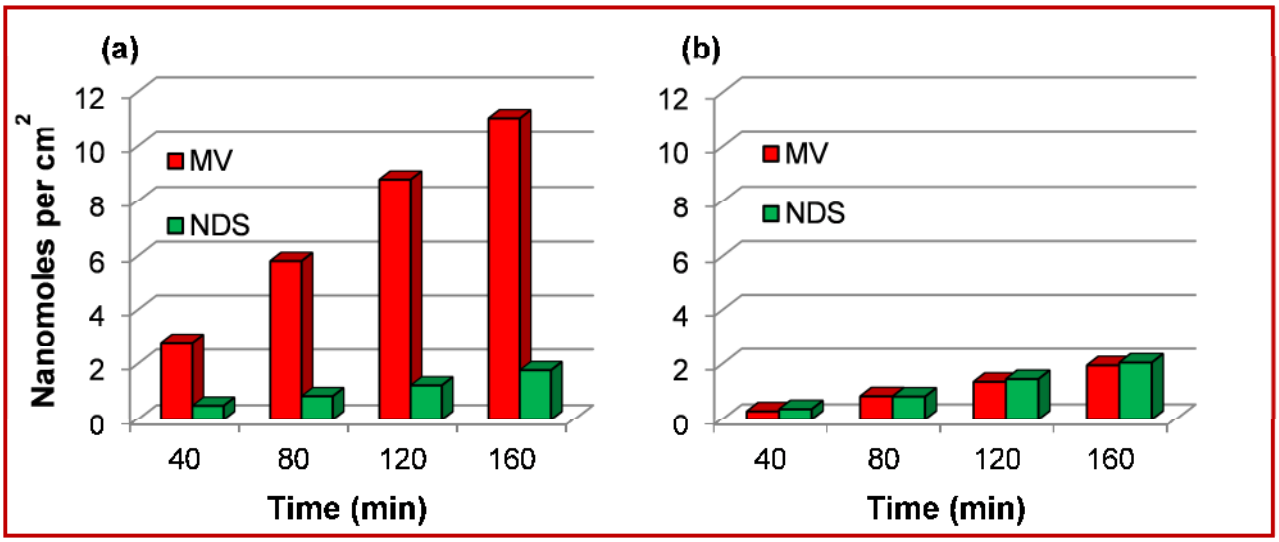

Figure 3.23: Diffusion of doubly charged organic analytes (MV^{2+} and NDS^{2-}) in the presence of lactoferrin (100 nM) in the analyte solution through nanoporous membrane containing an array of cylindrical nanopores (10^8 pores cm^{-2}) of ~26 nm in diameter, (a) before modification (carboxylated pore surface), and (b) after the immobilization of iron–terPy complexes onto the inner walls of nanopores.

However, the question may arise that this decrease in ionic permeation is either due to the formation of bioconjugates or only because of the physical adsorption of LFN molecules onto the nanopore surface. In order to assure this, we carried out the same diffusion experiment with another multi-pore membrane under the same set of experimental conditions. Figure 3.23 describes the ionic (MV^{2+} and NDS^{2-}) permeation *versus* time across the membrane before and after the iron–terPy immobilization in the presence of LFN dissolved in the feed solution. The diffusion data shown in Figure 3.23a reveals that the presence of LFN molecules did not cause any interference in the selective diffusion of MV^{2+} ions across the negatively charged ($–COO^-$) multipore membrane. However, when the same membrane was modified with metal–chelates, selective permeation of MV^{2+} was strongly reduced from 11.0 to 1.9 nanomoles after 160 minutes of diffusion time (Figure 3.23b). The above mentioned experimental results showed that the chelated metal ions affinity based LFN bioconjugation indeed diminishes the available effective pore diameter available for the transport of analyte molecules. This resulted in a decrease of ~82% in the permeation of MV^{2+} across the modified membrane. These results provided clear evidence that metal ions incorporated in the immobilized terPy monolayers onto the nanopore surface are accessible to analyte protein for successful binding through specific noncovalent interactions inside the confined environment.

3.4.4 Conclusions

In summary, the experiment demonstrated the construction of a nanobiosensor based on the immobilization of metal–ligand complexes inside a confined environment for the selective biomolecular recognition through metal–protein specific interactions. To achieve this goal, terpyridine ligands were covalently attached inside the track-etched nanopores by exploiting inherent COOH groups *via* EDC/sulfo-NHS coupling chemistry, followed by the iron complexation. The experimental results showed that the immobilized ligand (iron–terPy complex) acted as biorecognition element for the specific detection of LFN molecules. In addition, control experiments proved that the designed biosensor exhibit excellent biospecificity and non-fouling properties. For the further confirmation of noncovalent interaction of lactoferrin with iron complex, complementary experiments were also performed with multi-pore polymer membranes. The work demonstrated that in the presence of LFN in the feed solution, permeation of methyl viologen (MV^{2+}) and 1,5-naphthalenedisulfonate (NDS^{2-}) is drastically suppressed across the iron–terPy modified membranes, representing the occlusion of the nanopore upon the binding of LFN with metal ions incorporated into metal–chelating ligand. In this context, it is believed that metal affinity-based biomimetic system can be further extended for the molecular recognition of other protein analytes possessing specific receptors for coordination with metal ions in their polypeptide backbone. For instance, chelated nickel (Ni^{2+}) ions preferably bind to histidine rich proteins, or those proteins containing an exposed histidine tail (His-tagged proteins). Similarly, proteins containing zinc finger motifs (zinc finger proteins) can specifically coordinate and bind with zinc (Zn^{2+}) ions chelated with a ligand.

3.5 Carbohydrate-Mediated Biomolecular Recognition and Gating of Synthetic Ion Channels [XVI]

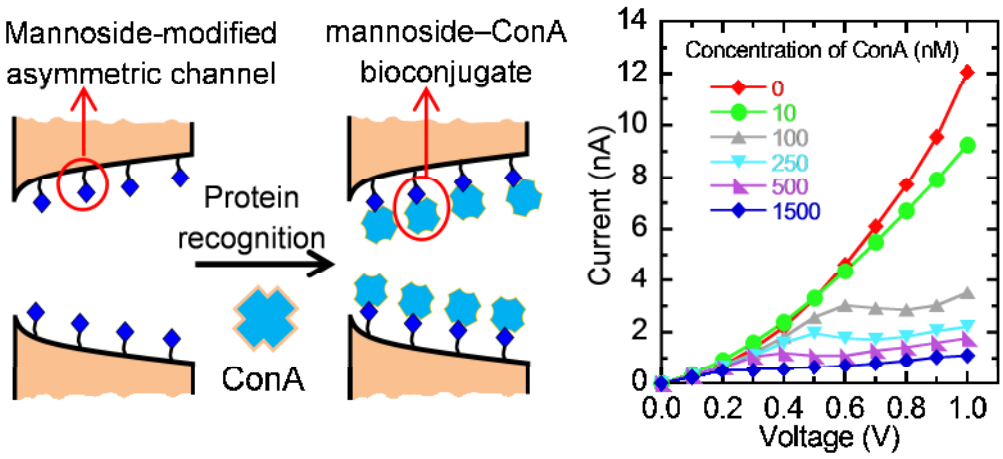

Nanochannel-based biosensing devices have been proposed for selective detection of protein analyte molecules. However, the design and miniaturization of reusable channel-based biosensors is still a challenge in nanoscience and biotechnology. In this study a reusable nanofluidic biosensor based on reversible lectin-carbohydrate interactions is demonstrated. The nanochannels are fabricated in heavy ion tracked polymer membranes. The channel walls are functionalized with p-aminophenyl α-D-mannopyranoside (APMP) monolayers through carbodiimide coupling chemistry. The chemical (mannopyranoside) groups on the inner channel walls serve as binding sites and interact with specific protein molecules. The binding (bioconjugation)/unbinding of proteins inside the confined geometry gives measurable changes in the electrical conductance for the case of a single channel and in the permeation rate for a multi-channel membrane. The modified-channel selectively recognizes concanavalin A (ConA) protein, but not the control proteins (lysozyme and bovine serum albumin), because ConA specifically binds with the mannopyranoside moieties. The method permits ConA detection in the range 10 nM to 1000 nM. Moreover, the ConA binding/unbinding is reversible, allowing several measuring cycles by washing the bioconjugated-channels with mannose solution. The experimental results are explained qualitatively by introducing a phenomenological model that incorporates the basic experimental trends observed in the current-voltage curves.

[XVI] Published work:

Ali, M.; Nasir, S.; Ramirez, P.; Cervera, J.; Mafe, S.; Ensinger, W. "Carbohydrate-mediated biomolecular recognition and gating of synthetic ion channels" *The Journal of Physical Chemistry C* **2013,** 117, (35), 18234-18242.

DOI: 10.1021/jp4054555

3.5.1 Introduction

Molecular recognition through lectin–carbohydrate interactions plays a pivotal role in life processes including immunochemical reactions in the immune response system, communication between the cells, embryogenesis, and infections caused by pathogens.[186] The cell surfaces carry various carbohydrate moieties such as glycoproteins, glycolipids and polysaccharides which have the potential for encoding biological information and participate in the cellular recognition system.[187] Lectins are ubiquitous in nature. The majority of membrane-bound lectins participate in the selective glycoproteins uptake and control the trafficking of glycoproteins in the cellular system of living organisms.[188]

Biorecognition can also be achieved in vitro by creating a natural-like environment into artificial sensors which exhibit some of the sensitivity of biological systems.[11] However, maintaining such a natural environment in artificial devices is a challenging task. Different strategies to obtain artificial nanofluidic devices mimicking the biological ion channels are possible.[6-8] Synthetic channels have emerged as "*abiotic*" equivalents to protein pores and ion channels with the ability to perform as specific biosensors.[10,29,118] Sensing with nanochannel-based systems depends on the nature of chemical groups (ligands) incorporated onto the inner channel walls. These groups act as binding sites for (bio)chemical analytes, and interact also with ions and molecules passing through the nanochannel. Different methods have been developed to introduce bio-recognition elements into gold nanotubes via thiol-chemistry[15,18,105] and onto the channel walls through the carbodiimide coupling chemistry in track-etched polymer membranes.[61,62,64,65,67,79,100,101]

The working principle of nanopore-based biosensing devices depends on the electronic readout, usually the current modulation. In the stochastic sensing approach (resistive-pulse method), an analyte translocates through the pore under the applied voltage and the transient current blockages result in downward current pulses that depend on the analyte molecule characteristics. In the "*steady-state*" approach, specific ligands are immobilized into the nanoscale architecture. Upon addition of the analyte molecules (receptors) in the surrounding environment, ligand-receptor interactions lead to volume exclusion (partial pore blocking) and/or electrostatic-based (changes in the surface pore charge) effects on the current-voltage curves. Sensing with nanopores relies on the traditional ligand–receptor interactions such as protein–protein, biotin–streptavidin/avidin, antigen–antibody, and peptide nucleic acid–DNA complexes.[60,63,69,111,113,115,178] However, these systems cannot be reversibly used due to very tight binding of the resulting bio-conjugates. For the dissociation of such ligand-receptor complexes, harsh conditions are required which can damage the sensory surface. The design and miniaturization of reversible and reusable biosensing devices still constitutes a challenge in biotechnology. Amongst the various ligand-receptor complexes, conjugates formed through lectin-carbohydrate interactions can be dissociated[110,189] without damage to the sensory surface. These devices can be miniaturized by immobilizing monolayers of carbohydrate (α-D-mannose/ α-D-glucose) moieties, which specifically recognize mannosyl/ glucosyl binding lectin protein, *e.g.*, concanavalin A (ConA).[190]

A variety of lectin proteins are isolated but ConA is studied extensively because of its well-known structure and remarkable contribution to biological processes.[186] ConA is isolated from the jack bean and exists as a tetramer with a molecular mass of 104 kDa at neutral pH. Each subunit of ConA possesses three binding sites: one site is specific for saccharide (α-D-mannose/ α-D-glucose) moieties; another site is for each divalent cation (Ca^{2+} and Mn^{2+}) required to activate the carbohydrate-combining site of ConA; and the third site is used for hydrophobic recognition.[191]

This study provides significant insights into the design, development and application of a ConA sensing and detection procedure. The method is based on the changes in the electrical conductance that are observed in the current–voltage (*I–V*) curves of a single nanochannel at different protein concentrations. Also ConA-mannopyranoside conjugates exhibit significant effects on the permeation rate of a multi-channel membrane. The sensing is specific to ConA protein and not to other control proteins, (*i.e,* lysozyme and bovine serum albumin, BSA) because of the particular chemical (α-D-mannopyranoside) moieties functionalized on the

channel surface. It is possible to detect the protein within a concentration range from 10 nM to 1000 nM and the ConA binding/unbinding is reversible, allowing several measuring cycles by washing the bioconjugated-nanochannel with mannose solution. The experimental results are explained qualitatively with a phenomenological model for the *I–V* curves that incorporates the basic experimental parameters (specific binding, protein concentration, voltage).

3.5.2 Ligand immobilization and bioconjugation

Single asymmetric nanochannels are prepared in 12 µm thick polyimide (PI) membranes (see experimental section 2.1.2 for details in chapter 2). The fabrication of the channels is achieved through the asymmetric chemical etching of the damage trails caused by the swift heavy ions along their trajectories.[41,156,179] Moreover, polyethylene terephthalate (PET) membranes containing an array of cylindrical nanochannels (5×10^8 channels cm^{-2}) are prepared by symmetric track-etching technique.[40] The track-etching process resulted in the generation of chemical (–COOH) groups onto the inner channel walls. The native –COOH moieties served as starting points for the covalent attachment of amine-terminated ligand molecules using carbodiimide coupling chemistry.

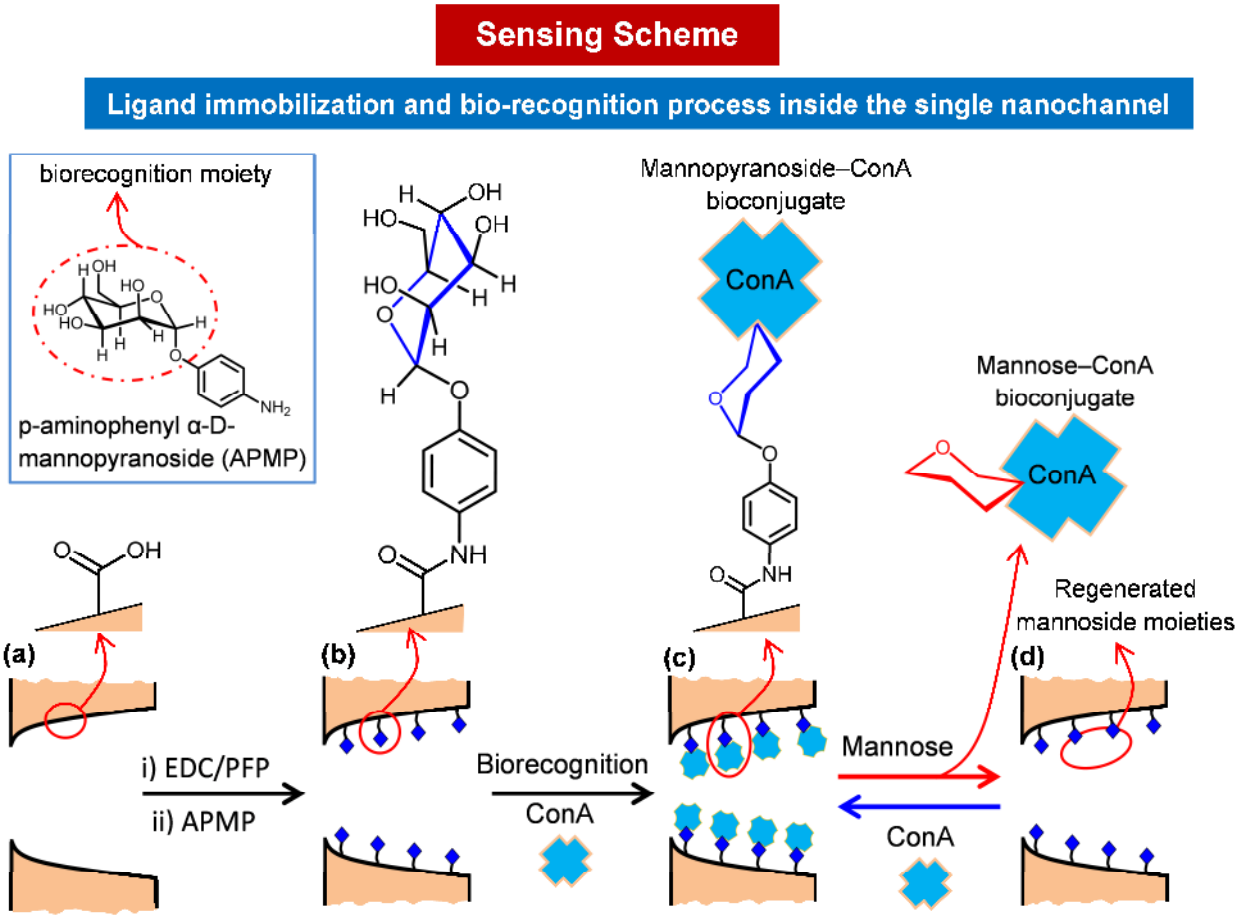

Figure 3.24: Schemes representing: (a) the as-prepared single asymmetric nanochannel containing native carboxylic acid (COOH) groups, (b) the covalent attachment of p-aminophenyl α-D-mannopyranoside (APMP) ligand molecules with COOH groups through carbodiimide coupling chemistry, (c) the selective recognition of ConA protein, and (d) the displacement of ConA by free mannose molecules and reversible ConA binding with regenerated mannopyranoside moieties on the nanochannel surface.

The covalent linkage of the channel surface –COOH groups with p-aminophenyl α-D-mannopyranoside (APMP) molecules is achieved by following a two-step reaction procedure. Firstly, the –COOH groups are converted into amine-reactive PFP-ester molecules. For this purpose, as-prepared channels (Figure 3.24a) are treated with an ethanolic solution containing a mixture of *N*-(3-dimethylaminopropyl)-*N'*-ethylcarbodiimide (EDC) and pentafluorophenol (PFP). Subsequently, the reactive intermediate, *i.e.*, PFP-ester molecules, are covalently coupled with the terminal-amine group of APMP ligand, as shown in Figure 3.24b. Figures 3.24c and 3.24d schematically show the recognition and displacement of ConA. For the experimental details of coupling reaction, see section 2.6.6 in chapter 2.

3.5.2.1 Single-channel membrane

The success of channel surface modification is evaluated through the *I–V* characteristics of the nanochannel before and after chemical modification (Figure 3.25a) recorded in symmetric electrolyte conditions (100 mM KCl aqueous solution at pH 7.2) on both sides of the single-channel membrane. The as-prepared channels are cation-selective due to the presence of ionized $–COO^-$ groups on the channel surface. [140,142,148,157] From Figure 3.25a, it is evident that channel modification leads to significant reduction of the current (from 24 to 13 nA) at a fixed positive voltage of 1 V. After modification, the channel surface charge is significantly decreased due to the presence of neutral mannopyranoside moieties in the APMP monolayers. This fact confirms the successful anchoring of APMP chains (Figure 3.24b) onto the inner channel walls.

The choice of APMP ligand is based on the presence of α-D-mannopyranoside moieties, which acted as bio-recognition elements for the specific detection of ConA. The interaction of ConA with these moieties occurred through hydrogen bonds and hydrophobic interactions (metal coordination bonds also play a decisive role in binding events). During the binding process, carbohydrate-combing sites are directed toward hydroxyl groups located at C-3, C-4, and C-6 positions of α-D-mannopyranoside to form hydrogen bonds with the NH groups, hydroxyls, and oxygen atoms in the amino acid sequence of the protein.[192]

After the anchoring of ligand monolayers onto the channel surface, we proceed to study the recognition and conjugation events inside the confined geometry. The sensing procedure is based on the modulation of ionic transport across the single-channel membranes in response to protein (receptor) binding/ unbinding with the biorecognition (ligand) elements. Upon addition of the analyte protein in the surrounding environment, the ligand-receptor interactions lead to volume exclusion and/or electrostatic-based effects. When the protein size is comparable with the channel tip opening, bioconjugation would lead to the partial occlusion of the channel and this occlusion hinders the flow of ions across the membrane.

To demonstrate the selective binding, the APMP-modified nanochannel is exposed to nonspecific (lysozyme and BSA) and specific (ConA) protein solutions. Figure 3.25b shows that the effects on the current are small even at high concentrations of the nonspecific analyte proteins in the electrolyte solution (0.1 M KCl containing 10 mM HEPES buffer to pH 7.2, 0.1 mM $CaCl_2$ and 0.1 mM $MnCl_2$). This fact confirms the low binding of lysozyme and BSA with the mannopyranoside units. Subsequently, when the same channel is subjected to a ConA protein solution of much lower concentration (1.5 µM) than those of lysozyme (7.0 µM) and BSA (8.0 µM), bio-conjugation inside the channel due to the specific ConA-mannoside binding interactions results in the significant decrease of current (from 13 to 1 nA at +1 V in Figure 3.25b). We observed only ~7% and ~28% decrease in the channel conductance for the case of lysozyme and BSA, respectively. On the contrary, after exposing the same channel to ConA protein, a decrease of ~92% in the conductance is observed when compared to the non-conjugated nanochannel. The specificity of ConA binding is associated with the carbohydrate binding sites in the protein molecules. Moreover, the results suggest that the changes in the conductance are only due to the specific ConA binding with mannopyranoside moieties, and not merely to the physical adsorption of proteins on the channel surface. In contrast at negative voltages (not shown here), the *I–V* curves at different

protein concentrations show low conductances and tend to overlap so that the nanopore is not useful for quantitative sensing.

To demonstrate the reversibility, the ConA-mannopyronoside conjugated channel is exposed to α-D-mannose solution for 30 min followed by washing with the same solution. ConA prefers to bind with free α-D-mannose molecules rather than to the bound mannopyranoside moieties. Therefore, the free α-D-mannose molecules dissociate the existing ConA-mannoside complexes on the inner channel surface. The displaced ConA binds and re-conjugates with the free mannose molecules (Figure 3.24d). This process regenerates the original sensor surface, providing undisturbed mannopyranoside moieties available to rebind with ConA molecules. Figure 3.25c demonstrates the reversibility (see also Figures 3.24c and 3.24d) for the case of the channel conductance at $V = +1$ V after several measuring cycles. It is obvious from Figure 3.25c that the ConA displacement from the channel surface leads to an increase in the conductance to levels of the non-conjugated channel (due to an increase in the effective channel diameter). Recently, Rant and co-workers have demonstrated the sensing of proteins through reversible binding/unbinding events inside receptor-modified synthetic nanochannels.[193] Our findings further suggest that the use of dissociable bio-conjugates incorporated into a single nanochannel may constitute a useful approach for sensing and controlled release processes.

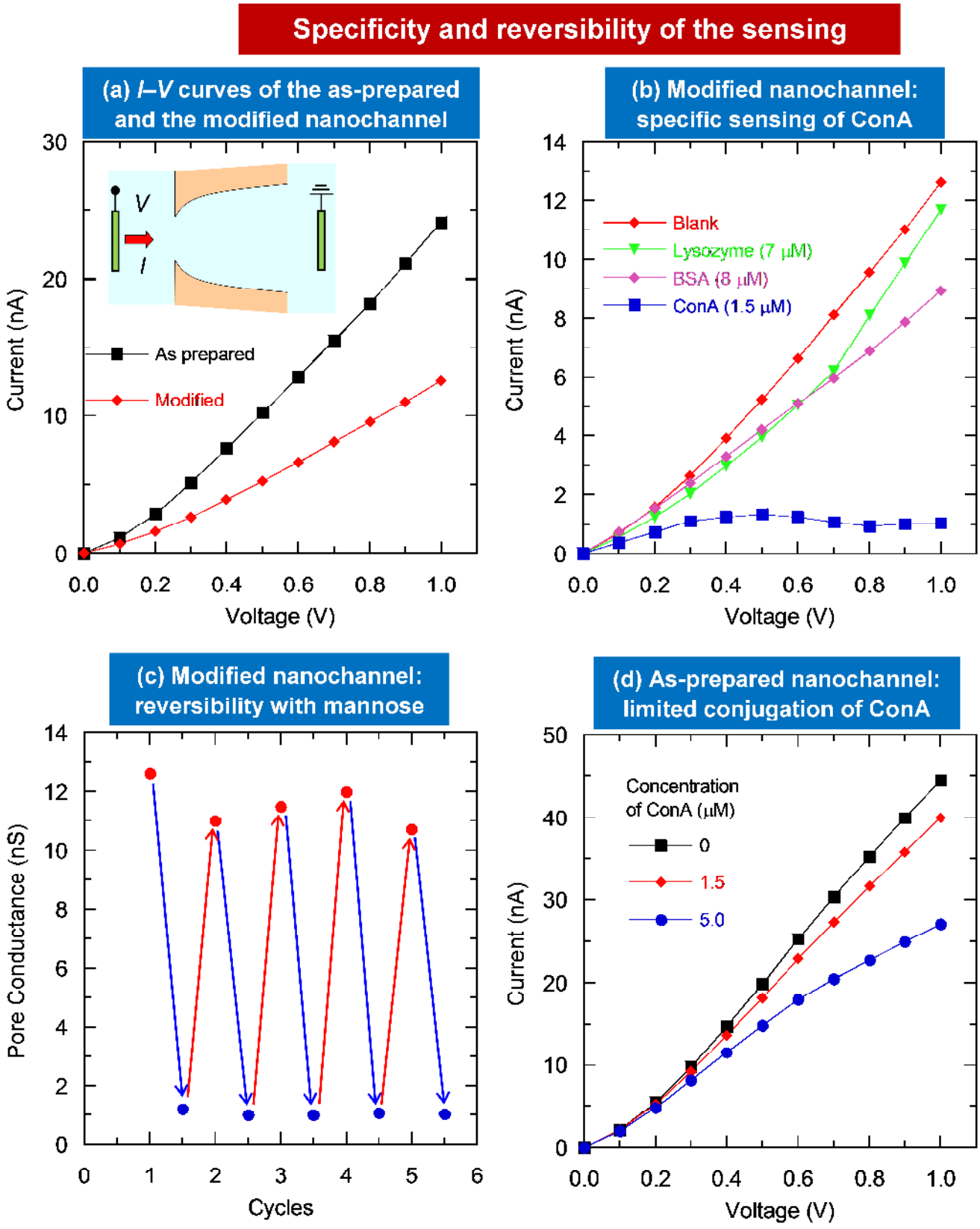

Figure 3.25: (a) The *I–V* curves for the as-prepared (carboxylated) and APMP-modified single asymmetric nanochannels. (b) The *I–V* characteristics of the modified nanochannel upon exposing to electrolyte solutions containing lysozyme, BSA and ConA proteins, separately. (c) The channel conductance at $V = 1$ V after several measuring cycles exhibiting the reversibility of ConA binding. (d) The *I–V* curves for the as-prepared nanochannels at high ConA concentrations in the micro-molar regime show a small to moderate decrease in the current.

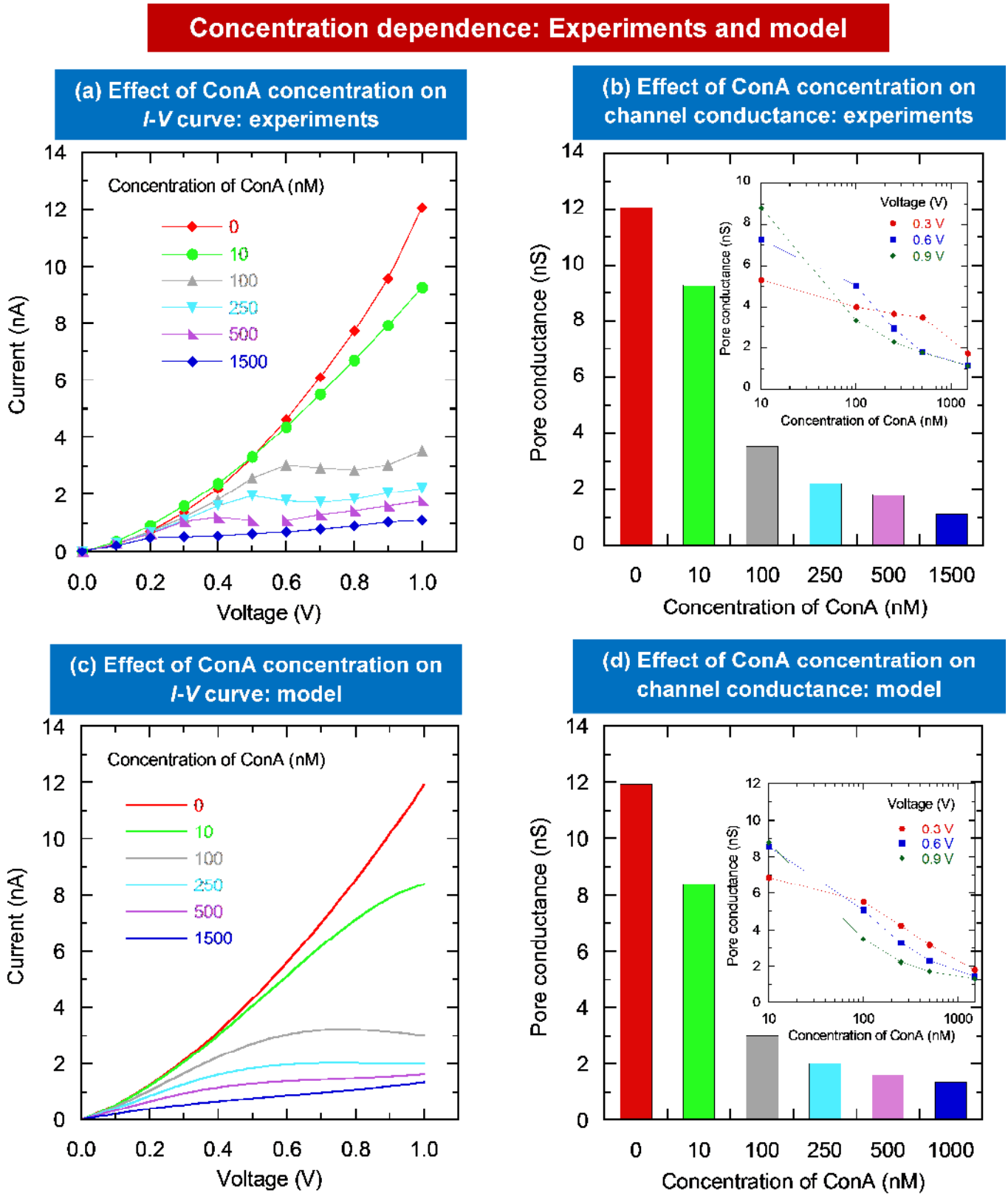

Figure 3.26: (a) *I–V* curves obtained for modified channel at different protein concentrations. (b) The experimental channel conductance values estimated from the *I–V* curves at V = 1 V. The inset shows the conductance values at three different voltages *V*. (c) The theoretical *I–V* curves reproduced the experimental trends of Figure 3.26a. (d) The calculated channel conductances agree with the experimental ones of Figure 3.26b. The pore basis radius (750 ± 10 nm) is determined from microscopy using multichannel samples etched at the same time as the single pore while the pore tip radius (15 ± 3 nm) is estimated by fitting the experimental data to the continuous model.

An additional negative control experiment is conducted using the as-prepared (carboxylated) nanochannel without any chemical modification. Figure 3.25d shows only a small decrease in the nanochannel conductance at ConA concentrations of the order of 1 μM. This fact strongly suggests that ConA can only specifically bind to the mannopyranoside moieties on the inner walls of the modified nanochannel. Recently, we have reported the supramolecular bio-conjugation of HRP enzyme and ConA protein inside the single nanopores, where mannose residues on the enzyme surface served as recognition elements for the binding of ConA molecules.[192] In the present study the immobilized APMP monolayers have several advantages over the previously reported method: a) mannopyranoside moieties served as recognition units for ConA instead of HRP enzymes and b) the APMP monolayer could not block the effective channel diameter compared to immobilized HRP enzyme molecules. Importantly, it is feasible here to determine the lowest possible detection limit of ConA using a monolayer of mannopyranoside moieties on the inner pore walls.

Finally, the sensitivity of the sensor is also evaluated by exposing the modified channel to different ConA concentrations. The conductances obtained from the *I–V* curves of Figure 3.26a at $V = 1$ V are shown in Figure 3.26b for ConA concentrations in the range $c_p = 10$ nM to 1 μM. The inset of Figure 3.26b shows the measured conductance values at three different voltages V for the protein concentrations in Figure 3.26a. Remarkably, the voltage may constitute an additional parameter for detection because different electrical potential windows can be used for the different protein concentration regimes (in Figure 3.26b, the 0.3 V curve should be employed at high concentrations, while that of 0.9 V should be used at low concentrations because of the improved discrimination).

From the results shown in Figures 3.25b, 3.26a, and 3.26b one can conclude that the modified channel is highly sensitive to ConA protein and that the channel conductance changes observed due to protein binding are useful for sensing and detection.

3.5.2.2 Modelling [XVII]

The modelling is carried out by theoretician collaborators. The conductance changes observed in the *I–V* curves are now interpreted in terms of the partial channel occlusion due to protein binding to the channel tip surface (see the channel scheme in Figure 3.25a). The binding should give a decrease of the cross-section area available for ionic conduction, though changes in the number of effective charges fixed at the channel surface might also occur.[62] Pore tip occlusion could be expected because the typical radius of the tip[157] is not much higher than the effective protein diameter (the physical size of ConA obtained by X-ray crystallographic methods and tapping mode AFM is between 6 and 9 nm.[194])

I–V curves obtained in the absence of ConA should be corrected by a factor lower than unity when the protein is present (Figure 3.26a). This factor accounts for the limited available area in the channel tip solution when the protein partially blocks this small region. The experimental *I–V* curves of Figure 3.26a show that this empirical factor depends not only on the protein concentration c_p but also on the voltage V. Also, the curves of Figures 3.25b and 3.25d show clearly that specific binding occurs only in the case of the APMP-modified channel. This experimental fact makes it necessary to incorporate a specific binding constant k in the model that takes high values only for the case of the ConA protein (Figures 3.25b and 3.26a) and the functionalized channel (Figure 3.25d). The following empirical equation for the *I–V* curves obtained in the presence of protein is proposed:

[XVII] Prof. Dr. P. Ramirez (Universitat Politècnica de València, Spain) and Prof. Dr. S. Mafe (Universitat de València, Spain) are highly acknowledged for the theoretical modelling of experimental results.

$$I(V) = I_0(V)\left\{1 - f\left[\frac{kc_p \exp(\alpha FV/RT)}{1 + kc_p \exp(\alpha FV/RT)}\right]\right\} \quad (1)$$

where $I_0(V)$ is the theoretical curve calculated in absence of protein (free pore). Constants *T, F* and *R* are the temperature, the Faraday constant and the gas constant, respectively. The curve $I_0(V)$ results from the fitting of the experimental data for the APMP-modified nanochannel with zero protein concentration (Figure 3.26a) to a model based on the Nernst-Planck equations, assuming a quasi-conical, slightly concave channel shape with approximate radii of ~15 ± 3 nm (tip opening) and ~750 ± 10 nm (base opening).[157,148] The parameter *f* is the maximum fraction of the cross-section area at the channel tip which is not available for ionic conduction when protein ConA is present (this fraction may also indirectly account for changes in the surface charge density of the channel). The parameter *f* can be estimated by comparing the *I–V* curve for the maximum protein concentration with that obtained for zero protein concentration in the high voltage limit of Figure 3.26a.

To incorporate the effects of the intermediate protein concentrations c_p and the voltage *V* (Figure 3.26a) in equation 1, *f* should be multiplied by the Langmuir-type binding isotherm between brackets. The binding constant *k* should assume low values for all proteins used here except for ConA (Figure 3.25b). The voltage-dependent exponential term accounts for the activated process allowing protein transport to the binding (mannopyranoside) groups located at the channel tip. We assume that it is protein binding over a small region around the channel tip which causes the observed conductance changes. Indeed, the channel tip dictates the experimental *I–V* curves of asymmetric nanochannels[140,148,157] and protein binding over most of the channel, which is characterized by a relatively wide cross-section area, should not block the current significantly (see the channel scheme of Figure 3.25a; the basis has a diameter much larger than the channel tip).[62,140,148,157]

The channel tip and ConA are negatively charged at the neutral pH of the experiments[110,194] Therefore, the protein entering the channel basis and proceeding across the axis in the channel scheme of Figure 3.25a should overcome an electrostatic barrier to reach finally the small region around the channel tip where binding occurs. It is conceivable that the protein could surmount this barrier due to the fixed charges assisted by the local potential drop at the channel end. This effective potential drop should then be only a small fraction α of the total voltage *V* applied across the whole nanochannel and the external solutions. Note that we do not assume bulk diffusion for the protein adsorption to the pore tip but a thermally activated process where the argument of the exponential contains an electrostatic barrier which is partly decreased by a fraction of the total potential. We introduce $f = 0.9$ from the maximum current decrease observed in Figure 3.26a and tentatively assume $\alpha = 0.1$. The binding constant *k* can then be estimated taking into account that $kc_p \exp(\alpha FV/RT)$ in eq. (1) should be of the order of unity at $V = 1$V when $c_p = 10 - 100$ nM (see Figure 3.26a). This procedure gives $k = 10^6$ M^{-1} which is in the lower range of binding constants reported for ConA-mannose binding,[194] in agreement with the approximate reversibility of the protein binding (Figure 3.25c) when the channel is washed with a mannose solution (Figure 3.24d)

The results shown in Figure 3.26c (*I–V* curves) and 3.26d (nanochannel conductance values) reproduce the experimental trends of Figures 3.26a and 3.26b. The model offers a qualitative explanation for the effects of ConA concentration and voltage on the channel conductance and reproduces the change in the concavity of the *I–V* curves observed at high protein concentrations and voltages.

3.5.2.3 Multichannel membrane

To extend further the results obtained for the single-channel, I have studied the effect of ConA binding/unbinding on the permeation rate of molecules across a nanoporous membrane containing cylindrical

nanochannels. Since cylindrical nanochannels of small diameter (< 50 nm) are not etchable in the PI membrane,[195] the polyethylene terephthalate (PET) membrane is used as an alternative material for the fabrication of cylindrical nanochannels. The pore surface chemistry in both membranes (PI and PET) is the same, *i.e.,* the inner pore walls contain carboxylic acid groups. The nanoporous membrane contains an array of cylindrical nanochannels (5×10^8 channels cm^{-2}) of 28 ± 3 nm in diameter and is modified with APMP monolayer. The mass transport through nanochannels is mainly governed by volume exclusion and electrostatic effects. The volume exclusion is significant because the formation of ConA-mannopyranoside bioconjugates can affect the effective channel diameter available for the permeation of molecules across the membrane. Therefore, to avoid any influence of electrostatic interactions on the permeation process, the uncharged 2,2′-dipyridine (DPy) molecules is used for the mass transport experiments.

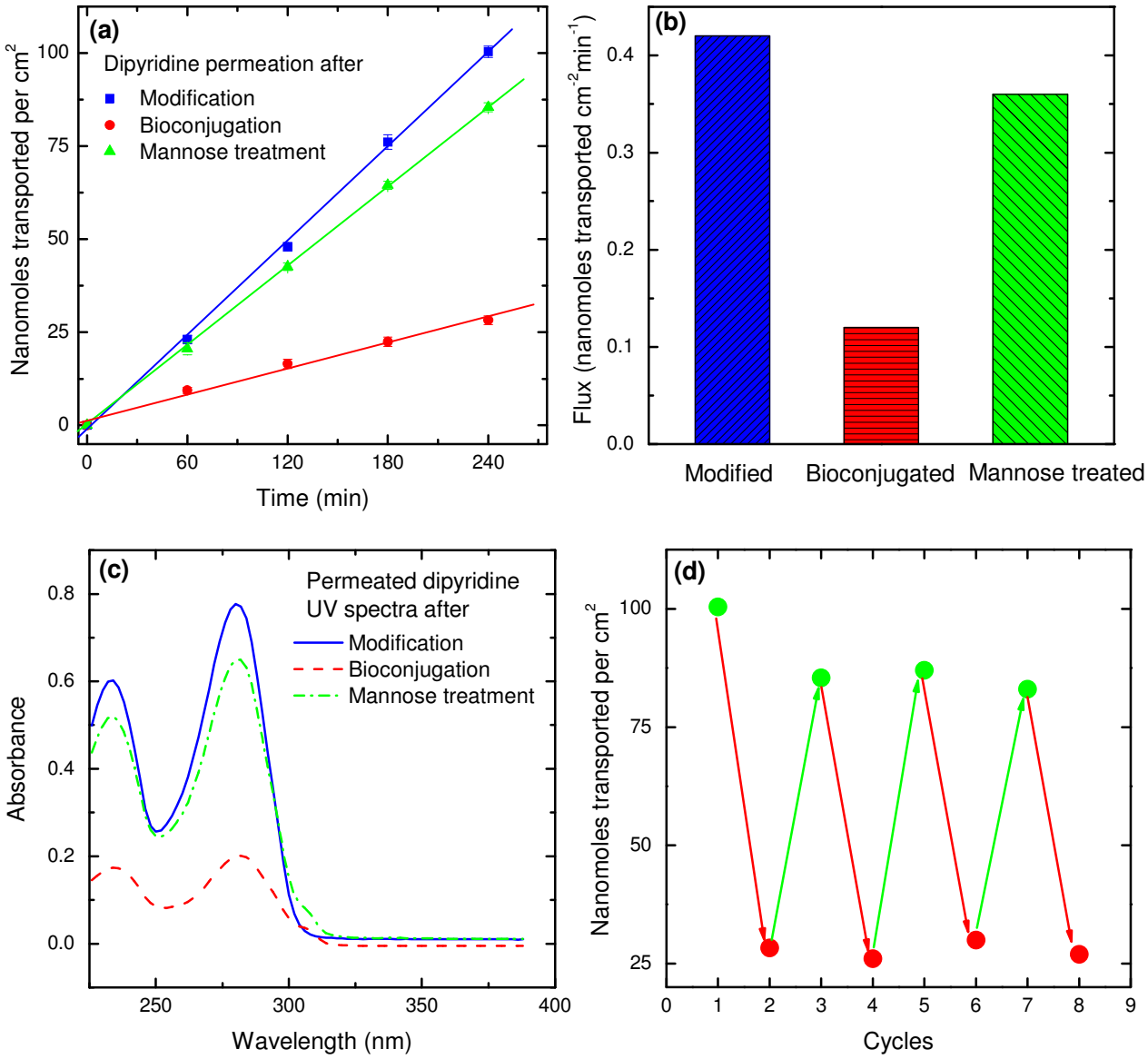

Figure 3.27: Permeation data for dipyridine: a) number of nanomoles transported versus time, (b) permeation rate (flux), and (c) absorption spectra of the permeate solution after 240 min of diffusion time across the non-bioconjugated, bioconjugated and mannose treated membranes. (d) Different cycles showing the dipyridine nanomoles permeated after reversible bioconjugation on and displacement from the channel surface by membrane exposition to ConA and mannose solutions, respectively.

The APMP-modified nanoporous membrane is fixed between the two compartments of the conductivity cell and the feed compartment is filled with an aqueous solution of DPy (10 mM) prepared in HEPES (pH 7.2) buffer containing 0.1 mM of Ca^{2+} ion and 0.1 mM of Mn^{2+} ion. The other chamber referred to as permeate compartment is filled only with buffer solution. After regular time intervals, the concentration of DPy molecules in the permeate compartment is estimated by measuring the UV absorbance with an UV/Vis spectrophotometer (Figures 3.27a, 3.27b, and 3.27c).

Figure 3.27a shows the number of nanomoles of DPy molecules permeated per cm^2 obtained with the non-bioconjugated (APMP-modified), bioconjugated (ConA-mannopyranoside conjugated) and mannose treated (washed with free mannose solution) membranes *versus* time. Figure 3.27b shows that bioconjugation results in a four-fold decrease (from ~100 to 28 nanomoles) in the permeation of DPy molecules after 240 min of diffusion time. Note that conjugation of ConA molecules with mannopyranoside moieties on the channel walls should decrease the effective cross-section of the nanochannels. Figure 3.27a shows that after mannose treatment the permeation of DPy molecules is increased from ~28 to ~85 nanomoles because the ConA-mannopyranoside conjugates on the inner walls are dissociated by the free mannose molecules, leading to the widening of the nanochannels. The DPy permeation flux can be determined from the slope of the experimental lines in Figure 3.27a, giving ~0.42, 0.12 and 0.36 nanomoles cm^{-2} min^{-1} transported across the modified, bioconjugated and mannose treated membrane, respectively (Figure 3.27b). Finally, the reversibility of ConA conjugation on and displacement from the channel surface is shown in Figure 3.27d.

3.5.3 Conclusions

In summary, the reversible biomolecular recognition/conjugation in single-channel and multichannel membranes mediated by carbohydrates was demonstrated. For this purpose, channel surface was decorated with mannopyranoside moieties. The protein recognition events, based on the observed changes in the electrical conductance for the case of the single-channel membrane, have also been studied in dipyridine permeation experiments for the multichannel membrane. The nanofluidic sensor specifically recognized ConA protein for concentrations in the range from 10 nM to 1000 nM, but not the control proteins (lysozyme and BSA) due to the specific ConA affinity towards mannopyranoside moieties functionalized onto the channel surface. The conjugated ConA protein was displaced by simple membrane washing with a mannose solution, allowing further use of the sensor. Finally, the experimental results were explained with a phenomenological model incorporating the basic experimental trends observed in the *I–V* curves.

4. Summary and outlook

5.1 Summary

In a nutshell, this thesis described the following goals which I have achieved experimentally during my PhD research work.

- Single- and multi-ion tracked polymer membrane samples were prepared by irradiation with swift heavy ions at the GSI (UNILAC accelerator). These latent tracks were then converted into nanosized pores by exposing to a chemical etchant. The membranes containing conical and cylindrical nanopores were fabricated by using asymmetric and symmetric track-etching techniques, respectively. The process of heavy ion irradiation and the concomitant chemical etching led to the generation of chemical moieties (–COOH) on the surface and inner pore walls. These groups were further exploited for the chemical attachment of stimuli-responsive molecules having amine in their backbone through carbodiimide coupling chemistry. The ionic/moleuclar flux across the membrane was tuned in response to variations in the external environmental conditions.
- Thermo-responsive membranes were prepared by the immobilisation of amine-terminated polymer chains (PNIPAAM–NH_2) on the inner pore wall via "grafting-to" approach through carbodiimide chemistry. In this case, the effective pore diameter was tuned due to swelling/shrinking of the polymer chains by changing the environmental temperature, leading to decrease/increase in the ionic transport through the modified nanopores. Single conical pore membrane and multi-pore membranes containinig cylindrical and conical nanopores were studied in this experiment. The experimental results demonstrated the reversible temperature-dependent analyte permeation across the multi-pore membranes and ionic transport through single-pore membrane in response to changes in the electrolyte solution in contact with the nanopores.
- For the preparation of light-sensitive nanopores, the inner pore walls were decorated with monolayers of photolabile molecules. The terminal hydrophobic and uncharged pyrene moeities were removed via UV irradiation, leading to the generation of hydrophilic and negatively charged (–COOH) groups. The photo-responsive behaviour of the nanopores was characterized experimentally and theoretically through the *I-V* curves for the case of single-pore membrane and selective permeation of anayltes through the multi-pore membrane.
- Dual-responsive nanopores, i.e., nanpores that respond to both light and pH, were also fabricated in this work. For this purpose, the pore walls were modified with photosensitive "caged" lysine chains. The uncharged hydrophobic NVOC groups were cleaved from the protected lysine by exposing to UV light. This resulted in the production of hydrophilic zwitterionic groups on the inner pore walls. In this experiment polymer membranes having single and arrays of asymmetric nanopores were studied for the pH-controlled transport of ionic and molecular analytes before and after the UV-light irradiation.
- The next step in this work was to modulate the ionic transport via biomolecular conjugation inside the confined environment. To this end, nanopore surface is modified with a suitable biorecognition element (ligand). In the first case, iron-terPy ligands were immobilized on the inner pore walls. These ligands specifically recognize and bioconjugate with lactoferrin protein. The biocojugates inside the nanopore significantly reduced the effective pore diameter available for the transport of ion which in turn resulted in reduction of ionic flux across the membrane. But this process was irreversible, i.e., the pore surface with initial ligand moieties can not be regenerated.

- In the second experiment, an attempt was made to fabricate biomolecular-responsive nanopore in which after use the original surface can be reproduced without any damage to the nanopore. For this purpose, the nanopore surface was decorated with manopyranoside moieties. The mannopyranoside groups can selectively recognize and bioconjugate with lectin (ConA) protein. The biomolecular conjugation and biorecognition events inside the confined geometries have been studied based on conductance changes for the case of single-pore membrane and permeation experiments for the case of multipore membrane. The ConA protein molecules were displaced by simply washing the bioconjugated membrane with a mannose solution, allowing the further use of ligand-modified pores.

5.2 Outlook

The goal of experiments and results obtained in this PhD work was to provide a framework for future development in the field of nanopore-based responsive systems, where the track-etched polymer membranes are still the materials of choice to miniaturize new "smart" nanodevices. To this end, following experiments are planned to explore the responsive behaviour of these nanoporous membranes in more detail:

- In addition to PET and PI, other polymer membranes like polycarbonate (PC) and polyetheretherketone (PEEK) will be employed to chemically modify and study the responsiveness of nanopores.
- The "grafting-to" route will also be used to attach end-functionalized "smart" polymer brushes on the pore surface. These responsive polymer chains will act as "ON" / "OFF" valve which can be opened or closed at will upon the application of external stimuli like temperature, pH, transition metal ions, electrical field, or small molecules. It will also be managed to graft the polymer brushes which respond to more than one stimulus, *i.e.,* pH–temperature, light–temperature, pH–light, *etc.* The responsive membranes would be used for the separation/drug delivery processes.
- In order to achieve reversible light-responsive control over nanopore transport properties, photo-responsive monolayer assemblies of coumarin, azobenzene or spiropyran derivatives will be functionalized on the pore surface. Irradiating the coumarin functionalized membrane with a specific wavelength of light will lead to the formation of cyclobutane dimer which in turn close the pore. The opening of the channel will be achieved by the regeneration of coumarin monomers through irradiating with high energy irradiation which will permit the molecules to pass through nanopores. For the case of azobenzene and spiropyran assemblies, the effective cross-section would be controlled upon the application of UV light via the reversible *cis-trans* photo-isomerization of these molecules anchored on the inner walls and surface of the nanochannel.
- It will also be interesting to investigate the bio-catalysed redox reactions inside the confined environment by immobilizing the desired enzyme on the inner pore walls. The membranes containing enzyme modified nanochannels will be able to very efficiently perform redox reactions inside the nano-sized pores. This can be visualised from the products of the redox reactions occurring in the nanopore.
- Moreover, in future work the opening/closing of the pores will be triggered by the modulation of pH of the surrounding environment. This will be accomplished by first anchoring the recognition elements on the outer pore openings. Subsequently, these recognition elements will interact with specifically functionalized nanoparticles, acting as a gate-keeper on the pore opening. The reversible detachment/attachment of particles will be achieved simply by tuning the solution pH in contact with membrane.

5. References

(1) Hille, B.: *Ionic channels of excitable membranes*; 3rd ed.; Sinauer Associates Inc.: Sunderland, MA, 2001.

(2) Doyle, D. A.; Cabral, J. M.; Pfuetzner, R. A.; Kuo, A.; Gulbis, J. M.; Cohen, S. L.; Chait, B. T.; MacKinnon, R. The Structure of the Potassium Channel: Molecular Basis of K+ Conduction and Selectivity. *Science* **1998**, *280*, 69-77.

(3) Doupnik, C. A.; Davidson, N.; Lester, H. A. The inward rectifier potassium channel family. *Curr. Opin. Neurobiol.* **1995**, *5*, 268-277.

(4) Lev, S.; Moreno, H.; Martinez, R.; Canoll, P.; Peles, E.; Musacchio, J. M.; Plowman, G. D.; Rudy, B.; Schlessinger, J. Protein tyrosine kinase PYK2 involved in Ca2+-induced regulation of ion channel and MAP kinase functions. *Nature* **1995**, *376*, 737-745.

(5) Gouaux, E.; MacKinnon, R. Principles of selective ion transport in channels and pumps. *Science* **2005**, *310*, 1461-1465.

(6) Dekker, C. Solid-state nanopores. *Nat. Nanotechnol.* **2007**, *2*, 209-215.

(7) Gyurcsanyi, R. E. Chemically-modified nanopores for sensing. *TrAC, Trends Anal. Chem.* **2008**, *27*, 627-639.

(8) Healy, K.; Schiedt, B.; Morrison, A. P. Solid-state nanopore technologies for nanopore-based DNA analysis. *Nanomedicine* **2007**, *2*, 875-897.

(9) de la Escosura-Muñiz, A.; Merkoçi, A. Nanochannels Preparation and Application in Biosensing. *ACS Nano* **2012**, *6*, 7556-7583.

(10) Hou, X.; Guo, W.; Jiang, L. Biomimetic smart nanopores and nanochannels. *Chem. Soc. Rev.* **2011**, *40*, 2385-2401.

(11) Howorka, S.; Siwy, Z. Nanopore analytics: sensing of single molecules. *Chem. Soc. Rev.* **2009**, *38*, 2360-2384.

(12) Jeon, G.; Yang, S. Y.; Kim, J. K. Functional nanoporous membranes for drug delivery. *J. Mater. Chem.* **2012**, *22*, 14814-14834.

(13) Stroeve, P.; Ileri, N. Biotechnical and other applications of nanoporous membranes. *Trend. Biotechnol.* **2011**, *29*, 259-266.

(14) Wandera, D.; Wickramasinghe, S. R.; Husson, S. M. Stimuli-responsive membranes. *J. Membr. Sci.* **2010**, *357*, 6-35.

(15) Jirage, K. B.; Hulteen, J. C.; Martin, C. R. Nanotubule-based molecular-filtration membranes. *Science* **1997**, *278*, 655-658.

(16) Kontturi, K.; Murtomäki, L.; Manzanares, J. A.: *Ionic Transport Processes*; Oxford University: Oxford, 2008.

(17) Lee, S. B.; Martin, C. R. pH-switchable, ion-permselective gold nanotubule membrane based on chemisorbed cysteine. *Anal.Chem.* **2001**, *73*, 768-775.

(18) Lee, S. B.; Mitchell, D. T.; Trofin, L.; Nevanen, T. K.; Soderlund, H.; Martin, C. R. Antibody-based bio-nanotube membranes for enantiomeric drug separations. *Science* **2002**, *296*, 2198-2200.

(19) Savariar, E. N.; Krishnamoorthy, K.; Thayumanavan, S. Molecular discrimination inside polymer nanotubules. *Nat. Nanotechnol.* **2008**, *3*, 112-117.

(20) Sinner, E. K.; Knoll, W. Functional tethered membranes. *Curr. Opinion Chem. Biol.* **2001**, *5*, 705-711.

(21) Song, L.; Hobaugh, M. R.; Shustak, C.; Cheley, S.; Bayley, H.; Gouaux, J. E. Structure of Staphylococcal α-Hemolysin, a Heptameric Transmembrane Pore. *Science* **1996**, *274*, 1859-1865.

(22) Nguyen, T. L. Three-dimensional Model of the Pore Form of Anthrax Protective Antigen. Structure and Biological Implications. *J. Biomol. Struct. Dyn.* **2004**, *22*, 253-265.

(23) Benz, R.: *Bacterial and Eukaryotic Porins: Structure, Function, Mechanism*; Wiley-VCH Verlag GmbH & Co. KGaA, 2004.

(24) Butler, T. Z.; Pavlenok, M.; Derrington, I. M.; Niederweis, M.; Gundlach, J. H. Single-molecule DNA detection with an engineered MspA protein nanopore. *Proc. Nat. Acad. Sci. U.S.A.* **2008**, *105*, 20647-20652.

(25) Menestrina, G.; Serra, M. D.; Lazarovici, P.: *Pore-forming Peptides and Protein Toxins*; Taylor & Francis Inc, CRC, 2003.

(26) Gu, L. Q.; Braha, O.; Conlan, S.; Cheley, S.; Bayley, H. Stochastic sensing of organic analytes by a pore-forming protein containing a molecular adapter. *Nature* **1999**, *398*, 686-690.

(27) Sakai, N.; Mareda, J.; Matile, S. Ion channels and pores, made from scratch. *Mol. Biosyst.* **2007**, *3*, 658-666.

(28) Bayley, H.; Braha, O.; Cheley, S.; Gu, L.-Q.: Engineered Nanopores. In *Nanobiotechnology*; Wiley-VCH Verlag GmbH & Co. KGaA: Weinheim, Germany, 2005; pp 93-112.

(29) Bayley, H.; Cremer, P. S. Stochastic sensors inspired by biology. *Nature* **2001**, *413*, 226-230.

(30) Braha, O.; Walker, B.; Cheley, S.; Kasianowicz, J. J.; Song, L. Z.; Gouaux, J. E.; Bayley, H. Designed protein pores as components for biosensors. *Chem. Biol.* **1997**, *4*, 497-505.

(31) Cheley, S.; Gu, L. Q.; Bayley, H. Stochastic sensing of nanomolar inositol 1,4,5-trisphosphate with an engineered pore. *Chem. Biol.* **2002**, *9*, 829-838.

(32) Howorka, S.; Movileanu, L.; Braha, O.; Bayley, H. Kinetics of duplex formation for individual DNA strands within a single protein nanopore. *Proc. Nat. Acad. Sci. U.S.A.* **2001**, *98*, 12996-13001.

(33) Chen, M.; Khalid, S.; Sansom, M. S. P.; Bayley, H. Outer membrane protein G: Engineering a quiet pore for biosensing. *Proc. Nat. Acad. Sci. U.S.A.* **2008**, *105*, 6272-6277.

(34) Alcaraz, A.; Ramirez, P.; Garcia-Gimenez, E.; Lopez, M. L.; Andrio, A.; Aguilella, V. M. A pH-tunable nanofluidic diode: Electrochemical rectification in a reconstituted single ion channel. *J. Phys. Chem. B* **2006**, *110*, 21205-21209.

(35) Li, J.; Stein, D.; McMullan, C.; Branton, D.; Aziz, M. J.; Golovchenko, J. A. Ion-beam sculpting at nanometre length scales. *Nature* **2001**, *412*, 166-169.

(36) Storm, A. J.; Chen, J. H.; Ling, X. S.; Zandbergen, H. W.; Dekker, C. Fabrication of solid-state nanopores with single-nanometre precision. *Nat. Mater.* **2003**, *2*, 537-540.

(37) Wu, S. S.; Park, S. R.; Ling, X. S. Lithography-free formation of nanopores in plastic membranes using laser heating. *Nano Lett.* **2006**, *6*, 2571-2576.

(38) Zhang, B.; Zhang, Y.; White, H. S. The Nanopore Electrode. *Anal. Chem.* **2004**, *76*, 6229-6238.

(39) Yuan, J. H.; He, F. Y.; Sun, D. C.; Xia, X. H. A Simple Method for Preparation of Through-Hole Porous Anodic Alumina Membrane. *Chem. Mater.* **2004**, *16*, 1841-1844.

(40) Apel, P. Y. Heavy Particle Tracks in Polymers and Polymeric Track Membranes. *Radiat. Meas.* **1995**, *25*, 667-674.

(41) Apel, P. Y.; Korchev, Y. E.; Siwy, Z.; Spohr, R.; Yoshida, M. Diode-like single-ion track membrane prepared by electro-stopping. *Nucl. Instrum. Methods Phys. Res., Sect. B* **2001**, *184*, 337-346.

(42) Spohr, R. Status of ion track technology - Prospects of single tracks. *Radiat. Meas.* **2005**, *40*, 191-202.

(43) Park, S. R.; Peng, H.; Ling, X. S. Fabrication of Nanopores in Silicon Chips Using Feedback Chemical Etching. *Small* **2007**, *3*, 116-119.

(44) Leoni, L.; Boiarski, A.; Desai, T. Characterization of Nanoporous Membranes for Immunoisolation: Diffusion Properties and Tissue Effects. *Biomed. Microdevices* **2002**, *4*, 131-139.

(45) Wei, C.; Bard, A. J.; Feldberg, S. W. Current rectification at quartz nanopipet electrodes. *Anal. Chem.* **1997**, *69*, 4627-4633.

(46) Umehara, S.; Pourmand, N.; Webb, C. D.; Davis, R. W.; Yasuda, K.; Karhanek, M. Current rectification with poly-L-lysine-coated quartz nanopipettes. *Nano Lett.* **2006**, *6*, 2486-2492.

(47) Uram, J. D.; Ke, K.; Hunt, A. J.; Mayer, M. Label-Free Affinity Assays by Rapid Detection of Immune Complexes in Submicrometer Pores. *Angew. Chem. Int. Ed.* **2006**, *45*, 2281-2285.

(48) Merchant, C. A.; Healy, K.; Wanunu, M.; Ray, V.; Peterman, N.; Bartel, J.; Fischbein, M. D.; Venta, K.; Luo, Z.; Johnson, A. T. C.; Drndić, M. DNA Translocation through Graphene Nanopores. *Nano Lett.* **2010**, *10*, 2915-2921.

(49) Vlassiouk, I.; Krasnoslobodtsev, A.; Smirnov, S.; Germann, M. "Direct" detection and separation of DNA using nanoporous alumina filters. *Langmuir* **2004**, *20*, 9913-9915.

(50) Vlassiouk, I.; Takmakov, P.; Smirnov, S. Sensing DNA hybridization via ionic conductance through a nanoporous electrode. *Langmuir* **2005**, *21*, 4776-4778.

(51) Martin, C. R.; Nishizawa, M.; Jirage, K.; Kang, M. S.; Lee, S. B. Controlling ion-transport selectivity in gold nanotubule membranes. *Adv. Mater.* **2001**, *13*, 1351-1362.

(52) Chen, P.; Mitsui, T.; Farmer, D. B.; Golovchenko, J.; Gordon, R. G.; Branton, D. Atomic Layer Deposition to Fine-Tune the Surface Properties and Diameters of Fabricated Nanopores. *Nano Lett.* **2004**, *4*, 1333-1337.

(53) Wanunu, M.; Meller, A. Chemically modified solid-state nanopores. *Nano Lett.* **2007**, *7*, 1580-1585.

(54) Nilsson, J.; Lee, J. R. I.; Ratto, T. V.; Letant, S. E. Localized functionalization of single nanopores. *Adv. Mater.* **2006**, *18*, 427-431.

(55) Vlassiouk, I.; Park, C. D.; Vail, S. A.; Gust, D.; Smirnov, S. Control of nanopore wetting by a photochromic spiropyran: A light-controlled valve and electrical switch. *Nano Lett.* **2006**, *6*, 1013-1017.

(56) Wang, G. L.; Bohaty, A. K.; Zharov, I.; White, H. S. Photon gated transport at the glass nanopore electrode. *J. Am. Chem. Soc.* **2006**, *128*, 13553-13558.

(57) Zhang, L.-X.; Cai, S.-L.; Zheng, Y.-B.; Cao, X.-H.; Li, Y.-Q. Smart Homopolymer Modification to Single Glass Conical Nanopore Channels: Dual-Stimuli-Actuated Highly Efficient Ion Gating. *Adv. Funct. Mater.* **2011**, *21*, 2103-2107.

(58) Ali, M.; Bayer, V.; Schiedt, B.; Neumann, R.; Ensinger, W. Fabrication and functionalization of single asymmetric nanochannels for electrostatic / hydrophobic association of protein molecules. *Nanotechnology* **2008**, *19*, 485711.

(59) Ali, M.; Nasir, S.; Ahmed, I.; Fruk, L.; Ensinger, W. Tuning nanopore surface polarity and rectification properties through enzymatic hydrolysis inside nanoconfined geometries. *Chem. Commun.* **2013**, *49*, 8770-8772.

(60) Ali, M.; Nasir, S.; Nguyen, Q. H.; Sahoo, J. K.; Tahir, M. N.; Tremel, W.; Ensinger, W. Metal Ion Affinity-based Biomolecular Recognition and Conjugation inside Synthetic Polymer Nanopores Modified with Iron-Terpyridine Complexes. *J. Am. Chem. Soc.* **2011**, *133*, 17307-17314.

(61) Ali, M.; Nasir, S.; Ramirez, P.; Ahmed, I.; Nguyen, Q. H.; Fruk, L.; Mafe, S.; Ensinger, W. Optical Gating of Photosensitive Synthetic Ion Channels. *Adv. Funct. Mater.* **2012**, *22*, 390-396.

(62) Ali, M.; Nasir, S.; Ramirez, P.; Cervera, J.; Mafe, S.; Ensinger, W. Calcium Binding and Ionic Conduction in Single Conical Nanopores with Polyacid Chains: Model and Experiments. *ACS Nano* **2012**, *6*, 9247-9257.

(63) Ali, M.; Neumann, R.; Ensinger, W. Sequence-Specific Recognition of DNA Oligomer Using Peptide Nucleic Acid (PNA)-Modified Synthetic Ion Channels: PNA/DNA Hybridization in Nanoconfined Environment. *ACS Nano* **2010**, *4*, 7267-7274.

(64) Ali, M.; Nguyen, Q. H.; Neumann, R.; Ensinger, W. ATP-modulated ionic transport through synthetic nanochannels. *Chem. Commun.* **2010**, *46*, 6690-6692.

(65) Ali, M.; Ramirez, P.; Mafe, S.; Neumann, R.; Ensinger, W. A pH-tunable nanofluidic diode with a broad range of rectifying properties. *ACS Nano* **2009**, *3*, 603-608.

(66) Siwy, Z. S.; Howorka, S. Engineered voltage-responsive nanopores. *Chem. Soc. Rev.* **2010**, *39*, 1115-1132.

(67) Vlassiouk, I.; Siwy, Z. S. Nanofluidic diode. *Nano Lett.* **2007**, *7*, 552-556.

(68) Ali, M.; Yameen, B.; Cervera, J.; Ramirez, P.; Neumann, R.; Ensinger, W.; Knoll, W.; Azzaroni, O. Layer-by-Layer Assembly of Polyelectrolytes into Ionic Current Rectifying Solid-State Nanopores: Insights from Theory and Experiment. *J. Am. Chem. Soc.* **2010**, *132*, 8338-8348.

(69) Ali, M.; Yameen, B.; Neumann, R.; Ensinger, W.; Knoll, W.; Azzaroni, O. Biosensing and supramolecular bioconjugation in single conical polymer nanochannels. Facile incorporation of biorecognition elements into nanoconfined geometries. *J. Am. Chem. Soc.* **2008**, *130*, 16351-16357.

(70) Pan, K.; Ren, R. M.; Dan, Y.; Cao, B. Synthesis of Controlled Thermoresponsive PET Track-Etched Membranes by ATRP Method. *J. Appl. Polym. Sci.* **2011**, *122*, 2047-2053.

(71) Yameen, B.; Ali, M.; Neumann, R.; Ensinger, W.; Knoll, W.; Azzaroni, O. Single conical nanopores displaying pH-tunable rectifying characteristics. Manipulating ionic transport with zwitterionic polymer brushes. *J. Am. Chem.Soc.* **2009**, *131*, 2070-2071.

(72) Yameen, B.; Ali, M.; Neumann, R.; Ensinger, W.; Knoll, W.; Azzaroni, O. Synthetic Proton-Gated Ion Channels via Single Solid-State Nanochannels Modified with Responsive Polymer Brushes. *Nano Lett.* **2009**, *9*, 2788-2793.

(73) Yameen, B.; Ali, M.; Neumann, R.; Ensinger, W.; Knoll, W.; Azzaroni, O. Ionic Transport Through Single Solid-State Nanopores Controlled with Thermally Nanoactuated Macromolecular Gates. *Small* **2009**, *5*, 1287-1291.

(74) Yameen, B.; Ali, M.; Neumann, R.; Ensinger, W.; Knoll, W.; Azzaroni, O. Proton-regulated rectified ionic transport through solid-state conical nanopores modified with phosphate-bearing polymer brushes. *Chem. Commun.* **2010**, *46*, 1908-1910.

(75) Hou, X.; Liu, Y. J.; Dong, H.; Yang, F.; Li, L.; Jiang, L. A pH-Gating Ionic Transport Nanodevice: Asymmetric Chemical Modification of Single Nanochannels. *Adv. Mater.* **2010**, *22*, 2440-2443.

(76) Hou, X.; Yang, F.; Li, L.; Song, Y. L.; Jiang, L.; Zhu, D. B. A Biomimetic Asymmetric Responsive Single Nanochannel. *J. Am. Chem. Soc.* **2010**, *132*, 11736-11742.

(77) Nasir, S.; Ali, M.; Ensinger, W. Thermally controlled permeation of ionic molecules through synthetic nanopores functionalized with amine-terminated polymer brushes. *Nanotechnology* **2012**, *23*, 225502.

(78) Huck, W. T. S. Responsive polymers for nanoscale actuation. *Mater. Today* **2008**, *11*, 24-32.

(79) Hou, X.; Zhang, H. C.; Jiang, L. Building Bio-Inspired Artificial Functional Nanochannels: From Symmetric to Asymmetric Modification. *Angew. Chem. Int. Ed.* **2012**, *51*, 5296-5307.

(80) Huang, J.; Zhang, X.; McNaughton, P. A. Modulation of temperature-sensitive TRP channels. *Semin. Cell Dev. Biol.* **2006**, *17*, 638-645.

(81) Latorre, R.; Brauchi, S.; Orta, G.; Zaelzer, C.; Vargas, G. Thermo TRP channels as modular proteins with allosteric gating. *Cell Calcium* **2007**, *42*, 427-438.

(82) Alem, H.; Duwez, A. S.; Lussis, P.; Lipnik, P.; Jonas, A. M.; Demoustier-Champagne, S. Microstructure and thermo-responsive behavior of poly (N-isopropylacrylamide) brushes grafted in nanopores of track-etched membranes. *J. Membr. Sci.* **2008**, *308*, 75-86.

(83) Jung, Y.; Bayley, H.; Movileanu, L. Temperature-responsive protein pores. *J. Am. Chem. Soc.* **2006**, *128*, 15332-15340.

(84) Chu, L.-Y.; Niitsuma, T.; Yamaguchi, T.; Nakao, S.-i. Thermoresponsive transport through porous membranes with grafted PNIPAM gates. *AlChE J.* **2003**, *49*, 896-909.

(85) Spohr, R.; Reber, N.; Wolf, A.; Alder, G. M.; Ang, V.; Bashford, C. L.; Pasternak, C. A.; Omichi, H.; Yoshida, M. Thermal control of drug release by a responsive ion track membrane observed by radio tracer flow dialysis. *J. Controlled Release* **1998**, *50*, 1-11.

(86) Guo, W.; Xia, H. W.; Cao, L. X.; Xia, F.; Wang, S. T.; Zhang, G. Z.; Song, Y. L.; Wang, Y. G.; Jiang, L.; Zhu, D. B. Integrating Ionic Gate and Rectifier Within One Solid-State Nanopore via Modification with Dual-Responsive Copolymer Brushes. *Adv. Funct. Mater.* **2010**, *20*, 3561-3567.

(87) Nicoletta, F. P.; Cupelli, D.; Formoso, P.; De Filpo, G.; Colella, V.; Gugliuzza, A. Light Responsive Polymer Membranes: A Review. *Membranes* **2012**, *2*, 134-197.

(88) Kramer, R. H.; Chambers, J. J.; Trauner, D. Photochemical tools for remote control of ion channels in excitable cells. *Nat Chem Biol* **2005**, *1*, 360-365.

(89) Liu, N. G.; Dunphy, D. R.; Atanassov, P.; Bunge, S. D.; Chen, Z.; Lopez, G. P.; Boyle, T. J.; Brinker, C. J. Photoregulation of mass transport through a photoresponsive azobenzene-modified nanoporous membrane. *Nano Lett.* **2004**, *4*, 551-554.

(90) Kocer, A.; Walko, M.; Meijberg, W.; Feringa, B. L. A light-actuated nanovalve derived from a channel protein. *Science* **2005**, *309*, 755-758.

(91) Mal, N. K.; Fujiwara, M.; Tanaka, Y. Photocontrolled reversible release of guest molecules from coumarin-modified mesoporous silica. *Nature* **2003**, *421*, 350-353.

(92) Zhang, M.; Hou, X.; Wang, J.; Tian, Y.; Fan, X.; Zhai, J.; Jiang, L. Light and pH Cooperative Nanofluidic Diode Using a Spiropyran-Functionalized Single Nanochannel. *Adv. Mater.* **2012**, *24*, 2424-2428.

(93) Patchornik, A.; Amit, B.; Woodward, R. B. Photosensitive protecting groups. *J. Am. Chem. Soc.* **1970**, *92*, 6333–6335.

(94) Pelliccioli, A. P.; Wirz, J. Photoremovable protecting groups: reaction mechanisms and applications. *Photochem. Photobiolog. Sci.* **2002**, *1*, 441-458.

(95) Brunsen, A.; Cui, J.; Ceolin, M.; del Campo, A.; Soler-Illia, G.; Azzaroni, O. Light-activated gating and permselectivity in interfacial architectures combining ‘‘caged’’ polymer brushes and mesoporous thin films. *Chem. Commun.* **2012**, *48*, 1422-1424.

(96) Lai, J. P.; Mu, X.; Xu, Y. Y.; Wu, X. L.; Wu, C. L.; Li, C.; Chen, J. B.; Zhao, Y. B. Light-responsive nanogated ensemble based on polymer grafted mesoporous silica hybrid nanoparticles. *Chem. Commun.* **2010**, *46*, 7370-7372.

(97) Nasir, S.; Ramirez, P.; Ali, M.; Ahmed, I.; Fruk, L.; Mafe, S.; Ensinger, W. Nernst-Planck model of photo-triggered, pH-tunable ionic transport through nanopores functionalized with ``caged" lysine chains. *J. Chem. Phys.* **2013**, *138*, 034709.

(98) Ito, Y.; Ochiai, Y.; Park, Y. S.; Imanishi, Y. pH-Sensitive Gating by Conformational Change of a Polypeptide Brush Grafted onto a Porous Polymer Membrane. *J. Am. Chem. Soc.* **1997**, *119*, 1619-1623.

(99) Ali, M.; Ramirez, P.; Nguyen, H. Q.; Nasir, S.; Cervera, J.; Mafe, S.; Ensinger, W. Single Cigar-Shaped Nanopores Functionalized with Amphoteric Amino Acid Chains: Experimental and Theoretical Characterization. *ACS Nano* **2012**, *6*, 3631-3640.

(100) Ali, M.; Mafe, S.; Ramirez, P.; Neumann, R.; Ensinger, W. Logic Gates Using Nanofluidic Diodes Based on Conical Nanopores Functionalized with Polyprotic Acid Chains. *Langmuir* **2009**, *25*, 11993-11997.

(101) Ali, M.; Schiedt, B.; Healy, K.; Neumann, R.; Ensinger, W. Modifying the surface charge of single track-etched conical nanopores in polyimide. *Nanotechnology* **2008**, *19*, 085713.

(102) Siwy, Z.; Heins, E.; Harrell, C. C.; Kohli, P.; Martin, C. R. Conical-nanotube ion-current rectifiers: The role of surface charge. *J. Am. Chem. Soc.* **2004**, *126*, 10850-10851.

(103) Kalman, E. B.; Vlassiouk, I.; Siwy, Z. S. Nanofluidic bipolar transistors. *Adv. Mater.* **2008**, *20*, 293-297.

(104) Xia, F.; Guo, W.; Mao, Y. D.; Hou, X.; Xue, J. M.; Xia, H. W.; Wang, L.; Song, Y. L.; Ji, H.; Qi, O. Y.; Wang, Y. G.; Jiang, L. Gating of single synthetic nanopores by proton-driven DNA molecular motors. *J. Am. Chem. Soc.* **2008**, *130*, 8345-8350.

(105) Harrell, C. C.; Kohli, P.; Siwy, Z.; Martin, C. R. DNA - Nanotube artificial ion channels. *J. Am. Chem. Soc.* **2004**, *126*, 15646-15647.

(106) Powell, M. R.; Sullivan, M.; Vlassiouk, I.; Constantin, D.; Sudre, O.; Martens, C. C.; Eisenberg, R. S.; Siwy, Z. S. Nanoprecipitation-assisted ion current oscillations. *Nat. Nanotechnol.* **2008**, *3*, 51-57.

(107) Siwy, Z. S.; Powell, M. R.; Petrov, A.; Kalman, E.; Trautmann, C.; Eisenberg, R. S. Calcium-induced voltage gating in single conical nanopores. *Nano Lett.* **2006**, *6*, 1729-1734.

(108) Hou, X.; Guo, W.; Xia, F.; Nie, F. Q.; Dong, H.; Tian, Y.; Wen, L. P.; Wang, L.; Cao, L. X.; Yang, Y.; Xue, J. M.; Song, Y. L.; Wang, Y. G.; Liu, D. S.; Jiang, L. A Biomimetic Potassium Responsive Nanochannel: G-Quadruplex DNA Conformational Switching in a Synthetic Nanopore. *J. Am. Chem. Soc.* **2009**, *131*, 7800-7805.

(109) Tian, Y.; Hou, X.; Wen, L. P.; Guo, W.; Song, Y. L.; Sun, H. Z.; Wang, Y. G.; Jiang, L.; Zhu, D. B. A biomimetic zinc activated ion channel. *Chem. Commun.* **2010**, *46*, 1682-1684.

(110) Ali, M.; Ramirez, P.; Tahir, M. N.; Mafe, S.; Siwy, Z.; Neumann, R.; Tremel, W.; Ensinger, W. Biomolecular conjugation inside synthetic polymer nanopores via glycoprotein-lectin interactions. *Nanoscale* **2011**, *3*, 1894-1903.

(111) Ali, M.; Schiedt, B.; Neumann, R.; Ensinger, W. Biosensing with Functionalized Single Asymmetric Polymer Nanochannels. *Macromol. Biosci.* **2010**, *10*, 28-32.

(112) Sexton, L. T.; Horne, L. P.; Sherrill, S. A.; Bishop, G. W.; Baker, L. A.; Martin, C. R. Resistive-pulse studies of proteins and protein/antibody complexes using a conical nanotube sensor. *J. Am. Chem. Soc.* **2007**, *129*, 13144-13152.

(113) Siwy, Z.; Trofin, L.; Kohli, P.; Baker, L. A.; Trautmann, C.; Martin, C. R. Protein biosensors based on biofunctionalized conical gold nanotubes. *J. Am. Chem. Soc.* **2005**, *127*, 5000-5001.

(114) Tahir, M. N.; Ali, M.; Andre, R.; Muller, W. E. G.; Schroder, H.-C.; Tremel, W.; Ensinger, W. Silicatein conjugation inside nanoconfined geometries through immobilized NTA-Ni(ii) chelates. *Chem. Commun.* **2013**, *49*, 2210-2212.

(115) Vlassiouk, I.; Kozel, T. R.; Siwy, Z. S. Biosensing with Nanofluidic Diodes. *J. Am. Chem. Soc.* **2009**, *131*, 8211-8220.

(116) Ali, M.; Nasir, S.; Ramirez, P.; Cervera, J.; Mafe, S.; Ensinger, W. Carbohydrate-Mediated Biomolecular Recognition and Gating of Synthetic Ion Channels. *J. Phys. Chem. C* **2013**, *117*, 18234-18242.

(117) Fologea, D.; Gershow, M.; Ledden, B.; McNabb, D. S.; Golovchenko, J. A.; Li, J. L. Detecting single stranded DNA with a solid state nanopore. *Nano Lett.* **2005**, *5*, 1905-1909.

(118) Healy, K. Nanopore-based single-molecule DNA analysis. *Nanomedicine* **2007**, *2*, 459-481.

(119) Iqbal, S. M.; Akin, D.; Bashir, R. Solid-state nanopore channels with DNA selectivity. *Nat. Nanotechnol.* **2007**, *2*, 243-248.

(120) Ali, M.; Tahir, M. N.; Siwy, Z.; Neumann, R.; Tremel, W.; Ensinger, W. Hydrogen Peroxide Sensing with Horseradish Peroxidase-Modified Polymer Single Conical Nanochannels. *Anal. Chem.* **2011**, *83*, 1673-1680.

(121) Fischer, B. E.; Spohr, R. Production and use of nuclear tracks-imprinting structure on solids. *Rev. Mod. Phys.* **1983**, *55*, 907-948.

(122) Ziegler, J. F.; Biersack, J. P.; Ziegler, M. D.: *SRIM: The Stopping and Range of Ions in Matter*.Lulu Press Co., Morrisville, NC, USA, 2008.

(123) Trautmann, C.; Bouffard, S.; Spohr, R. Etching threshold for ion tracks in polyimide. *Nucl. Instrum. Methods Phys. Res., Sect. B* **1996**, 429-433.

(124) Sun, Y.; Zhu, Z.; Wang, Z.; Jin, Y.; Liu, J.; Hou, M.; Zhang, Q. Swift heavy ion induced amorphisation and chemical modification in polycarbonate. *Nucl. Instr. & Method. B* **2003**, *209*, 188-193.

(125) Zhu, Z.; Maekawa, Y.; Liu, Q.; Yoshida, M. Influence of UV light illumination on latent track structure in PET. *Nucl. Instrum. Methods Phys. Res., Sect. B* **2005**, 61-67.

(126) Dobrev, D.; Trautmann, C.; Neumann, R. Novel two-step etching process for ion tracks in polyimide. *GSI Scientific Report* **2006**, 321.

(127) Apel, P. Y.; Blonskaya, I. V.; Oganessian, V. R.; Orelovitch, O. L.; Trautmann, C. Morphology of latent and etched heavy ion tracks in radiation resistant polymers polyimide and poly(ethylene naphthalate). *Nucl. Instrum. Methods Phys. Res., Sect. B* **2001**, *185*, 216-221.

(128) Apel, P. Y.; Blonskaya, I. V.; Orelovitch, O. L.; Root, D.; Vutsadakis, V.; Dmitriev, S. N. Effect of nanosized surfactant molecules on the etching of ion tracks: New degrees of freedom in design of pore shape. **2003**, 329-334.

(129) Wolf-Reber, A. Aufbau eines Rasterionenleitwertmikroskops. Stromfluktuationen in Nanoporen Johann Wolfgang Goethe Universität, Frankfurt am Main, Germany, 2002.

(130) Hermanson, G. T.: *Bioconjugate Techniques*; Academic Press: San Diego, 1996.

(131) Jiang, J. Q.; Tong, X.; Zhao, Y. A new design for light-breakable polymer micelles. *J. Am. Chem. Soc.* **2005**, *127*, 8290-8291.

(132) Iwamura, M.; Ishikawa, T.; Koyama, Y.; Sakuma, K.; Iwamura, H. 1-Pyrenylmethyl esters, photolabile protecting groups for carboxylic acids. *Tetrahedron Lett.* **1987**, *28*, 679-682.

(133) Sahoo, J. K.; Tahir, M. N.; Yella, A.; Branscheid, R.; Kolb, U.; Tremel, W. Soluble IF-ReS2 Nanoparticles by Surface Functionalization with Terpyridine Ligands. *Langmuir* **2011**, *27*, 385-391.

(134) *Membrane Science and Technology*; Osada, Y.; Nakagawa, T., Eds.; Marcel Dekker, Inc: New York, 1992.

(135) Ermakova, L. E.; Sidorova, M. P.; Bezrukova, M. E. Filtration and electrokinetic characteristics of track membranes. *Colloid J. (USSR)* **1998**, *60*, 705-712.

(136) Nishizawa, M.; Menon, V. P.; Martin, C. R. Metal nanotubule membranes with electrochemically switchable ion-transport selectivity *Science* **1995**, *268*, 700-702.

(137) Reber, N.; Kuchel, A.; Spohr, R.; Wolf, A.; Yoshida, M. Transport properties of thermo-responsive ion track membranes. *J. Membr. Sci.* **2001**, *193*, 49-58.

(138) Zhao, B.; Brittain, W. J. Polymer brushes: surface-immobilized macromolecules. *Prog. Polym. Sci.* **2000**, *25*, 677-710.

(139) Nguyen, Q. H.; Ali, M.; Bayer, V.; Neumann, R.; Ensinger, W. Charge-selective transport of organic and protein analytes through synthetic nanochannels. *Nanotechnology* **2010**, *21*, 365701.

(140) Cervera, J.; Ramirez, P.; Mafe, S.; Stroeve, P. Asymmetric nanopore rectification for ion pumping, electrical power generation, and information processing applications. *Electrochim. Acta* **2011**, *56*, 4504-4511.

(141) Karnik, R.; Duan, C. H.; Castelino, K.; Daiguji, H.; Majumdar, A. Rectification of ionic current in a nanofluidic diode. *Nano Lett.* **2007**, *7*, 547-551.

(142) Siwy, Z. S. Ion-current rectification in nanopores and nanotubes with broken symmetry. *Adv. Funct. Mater.* **2006**, *16*, 735-746.

(143) White, H. S.; Bund, A. Ion current rectification at nanopores in glass membranes. *Langmuir* **2008**, *24*, 2212-2218.

(144) Kontturi, K.; Mafe, S.; Manzanares, J. A.; Svarfvar, B. L.; Viinikka, P. Modeling of the salt and pH ffects on the permeability of grafted porous membranes. *Macromolecules* **1996**, *29*, 5740-5746.

(145) Griffiths, J. The realm of the nanopore. *Anal. Chem.* **2008**, *80*, 23-27.

(146) Cervera, J.; Alcaraz, A.; Schiedt, B.; Neumann, R.; Ramirez, P. Asymmetric selectivity of synthetic conical nanopores probed by reversal potential measurements. *J. Phys. Chem. C* **2007**, *111*, 12265-12273.

(147) Cervera, J.; Schiedt, B.; Ramirez, P. A Poisson/Nernst-Planck model for ionic transport through synthetic conical nanopores. *Europhys. Lett.* **2005**, *71*, 35-41.

(148) Ramirez, P.; Apel, P. Y.; Cervera, J.; Mafe, S. Pore structure and function of synthetic nanopores with fixed charges: tip shape and rectification properties. *Nanotechnology* **2008**, *19*, 315707.

(149) Bochet, C. G. Photolabile protecting groups and linkers. *J. Chem. Soc., Perkin Trans. 1* **2002**, 125-142.

(150) Reinhard, R.; Schmidt, B. F. Nitrobenzyl-based photosensitive phosphoramide mustards: Synthesis and photochemical properties of potential prodrugs for cancer therapy. *J. Org. Chem.* **1998**, *63*, 2434-2441.

(151) Zehavi, U.; Amit, B.; Patchornik, A. Light-sensitive glycosides. I. 6-Nitroveratryl .beta.-D-glucopyranoside and 2-nitrobenzyl .beta.-D-glucopyranoside. *J. Org. Chem.* **1972**, *37*, 2281-2285.

(152) *Dynamic Studies in Biology: Phototriggers, Photoswitches and Caged Biomolecules*: 1 ed.; Goeldner, M.; Givens, R., Eds.; Wiley- VCH: Weinheim, Germany, 2005.

(153) Orain, D.; Ellard, J.; Bradley, M. Protecting groups in solid-phase organic synthesis. *J. Comb. Chem.* **2002**, *4*, 1-16.

(154) Cui, W.; Lu, X. M.; Cui, K.; Wu, J.; Wei, Y.; Lu, Q. H. Photosensitive nanoparticles of chitosan complex for controlled release of dye molecules. *Nanotechnology* **2011**, *22*.

(155) Zhao, B.; Moore, J. S.; Beebe, D. J. Surface-directed liquid flow inside microchannels. *Science* **2001**, *291*, 1023-1026.

(156) Siwy, Z.; Apel, P.; Dobrev, D.; Neumann, R.; Spohr, R.; Trautmann, C.; Voss, K. Ion transport through asymmetric nanopores prepared by ion track etching. *Nucl. Instrum. Methods Phys. Res., Sect. B* **2003**, *208*, 143-148.

(157) Cervera, J.; Schiedt, B.; Neumann, R.; Mafe, S.; Ramirez, P. Ionic conduction, rectification, and selectivity in single conical nanopores. *J. Chem. Phys.* **2006**, *124*, 104706.

(158) Pita, M.; Katz, E. Multiple logic gates based on electrically wired surface-reconstituted enzymes. *J. Am. Chem. Soc.* **2008**, *130*, 36-37.

(159) Han, J. H.; Kim, K. B.; Kim, H. C.; Chung, T. D. Ionic Circuits Based on Polyelectrolyte Diodes on a Microchip. *Angew. Chem. Int. Ed.* **2009**, *48*, 3830-3833.

(160) de Silva, A. P.; Dixon, I. M.; Gunaratne, H. Q. N.; Gunnlaugsson, T.; Maxwell, P. R. S.; Rice, T. E. Integration of logic functions and sequential operation of gates at the molecular-scale. *J. Am. Chem. Soc.* **1999**, *121*, 1393-1394.

(161) Zong, G. Q.; Lu, G. X. An Anthracene-Based Chemosensor for Multiple Logic Operations at the Molecular Level. *J. Phys. Chem. C* **2009**, *113*, 2541-2546.

(162) Smaali, K.; Lenfant, S.; Karpe, S.; Ocafrain, M.; Blanchard, P.; Deresmes, D.; Godey, S.; Rochefort, A.; Roncali, J.; Vuillaume, D. High On-Off Conductance Switching Ratio in Optically-Driven Self-Assembled Conjugated Molecular Systems. *ACS Nano* **2010**, *4*, 2411-2421.

(163) Perry, J. M.; Zhou, K.; Harms, Z. D.; Jacobson, S. C. Ion Transport in Nanofluidic Funnels. *ACS Nano* **2010**, *4*, 3897-3902.

(164) Nam, S.-W.; Rooks, M. J.; Kim, K.-B.; Rossnagel, S. M. Ionic Field Effect Transistors with Sub-10 nm Multiple Nanopores. *Nano Lett.* **2009**, *9*, 2044-2048.

(165) Striemer, C. C.; Gaborski, T. R.; McGrath, J. L.; Fauchet, P. M. Charge- and size-based separation of macromolecules using ultrathin silicon membranes. *Nature* **2007**, *445*, 749-753.

(166) Apel, P. Y.; Blonskaya, I. V.; Dmitriev, S. N.; Mamonova, T. I.; Orelovitch, O. L.; Sartowska, B.; Yamauchi, Y. Surfactant-controlled etching of ion track nanopores and its practical applications in membrane technology. *Radiat. Meas.* **2008**, *43*, S552-S559.

(167) Harrell, C. C.; Siwy, Z. S.; Martin, C. R. Conical nanopore membranes: Controlling the nanopore shape. *Small* **2006**, *2*, 194-198.

(168) Mafe, S.; Manzanares, J. A.; Ramirez, P. Gating of Nanopores: Modeling and Implementation of Logic Gates. *J. Phys. Chem. C* **2010**, *114*, 21287-21290.

(169) Ramirez, P.; Ali, M.; Ensinger, W.; Mafe, S. Information processing with a single multifunctional nanofluidic diode. *Appl. Phys. Lett.* **2012**, *101*, 133108.

(170) Manzanares, J. A.; Mafe, S.; Pellicer, J. Current efficiency enhancement in membranes with macroscopic inhomogeneities in the fixed charge distribution. *J. Chem. Soc., Faraday Trans.* **1992**, *88*, 2355-2364.

(171) MacGillivray, A. D. Nernst-Planck Equations and the Electroneutrality and Donnan Equilibrium Assumptions *J. Chem. Phys.* **1968**, *48*, 2903.

(172) Burger, M. Inverse problems in ion channel modelling *Inverse Probl.* **2011**, *27*, 083001.

(173) Robinson, R. A.; Stokes, R. H.: *Electrolyte Solutions*; Butterworths, London, 1955.

(174) Mathews, C. K.; van Holde, K. E.: *Biochemistry*; Benjamin/Cummings: Redwood City, 1990.

(175) Kohli, P.; Harrell, C. C.; Cao, Z. H.; Gasparac, R.; Tan, W. H.; Martin, C. R. DNA-functionalized nanotube membranes with single-base mismatch selectivity. *Science* **2004**, *305*, 984-986.

(176) Sinha, P. M.; Valco, G.; Sharma, S.; Liu, X. W.; Ferrari, M. Nanoengineered device for drug delivery application. *Nanotechnology* **2004**, *15*, S585-S589.

(177) Siwy, Z.; Fulinski, A. Fabrication of a synthetic nanopore ion pump. *Phys. Rev. Lett.* **2002**, *89*, 198103.

(178) Hou, X.; Jiang, L. Learning from Nature: Building Bio-Inspired Smart Nanochannels. *ACS Nano* **2009**, *3*, 3339-3342.

(179) Siwy, Z.; Dobrev, D.; Neumann, R.; Trautmann, C.; Voss, K. Electro-responsive asymmetric nanopores in polyimide with stable ion-current signal. *Appl. Phys.* **2003**, *76*, 781-785.

(180) Holyer, R. H.; Hubbard, C. D.; Kettle, S. F. A.; Wilkins, R. G. The Kinetics of Replacement Reactions of Complexes of the Transition Metals with 2,2',2"-Terpyridine. *Inorg. Chem.* **1966**, *5*, 622-625.

(181) Tuccitto, N.; Giamblanco, N.; Licciardello, A.; Marletta, G. Patterning of lactoferrin using functional SAMs of iron complexes. *Chem. Commun.* **2007**, 2621-2623.

(182) Baker, E. N.; Baker, H. M. Molecular structure, binding properties and dynamics of lactoferrin. *Cell. Mol. Life Sci.* **2005**, *62*, 2531-2539.

(183) Hu, K. L.; Li, J. W.; Shen, Y. H.; Lu, W.; Gao, X. L.; Zhang, Q. Z.; Jiang, X. G. Lactoferrin-conjugated PEG-PLA nanoparticles with improved brain delivery: In vitro and in vivo evaluations. *J. Controlled Release* **2009**, *134*, 55-61.

(184) Marchetti, M.; Pisani, S.; Antonini, G.; Valenti, P.; Seganti, L.; Orsi, N. Metal complexes of bovine lactoferrin inhibit in vitro replication of herpes simplex virus type 1 and 2. *Biometals* **1998**, *11*, 89-94.

(185) Jenssen, H.; Hancock, R. E. W. Antimicrobial properties of lactoferrin. *Biochimie* **2009**, *91*, 19-29.

(186) Sharon, N.; Lis, H. Lectins: Cell-Agglutinating and Sugar-Specific Proteins. *Science* **1972**, *177*, 949-959.

(187) Sharon, N.; Lis, H. Carbohydrates in cell recognition. *Sci. Am.* **1993**, *268*, 82-89.

(188) Ashwell, G.; Harford, J. Carbohydrate-specific receptors of the liver. *Ann. Rev. Biochem.* **1982**, *51*, 531-554.

(189) Cella, L. N.; Chen, W.; Myung, N. V.; Mulchandani, A. Single-Walled Carbon Nanotube-Based Chemiresistive Affinity Biosensors for Small Molecules: Ultrasensitive Glucose Detection. *J. Am. Chem. Soc.* **2010**, *132*, 5024-5025.

(190) Goldstein, I. J.; Hollerman, C. E.; Smith, E. E. Protein-carbohydrate interaction. II. Inhibition studies on the interaction of concanavalin A with polysaccharides. *Biochemistry* **1965**, *4*, 876-883.

(191) Derewenda, Z.; Yariv, J.; Helliwell, J. R.; Kalb, A. J.; Doson, E. J.; Papiz, M. Z.; Wan, T.; Campbell, J. The structure of the saccharide-binding site of concanavalin A. *EMBO J.* **1989**, *8*, 2189-2193.

(192) Lis, H.; Sharon, N. Lectins: Carbohydrate-specific proteins that mediate cellular recognition. *Chem. Rev.* **1998**, *98*, 637-674.

(193) Wei, R. S.; Gatterdam, V.; Wieneke, R.; Tampe, R.; Rant, U. Stochastic sensing of proteins with receptor-modified solid-state nanopores. *Nat. Nanotechnol.* **2012**, *7*, 257-263.

(194) Zhang, Y.; Luo, S. Z.; Tang, Y. J.; Yu, L.; Hou, K. Y.; Cheng, J. P.; Zeng, X. Q.; Wang, P. G. Carbohydrate-protein interactions by "clicked" carbohydrate self-assembled monolayers. *Anal. Chem.* **2006**, *78*, 2001-2008.

(195) Trautmann, C.; Brüchle, W.; Spohr, R.; Vetter, J.; Angert, N. Pore geometry of etched ion tracks in polyimide. *Nucl. Instrum. Methods Phys. Res., Sect. B* **1996**, *111*, 70-74.

Appendix

List of Abbreviations

αHL ..... α-Hemolysin
AAO ..... Anodic aluminum oxide
AEE ..... 2-(2-Aminoethoxyethanol)
APBA ..... 3-Aminophenylboronic acid
APMP ..... p-Aminophenyl α-D-mannopyranoside
BSA ..... Bovine serum albumin
ConA ..... Concanavalin A
COOH ..... Carboxylic acid
DCC ..... *N,N′*-dicyclohexylcarbodiimide
DEG-NH_2 ..... Diethylene glycolamine
DIPEA ..... *N,N*-diisopropylethylamine
DMAP ..... 4-(Dimethyl amino)-pyridine
DMSO ..... Dimethyl sulfoxide
DPy ..... 2,2′-Dipyridine
EDA ..... Ethylene diamine
EDC ..... *N*-(3-Dimethyl-aminopropyl)-*N′*-ethylcarbodiimide
FESEM ..... Field emission scanning electron microscopy
$FeSO_4 \cdot 7H_2O$ ..... Ferrous sulphate heptahydrate
FIB ..... Focused ion beam
HCl ..... Hydrochloric acid
HCOOH ..... Formic acid
HEPES ..... 4-(2-Hydroxyethyl)-1-piperazineethanesulfonic acid)
I–V ..... Current–voltage
KCl ..... Potassium chloride
KOH ..... Potassium hydroxide
LCST ..... Lower critical solubility temperature
LFN ..... Lactoferrin
MES ..... 2-(*N*-morpholino)ethanesulfonic acid
MV^{2+} ..... Methyl viologen (cation)
NaOCl ..... Sodium hypochloride
NaOH ..... Sodium hydroxide
NDS^{2-} ..... 1,5-Naphthalene disulfonate (anion)
NP ..... Nernst-Planck

NVOC 4,5-Dimethoxy-2-nitrobenzyl
PA ..... Propylamine
PC ..... Polycarbonate
PCTFE ..... Ploychlorotrifluoroethylene
PEI ..... Polyethyleneimine
PET ..... Polyethylene terephthalate
PFP ..... Pentafluorophenol
pI ..... Isoelectric point
PI ..... Polyimide
PNIPAAM ..... Poly(*N*-isopropyl acrylamide)
PNP ..... Poisson and Nernst-Planck
PPGs ..... Photo-labile protecting groups
PYBA ..... 4-Oxo-4-(pyren-4-ylmethoxy) butanoic acid
SEM ..... Scanning electron microscope
Si ..... Silicon
Si_3N_4 ..... Silicon nitride
SiO_2 ..... Silicon dioxide
sulfo-NHS ..... *N*-hydroxysulfosuccinimide
TEM ..... Transmission electron microscope
terPy–DEG-NH_2 ..... 1-Amino-5-(2,2′:6′,2″-terpyrid-4′-yl-oxy)pentane
UNILAC ..... UNIversal Linear Accelerator

List of Chemicals

1,5-Naphthalene disulfonate di-sodium salt (Sigma-Aldrich, Germany)

1-Pyrenemethanol (98%, Sigma-Aldrich, Germany)

2-(2-Aminoethoxyethanol) (Sigma-Aldrich, Germany)

2-(*N*-morpholino)ethanesulfonic acid (SL Labor-Service GmbH, Germany)

2,2′-Dipyridine (Sigma-Aldrich, Germany)

4,5-Dimethoxy-2-nitrobenzyl chloroformate (97 %, Sigma-Aldrich, Germany)

4′-Chloro,2,2′,6′,2"-terpyridine (Sigma-Aldrich, Germany)

4-Aminophenyl α-D-mannopyranoside (Sigma-Aldrich, Germany)

4-Dimethylaminopyridine (Sigma-Aldrich, Germany)

6-Nitroveratryl alcohol, (99 %, Sigma-Aldrich, Germany)

Amine-terminated poly(*N*-isopropyl acrylamide) [P10405A-NIPAMNH$_2$, Mn = 82,000, Polymer Source, Inc.]

Bovine serum albumin (BSA; fraction V, Sigma-Aldrich, Germany)

Concanavalin A (Sigma-Aldrich, Germany)

Dimethyl sulfoxide (anhydrous, DMSO, Sigma-Aldrich, Germany)

Ethanol (Sigma-Aldrich, Germany)

Ethylenediamine (99+%, Sigma-Aldrich, Germany)

Ferrous sulphate heptahydrate ($FeSO_4 \cdot 7H_2O$, Sigma-Aldrich, Germany)

Lactoferrin human (Sigma-Aldrich, Germany)

Lysozyme (Sigma-Aldrich, Germany)

Methylviologen dichloride (Sigma-Aldrich, Germany)

N-(3-Dimethylaminopropyl)-*N*′-ethylcarbodiimide hydrochloride (98%, Sigma-Aldrich, Germany)

N,N′-Dicyclohexylcarbodiimide (DCC, 98 %, Sigma-Aldrich, Germany)

N,N-Diisopropylethylamine (Sigma-Aldrich, Germany)

N-Hydroxysulfosuccinimide (Sigma-Aldrich, Germany)

Pentafluorophenol (PFP, 99+ %, Sigma-Aldrich, Germany)

Piperidine (Sigma-Aldrich, Germany)

Succinic anhydride (Sigma-Aldrich, Germany)

List of Figures

Figure 2.1: a-f) Presentation of steps for the preparation of samples and packing of samples in magazine. 10

Figure 2.2: a) Electronic and nuclear energy loss of lead (^{206}Pb) ion during the irradiation of a stack of PET membrane samples of 72µm thickness. b) Energy loss versus specific energy E (GeV) at low energies. c) Projectile range of ^{206}Pb ion in PET sample with respect to specific energy. The energy loss and projectile range for ^{206}Pb ion was calculated by using SRIM code. 11

Figure 2.3: Scheme representing the setup for single ion irradiation experiments. 12

Figure 2.4: Schematic representation of chemical etching of latent track in heavy ion irradiated polymer membrane. 14

Figure 2.5: a) Conductivity cell with ion tracked PET polymer membranes. b) Experimental setup used for the asymmetric track-etching of polymer membranes. c) Scheme showing the fabrication process of conical nanopores. d) Current versus time curve recorded during asymmetric etching of single latent track in PET membrane. 15

Figure 2.6: a) Sample holder with PET membranes used for the preparation of cylindrical nanopores. b) Experimental setup used for symmetric track-etching technique. c) Schematic representation of symmetric track-etching process. 16

Figure 2.7: FESEM images of track-etched PET membrane surface with conical (a), and cylindrical nanopore (c). The FESEM images of conical nanowires (b) and cylindrical nanowires (d) formed by electrochemical deposition of Au in asymmetrically and symmetrically etched PET membranes, respectively. 18

Figure 2.8: A labview window image showing current-voltage (*I–V*) characteristics of a single conical nanopore (a) and single cylindrical nanopore (b) in 100 mM KCl (pH 7.0) solution. 19

Figure 2.9: Schematic representation of the geometrical dimensions of a track-etched single conical nanopore (a), and cylindrical (b) nanopores. 20

Figure 2.10: a) Scheme representing the hydrolysis of ester bonds via chemical etching of ion tracks in PET membrane. b) Track-etched nanopores with surface carboxylic acid groups on the inner pore walls. 21

Figure 2.11: A general reaction scheme representing the tuning of nanopore surface functionalities via carbodiimide coupling chemistry. The terminal –R can be a primary amine, zwitterionic group or stimuli-responsive molecule / group. 22

Figure 2.12: A simplified cartoon representing the process of analyte permeation across the track-etched nanoporous membrane. 23

Figure 2.13: Concentration-dependent absorption spectra and linear fit for λ_{max} versus analyte concentration: a) methylviologen (MV), b) 1,5-naphthalene disulfonate (NDS), c) 2,2′-dipyridine (DPy). The different analyte concentrations are prepared in phosphate buffer solution. 24

Figure 2.14: Reaction scheme for the synthesis of photosensitive “caged” lysine amino acid (7). 28

Figure 3.1: The thermally-driven conformational transitions of the attached polymer brushes and respective transport of ionic molecules through an array of cylindrical nanopores across the modified membrane below (left) and above (right) the lower solubility temperature (LCST) of the PNIPAAM chains. 38

Figure 3.2: Thermally controlled permeation of MV^{2+} and NDS^{2-} molecules through cylindrical nanopore arrays before (a) and after (b) modification with PNIPAAM brushes at low and high temperatures. 38

Figure 3.3: Reversible switching of thermal gating of the modified membrane; (a) for the transport of MV^{2+} and (b) NDS^{2-} molecules through the cylindrical nanopore arrays at low and high temperature. 39

Figure 3.4: The thermally-driven conformational transitions of the attached polymer brushes and respective transport of ionic molecules through an array of conical nanopores across the modified membrane below (left) and above (right) the lower critical solubility temperature (LCST) of the PNIPAAM chains. 40

Figure 3.5: Temperature-dependent permeation of NDS^{2-} and MV^{2+} molecules prior to (a) and after (b) modification of an array of conical nanopores (5×10^7 pores cm^{-2}) with tip and base openings of ~18±3 and 500±5 nm in diameters, respectively. 41

Figure 3.6: Reversible switching of thermal gating of the modified membrane; (a) for the transport of MV^{2+} and (b) NDS^{2-} molecules through arrays of conical nanopores at low and high temperature.....42

Figure 3.7: Temperature-dependent current–voltage (*I–V*) curves of a single conical nanopore prior to (a) and after (b) modification with PNIPAAM molecules. The tip diameter of the conical pore is ~15 nm. 43

Figure 3.8: (a) *I–V* curves of single conical nanochannels bearing ionised carboxyl and amine groups in a 0.1 M KCl (pH = 6.0) aqueous solution. (b) *I–V* characteristics of the same nanochannel modified with photosensitive PYBA molecules before and after UV light irradiation. (c) and (d) *I–V* theoretical curves corresponding to the experimental curves (a) and (b) respectively. The approximate radii are a_B = 140 nm for the channel base and a_T = 2 nm for the channel tip (COO^- and NH_3^+ pores). For the PYBA pore, a_B = 139 nm and a_T = 1 nm.....48

Figure 3.9: Schematic illustration of the wettability changes produced by UV light irradiation of a single conical nanochannel modified with photoremovable protecting molecules. 49

Figure 3.10: (a) Schematic illustration of the transport of ionic species through the multi-channel membrane before and after UV irradiation. (b) Permeation data for MV^{2+} and NDS^{2-} prior to and after UV treatment of the PYBA-modified membrane. The fluxes are obtained for an array of cylindrical nanochannels with an average diameter (20 ± 3) nm in a multipore membrane.....50

Figure 3.11: a) Scheme (not to scale) of the asymmetric nanopore. b) Reaction scheme for the synthesis of "caged" amino acid lysine (7) with caged amine and carboxylic acid groups attached to the α-carbon.....55

Figure 3.12: Schematic pore and *pH*-dependent *I–V* curves of a single asymmetric nanopore with carboxylate groups (a), "caged" (b), and "uncaged" amphoteric lysine chains (c). The *I–V* curves are measured in a 0.1 M KCl solution prepared in a phosphate buffer at different *pH* values. 56

Figure 3.13: Schematic cartoon describing the (a) phototriggered permeation through the asymmetric nanopore arrays bearing "caged" lysine chains ("off" state) and "uncaged" lysine chains ("on" state) on the inner pore walls. (b) The *pH*-tunable permselective transport of ionic analytes across the multipore membrane containing "uncaged" amphoteric lysine chains. 57

Figure 3.14: pH-dependent permeation of MV^{2+} through the multipore membrane prior to (a) and after (b) UV irradiation. (c) Absorption spectra recorded for MV^{2+} in the permeate solution obtained after 4 hours of analyte transport at *pH* = 9.5 before and after UV irradiation of the membrane. (d) MV^{2+} permeation rates through the multipore membrane before and after UV treatment, respectively. ...58

Figure 3.15: pH-dependent permeation of NDS^{2-} through the multipore membrane prior to (a) and after (b) UV irradiation. (c) Absorption spectra recorded for NDS^{2-} in the permeate solution obtained after 4 hours of analyte transport at pH = 3.0 before and after UV irradiation of the membrane. (d) NDS^{2-} permeation rates through the multipore membrane before and after UV treatment, respectively. ...59

Figure 3.16: Sketch of the asymmetric nanopore (not to scale). 60

Figure 3.17: Calculated *I–V* curves of a single asymmetric nanopore with carboxylate groups (a), "caged" lysine chains (b), and "uncaged" lysine chains (7c), for the same experimental conditions as in Figure 3.12. The nanopore parameters used in the calculations are shown in the insets. 66

Figure 3.18: Schematic representation of (a) as-prepared single conical nanopore containing surface carboxylic acid groups , (b) covalent immobilization of amine-terminated terpyridine ligand with carboxyl groups via carbodiimide coupling chemistry, (c) subsequent treatment with iron(II) salt solution to obtain iron–terPy complexes (X represents any counter-ion or coordinating solvent molecule), and (d) biorecognition of lactoferrin molecules.....74

Figure 3.19: *I–V* characteristics of a single conical nanopore with tip $d \approx 13$ nm measured in 0.1 M KCl (pH 7.0) solutions corresponding to pore surfaces with carboxylate groups (black square), and iron–terpyridine complexes (red filled circle); and upon exposing the modified pore to different concentration of lactoferrin prepared (separately) in the same electrolyte solution, respectively. ...75

Figure 3.20: Current-voltage characteristics of a single conical nanopore with tip $d \approx 11$ nm and base $D \approx 575$ nm in 0.1 M KCl prior to and after the covalent immobilization of iron–terPy ligand followed by the addition (separately) of 100 nM of each, bovine serum albumin (BSA) and lactoferrin (LFN) protein in the electrolyte solution, respectively. 76

Figure 3.21: Current–voltage (*I–V*) characteristics of a single conical nanopore with tip $d \approx 10$ nm in 0.1M KCl solution (a) before, and (b) after the covalent attachment of terpyridine followed by the addition of various concentration of lactoferrin the background electrolyte solution. 77

Figure 3.22: Diffusion of doubly charged organic analytes (MV^{2+} and NDS^{2-}) through nanoporous membrane containing an array of cylindrical nanopores (10^8 pores cm^{-2}) of ~18 nm in diameter, (a) before modification (carboxylated pore surface) without lactoferrin in the feed solution, and (b) after the immobilization of iron–terPy complexes in the presence of lactoferrin (100 nM) in the feed solution.....78

Figure 3.23: Diffusion of doubly charged organic analytes (MV^{2+} and NDS^{2-}) in the presence of lactoferrin (100 nM) in the analyte solution through nanoporous membrane containing an array of cylindrical nanopores (10^8 pores cm^{-2}) of ~26 nm in diameter, (a) before modification (carboxylated pore surface), and (b) after the immobilization of iron–terPy complexes onto the inner walls of nanopores. 79

Figure 3.24: Schemes representing: (a) the as-prepared single asymmetric nanochannel containing native carboxylic acid (COOH) groups, (b) the covalent attachment of p-aminophenyl α-D-mannopyranoside (APMP) ligand molecules with COOH groups through carbodiimide coupling chemistry, (c) the selective recognition of ConA protein, and (d) the displacement of ConA by free mannose molecules and reversible ConA binding with regenerated mannopyranoside moieties on the nanochannel surface. 83

Figure 3.25: (a) The *I–V* curves for the as-prepared (carboxylated) and APMP-modified single asymmetric nanochannels. (b) The *I–V* characteristics of the modified nanochannel upon exposing to electrolyte solutions containing lysozyme, BSA and ConA proteins, separately. (c) The channel conductance at $V = 1$ V after several measuring cycles exhibiting the reversibility of ConA binding. (d) The *I–V* curves for the as-prepared nanochannels at high ConA concentrations in the micro-molar regime show a small to moderate decrease in the current. 86

Figure 3.26: (a) *I–V* curves obtained for modified channel at different protein concentrations. (b) The experimental channel conductance values estimated from the *I–V* curves at V = 1 V. The inset shows the conductance values at three different voltages *V*. (c) The theoretical *I–V* curves reproduced the experimental trends of Figure 3.26a. (d) The calculated channel conductances agree with the experimental ones of Figure 3.26b. The pore basis radius (750 ± 10 nm) is determined from microscopy using multichannel samples etched at the same time as the single pore while the pore tip radius (15 ± 3 nm) is estimated by fitting the experimental data to the continuous model. 87

Figure 3.27: Permeation data for dipyridine: a) number of nanomoles transported versus time, (b) permeation rate (flux), and (c) absorption spectra of the permeate solution after 240 min of diffusion time across the non-bioconjugated, bioconjugated and mannose treated membranes. (d) Different cycles showing the dipyridine nanomoles permeated after reversible bioconjugation on and displacement from the channel surface by membrane exposition to ConA and mannose solutions, respectively. 90

List of Tables

Table 3.1: Analyte permeation rates (nanomoles cm^{-2} min^{-1}) before and after modification through cylindrical nanopore arrays at low and high temperature. 39

Table 3.2: Analyte permeation rates (nanomoles cm^{-2} min^{-1}) before and after modification through conical nanopore arrays at low and high temperature. 42

Table 3.3: YES logic function for the single nanochannel with an optical input and an electrical output. 51

Table 3.4: YES logic function for the multichannel membrane with an optical input and a chemical output. 51

Table 3.5: AND logic function for single nanochannel with electro-optical inputs and an electrical output.....51

Table 3.6: Estimation of pore parameters from least-square fittings of linear *I–V* curves in Figures 3.12b and 3.12c. 65

Table 3.7: The flux ratios at different pH values obtained with the NP model and the experimental ratios for the permeation of MV^{2+} and NDS^{2-} through the multipore membrane. 68

List of Publications

[1] **Saima Nasir**, Mubarak Ali and Wolfgang Ensinger, "Thermally Controlled Permeation of Ionic Molecules through Synthetic Nanopores Functionalized with Amine-Terminated Polymer Brushes" *Nanotechnology* **2012**, 23, 225502.

[2] **Saima Nasir**, Patricio Ramirez, Mubarak Ali, Ishtiaq Ahmed, Ljiljana Fruk, Salvador Mafé, and Wolfgang Ensinger, "Nernst-Planck Model of Photo-Triggered, pH–Tunable Ionic Transport through Nanopores Functionalized with "Caged" Lysine Chains"
Journal of Chemical Physics **2013**, 138, 034709.

[3] **Saima Nasir**, Mubarak Ali, Patricio Ramirez, Vicente Gómez, Bernd Oschmann, Falk Muench, Muhammad Nawaz Tahir, Salvador Mafé, and Wolfgang Ensinger, "Fabrication of Single Cylindrical Au-Coated Nanopores with Non-Homogeneous Fixed Charge Distribution Exhibiting High Current Rectifications"
ACS Applied materials and Interfaces **2014**, 6, 12486–12494.

[4] **Saima Nasir**, Mubarak Ali, Quoc Hung Nguyen and Wolfgang Ensinger, "Stimuli-Triggered Permeation of Ionic Analytes through Nanopores Functionalised with Responsive Molecules"
Nanopores for Bioanalytical Applications: Proceedings of the International Conference, The Royal Society of Chemistry **2012**, 76–82.

[5] Mubarak Ali, **Saima Nasir**, Quoc Hung Nguyen, Jugal Kishore Sahoo, Muhammad Nawaz, Tahir, Wolfgang Tremel, and Wolfgang Ensinger ,"Metal Ion Affinity-Based Biomolecular Recognition and Conjugation inside Synthetic Polymer Nanopores Modified with Iron–Terpyridine Complexes"
Journal of the American Chemical Society **2011**, 133, 17307−17314.

[6] Mubarak Ali, **Saima Nasir**, Patricio Ramirez, Ishtiaq Ahmed, Quoc Hung Nguyen, Ljiljana Fruk, Salvador Mafe, and Wolfgang Ensinger, "Optical Gating of Photosensitive Synthetic Ion Channels" *Advanced Functional Materials* **2012**, *22*, 390−396.

[7] Mubarak Ali, **Saima Nasir**, Patricio Ramirez, Javier Cervera, Salvador Mafe, and Wolfgang Ensinger, "Calcium Binding and Ionic Conduction in Single Conical Nanopores with Polyacid Chains: Model and Experiments"
ACS Nano **2012**: 6, 9247–9257.

[8] Mubarak Ali, **Saima Nasir**, Quoc Hung Nguyen, Reinhard Neumann and Wolfgang Ensinger, Biochemical Sensing with Chemically Modified Synthetic Ion Channels,
Nanopores for Bioanalytical Applications: Proceedings of the International Conference, The Royal Society of Chemistry **2012**, 32-37.

[9] Mubarak Ali, **Saima Nasir**, Patricio Ramirez, Javier Cervera, Salvador Mafe and Wolfgang Ensinger, "Carbohydrate-Mediated Biomolecular Recognition and Gating of Synthetic Ion Channels"
The Journal of Physical Chemistry C **2013**, 117, 18234−18242.

[10] Mubarak Ali, **Saima Nasir**, Ishtiaq Ahmed, Ljiljana Fruk and Wolfgang Ensinger, "Tuning Nanopore Surface Polarity and Rectification Properties through Enzymatic Hydrolysis inside Nanoconfined Geometries"
Chemical Communications **2013**, 49, 8770−8772.

[11] Quoc Hung Nguyen, Mubarak Ali, **Saima Nasir** and Wolfgang Ensinger, "Fabrication of Nanochannel Arrays for the Selective Transport of Ionic Species" *Nanopores for Bioanalytical Applications: Proceedings of the International Conference, The Royal Society of Chemistry* **2012**, 83–88.

[12] Mubarak Ali, Patricio Ramirez, **Saima Nasir**, Quoc Hung Nguyen, Wolfgang Ensinger, Salvador Mafe "Nanoparticle-Induced Rectification in a Single Cylindrical Nanopore: Net Currents from Zero Time-Average Potentials"
Applied Physics Letters **2014**, 104, 043703.

[13] Mubarak Ali, Patricio Ramirez, **Saima Nasir**, Quoc Hung Nguyen, Wolfgang Ensinger, Salvador Mafe "Current Rectification by Nanoparticle Blocking in Single Cylindrical Nanopores"
Nanoscale **2014**, *6*, 10740–10745.

[14] Mubarak Ali, Patricio Ramirez, Quoc Hung Nguyen, **Saima Nasir**, Javier Cervera, Salvador Mafe and Wolfgang Ensinger, "Single Cigar-Shaped Nanopores Functionalized with Amphoteric Amino Acid Chains: Experimental and Theoretical Characterization"
ACS Nano **2012**, *6*, 3631–3640.

[15] Antonio Alcaraz, Mubarak Ali, Wolfgang Ensinger, Salvador Mafe, Falk Münch, **Saima Nasir** and Patricio Ramirez, "Biomimetic Nanopores with Amphoteric Amino Acid Groups. Effects of a pH Gradient on the Ionic Conductance and Selectivity"
Nanopores for Bioanalytical Applications: Proceedings of the International Conference, The Royal Society of Chemistry **2012**, 57–61.

Curriculum Vitae

Name:	Saima Nasir
Date of birth:	1st December 1979
Palce of birth:	Sahiwal, Pakistan
Nationality:	Pakistani
Marital status:	Married
Present address:	In Den Wingerten 39, 64291 Darmstadt, Germany
Permanent address:	Post office Dhabli Wala, Teh. & Distt. Narowal, Pakistan

Academic Career

1997 – 1999	**B.Sc.** in Chemistry, Botany and Zoology. Institution: Bahauddin Zakariya University, Multan.
1999 – 2001	**M.Sc.** in Chemistry. Institution: Islamia University Bahawalpur, Pakistan.
2002 – 2004	**M.Phil.** Specialization in Organic Chemistry. Institution: Quaid-i-Azam University Islamabad, Pakistan.

Since April 2011 **Doctoral thesis** under the supervision of Prof. Dr. Wolfgang Ensinger at Darmstadt University of Technology, Darmstadt, Germany.

Teaching Experience

Served as a Lecturer (Chemistry) in the Department of Chemistry, Bahauddin Zakariya University, Multan (Pakistan), from. Jan 2005 to Jan 2008.